Queen Mary
University of London

POLYOXAZOLINE DERIVATIVES FOR THE DESIGN OF POLYMER BRUSHES AND HYDROGELS

Pei Tang

School of Engineering and Materials science

Queen Mary University of London

This dissertation is submitted for the degree of Doctor of Philosophy

2017

STATEMENT OF ORIGINALITY FOR INCLUSION IN RESEARCH DEGREE THESES

I, Pei Tang, confirm that the research included within this thesis is my own work or that where it has been carried out in collaboration with, or supported by others, that this is duly acknowledged below and my contribution indicated. Previously published material is also acknowledged below.

I attest that I have exercised reasonable care to ensure that the work is original, and does not to the best of my knowledge break any UK law, infringe any third party's copyright or other Intellectual Property Right, or contain any confidential material.

I accept that the College has the right to use plagiarism detection software to check the electronic version of the thesis.

I confirm that this thesis has not been previously submitted for the award of a degree by this or any other university.

Signature:

Date:

Details of collaboration and publications:

Stefania Di Cio performed the AFM measurements, and Burcu Colak performed the fluorescent microscopy. All analysis of the data was performed by me.

ACKNOWLEDGEMENT

This thesis could not exist without the funding provided by China Scholarship Council and Queen Mary University of London and the support of my supervisors Julien E. Gautrot and Professor Wen Wang. I am extremely grateful that I have had this opportunity being part of Julien's team member. I am really appreciative of everything he has taught me, his patience and kind support.

I would like to thank Burcu Colak for her assistance on the synthesis of poly (oxazolines)s and fluorescent microscopy, and Stefania Di Cio provided the AFM scans and cell work. I would also like to express my appreciation to Dexu Kong for her assistance on preparation of proteins and William Megone for training and helping with the rheology.

Many thanks to the group members in the Gautrot lab: Khai Duong Quang Nguyen, Maria Crespo Ribadeneyra, Shoghik Hakobyan, Xi Zhang and so on for happy memories in the lab.

Finally, I would like to thank my parents, for their selfless love and support throughout my life, and also Miao Lin, Li Zhao for their emotional support throughout the last year and Kaz Janowski for proof reading my thesis.

Abstract

Hydrophilic POx have very similar behaviour with PEG owing to its peptdomimetic structure, however, POx shows higher chemical stability than PEG and can be further functionalised via substitute R in the side chains or at the end of the chain. In addition, PEtOx has been approved as an indirect food additive by FDA which may indicate the possibility of good immunogenicity of POx-based materials. Synthetic surfaces with reproducibility and biocompatibility for in vitro cell culture offer lots of advantages on adherent cells. A variety of synthetic polymers as well as properties like mechanical and chemical robustness resulting polymer brushes prior to other surface modification methods. Synthetic hydrogels can be further modified and allow a variety of mechanical and biochemical properties that determine the cell phenotype which makes it a good candidate for biomedical applications.

Our work has focused on the design of polyoxazolines with controlled end chains for the design of such hydrogels and polymer brushes. In the second chapter, we review the synthesis of defined polyoxazoline and its applications, synthesis of non-fouling surfaces, fabricated hydrogels and characterisations. In the third chapter, we explore the design of poly(2-oxazolines) with controlled end chains and characterise the structure and control of initiation and termination steps. A range of initiators (bromide, iodide as well as tosylates) and termination agents were used to introduce functionalisable or polymerisable end groups on poly(2-oxazolines). Microwave assisted synthesis was used for polyoxazoline synthesis. Polyoxazolines can be simply synthesized in relatively mild conditions using this approach. The structure of the resulting polymers is characterised by NMR, MALDI-ToF and FTIR. In the third chapter, we explore the use of polymerisable polyoxazolines for the design of grafted from polymer brushes. The

growth of poly(oxazoline) brushes was studied first and the resulting polymer brushes characterised. We then explored the functionalization of polymer brushes using thiol-ene chemistry and their protein resistance for cell and protein patterning. Hence, we explored the design of polyoxazoline nonfouling coatings. These surfaces allow the control of surface properties such as protein adsorption and bio-functionalization. In the fourth chapter, we designed a series of thiolated poly(oxazolines) to be used for the design of hydrogels crosslinked via thiol-ene chemistry. We fully characterised the thiolated polymers designed and studied the formation of hydrogels using an alkene-functionalised polyoxazoline and a range of thiolated crosslinkers with polyethylene glycol and poly(oxazoline) backbones. Synthetic hydrogels have attracted much attention recently for in vitro cell culture as they allow the control of the properties of soft biomaterials (mechanics, cell adhesion, degradation). Importantly, the gelation conditions used for 3D cell encapsulation are essential as they allow controlling the mechanics and stability of the gel, whilst curing in mild, non-toxic conditions. Properties such as hydrogel chemistry, macroscopic and nanoscale mechanical properties and degradation have indeed been shown to strongly affect cell phenotype and the use of these materials for tissue engineering. To study gelation in situ, photo-rheology was used to characterise the properties and kinetics of the resulting hydrogels. Here, we investigated the formation of hydrogels with different multi-arm PEG thiols. This allowed us to improve the properties of hydrogel even at low weight concentration of materials where gelation is particularly challenging.

CONTENTS

Abbreviations

2I-PMeOx-acry acrylic acid	MeOx initiated with 1, 2-Diiodoethane and terminated with
2I-PMeOx-SH thiol	MeOx initiated with 1, 2-Diiodoethane and terminated with
4I-PMeOx-acry	MeOx initiated with Pentaerythrityl tetraiodide and terminated with acrylic acid
ACN	acetonitrile
AFM	Atomic force microscopy
ATRP	atom transfer radical polymerisation
BBBs	bottle-brush brushes
BF3-OEt2	boron trifluoride
BPEI	branched polyethyleneimine
BSA	bovine serum albumin
BuPEtOxOH oxazoline)	Poly (2-ethyl-2-oxazoline)-co-poly (2-(3-butenyl)-2-
Bu-PMeOx-acry	acrylic acid end capped copolymer Poly (2-methyl-2-oxazoline)-co-poly (2-(3-butenyl)-2-oxazoline)
BuPMeOxOH oxazoline)	Poly (2-methyl-2-oxazoline)-co-poly (2-(3-butenyl)-2-
BuPMeOxSH	thiol end capped copolymer Poly (2-methyl-2-oxazoline)-co-poly (2-(3-butenyl)-2-oxazoline)
Bu-PMeOx-thioacetate	thioacetic acid end capped copolymer Poly (2-methyl-2-oxazoline)-co-poly (2-(3-butenyl)-2-oxazoline)
ButNOx	2-(3-butenyl)-2-oxazoline
CROP	cationic ring opening polymerization
CRP	controlled/living radical polymerization
CuAAC	copper-catalysed azide-alkyne cycloaddition
DAPI	4',6-Diamidino-2-phenylindole

DCM	Dichloromethane
DMF	Dimethylformamide
DP	degree of polymerization
DT	degenerative transfer
DTT	dithiothreitol
EBs	embryoid bodies
ECM	extracellular matrix
EGDMA	ethylene glycol dimethacrylate
EPR	permeability and retention
FBS	foetal bovine serum
Fn	fibronectin
FRAP	fluorescence recovery after photo bleaching
FTIR	Fourier-transform infrared spectroscopy
HA	hyaluronic acid
His-tagged	histidine-tagged
HMTETA	1,1,4,7,10,10-hexamethyltriethylenetetramine
HOEGMA	poly (ethylene glycol) end capped with OH
IgG	immunoglobulin G
Irgacure 2959	2-hydroxy-1-[4-(2-hydroxyethoxy)phenyl]-2-methyl-1-propanone
LDA	Lithium diisopropylamide solution
LVE	linear viscoelastic
MAA	methacrylic acid
MALDI	matrix-assisted laser desorption/ionization
MBA	methylene bisacrylamide
MeOTf	methyl triflate
MeOTs	methyl tosylate

NHS	N-hydroxysuccinimide
NMP	nitroxide mediated polymerisation
NMP	N-Methyl-2-pyrrolidone
OAMeOxMA	Allyl-PMeOx-MA
OEGMA	oligo(ethylene glycol)
OEGMA	oligo(ethylene oxide) methacrylate
PBS	Phosphate-buffered saline
PEG	poly(ethylene glycol)
PEG-2SH	poly(ethylene glycol) dithiol
PEG-4Mal	PEG - Methoxypolyethylene glycol maleimide
PEG4NB	PEG-tetra-norbornene
PEG-4SH	4arm PEG thiol
PEG-4SH	four arms poly(ethylene glycol) end capped with thiols
PEG-8SH	eight arms poly(ethylene glycol) end capped with thiols
PEI	polyethylenimines
PETA	pentaerythritol triacrlylate
PEtOx	poly(2-ethyl-2-oxazoline)
PEtOxMA	Me- poly(2-ethyl) oxazoline- methacrylate
PEtOx-PEG- PEtOx poly(2-ethyl-2-oxazoline)	Poly (2-ethyl-2-oxazoline)-b-poly (ethylene oxide)-b-
PETTA	pentaerythritol tetraacrylate
PGMA	polyglycidyl methacrylate
PMDETA	N,N,N’,N’’,N’’-Pentamethyldiethylenetriamine-bute
PMeOx	poly(2-methyl) oxazoline
PMeOx-2SH	two arms PMeOx end capped with thiols
PMeOxMA	Me- poly(2-methyl) oxazoline- methacrylate
PNonOx	2-nonyl-2-oxazoline

POx	poly(2-oxazoline)
PPhOx	2-phenyl-2-oxazoline
RAFT polymerisation	reversible addition-fragmentation chain-transfer
ROMP	metathesis polymerization
SAM	Self-assembled monolayer
SAPs	Superabsorbents
SET	single electron transfer
SET-LRP	single-electron-transfer living radical polymerization
SPR	surface plasmon sensor
SR	swelling ratio
TEA	Triethylamine
TEC	thiol-ene coupling
THF	Tetrahydrofuran
TMPTA	hexafunctional trimethylpropane trimethacrylate
TPT	trimethylolpropane trimethacrylate
VP-BA	N-vinyl-2-pyrrolidone-co-butyl acrylate
XPS	X-ray photoelectron spectroscopy

List of figures

Chapter 1

INTRODUCTION

Although poly(ethylene glycol) (PEG) has been widely used in biomedical applications, For example, PEGylated drugs were used as inert molecules to biologic molecules to improve the pharmacodynamics properties regarding to rheumatic diseases.[1] However, its chemistry and synthesis present several drawbacks. Moreover, the synthesis of PEG is not simple to carry out routinely in the lab, as the monomer, ethylene oxide is a gas, and cannot be readily functionalised with reactive side-chains. This contrasts with poly(oxazolines), which can be readily synthesised in the lab, in relatively mild conditions and can be substituted with reactive side groups. Furthermore, PEG degradation was reported before as both in solution[2] and of surface bound thin film[3-5]. In addition, it has been shown that PEG displays immunogenicity; either from the polymer structure itself or some of the by-products of its degradation[6].

Furthermore, Textor and studied the stability of PLL-g-PEG brushes and PLL-g-PMOXA brushes, although both thin films proved equally excellent anti-fouling properties under protein and bacterial, PLL-g-PMOXA brushes showed superior stable actions during longer term applications when exposed to oxidative environment[7].

Importantly, the ease of incorporate functional and reactive moieties at both the termini and side chains together allowing this class of polymers suitable for the preparation of polymer conjugates, drug delivery systems, and targeted drug delivery.

Polyethylene glycol derived polymers (PEGs) were widely utilized in drug and medical device applications. A majority of novel applications for PEG derivatives on drug

delivery and targeted diagnostics were studied, either from direct PEGylation of therapeutics[8-11] or via nanoparticles[10, 11], liposomes[12], micelles[13, 14]. Moreover, Polyethylene Glycol hydrogels were applied in would healing and tissue regeneration, especially for the regeneration of the cartilage tissue[15, 16]. Furthermore, PEG hydrogels were fabricated for cell culture of valvular interstitial cells and valvular endothelial cells, which pave the way of application for cell culture and tissue models[17]. In addition, PEG and methoxypolyethylene glycols are manufactured by Dow Chemical under the tradename Carbowax for industrial use, and Crbowax Sentry for food and pharmaceutical use. With different molecular weight, they vary from liquid to solid. Nowadays, they are been used commercially in different applications, such as surfactants[18], foods[19], cosmetics[20, 21], pharmaceutics[22, 23], biomedicine[24] and so on.

Regarding to those enormous biomedical applications, the eager to identify more stable polymer upon long term storage compared to PEGs was proposed and polyoxazolines was selected as promising alternatives to PEG derivatives.

Aim of the thesis: herein in this thesis, we synthesised low molecular weight polyoxazolines with controlled end groups and pave the way for its role as alternative of PEG. Moreover, polyoxazoline brushes were grown on gold wafers to confirm the non fouling ability among non-specific proteins which may in turn be applied to biomedical surface materials. In particular, we applied these promising nonfouling polyoxazolines in fabricating hydrogels, which can be further used as cell matrix.

Chapter 2

Synthesis of well-defined poly(2-ethyl-2-oxazoline)s for biomedical applications

2.1 Synthesis of polyoxazolines and its biomedical applications

2-oxazolines are a type of heterocyclic compounds that is known since the 19th century. The first synthesis and dedicated chemical structure were reported in 1889[25]. However since 1966, the class of poly(2-oxazoline)s started to attract a lot of attention owing to its use to generate materials with well controlled and defined properties[26]. Recently researchers have shown a great interest in these well-defined materials for their potential application to the field of biomaterials. This has been fostered partly because of their efficient synthesis using microwave-assisted reactors[27].

One of the advantages of the cationic ring-opening polymerization of 2-oxazoline monomers is the possibility to end-functionalize the living oligo(2-oxazolinium) species with a suitable nucleophile. According to the first-order kinetics of the monomer consumption, the polymers have got narrow molar mass distributions, which pave the way for the synthesis of block copoly(2-oxazoline)s as well as other copolymers containing blocks of poly(2-oxazoline)s. In addition, by using the dedicated termination group, synthesis of telechelic and semitelechelic poly(2-oxazoline)s can be carried out. Notably, telechelic polymer has a reactive functional group on both ends while the semitelechelic polymer has at least one reactive group on one end. The initiation of the polymerization is highly regioselective and only occurs at the nitrogen atom of a 2-oxazoline monomer, not at the oxygen atom.[25] These features ensure an excellent control of the polymer chemical structure and therefore properties.

POx-based materials were found to be obtained with a lower critical solution temperature in water which opened up a new research area on thermoresponsive materials, this phenomenon is sensitive to the nature of the alkyl group in the pendant chain.[28] Moreover, the easy accesses to hydrophilic, hydrophobic as well as fluorophilic polymers by simply change the side chain of the monomer accelerates investigation into the synthesis and self-assembly of a range of amphiphilic copolymer structure. In addition water-soluble POx derivatives such as poly(2-methyl) oxazoline (PMeOx), poly(2-ethyl-2-oxazoline) (PEtOx), poly(2-propyl-2-oxazoline) have shown similar protein resistance and hydrophilicity properties to poly(ethylene glycol) (PEG)[7, 29]. Hence these polymers can be used for drug delivery applications. It has been shown that PEG has some drawbacks (such as immunogenicity) not only due to the polymer itself but also unstable side products[30]. PEG is easily to oxide and can form explosive polyoxides when stored, making it a little bit hazardous[3, 7, 30]. Hence unexpected pharmacokinetic behaviour has been reported for the PEG carriers[31]. These problems have led to the development of polyoxazoline derivatives as a promising alternative to PEG.

This section will summarize progress in the synthesis and characterisation of poly(2-oxazoline)s and in particularly will focus on the poly(2-ethyl-2-oxazoline), precisely controlled molecular structure and bio-functionality.

2.1.1 Polyoxazolines synthesis

Living cationic polymerization of oxazoline monomers provide the possibility to synthesise a wide range of polymers with defined composition and especially narrow molar mass distribution and also more complex architecture such as star-shaped and comb shaped architecture[32, 33]. Monomers are relatively accessible and can be

synthesised easily, the cationic ring opening polymerization (CROP) plays an important role in this field, and different substituent of 2-oxazolines were prepared. The CROP of 2-oxazolines was reported since 1966 by four different research groups[34-37]. Scheme 1 represents the mechanism of the CROP of 2-oxazolines. Different electrophile initiators namely: methyl tosylate, methyl triflate, methyl iodide, or benzyl bromide can be used, and after this step, a nucleophilic attack of the nitrogen of another monomer prone to occur with the weaked CO-bond which was in the formed oxazolinium species[38]. Subsequently, the propagation species is growing by the addition of further monomer.

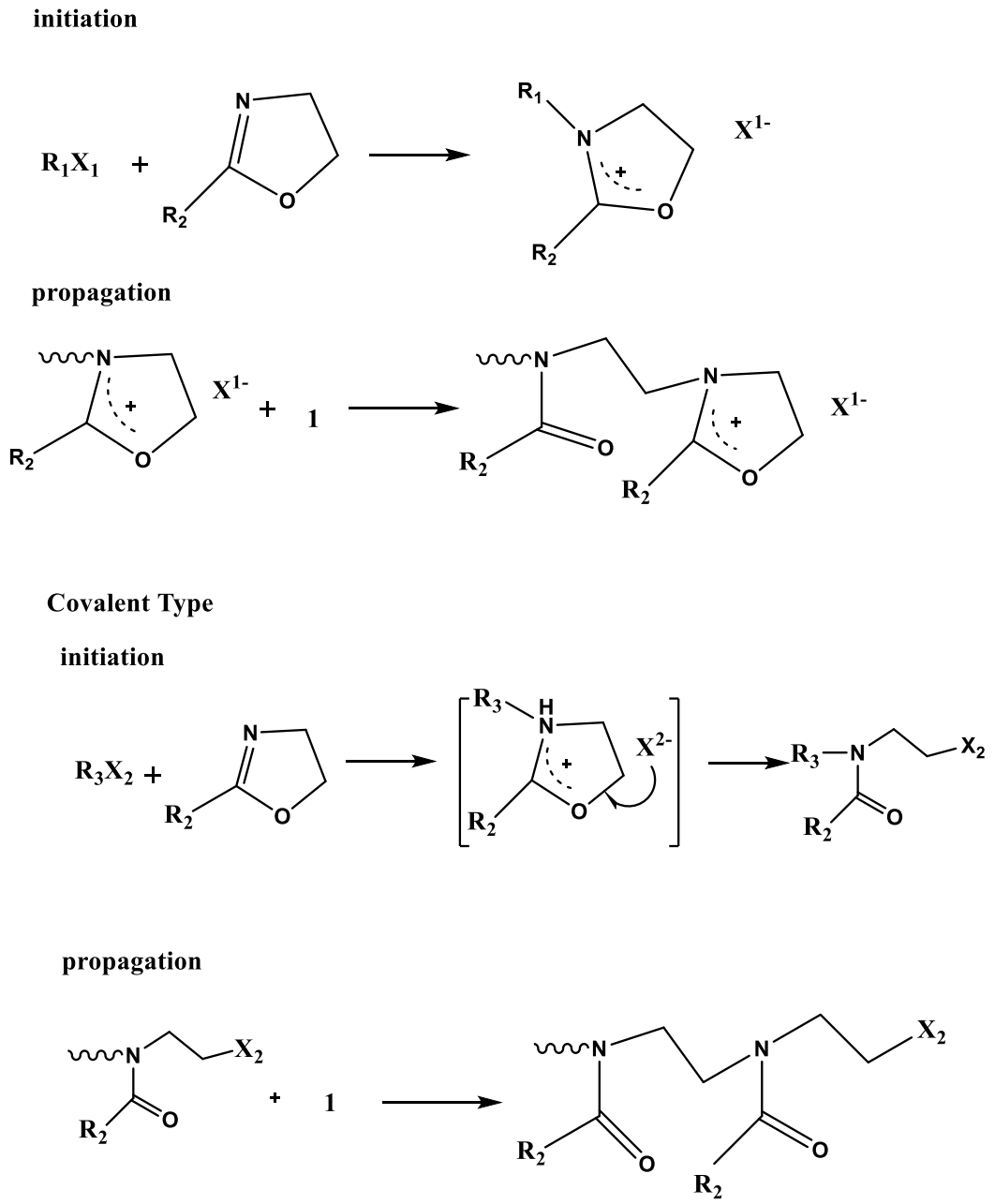

Scheme 2.1 Schematic representation of the mechanism of the living cationic ring opening polymerization of 2-substituted-2-oxazolines

2.1.1.1 Initiators of polyoxazoline

2.1.1.1 a Lewis acids and alkyl halides

To date, Lewis acid such as boron trifluoride (BF_3-OEt_2) zirconium/tris (pentafluorophenyl) borate, trihalogenobismuthine have been widely used as the initiator for the polymerization of 2-oxazolines. Kricheldorf and co-workers using Bi(3)

salts as initiators for the polymerization of EtOx and MeOx, and they also found that normal or neutral Bi-salts such as the oxide, the acetate were inactive when the polymerization go through the cationic mechanism[39]. Bismuth triflate has the highest Lewis acidity against $BiCl_3$, $BiBr_3$, and BiJ_3, and it was proved to be the most reactive initiator in the mentioned Lewis acid. In addition, $BiCl_3$ was more reactive than the higher halogenides[39]. Alkyl halide such as alkyl chloride, bromide and iodide can be used as initiators as well[40, 41]. Lewis acids, strong protonic acids and their esters, and alkyl halides are typical initiators that are listed in table 2.1.

Table 2.1 Types of initiators for the polymerization of cyclic imino ethers ([42])

Type of initiator	Example	Type of initiator	Example
sulfonate esters	p-$MeC_6H_4SO_3Me$ p-$O_2NC_6H4SO_3Me$ CF_3SO_3Me FSO_3Me	Lewis acids	BF_3 $AlCl_3$ $TiCl_4$ PF_5
sulfate esters	$(MeO)_2SO_2$		SbF_5
sulfate anhydrides	$(MeSO)_2O$	salts of Lewis acids alkyl haloformates	$Et_3O^+BF_4^-$ MeOCOCl
alkyl halides	$PhCH_2Cl$ $PhCH_2Br$ MeI	oxazolinium salts electron acceptors	$(NC)_2C=C(CN)_2$
protonic acids	$HClO_4$ CF_3SO_3H H_2SO_4 HBr		7,7,8,8-tetracyanoquinodimethane

2.1.1.1 b Acetyl halides

Schubert and co-workers used acetyl halide as the initiators for the CROP of 2-ethyl-2-oxazolines[43]. Three different initiators (acetyl chloride, acetyl bromide and acetyl iodine) were used at different polymerization temperature. In terms of polymerization rates, the initiators that contain acetyl during the initiation were ranked: acetyl iodine > acetyl bromide > acetyl chloride, which in agreement with the decreasing electrophilicity of the halide. In addition, at higher temperature, the polymerization rates increased and the well-defined polymers with narrow molecular weight distribution as well as low polydistribution index were discovered.

2.1.1.1 c Tosylates

Schubert and co-workers synthesis a library of homopolymers of the composition MeOx, PEtOx, PPhOx, and PNonOx and by using four different initiators for the corresponding of the CROP reactions, which are benzyl bromide, methyl triflate, methyl tosylate, and methyl iodide. There is a loss of control over the polymerization initiated with methyl triflate (MeOTf) or methyl tosylate (MeOTs), it may be as a result of the higher concentration of reactive cationic centres. The order in polymerization rate for these four different initiators came out as the decreasing electrophilicity: MeOTf > MeOTs >MeI >BB[44]. In addition, MeOTf is the best initiator to control the chain length[42].

2.1.1.2 Terminating agents of polyoxazolines

The nature of the living cationic polymerization and the requirement of persisting oxazolinium propagating species in the terminal position of the polymer chains need a nucleophilic reagent to stop the propagation. Such nucleophilic termination reagent as water[44], alcohols, amines have been widely used.

2.1.1.2 a Termination of poly(2-oxazoline) polymerisation with water

Schubert and co-workers reported kinetic investigations for the polymerization of four different monomers with four different initiators and two different reaction temperatures. All of them are terminated by water[44]. Schubert et al. investigated three methods for the functionalisation of 2-ethyl-2-oxazoline (EtOx) oligomers with a methacrylate or methacrylamide unit, use water as the termination agent for two methods and found hydrogen end-group was the easiest to be formed[45].

2.1.1.2 b Termination of poly(2-oxazoline) polymerisation with other nucleophiles

Self-assembly micelles of telechelic hydrophobically modified poly(2-oxazoline)s was carried out by Winnik and co-workers, by using n-octadecyl-4-chlorobenzenesulfonate as initiator and methanolic KOH or n-octadecyl isocyanate as terminating agent[46]. In order to control the LCST of PPhOx, Jorden et. al looked into initiators and terminating agent by various reactants as well as the sequential of the block copolymers with MeOx[47]. Telechelic group such as methyl, n-nonyl, pipyridine, piperazine and oligo(ethylene glycol) as well as oligo MeOx were used. Lipophilic reactants decreased the LCST while hydrophilic tailor increased the LCST.

2.1.1.3 Different effect of the alkyl substituent for poly(2-oxazoline)s

By simply varying the side chain of the 2-oxazoline monomer it is possible to tune the properties of poly(2-oxazoline)s. Schubert et. al[48] investigated four representative 2-oxazolines, namely 2-methyl-, 2-ethyl-, 2-Nonyl-, and 2-Phenyl-2-oxazolines in single living CROP polymerization mode. Different samples under different reaction time for each different temperature were performed and it was found that with increasing temperature, the conversion increased. Furthermore, at the same reaction temperature, the rate of polymerisation of 2-methyl-oxazoline is the fastest, because of the higher nucleophilicity. The activation energies were determined for these monomers according

to Arrhenius plots and showed that 2-methyl-, 2-ethyl-, and 2-Nonyl-2-oxazoline had similar activation energies, however, 2-phenyl-2-oxazoline is obviously higher owing to the ＋M stabilization of the propagating species.

2.1.1.4 Effect of microwave heating

As a consequence of easy access to high temperature and high pressure synthesis in a single mode of microwave reactor, and some poly(2-oxazoline)s have very poor solubility in organic solvents, the halogen-free and low boiling solvent (good absorption of the microwave irradiation) could be used, such as acetonitrile. It was reported that under microwave reactor, the reaction time for the polymerization of 2-ethyl-2-oxazoline in acetonitrile can be decreased to 6 h under standard conditions. Moreover, side reactions were reduced to a minimum at 140ºC, which was the most suitable temperature for the polymerization.

2.1.2 Applications of polyoxazolines

In the last few decades, the interaction between polymer science and medicine has significantly expanded and this has even open a new research area such as polymeric biomaterials, tissue engineering, implant techonology as well as polymer therapeutics[49].

Poly(2-oxazoline)s are promising materials for application in biomedical as it allow to control properties such as blood clearance, biodistribution, and protein adsorption. POx have very similar behaviour to PEG owing to its peptdomimetic structure[50]. In addition, POx exhibit higher chemical stability. These confer to these polymers properties such as low toxicity and high stability in biological conditions. In addition, PMeOx and PEtOx display low viscosity and thermo-responsive behaviours, which increase their range of applications as biomaterials[51]. Compared to polypeptides,

polyoxazolines are tertiary polyamides and usually lack chiral centers in the main chain, therefore unable to form distinct secondary structures via hydrogen bonding. However, polyoxazolines have the chirality and biofunctionality via substitute R in the side chains or at the end of the side chains[42]. POx-based materials have expected pharmacokinetic behaviour as well as the thermosensitivity make them able to be drug carriers. It was also demonstrated that functionalisation of the lateral chain and end groups can confer bioactivity such as antimicrobial activity[52] and hemocompatibility[53].

In the case of using poly (2-oxazoline)s as therapeutics, we classify them as polymer protein conjugates, polyplexes, polymer drug conjugates and polymeric micelles, aggregates and polymer nanoparticles. (as we can see from Figure 2.1)

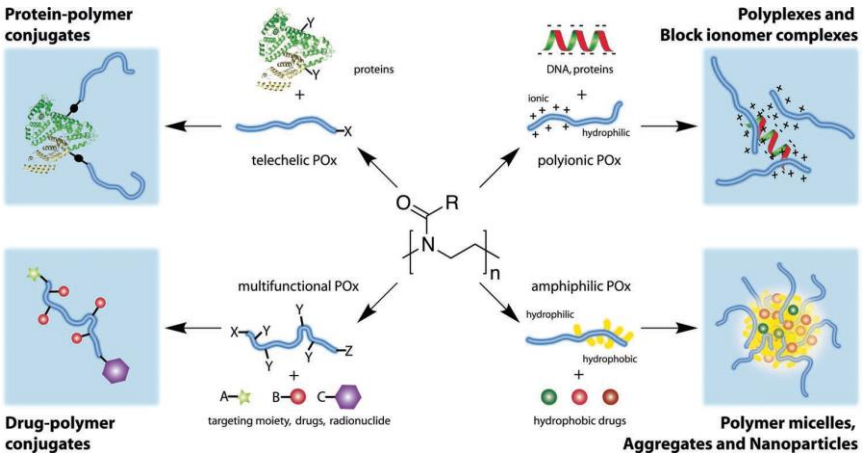

Figure 2.1 Polymer therapeutics based on poly(2-oxazoline)s ([54])

2.1.2.1 POx-protein conjugates

Protein delivery has been proposed as a suitable strategy for therapeutic angiogenesis. The recombination of protein therapeutics, human insulin were introduced 30 years ago, while further studies of protein therapeutic still play an important role in medicine[55]. Poly(2-oxazoline)s are currently as an important polymer platform for the design of

biomaterials. Some of the limitation of the first generations of drug delivery vehicles include toxicity, suboptimal pharmacokinetics, physicochemical instability, immunogenicity, short elimination half-life[51]. Conjugation of the protein with PEG, termed PEGylation has been used as a successful method to overcome these problems and have given rise to successful drugs. For example, Adagen, which has become a blockbuster drug after a few PEGylation protein medicine[56]. However, PEGylation has been associated with immunogenicity concerns. It was reported that 5 kDa PEtOx and 10 kDa PEG conjugates yield significantly lower immunological response especially for the larger conjugates, and PEtOx perform better than PEG[53]. Veronese and co-workers conjugated 5 kDa PEtOx which was functionalised by N-hydroxysuccinimide (NHS) to trypsine to investigate the steric influence of the polymer chain to the enzyme activity towards different substrates[57]. It seems that the POx-based conjugations work similarly to PEG-based conjugations, both partially losing activity towards large substrates. In addition, both in vivo activity and pharmacodynamics of POxylated conjugation were studied by using a PEtOx 10 kDa insulin conjugate in rats. Although the conjugate lowered the blood glucose as free insulin did, insulin activity reversed after 2 h while PEtOx insulin kept the lowering effect for 8 h, which means that PEtOx keep insulin from rapid proteolysis and clearance[51].

2.1.2.2 Polymer-drug and polymer-peptide conjugates

For a pioneering study, Riffle and co-workers used living POx chains to directly attach a short dodecapeptide[58], though the yield was not high, it still a promising area to discover. The avidity of the peptide to a specific antibody has been performed. Well-defined poly(2-oxazoline)s play an important role as their character and aggregates are fundamental issues such as the solubility, variation of size, architecture as well as

chemical functionality to the potential problems and pitfall[59]. Polymer – drug conjugations was regarded as a good way to improve drug solubility, specific targeting via the inclusion of homing moieties in the polymer chain, may contribute to the regenerative medicine as well as to improve permeability and retention (EPR) effect of cancer treatment[60].

In the range of 1-10 kDa, to some extent PMeOx and PEtOx did diminish the binding of dodecapeptide to the antibody. Increased the inhibitory concentration (IC90) in half-maximal were occurred by a factor of 25 at maximum[61]. Luxenhofer et. al conjugated diverse POx with a variety of small peptides, such as cyclic RGD binding integrin $\alpha_v\beta_3$. Using chemoselective reactions to get diverse side chains of POx for conjugations.

Finally, Serina therapeutic Inc. developed folate-terminated POx conjugated anticancer drugs. Furthermore, a lot of POx-based conjugates for the treatment of dopamine-responsive disorders as well as restless leg syndrome have been exploited (see table 2.2). In part, POx-rot-igotine conjugates allowed longer lasting therapeutically relevant to plasma levels of rotigotine in normal rats and macaque monkeys, in addition enabling Parkinson's disease patients to have injection once a week for treatment[62].

Table 2.2 POxylated targeting or therapeutic small molecules ([49])

Polymer	Peptide/drug	Linking chemistry
PMeOx, PEtOx	HCPC	Direct termination with protein-NH_2
(1-10 kDa)		
PMeOx, PEtOx	RGD	POx-alkyne + Peptide-azide, POx-aldehyde + Peptide-aminooxy
PEtOx	CREKA	Native ligation
PMeOx	MTII	POx-aldehyde + Peptide-aminooxy
PEtOx	Ara-C	P-COOH/DCC/NHS + Protein-NH_2
Unknown, presumably PEtOx	Irinotecan/folate (SER203)	Presumably POx-alkyne + drug azide

Unknown, presumably PEtOx	**Irinotecan (SER201)**	**Presumably POx-alkyne + drug azide**
Unknown, presumably PEtOx	**Unkown/folate (SER207)**	**Presumably POx-alkyne + drug azide**

2.1.2.3 Gene delivery therapy

Gene therapy has been regarded as the prominent invention in medicine, to treat genetic inherited disease. In fact, at the end of 2012, Glybera became the first approved gene therapy in the European Union, which open a new therapy area. Polyplexes are formed by a positively charged polymer with the phosphate anions present along the genetic material (see figure 2.2), protecting and enabling passage through the cell membrane[63].

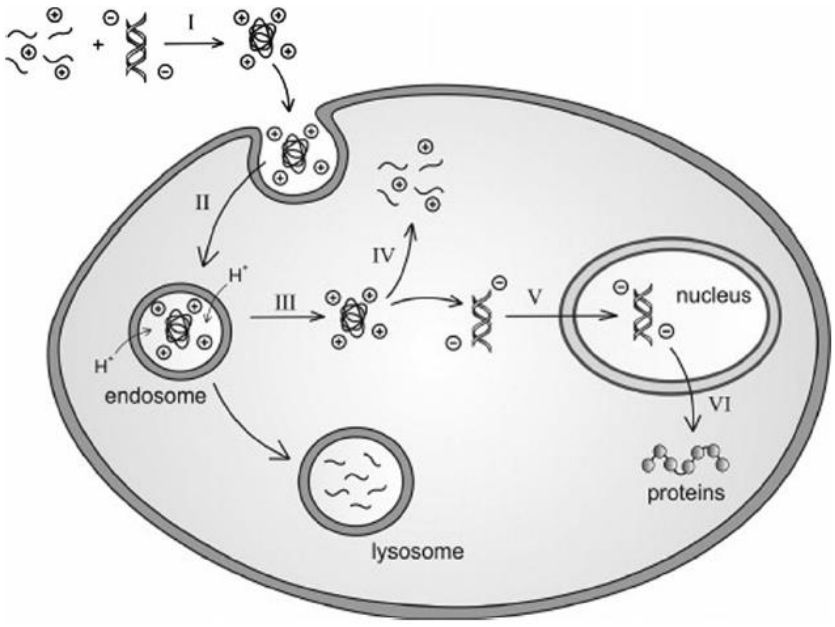

Figure 2.2 Barriers to gene delivery. Design requirements for gene delivery systems include the ability to (Ⅰ) package therapeutic gene; (Ⅱ) gain entry into cells; (Ⅲ)

escape the endo-lysosomal pathway; (Ⅳ) effect DNA/vector release; (Ⅴ) enable gene expression; and (Ⅵ) remain biocompatible[51].

High molar mass, polyethylenimines (PEIs) are widely used for nucleic acid delivery. Thomas and co-worker found that removal of the residual N-acyl moieties from commercial linear 25 kDa PEI enhanced its plasmid DNA delivery efficiency in vitro, as well as the lung specificity in mice[64]. Furthermore, the author used the polyplexes to deliver siRNA to treat influenza-infected mice reducing virus titer by 94%, which is acceptable to our expectation as effectively cure a patient from a life treatment infection.

POx hydrolysis yields well defined PEI with a variety of architectures, enabling the success of gene carrier, as well as conjugation with other polymers[65]. Hsiue et. al associated partially hydrolysed PEtOx with a PEtOx chain via a disulphide linkage, enabling high transfection efficiencies to Henrietta Lacks' 'Immortal' (HeLa) cells and significantly reducing the cytotoxicity related to pure PEI[66]. It should be noted that cytotoxicity of the polymers was especially dependent on the degree of the hydrolysis PEtOx within PEtOx-co-PEI. In general, polycations are toxic because of their strong potential to interact with cell membranes (leading to their disruption and cell death) and proteins. In the case of POx-PEI copolymers it can be concluded that with similar transfection, the lower cytotoxicity can be obtained[65].

Uptaking cellular and efficiently express gene by gene delivery vehicle strongly depend on the diameter. Lumann and co-workers discovered a new strategy of obtaining protected polyplexes to get lower cytotoxicity by grafting poly(L-lysine) on PMeOx.

Only when grafted density is around 10% or even lower, efficient transfection can be performed in COS-7 cells. This can be explained to the steric hindrance. The most interesting founding is that excellent stability against serum and DNAse digestion was observed by using PLL-g-PMeOx-DNA condensates[67].

2.1.2.4 POx-based micellar systems

One of the issues associated with some cancer treatments is the poor solubility of many effective anti-cancer drugs and the need for combination therapy to tackle tumours. In addition, the inherent resistance of tumour initiating cells and cancer stem cells require higher capacity treatments and drug delivery vehicles.

Micelles can be formed by self-assembly of amphiphilic block copolymers and have been exploited as drug carrier as well as conjugated with polymer-drug. Micellar systems are extensively applied as their excellent capability to transport poorly soluble drugs even at high loading, hence enabling the use of such drugs to the cancer treatment. In addition, micelles can be functionalised in both passive and active targeting, leading the accumulation in the tumour site of the EPR effect and also as a platform for the targeting, as can be seen in figure 2.3.

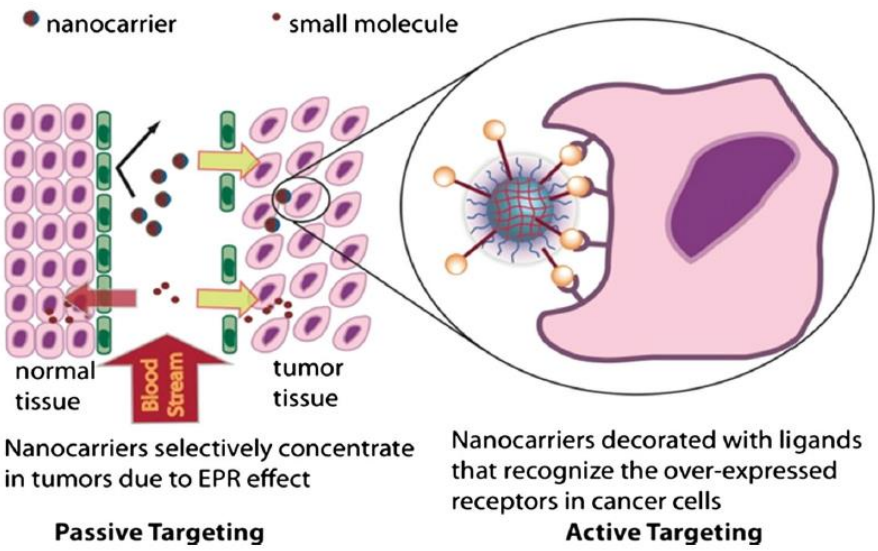

Figure 2.3 Representation displaying the concept of passive targeting through EPR effect and active targeting via inclusion of homing moieties ([68])

Using a nanocarrier system can increase blood circulation times as well as the whole efficacy of drugs, which strongly lower the side effects and the required quantities[69, 70]. Moreover, the conjugations are not only simply bond to the polymeric system, it also managing the combination therapy. As reported, the micelles properties such as size, critical micelle concentration and the ability to release drug can be tuned via a straightforward synthesis of block copolymer[71, 72].

The association of hydrophilic POx with hydrophobic polymers yields amphiphilic polymers can form polymersomes and polymer micelles as nanocarrier systems. These copolymers are suitable for drug and gene delivery. One typical example is the work Meier and colleagues have done. They observed the constitutions of the stable polymersomes in diluted aqueous solutions (PMeOx-PDMS-PMeOx ABA triple block copolymers). The solutions finely controlled the vesicle size from 50 to 300 nm. Some similar copolymers were used as the encapsulation of various drugs and proteins,

namely, trypsin[73], pravastatin[74], or trypanosome vivax nucleoside hydrolase (TvNH)[75].

2.1.2.5 Polyoxazolines as Non-fouling surface coatings

The prevention of protein adhesion to surfaces, termed the anti-fouling effect, is important for the development of anti-bacterial medical implants, biosensors with increased signal-to-noise ratio, as well as low-fouling of membranes. It is also used to control cell adhesion and cell micro-patterning.

Antifouling surface coating still remain a hot topic for medical device technology, food industry, biosensors, microarrays, drug delivery carriers, water supply (membranes), and mobility. Fouling, the deterioration of device/surface function results of the deposition of biological matter (especially microorganisms) accompanied with organic and inorganic material deposition. One advantage of the antifouling surface is it can facilitate the release of deposits, and coatings can also avoid the deposition of mostly biological media in a passive way at first[76].

The effective coatings prevent the adsorption of proteins, bacteria, and mammalian cells[77]. Their properties are controlled with different parameters, namely: hydrophilic (polar functional groups), hydrogen-bond-accepting groups, while there is no hydrogen-bond-donating groups, no net charge.

The control of these parameters enabled the design of antithrombogenic surfaces, as was developed by Merrill and co-workers. The best polymers were those possessing a combination of the properties described above. Figure 2.4 give the examples for some structures of materials displaying such anti-fouling properties.

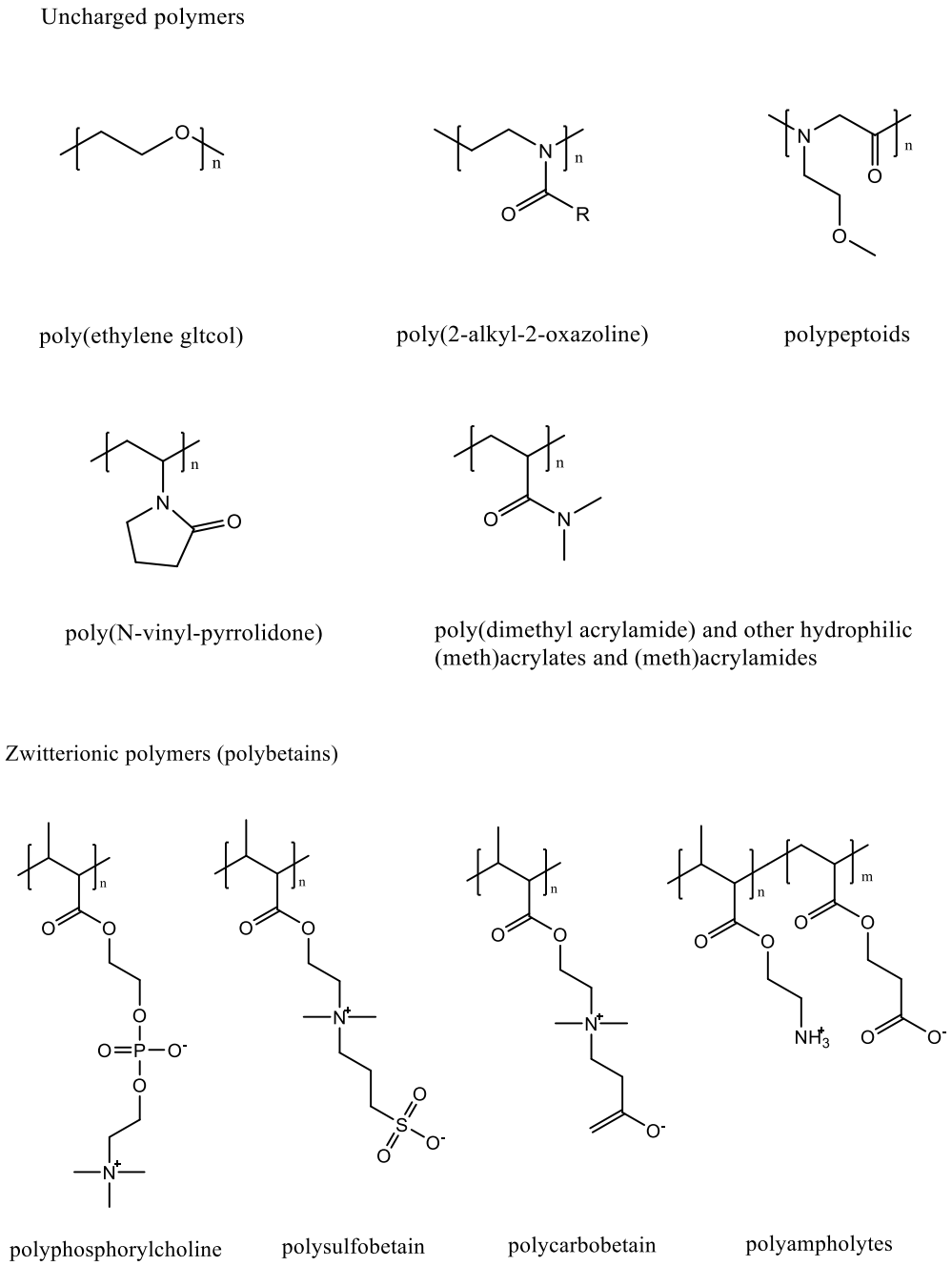

Figure 2.4 Structures of typical polymers that have been employed to prepare highly biopassive/non-fouling surface coatings (inspired by[50])

In order to ensure the adhesion of such antifouling polymers to surfaces, electrostatic interactions have been used. For example, polycationic graft copolymers were designed for surface self-assembly on negatively charged substrates. In particular, PEG and

PMeOxMA were used in such works and grafted side chain via active ester chemistry onto poly(L-Lysine) (PLL) backbones[67]. Konradi and co-workers tuned the side chain by using per lysine monomer unit and well controlled it via graft traction. The PLL-g-PEG and PLL-g-PMeOxMA copolymers spontaneously self-assemble from buffered aqueous solutions on negatively charged substrates such as on transition metal oxides, glass, or tissue culture polystyrene due to the properties of PLL backbone. Typically, sputter-coated niobium oxide was used as a substrate material owing to its good chemical stability, high surface charge density and low electric point of around 4.3[50]. Tiller and co-workers reported that POx terminating with quaternary ammonium compounds (PMeOxMA-QACs) with 12 or more carbon atoms is antibacterial. They hypothesis that non-fouling polymers would be perfect to penetrate through the glycocalix of the bacterial cell wall[78].

2.1.2.6 Polymer brush

Nowadays, interfaces play an important role in a wide range of areas, such as biosensing[79], electronic materials to store energy[80], cell culture and regeneration of tissue engineering, and antibacterial coatings. The polymer chain that for the polymer brush are attached one end to the underlying substrate, usually a solid, this allows a good control of grafting density. The thickness of the coating depends on the length of the polymer chain and the grafting density. An example of electrode architecture making use of such a polymer coating is shown in figure 2.5.

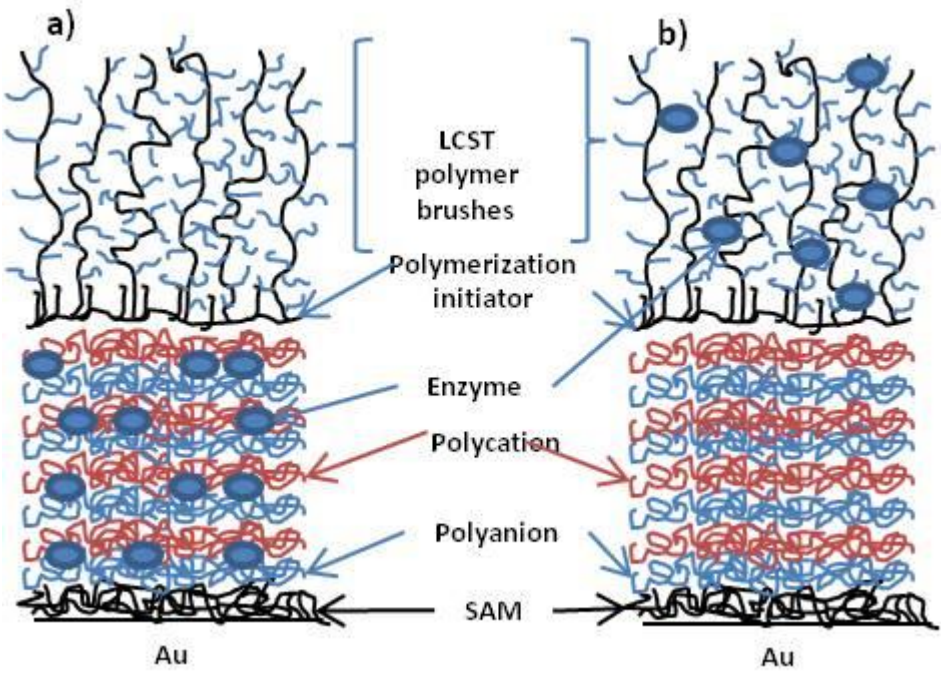

Figure 2.5 electrode architecture with enzyme immobilized in the LBL assembly or in the LCST polymer matrix([81])

Polymer brush can be prepared via different radical chemistry polymerisation techniques, such as atom transfer radical polymerisation (ATRP)[82], reversible addition-fragmentation chain-transfer (RAFT) polymerisation, nitroxide mediated polymerisation (NMP)[83] and iniferter polymerisation[84].

Some coatings did not show significant levels of protein adsorption, which makes them suitable as applied in protein resistant coatings. It was reported that POEGMA even show protein resistance from undiluted sera, the first case for such behaviour was reported. Non-fouling (below 1ng/cm^2) from lysozyme, bovine serum albumin (BSA), fibronectin (Fn) and foetal bovine serum (FBS, various applications for cell culture)[85].

Since polyethers are subject to oxidative degradation, the non-degradable peptide-like POx polymer might be the better choice for the long-term resistance to protein adsorption from complex biology mixture such as sera and plasma. The side chain of POx bottle-brush brushes (BBBs) is hydrophilic and polar, such as for poly (2-methyl-2-oxazoline) and poly(2-ethyl-2-oxazoline), and hence should provide some level of protein resistance. It has been showed that the protein has very low ability to be absorbed and cell is not easy to adhesion as well. In addition, the side chain length largely effect the adsorption and adhesion than terminal groups of the side chain[86].

2.1.2.7 LCST

Living and controlled polymerization techniques obtain various well-defined end groups and even more advanced polymers. The solubility of polymers can be tuned by temperature owing to their thermo-responsive properties. Such features significantly attracted researchers attention as their broad application in various fields, namely protein adsorption and tissue engineering[87] as well as drug delivery and regenerative medicine[88].

A lot of polymers show different solubility with different temperature in aqueous solution. It was reported that except polymers which have similar structure of polyacrylamide, there still some other polymers exhibit LCST behaviour in water such as methyl cellulose, polyethers, poly(2-oxazoline)s and so on[89]. The phase separation always happened with the changes of polymers, such effect can be described as coil to globule transition of the responsive polymer (figure 2.6).

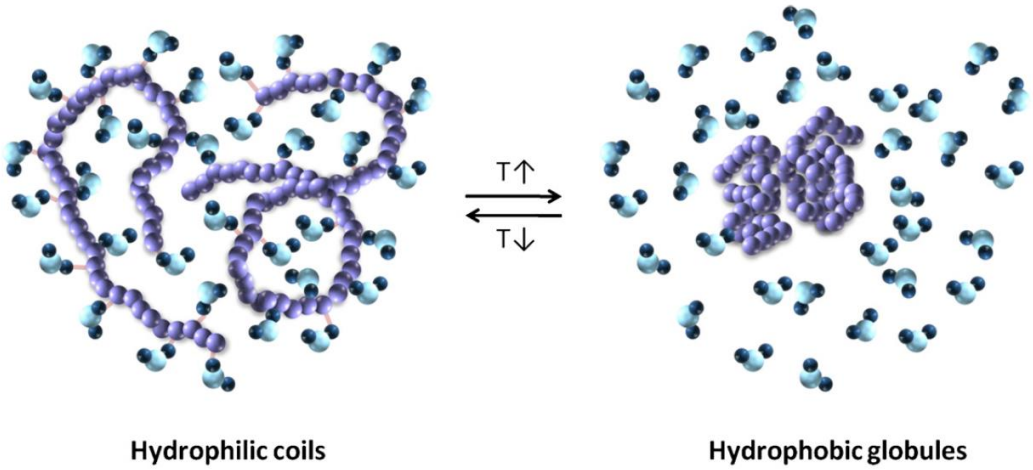

Figure 2.6 Coil to globule transition of a thermo-responsive polymer in aqueous solution ([90]).

It was reported that a variety of amphiphilic di- and tri-block copolymers perform a fast endocytosis especially the more hydrophilic polymers without affecting the activity of the cells[91]. David et. al as well as Rueda et. al were the first to report on graft copolymer which show LCST behaviour and based on PNiPAM backbone and hydrophilic PEtOx and PMeOx as side chains using macromonomer[92] or the graft-from method[93].

2.2 Non-fouling surface

Biofouling poses significant challenges across many sectors, for example, it affects the functioning of a wide range of crucial medical applications such as biosensors and biomedical implants and devices[94-96], it impacts the efficiency of food packing[97, 98] and the operation of industrial and marine equipment[68, 99]. As a consequence the development of antifouling surfaces and in particular those resistant to the non-specific adsorption of protein in materials for patterned cell culture[100, 101] have attracted considerable attention in recent years.

Most strategies for preventing biofoulants caused by proteins, bacteria, and marine organisms mainly follow two mechanisms: resistance to adhesion of biocontaminants or degradation of biocontaminants[76].

Kane and colleagues have summarised the most popular strategies that have been used recently to fabricate antifouling surfaces (figure 2.7) These include immobilizing poly(ethylene glycol) on surfaces, photoactivated self-cleaning coatings, structured surfaces, and the use of biocidal agents such as silver, antibiotics, nanoparticles, enzymes etc[76].

One of the most widely used strategies is the immobilization of PEG on surfaces, through chemical adsorption, physical adsorption, direct covalent attachment, and copolymerization[102].

Oligo(ethylene glycol) (OEG)-terminated self-assembled monolayers have been shown

To have a reversible ability of adhesive protein within limited time while irreversible BSA adsorption surfaces were found from short-chain OEG-terminated surfaces. The irreversible BSA adsorption may be due to the hydrated ethylene glycol surface

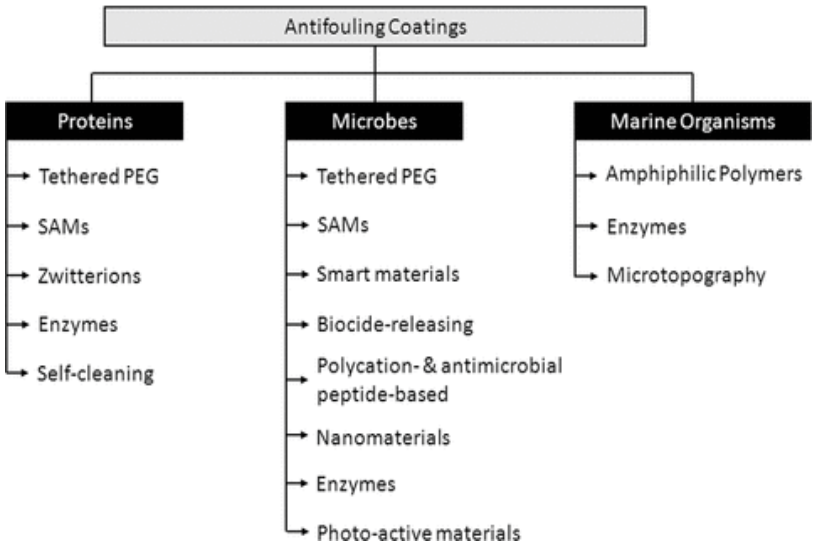

Figure 2.7 Schematic representation of the various approaches to fabricate antifouling surfaces.

preventing the protein from unfolding through irreversible bonding. By contrast, short-chain OEG-terminated surfaces interact with the protein in the presence of dynamic effects dominated by steric repulsion[103].

Polymer brushes consist of macromolecules tethered at one end to a substrate. Their wide range of functionality and ease of synthesis account for this technique being widely used recently. Generally, there are three methods of tethering brushes, namely: ‘grafting to’, ‘grafting from’ and ‘grafting through’. Figure 2.8 illustrates three methods i.e. grafting to (synthesis side chains and backbone with subsequent coupling), grafting from (polymerization of side chains starting from a macroinitiator backbone) and grafting through (polymerization of macromonomer).

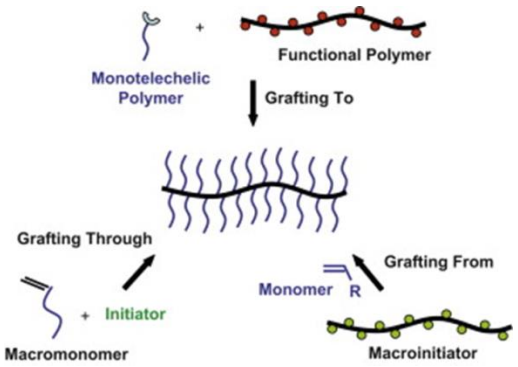

Figure 2.8 Three main strategies for preparing molecular brushes: grafting to, grafting through and grafting from.

'Grafting onto' strategy involves joining a well-defined polymer with a reactive end group on the surface attached polymer chain by reaction with a reactive end group. (Common reactive functional groups include thiols[104, 105], silane[106], amino[107, 108] and carboxylic group[109]). There are, however, some drawbacks with grafting onto brushes as the steric repulsion between the grafted chains and the incoming macromolecular units from solution inhibit new polymer chains attaching to grafting sites on the surface[110]. Moreover, film thickness is limited by the molecular weights of the polymer in solution (100 nm thickness range is inaccessible)[111].

"Grafting from" approaches take advantage of polymer chains growing on the initiated surface of the substrate. This "surface-initiated polymerization" can be explained as polymerization occurs on the solid surfaces. "Grafting from" has been widely used due to the versatility, reliability, and controllability of the formation of dense polymer brushes and can be accomplished with a variety of controlled/living radical polymerization (CRP) methods. These include the following: ring opening metathesis polymerization (ROMP)[112], nitroxide-mediated polymerization (NMP)[113], atom transfer radical polymerization (ATRP)[114], degenerative transfer (DT), where alkyl

halides as dormant chains; single-electron-transfer living radical polymerization (SET-LRP)[115], or reversible addition fragmentation chain transfer (RAFT)[116] polymerization.

“Grafting through” approaches allow a low molecular weight monomer to be radically polymerized with a (meth) acrylate functionalised macromonomer. A combination of polymerization can be employed here as macromonomers can be prepared via any controlled polymerization process. For example, Jürgen Rühe and colleagues have immobilized silica gel surface with methacryl moieties and further attached polymers previously prepared in solutions. However, they note that the higher molecular weight macroradicals limit the free polymers attached on the surface[117].

Atom transfer radical polymerization (ATRP), has proved to be a robust strategy for the synthesis of well-defined functional grafted polymers. This surface-initiated controlled radical polymerization can be affected by a range of factors such as the kind of monomer, initiator, catalyst and solvents. It allows the creation of a variety of polymers with site-specific tailored functionalities targeting specific properties for high value applications. For example, polymers created using ATRP have been used for coatings and adhesives[50, 118]. Moreover, polymer brushes have been widely used for medical and environmental applications[76].

ATRP, is an unconventional way of uniformly and precisely controlling the chemical composition and architecture of polymers as well as the uniform growth of each polymer chain. In addition, it suits a broad range of monomers. Structurally complex polymers can be prepared with a special catalyst that adds one or a few subunits (monomers) at a time to growing polymer chain via ATRP. This living, controlled process can be shut down and re-started at will depending on the temperature and other

conditions of the reaction. ATRP has been widely used recently in industry, and many companies incorporate the latest ATRP methodologies into the development of new products for their specific markets.

Matyjaszewski's group has focused on the development and use of copper based catalysts for Atom Transfer Radical Polymerizations conducted with a halogen as the transferable atom[113, 119]. A general mechanism of ATRP is shown in scheme 2.2:

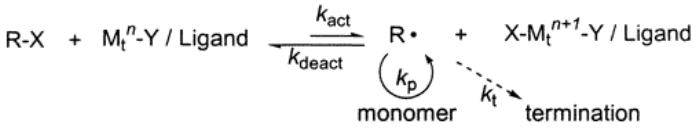

Scheme 2.2 Transition-Metal-Catalyzed ATRP[120]

The radicals, which can also be called active species, are generated through a reversible redox process catalysed by a transition metal complex (Mt^n−Y/Ligand, where Y might be another ligand or a counterion) which goes through a one-electron oxidation with concomitant abstraction of a (pseudo)halogen atom, X, from a dormant species, R-X. This process undergoes a rate constant of activation k_{act}, and deactivation k_{deact}. Chain growth by the addition of the intermediate radicals to monomers is achieved in a way similar to conventional radical polymerization, with the rate constant of propagation k_p. Also termination reactions (k_t) happen through radical coupling and disproportionation. In general, only a small percentage of polymer chains go through termination in a well-controlled ATRP[120]. The final molecular weight can be affected by the side reactions. During the termination stage, oxidized metal complexes, X−M_t^{n+1}, play the role of reducing the stationary concentration of growing radicals which in turn negates the advantage of termination[121]. A well-controlled growth of all chains as a result of fast

initiation and rapid reversible deactivation as well as a small contribution of terminated chains.

Components

ATRP is made up of a monomer, an initiator with a transferable (pseudo)halogen, and a catalyst (composed of a transition metal species with any suitable ligand). For a successful ATRP, other factors, such as solvent and temperature also affect the fate of the process.

1. Monomers

Monomers are substances such as styrene, (meth)acrylate, (meth)acrylamides, and acrylonitrile, that can stabilize the propagating radicals[122, 123]. Although under the same conditions, for example, by using the same catalyst, each monomer has its own atom transfer equilibrium constant for its active and dormant species. Regardless of any side reactions but radical termination by coupling or disproportionation, the polymerization rate relies on the magnitude of the equilibrium constant ($K_{eq} = k_{act}/k_{deact}$). If the equilibrium constant is too small the process will not even occur while too large an equilibrium constant can result in a large amount of termination because of high concentration of radicals. This phenomenon also occurs if the number of deactivating higher oxidation state metal complexes is too high, which can transfer the equilibrium to a dormant species and end up with slow polymerization[124].

2. Initiators

Initiators determine the number of the growing polymer chains. The theoretical molecular weight or degree of polymerization (DP) increases; by contrast the initial

concentration of an initiator in a living polymerization decreases when the concentration of monomer and conversion keep the same (eq 1).

(1)

Alkyl halides (RX) are common initiators and the rate of polymerization is related to their concentration. Rapid and selective migration between the growing chain and the transition-metal complex from the halide group can lead to well-defined polymers with a narrow molecular weight distribution.

The rate of activation depends on the structure of the initiator, for narrow polydispersity and high initiation efficiency; the rate of activation from the initiation should be as fast as the propagation process.

In general, any alkyl halides with activating substituents on the δ-carbon, such as acryl, carbonyl, or allyl groups, are candidates for initiators.

Matyjaszewski and colleagues have compared the rate of activation with different initiators for Cu-mediated ATRP and found that the activation rate constants increase with initiator substitution. Thus, for primary, secondary, and tertiary α-bromoesters the ratios are ∼1:10:80. With the radical stabilizing α -substituent (e.g., alkyl bromides with -C(O)NEt_2, -Ph, -C(O)OMe, and -CN groups) the ratios are ∼1:4:8:600 but with both α -Ph and α -C(O)-OEt the ratios are ∼ 140 000. With the leaving atom/group (e.g., for methyl 2-halopropionates: chloro:bromo:iodo) the ratios are ∼1:20:35 but benzyl bromide is ∼10 000 more reactive than the corresponding isothiocyanate/thiocyanate.

3. Ligands

Ligands play a variety of roles when incorporated with an ATRP catalyst complex. Firstly, a ligand can solubilize the transition metal salts in the polymerization medium; secondly, it can adjust the redox potential of the metal centre to provide an appropriate activity and dynamics for the repetitive halogen exchange reaction. The electron donating ability of the ligand can greatly affect the redox potential of the transition metal complex and influence the reactivity of the metal centre in halogen abstraction and transfer, meaning that the structure of the catalyst selected for a given reaction affects the kinetics of an ATRP and hence the degree of control over the polymerization reaction.

An overview of different structural parameters on the activation rate constants can be seen in figure 2.9[125].

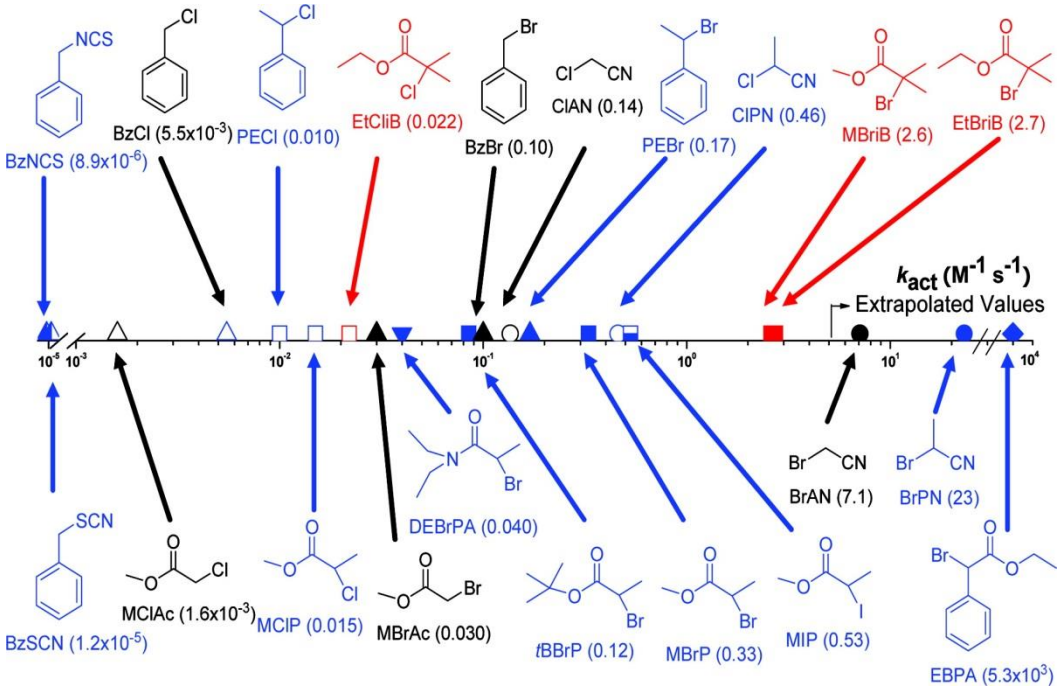

Figure 2.9 ATRP activation rate constants for various initiators with CuIX/PMDETA (X = Br or Cl) in MeCN at 35 °C: 3°, red; 2°, blue; 1°, black; isothiocyanate/thiocyanate,

left half-filled; chloride, open; bromide, filled; iodide, bottom half-filled; amide, ▼; benzyl, ▲; ester, □; nitrile, ○; phenyl ester, ◇[125].

4. Catalysts

Catalysts are one of the key parameters for balancing the process of ATRP as they determine the important role of the atom transfer equilibrium and the dynamics of exchange between the dormant and the active species. There are some requirements for an efficient transition metal catalyst. First, the metal centre must have at least two readily accessible oxidation states, only one-electron difference between each other. Secondly, the metal centre should have reasonable affinity towards a halogen. Thirdly, the spherical space around a metal should be enough to accommodate a (pseudo)-halogen. Finally, the ligand and metal should relatively attract each other strongly[120].

Copper-mediated polymerization has been widely used. For example, Jordan et al synthesised several molecular brushes of poly(2-oxazoline) (POx) with methacrylate end groups and grafting through polymerization by aqueous ATRP with $Cu^{I}Br$ at room temperature, and well-defined POx brushes with thermoresponsive behaviour were obtained[126].

5. Solvents

A solvent is required during ATRP especially when the obtained polymer is insoluble in its monomer. There should be little chain transfer in the solvent and the interaction between solvent and the catalyst system should be considered.

It is important to note that the structure of the catalyst may change in different solvents. For example, well-defined polymers with narrow polydispersity as well as controlled

molecular weight can be synthesised using ethylene carbonate as solvent with the rate of polymerization being even faster than in the bulk of monomer itself. Polydispersity was found to decrease when the level of $CuBr_2$ increased or when the amount of ethylene carbonate was reduced[127]. That the rate of polymerization increased in polar media was verified from other studies[128-130].

6. Temperature and reaction time

Increasing the temperature, results in an increase of both the radical propagation rate constant and the atom transfer equilibrium constant, which in turn leads to a higher rate of polymerization.

With longer reaction time a completed monomer conversion can be obtained, however, it may not result in a higher level of polydispersity of the final polymer and may lead to the loss of end groups[131].

2.3 Fabricating hydrogels with polyoxazolines

The aim of tissue engineering is to structurally and biochemically manipulate living tissues, which are similar to native tissues. Thus, determining a well-controlled gelation condition for cell encapsulation in vivo and related hydrogel chemistry, macroscopic properties and degradation to improve functional tissue growth all play a critical role in tissue engineering[132].

The nature of the matrix has been found to affect the shape of cells as well as their behaviour later on. Culturing cells in 2D (on a hydrogel film) or in 3D (encapsulated within a hydrogel) produces different results. In general, cells are less constrained in 2D than in a 3D hydrogel environment. Hyung-Do et al. found that cell migration in 3D is only partially due to cell-intrinsic effects, while in 2D hydrogels things are simpler. This

suggests that 3D hydrogel is more accurate and closer to in vitro conditions, especially in the context of pathophysiological environment[133].

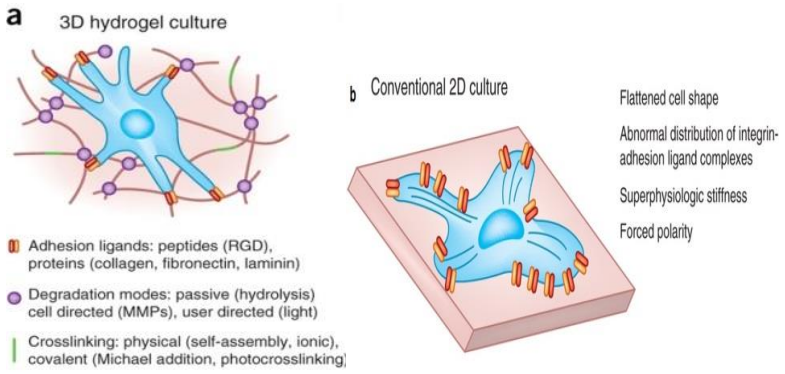

Figure 2.10 3D hydrogels can be engineered to present a more realistic microenvironment to cells; b. conventional 2D culture on super physiologically stiff plastic or glass substrate leads to cells displaying aberrant phenotypes.

The highly hydrated networks formed by polymer chains in 3D hydrogels, mimic the properties of natural tissues, for example, by performing similar elasticity. Highly cross-linked hydrogels contain hydrophilic chemical properties which can absorb large amount of water without dissolving and which resemble the native extracellular matrix (ECM) that surrounds many types of stem cells[132, 134]. This half liquid-like and half solid-like property is attracting much attention due to its showing neither pure solid nor pure liquid behaviours that cannot be found anywhere else.

The formation of 3D hydrogels allows cells to encapsulate. Ideally synthetic hydrogels should have low concentrations and reactions in buffers, which afford convenient space for structure of proteins and viability of cells.

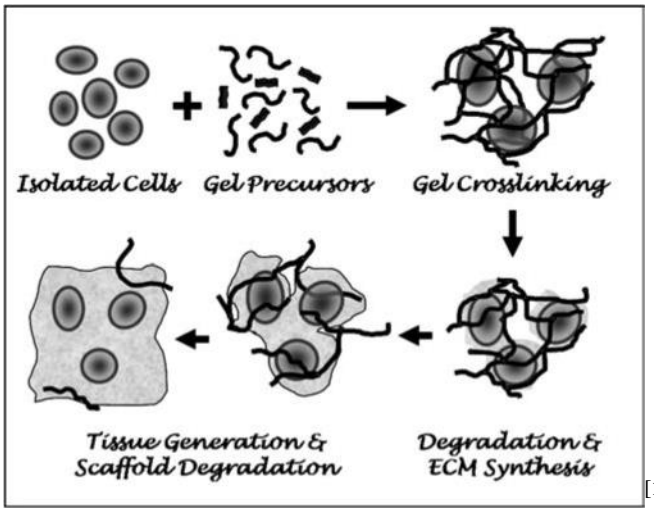

[112]

Figure 2.11 Cell encapsulation strategies involve mixing cells with precursors in a liquid solution followed by gelation and encapsulation of cells. The crosslinked structures will largely dictate diffusion of newly synthesized ECM molecules, and therefore, degradation of the scaffold must closely follow ECM synthesis and macroscopic tissue development. The gel precursors, gelation mechanisms, and degradation products must be cytocompatible.

In addition, before cell encapsulation, cells are suspended in a liquid precursor solution so this step (where gelation occurs) must be mild and cell friendly. The structure and chemistry of the hydrogel should be suitable for cells to survive and tissues to form. Moreover, degradation should follow tissue growth, and most importantly degradation products should not affect the encapsulated cells. Those critical steps are shown in figure 2.11[132].

For example, we can see from figure 2.12 that Melinda C. Cushing et al. have successfully used degradable poly(ethylene glycol) gels to promote attachment, migration, and differentiation of the encapsulated cells to bone-forming osteoblasts[134].

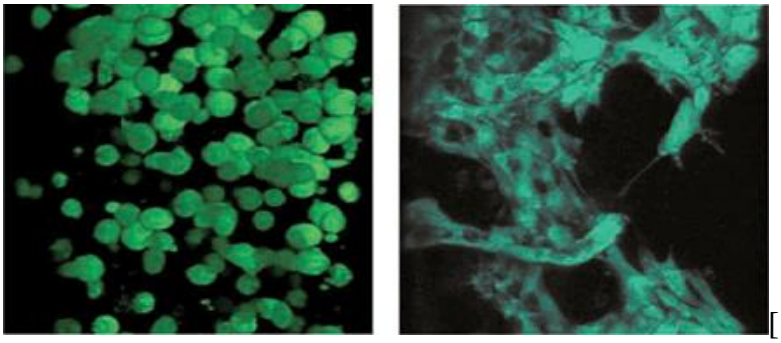 [134]

Figure 2.12 Scanning confocal microscopy of fluorescently labelled cells was used to visualize changes in cell morphology in the gel microenvironment. At the start of the experiment, the cell-laden gel contains rounded cells with few interactions (left). Over the course of 2 weeks, the gel forms a dynamic system with multiple cell-gel interactions that promote attachment, migration, and ultimately, differentiation of the encapsulated cells to bone-forming osteoblasts (right).

2.3.1 Hydrogel fabrication and characterization

2.3.1.1 Fabricating hydrogels

Hydrogels are formed via a variety of mechanisms where polymer chains are cross-linked by covalent, ionic, or physical bonds.

Generally, cell encapsulation strategies using covalently cross-linked hydrogels are start from macromolecular monomer other than monomer as lower toxicity. In general, molecular weight of 3 kDa or more compatible polymers are used during fabrication[135].

Hoogenboom et. al have synthesised water-soluble poly (2-oxazoline) copolymers containing vinyl groups on the side chain, they found that the structure of the copolymer deeply affects the cross-linking kinetics. For example, vinyl group on longer alkyl chains can be cured rapidly in a process which is almost independent of the thiol

concentration, while on shorter alkyl chains, the speed is highly dependent on the molar ratio of thiol to ene groups[136].

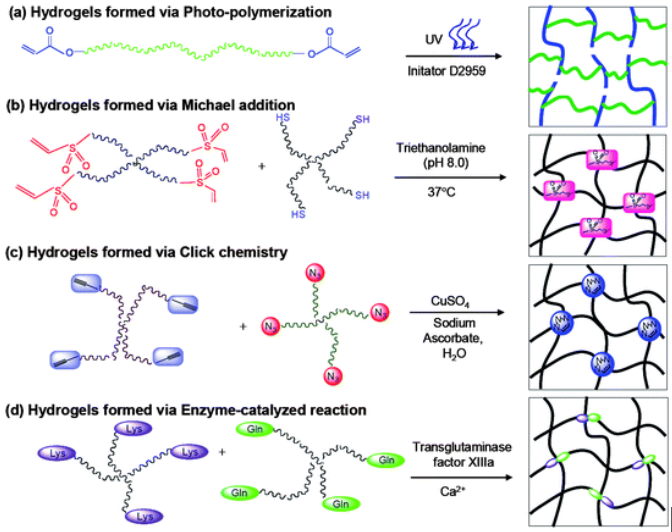

[137]

Figure 2.13 Reaction scheme for preparing PEG based hydrogels via (a) photo-polymerization; (b) Michael addition; (c) click chemistry; (d) catalysed reaction.

Chemically crosslinked gels were introduced as they are more robust than those formed from ionic and physical interactions. From figure 2.13 we can see the typical mechanisms of fabricating hydrogels based on PEG.

2.3.1.1 a Radical polymerization

The first time a polymerization technique was used to produce hydrogels dates back to the 1960s, Well-defined gels can be formed within minutes under physiological conditions[138]. Since then polymerization remains a popular strategy for forming PEG hydrogels for tissue engineering applications[139-141]. With suitable radical-generating initiators and other conditions, macromeres with at least two vinyl groups can be polymerized in a radical chain-growth process[132].

In addition to efficiently producing hydrogels, photo polymerization can be perfectly controlled during gel formation, as radical polymerization can be restricted in time and

space using focused beams of light[142]. In order to encapsulate cells, UV photo initiators have the priority because of their higher efficiency compared to visible light[143].

Radical concentration can be affected by several factors, such as the type and concentration of the initiator, the light intensity that also corresponds to the initiating signal, and polymerization kinetics. There are two methods of polymerization when fabricating hydrogels: chain polymerization and step-growth polymerization. Via radical thiol-ene chemistry, crosslinking occurs to form Homogeneous hydrogels.

Mark et. al found that hydrogels formed via step-growth polymerization compared to chain polymerization are softer, with higher tensile toughness and shear strain. This may indicate that improved mechanical properties can be obtained in homogeneous gels[144].

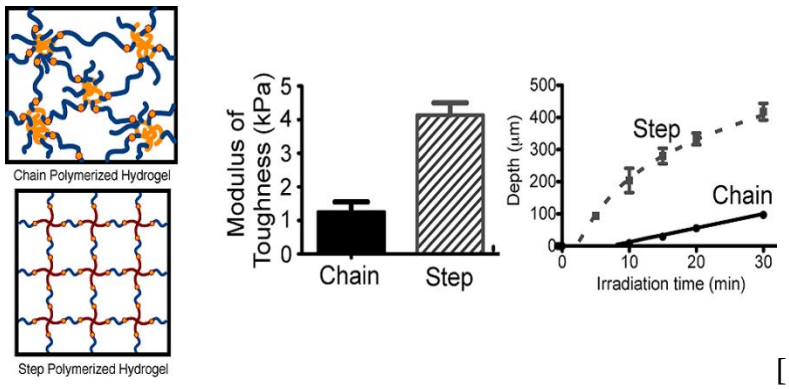

[144]

Figure 2.14 Mechanical properties of hydrogels formed via chain and step-growth polymerization.

Chain-growth polymerization always results in low macromere conversion and can be overcame by extending the polymerization time, however, it also increases the

possibility of cells being exposed to a highly radical environment which can damage the environment of forming hydrogels and which is also bad for cells.

High molecular weight polymers crosslinked at low monomer conversions in chain-growth polymerization lead to early gelation. Thus restricted movement of monomers through the gel, results in inhomogeneous regions in the structure of the fabricated hydrogels. However, step growth polymerization produces low polydispersity networks which can overcome this problem. It enables more homogeneous hydrogels to be formed compared to hydrogels formed from chain growth polymerization[145].

Photo polymerization has been widely used recently because it offers spatial and temporal control over polymerization, because of its fast curing rate (less than a second to a few minutes) and because it takes place under mild conditions with minimal heat production[146]. Moreover, one of the greatest advantages of photo polymerization is that hydrogels can be fabricated *in situ* from aqueous precursors which are less invasive for cells. Some photopolymerization systems are sufficiently mild (low light intensity, short irradiation time, physiological temperature, and low organic solvent levels) and can be carried out in the presence of cells and tissues for critical biological environment[147]. For example, Anseth KS et al. have synthesised hydrogels via photo polymerization to control induction of hMSC lineages by using simply functionalised hydrogels with small-molecule chemicals[148]. Moreover, they also incorporate other molecules in PEG hydrogels such as RGD and phosphate in the presence of osteogenesis of bone marrow stromal cells[149] and hMSCs[150].

Jennifer Elisseeff and colleagues have investigated the differentiation of chondrogenesis with PEG hydrogels in the presence of embryoid bodies (EBs). They found that the result from gene expression and protein analyses indicated EB-PEG hydrogel culture

upregulated cartilage-relevant markers compared with a monolayer environment[151, 152]. Christopher G. Williams has found that Irgacure 2959 shows minimal toxicity over a range of mammalian cell types and species even though different cell types have a variable response to the same photo initiators at the same concentration[153]. Irgacure 2959 showed toxicity at high concentrations; however, it showed cytocompatibility with concentrations below 0.05% when acrylate-PEG was cured with UV irradiation. In addition, photo polymerization can be accomplished with different light systems, which are dependent on the photo initiators. For example, Irgacure 2959 can be initiated with UV light and Irgacure 651 initiated with visible light. It has been reported that nearly all chondrocytes survived in the process with Irgacure 2959 at a concentration of 0.05% (w/w) while only a few chondrocytes survived the process with 0.01% (w/w) I651[154].

2.1.3.1 b Michael addition chemistry

In general, at least di-functional PEG macromers end functionalized with acrylate or vinyl sulfonate groups that reacted with similar macromere containing thiols end groups are needed for fabricate hydrogels via Michael addition chemistry.

HA hydrogels which are fabricated via thiolated HA in the presence of H_2O_2 solution can be used to encapsulate fibroblasts, although in vitro it can last for even three days, the gelation time is very long up to several hours[155].

Park Y and colleagues have successfully encapsulated bovine primary chondrocyte culture in synthetic PEG hydrogels. The PEG hydrogels are thiol functionalised peptides (GCRDGPQGIWGQDRCG) crosslinked with branched PEG-vinylsulfone macromers[156].

Andrew Metters et al. have synthesised four-arm and eight-arm PEG hydrogels, and hydrogels are fabricated via two different molecular weight (10 kDa and 20 kDa) of

hydroxyterminated PEGs with PEG dithiol (3.1 kDa). However, they found that only the highest functionality cross-linkers (octa-acrylate PEGs) polymerized at high precursor concentration (above ca. 50 wt.%) obtained an ideally networks with maximum cross-linking efficiencies[157].

Generally, thiolate was formed when PH was 8.0, thus the pKa of the thiol can be adjusted by altering the chemistry adjacent to the thiol to increase the reactivity when PH was neutral[158, 159].

Although the gelation rates are slower compared to radical chain polymerization, gelation occurs at high macromer concentrations. Hydrogels fabricated via chemistry crosslinking do not produce additional components during polymerization and degradation and the thiolate reactive species does not adversely affect cells[132].

2.1.3.1 c Mixed-mode polymerization

Recently, a mixed-mode polymerization composed of step-growth and chain polymerization was carried out to fabricate hydrogels. In the presence of an initiator or mediated with radicals, multifunctional macromers which contain thiol can be crosslinked with multifunctional macromers which contain acrylate and encapsulated cells *in situ*[160, 161].

Anseth and colleagues have investigated the concentration and thiol functionality on the molecular weight of the hydrogel's backbone when thiol-polyacrylate backbone was formed during photopolymerization[162].

Bowman et al. have synthesised degradable thiol-acrylate hydrogels via mixed-mode polymerization and found that by increasing the thiol concentration from 10 to 50 mol%, the gelation time decreased from 35 to 8 days. Similarly, by decreasing the thiol functionality from 4 to 1, a reverse gelation time was found from 18 to 8 days[163].

2.1.3.1 d Click chemistry

Click chemistry can form hydrogels in mild conditions, and the reactions are fast, high yielding and produce no additional components[164, 165]. For example, Hawker CJ and colleagues have compared PEG hydrogels fabricated via click chemistry and photo crosslinking, and found that a significantly mechanical property was obtained by PEG hydrogels formed with click chemistry mechanism[166]. However, gelation time is longer than with radical polymerization and the use of cytotoxic copper ions as catalyst prevents it becoming a popular method for fabricating hydrogels[167, 168]. Gelation needs to occur fast enough to prevent the settling of cells during the encapsulation process. Many factors determine the property of hydrogels and the most important requirements are adhesion to cells, stability in culture, and biophysical properties such as hydrogel elastic modulus[169].

Polyethylene glycol is a synthetic polymer which is outstanding for its hydrophilicity and relative inertness. PEG is verified as “blank gold” materials for biomedical engineering as a result of its non-fouling properties, also it is reasonably amenable to well-defined crosslinking chemistry and presentation of ligands to cells. PEG Hydrogels formed by step growth mechanisms have emerged as an attractive class of biomaterials as a result of being highly tuneable in network cross-linking and degradation: homogenous network structure, robust mechanical properties, and flexible modulate properties using responsive and orthogonal chemistries[166, 170, 171].

Anseth and colleagues found that PEG hydrogels formed via thiol-ene chemistry gained faster gel points and higher degree of networking crosslinking compared to hydrogels formed via Michael addition[107]. Thiol-ene hydrogels are susceptible to hydrolytic degradation due to their structure i.e. the presence of an ester bond between the cyclic olefin and PEG backbone. Moreover, the hydrolytic degradation of thiol-ene hydrogels

was not only dependent on ester bond hydrolysis but was also affected by the degree of network cross-liking[171].

2.1.3.2 Characterization of hydrogel properties

The design of robust hydrogels with good mechanical properties plays a vital role in many existing and potential application areas of soft materials. There are important features of hydrogels that affect the properties of hydrogels for cell culture applications; here we list the most intensively studied: mechanics, swelling, mesh size, and degradation. In addition, the structure of hydrogels plays a pivotal role in their mechanical properties. The equilibrium swelling degree and the elastic modulus of hydrogels were determined by the cross-link and charge densities of the polymer network as well as the cross-linked polymer concentration after the gel preparation[172].

2.1.3.2 a Mechanics

Cellular mechanotransduction is the ability of cells to convert mechanical signals into biochemical responses and is a very important process to study as it is closely related to mechanical properties. Mechanical properties affect the stability of hydrogels in culture[173]. Mechanical force sensing is determined by the architectural context in which the cell lives. Owing to force-induced stabilization of multiple bond formation and fast rebinding of broken bonds, cell adhesion under low shear stress will show better cell adhesion as well as rolling at higher levels of shear[174]. Typically hydrogel mechanical properties such as shear modulus (G) or elastic modulus (E), two values are related to each other as a function of the material's Poisson' ratio (ν) as shown by the equation (eq 2):

$$E = 2G (1+ \nu) \qquad \text{(eq 2)}$$

Most hydrogels are assumed to have a Poisson's ratio of around 0.45-0.5, meaning that $E \approx 3G$.

Generally, hydrogels are characterized by an elastic modulus which exhibits a significant plateau over time, while a viscous modulus is considerably smaller than the elastic modulus in the plateau region[175].

Compressive or tensile testing can measure the mechanical properties of a bulk of hydrogels by pushing or pulling a material[169], Time-dependent properties such as gelation time and shear modulus are measured with rheology, in which shear forces are applied in order to characterize the rate of hydrogel formation or the ability of a material to relax after gelation for 3D hydrogels[176]. The modulus of hydrogels highly affects the spreading, differentiation, migration and fate of stem cells during the encapsulation process[177, 178]. In order to mimic the elasticity of natural tissue, different stiffness of the substrates are required such as brain: about 0.2-1 kPa[179-181], muscle: about 10 kPa[182], osteoid: about 30-45 kPa[183].

2.1.3.2 b Swelling

Swelling which is the amount of water or buffer taken up into the hydrogel. It is a straight forward property to indicate the hydrophilicity of the polymer network as well as the relative crosslinking density. Swelling is a good indicator to measure the variation and consistency in hydrogel fabrication properties; moreover, it can also indicate whether the hydrogel mechanics are changing over time. The swelling ratio is measured by first allowing hydrogels to reach equilibrium swelling followed by blotting to remove excess solvent.

The swelling ratio (SR) was calculated using eqn:

$$SR = \frac{mw-md}{md}$$

Where SR is the swelling ratio, mw is the weight of the swollen hydrogel (g), and md is the weight of the dry hydrogel before swelling (g).

Okay has shown that at higher monomer concentrations, a more dense and effective cross-link network was formed, and a smaller swelling capacity observed[172]. Increasing the amount of counter-ions inside the gel can create additional osmotic pressure resulting in an increased swelling capacity[184].

2.1.3.2 c Inhomogeneity

Compared to ideal gels with a homogeneous distribution of cross-links, hydrogels always show an inhomogeneous cross-link density distribution, known as the spatial gel inhomogeneity. The spatial inhomogeneity has some defects as it reduces the transparency and elasticity of hydrogels. Since the gel inhomogeneity is related to the spatial concentration fluctuations, scattering methods such as light scattering, small angle X-ray scattering, and small angle neutron scattering have been employed to investigate the spatial inhomogeneity[172].

In general, the special inhomogeneity increases with the gel cross-link density due to the simultaneous increase of the extent of network defects more or less in cross-links. On the other hand, the inhomogeneity decreases with ionization degree of gels due to the effects of the mobile counter ions, electrostatic repulsion and the Donnan potential[185].

2.1.3.2 d Mesh size

The mesh size, or molecular porosity, to hydrogel is typically in the nanometre scale and can influence nutrient flux throughout the matrix. It is highly related to hydrogel swelling behaviour and mechanical properties, hydrogels show lower swelling and a

higher modulus implies a smaller mesh size. It was reported that fluorescence recovery after photo bleaching (FRAP)[186], DNA electrophoresis[187], or simply measuring the diffusion of fluorescently tagged polymers entrapped within the hydrogels are additional methods of characterizing mesh size and molecular transport.

2.1.3.2 e Degradation

Cell-matrix adhesive interactions are known to regulate stem cell differentiation, but the mechanism especially for direct three-dimensional encapsulation within hydrogels needs to be further studied.

Typically, hydrogels degrade through entire hydrolytic or enzymatic process. Hydrolysis occurs via hydrolytically unstable chemical bonds, and the rate of hydrolysis can be tuned by varying parameters such as crosslinking density or the conditions of the buffer such as PH. Crosslinking density was controlled via polymer concentration and extent of crosslinking over fabrication process. Hult and colleagues have studied mechanical properties of tetra functional PEG hydrogels, under alkaline conditions (PH 10) hydrogels were easier to hydrolyse with higher molecular weight of PEG hydrogels[188]. Burdick et al investigated how degradation affects the stem cell fate in three-dimensional hydrogels by mediated cellular traction, without affected by cell morphology nor matrix mechanics[189].

Chapter 3

Experimental section

3.1 Materials

Methyl p-toluenesulfonate (98%), Allyl p-toluenesulfonate (≥95.0% (GC)), p-Toluenesulfonyl chloride (ReagentPlus®, ≥99%), 3-Buten-1-ol (96%), 10-Undecen-1-ol (98%), PEG-di-p-tosylate (average Mn 3,500), Allyl iodide (98.0%), Acetonitrile (anhydrous, 99.8%) was stored under argon, methacrylic acid (MAA, contains 250 ppm MEHQ as inhibitor, 99%), 2-Bromo-2-methylpropionic acid (98%), Allylamine (≥99%), Allyl bromide (reagent grade, 97%, contains ≤1000 ppm propylene oxide as stabilizer), Pyridine (anhydrous, 99.8%), sodium chloride (99.5%), sodium bicarbonate (99.5%), magnesium sulfite (98%), Dithranol (≥90% (HPLC)), Lithium diisopropylamide solution (LDA, 1.0 M in THF/hexanes), Chloroform (AR), Copper(II) bromide 99.999% trace metals basis, 2,2'-Bipyridyl Green Alternative Reagent Plus® (≥99%) (bpy), Methanol was purchased from Aldrich, Poly(ethylene glycol) methyl ether methacrylate (average Mn 300, contains 100 ppm MEHQ as inhibitor, 300 ppm BHT as inhibitor) , L-glutathione reduced (98%), 2-Hydroxy-4′-(2-hydroxyethoxy)-2-methylpropiophenone (98%, Irgacure 2959), 4',6-Diamidino-2-phenylindole (DAPI), Phalloidin, 1, 2-Diiodoethane (99%), 1, 2-Dibromoethane (≥ 99%), Pentaerythrityl tetraiodide Aldrich^{CPR}, Pentaerythritol tetrabromide (96%), Acrylic acid anhydrous, contains 200 ppm MEHQ as inhibitor (99%), Thioacetic acid (96%), Sodium hydroxide (Sodium hydroxide pellets pure), Hydroxylamine solution 50 wt.% in H_2O (99.999%), 1-Methyl-2-pyrrolidinone anhydrous (99.5%), Diethyl ether, Deuterium oxide (deuteration degree min. 99.9% for NMR spectroscopy MagniSolv™), Methanol-d4 (Sigma), Chloroform-d (≥ 99.8 atom % D, contains 0.5 wt. % silver foil as stabilizer), 2-

Ethyl-2-oxazoline (EtOx, 99%, Aldrich) was dried over calcium hydride and distilled under argon prior to use. 2-methyl-2-oxzoline (MeOx, 98%, Aldrich) was dried over calcium hydride and distilled under argon prior to use. Triethylamine (≥99.5%) was dried over Potassium Hydroxide and distilled under argon prior to use.

3.2 Methods

3.2.1 General procedure for the microwave-assisted polymerization of EtOx

Methyl tosylate (0.188 g, 1.01 mmol), EtOx (0.500 g, 5.04 mmol) and acetonitrile (7.0 mL) were added in the pre-dried microwave vials. In all cases, the monomer concentration was adjusted to 4 mol/L, and a monomer to initiator ([M]/ [I]) ratio varied from 5-20 were used. The vessels were capped with dedicated vessel caps and placed in the microwave synthesizer. Therefore, the reaction solution was heated to the desired temperature (140℃) after around 20 s preheating, and kept at this temperature whilst stirring for the desired reaction time (5-30 min). Subsequently, reaction mixtures were cooled to room temperature under a gas flow. Triethylamine (0.408 g, 4.03 mmol) was added in a 4-fold excess. Subsequently, Methacrylic acid (0.024 g, 3.02 mmol) was added in a 3-fold excess via syringe through the microwave vessel cap to the living oligo (EtOx). The amounts of methacrylic acid and triethylamine were calculated from the used monomer to terminating agent's ratios. The reaction solution was heated to 80°C for 12 h. Acetonitrile was evaporated and the polymer was dissolved in chloroform. Therefore, the solution was washed with saturated sodium bicarbonate aqueous solution for three times, and then washed with brine for three times. Finally, the solution was dried with magnesium sulfate and filtered, then the solvent was evaporated under reduced pressure and the resulting yellow polymer was dried under high vacuum and stored in the fridge. (Yield: 89%) ^{1}H-NMR (400 MH_Z, $CDCl_3$): δ 6.07 (=C**H$_2$**), 5.58

(=C**H**$_2$), 4.27 (m, C**H**$_2$-COO), 3.44 (m, N-C**H**$_2$); 3.02 (m, N-C**H**$_3$), 2.35 (m, C-C**H**$_2$-C), 1.92 (m, CH_2=C-C**H**$_3$), 1.12 (m, C-C**H**$_3$). (NMR ratio calculated: the peak integrations were first divided by the number of expected protons corresponding to this peak and ratios were measured after such corrections were applied.)

3.2.2 Preparation of triblock copolymer PEtOx-PEG- PEtOx

General procedure of preparation copolymer PEtOx-PEG-PEtOx (10:1:10): PEG-di-p-tosylate (0.250 g, 0.07 mmol), 2-ethyl-2-oxazoline (0.142 g, 1.42 mmol) and anhydrous acetonitrile (2 mL) were added in a pre-dried microwave vial. The vessels were capped with dedicated vessel caps and placed in the microwave synthesizer. Therefore, the reaction solution was heated to the desired temperature (160℃) after around 30 s preheating, and kept at this temperature for the desired reaction time (10 min). Then, vessels were cooled to room temperature under a gas flow. The reaction solution was heated to 80ºC for 12 h. Acetonitrile was evaporated and the polymer was dissolved in chloroform. Therefore, the solution was washed with saturated sodium bicarbonate aqueous solution for three times, and then washed with brine for three times as well. Finally, the solution was dried with potassium sulfate and filtered, then the solvent was evaporated under reduced pressure and the resulting light yellowish polymer was dried under high vacuum. (Yield: 62.55%) ^{1}H-NMR (400 MH_Z, $CDCl_3$): δ 3.63 (m, O-C**H**$_2$-CH_2), 3.45 (m, N-C**H**$_2$), 2.34 (m, C-C**H**$_2$), 2.17 (m, HN-C**H**$_2$), 1.01 (m, CH_2-C**H**$_3$). FTIR: 2875 (C-H), 1718 (C=O), 1100 (C-H_2)

Similarly, for PEtOx-PEG-PEtOx (35:1:35): (53.34%) ^{1}H-NMR (400 MH_Z, D_2O): δ 3.63 (m, O-C**H**$_2$-CH_2), 3.45 (m, N-C**H**$_2$), 2.34 (m, C-C**H**$_2$), 2.17 (m, HN-C**H**$_2$), 1.01 (m, CH_2-C**H**$_3$). FTIR: 2875 (C-H), 1718 (C=O), 1100 (C-H_2). GPC: Mn= 9973 g/mol.

3.2.3 Hydrolysis of triblock copolymer PEtOx-PEG- PEtOx

Poly (2-ethyl-2-oxazoline)-b-poly (ethylene oxide)-b-poly(2-ethyl-2-oxazoline) (0.400 g, 0.1 mmol) was dissolved in 12 mL 0.5 M HCl in a one neck flask under reflux, the temperature was kept at 120°C overnight in a nitrogen atmosphere. After that, the acid solution was removed under reduced pressure. Then the solid can easily to be scratched out from flask. (Yield over than 95%) ^{1}H-NMR (400 MH_Z, D_2O): δ 3.63 (m, O-C**H₂**-CH_2), 3.45 (m, N-C**H₂**), 2.34 (m, C-C**H₂**), 2.17 (m, HN-C**H₂**). FTIR: 2983 (C-H), 3450, 1654 (N-H), 1465 (C-H).

Similarly, for PEtOx-PEG-PEtOx (35:1:35): ^{1}H-NMR (400 MH_Z, D_2O): δ 3.63 (m, O-C**H₂**-CH_2), 3.45 (m, N-C**H₂**), 2.34 (m, C-C**H₂**), 1.01 (m, CH_2-C**H₃**). FTIR: 2983 (C-H), 3450, 1654 (N-H), 1465 (C-H).

3.2.4 Synthesis of monomer: 2-butenyl-2-oxazoline (ButNOx)

A three neck flask was purged with argon and vacuum three times with a heat gun, and Lithium diisopropylamide (LDA) solution (100 mL, 0.1 mol, 1 M) was added into the three neck flask. The flask was cooled with dry ice and fresh acetone to -78°C, then distilled 2-methyl-2-oxazoline (7.78 mL, 0.09 mol, 0.9 eq) mixed with THF (1:1 volume ratio) were added dropwise from dropping funnel over 30 min. After stirring one hour at -78°C in an acetone/dry ice cooling bath, some yellow precipitate gradually formed. Allyl bromide (7.800 g, 0.06 mol) in THF (1:1) was added dropwise through a dropping funnel over than 30 min. After leaving the reaction at room temperature for overnight stirring, all the crude was transferred to a one neck flask containing anhydrous methanol (20 mL). All the volatiles were evaporated under reduced pressure, and after adding DCM, the crude was washed with water (2 × 50 mL) and brine (1 × 50 mL), after that it was purified through vacuum distillation.

3.2.5 Synthesis of copolymer BuPEtOxOH and BuPMeOxOH

For the synthesis of BuMeOxOH: 2-methyl-2-oxazoline (1.500 g, 17.6 mmol) distilled over calcium hydride and the synthesized monomer 2-butenyl-2-oxazoline (0.539 g, 4.31 mmol) were added into an air flowed microwave vessel. Then methyl tosylate (0.033 g, 0.18 mmol) was added into the tube and 2 mL anhydrous acetonitrile as solvent was added as well. The vessels were capped with dedicated vessel caps and placed in the microwave synthesizer. Therefore, the reaction solution was heated to the desired temperature (160℃) after 40 s preheating, and kept at this temperature for the desired reaction time (10 min). Then, vessels were cooled to room temperature under a gas flow. The reaction was quenched with a few drops of water and then precipitated in cold diethyl ether three times. Similarly, BuPEtOxOH was prepared from 2-methyl-2-oxazoline (1.500 g, 15.2 mmol), synthesized monomer 2-butenyl-2-oxazoline (0.470 g, 3.8 mmol), methyl tosylate (0.035 g, 0.18 mmol), and 2 mL anhydrous acetonitrile as solvent was added as well. ^{1}H-NMR (400 MHz, D_2O): δ 5.81 (=C**H**$_2$), 5.00 (=C**H**$_2$), 3.44 (m, N-C**H**$_2$); 2.37 (m, N-C**H**$_3$; m, C-C**H**$_2$-C), 2.00 (m, C-C**H**$_3$).

Similarly, for Bu-PEtOx, ^{1}H-NMR (400 MHz, $CDCl_3$): δ 5.81 (=C**H**$_2$), 5.00 (=C**H**$_2$), 3.44 (m, N-C**H**$_2$); 2.37 (m, N-C**H**$_3$; m, C-C**H**$_2$-C; m, C-C**H**$_2$-C**H**$_2$-C), 1.92 (m, CH_2=C-C**H**$_3$), 1.12 (m, C-C**H**$_3$).

3.2.6 Synthesis of POx-MAA monomers initiated with Allyl tosylate

General procedure to synthesis POxMA monomers: Allyl tosylate (0.374 g, 1.73 mmol), MeOx (0.750 g, 8.50 mmol) and acetonitrile (2.0 mL) were added in the pre-dried microwave vials. In all cases, the monomer concentration was adjusted to 4 mol/L, and a monomer to initiator ([M]/ [I]) ratio of 5-10 was used. The vessels were capped with dedicated vessel caps and placed in the microwave synthesizer. The reaction solution was heated to the desired temperature (140℃) after around 20 s preheating, and retained

for desired reaction time (5 min). Then, vessles were cooled to room temperature under a gas flow. Triethylamine (0.700 g, 6.92 mmol) was added in a 4-fold excess. Subsequently, methacrylic acid (0.447 g, 5.19 mmol) was added in a 3-fold excess via a syringe through the microwave vessel cap to the living oligo (EtOx). The amounts of MAA and triethyl amine were calculated from the used monomer to terminating agent's ratios. The reaction solution was heated to 80°C for 12 h. Acetonitrile was evaporated and the polymer was dissolved in chloroform. The solution was then washed with saturated sodium bicarbonate aqueous solution three times, and then washed with brine three times. Finally, the solution was dried with magnesium sulfate and filtered, then the solvent was evaporated under reduced pressure and the resulting orange polymer was dried under high vacuum and stored in the fridge. (Yield: 63%) ^{1}H-NMR (400 MHz, $CDCl_3$): δ 6.07 (=C**H**$_2$), 5.59 (=C**H**$_2$), 5.15 (=C**H**$_2$), 5.77 (m, CH_2=C**H**-CH_3) 4.27 (m, C**H**$_2$–COO), 3.44 (m, N–C**H**$_2$), 2.35 (m, C–C**H**$_2$–C), 1.92 (m, CH_2=C–C**H**$_3$).

Methyl tosylate (0.220 g, 1.18 mmol), MeOx (0.500g, 5.88 mmol), methacrylic acid (0.300 g, 3.54 mmol) (Yield: 56%) ^{1}H-NMR (400 MHz, $CDCl_3$): δ 6.05 (=C**H**$_2$), 5.56 (=C**H**$_2$), 4.24 (m, C**H**$_2$–COO), 3.42 (m, N–C**H**$_2$); 3.00 (m, N–C**H**$_3$), 2.09 (m, CH_2=C–C**H**$_3$).

3.2.7 Surface initiated growth of POxMA and POEGMA brushes

General growth of a 20 nm thick POx brush: a solution A of $CuBr_2$ (18 mg, 80 μmol), bpy (320 mg, 2.0 mmol) in water/ methanol 2/1 (15 mL) was degassed using nitrogen bubbling for 30 min. CuBr (82 mg, 0.57 mmol) was added to this solution A, and the resulting mixture further degassed for 10 min. Solution B of PEtOxMA (4.200 g, 7.2 mmol) in water/methanol 2:1 (5 mL) was degassed using nitrogen bubbling for 30 min. 5 mL of mixture solution A were transferred to solution B and stirred for 1 min, and

then transferring to a flask containing the initiator-coated gold surface (immersion in 25 mL ethanol solution of 39 mg thiol initiator overnight) under inert atmosphere. The polymerization was stopped after different time intervals by immersing the surface in deionized water and subsequently washed with large amount of water and ethanol before drying in a stream of nitrogen.

Growth of PAMeOxMA brush and Me-PMeOxMA brush use the same condition as PEtOxMA.

Similarly, for copolymer brushes, re-initiation of POEGMA brush growth with oligomer OAMeOxMA can be obtained via the following procedure. First, the growth of 20 nm thick POEGMA brushes was carried out: a solution of $CuBr_2$ (9 mg, 40 μmol), bpy (160 mg, 1.0 mmol) and OEGMA (6.300 g, 17.5 mmol) in water/ethanol 4/1 (15 mL) was degassed using nitrogen bubbling for 30 min. CuCl (82 mg, 410 μmol) was added to this solution and the resulting mixture further degassed for 15 min before transferring to a degassed column containing the initiator-coated silicon wafer under inert atmosphere. The polymerization was stopped after 15 min by immersing the surface in 5 ml solution D (bpy 320 mg and $CuBr_2$ 180 mg fully dissolved in 30 ml water/ethanol 4/1 that was degassed for 30 min). After 5 min of incubation, samples were removed from this solution and subsequently washed with copious amount of water and ethanol before drying in a stream of nitrogen. The thickness of POEGMA brushes was measured by ellipsometry. Finally, a second block of PAMeOxMA brushes was grown on top of the first block of POEGMA brush, in identical conditions and procedures as for the growth of POx brushes.

3.2.8 Microcontact printing of POx brushes

Solution E (39 mg thiol in 25 mL ethanol) was spread on a PDMS stamp using a cotton bud for 10 s. The stamp was dried in a stream of nitrogen and deposited on a gold substrate, allowing the contact to occur for 30 s. Afterwards, the stamp was gently removed from the gold substrate and stored in a polymerization jar under inert atmosphere until all samples were ready for polymerisation. A monomer solution (prepared as for the growth of POx brushes from non-patterned substrates) was added to the jar under inert atmosphere.

3.2.9 Thiol-ene chemistry on PAMeOxMA brushes

25 μL photo initiator solutions (Irgacure 2959 with concentration of 250 mg/mL in methanol) were added to 1 mL solution F (14 mg/mL of glutathione in PBS). 10 μL of mixture solution was on a quartz plate and polymer brush functionalised gold substrates were placed on top. Substrates were exposed to UV radiation (Intensity: 17mW/cm^2) for 300s and washed with deionised water before being measured by ellipsometry (figure 4.16 B).

3.2.10 Patterning peptides on PAMeOxMA brushes

Patterned substrates were prepared via PAMeOxMA brushes reacted with FITC labbled RGE. Instead of adding the reaction mixture to the quartz, it was added to the photomask (acetate mask-circles) as shown in figure 4.16 A and follow the same process as thiol-ene chemistry on PAMeOxMA brushes. Substrates were washes with DMF, deionised water and ethanol before performed with epifluorescent microscopy.

3.2.11 Fibronectin deposition and staining

For the deposition of fibronectin onto patterned substrates, samples with patterned polymer brushes were incubated in a fibronectin solution (10 μg/mL in PBS solution) for 45 min. Following this step, samples were washed with PBS, starting by diluting

twice with PBS and then fully replacing the buffer twice more, to avoid protein depositing and drying onto the surface of brushes when no dilution is carried out.[228] Samples were then blocked with blocking buffer (composed of 10 mL PBS, 1 mL FBS, 25 µL gelatine) for 30 min. Samples were then incubated in the first rabbit antibody solution raised against fibronectin (human-fibronectin, 10 µg/mL, Millipore) at a concentration of 1 mg/mL (dilution of 200:1), for one hour. Samples were washed with PBS three times and then incubated in the secondary antibody solution (rabbit-antibody, 1mg/mL, abcam) at a dilution of 1000X for 1 h. Samples were washed three times with PBS and imaged as soon as possible.

3.2.12 Cell culture and seeding

GEβ3 cells were cultured in DMEM supplemented with 10% FBS, glutamine and antibiotics. GEβ3 cells were obtained by retroviral expression from GEβ1-deficient epithelial cells (GE) and stably express αvβ3 integrins (Danen et al., 2002). Cells were cultured to confluency (about 80% densities) and were detached using trypsin/versene (1:9) and reseeded on the samples in a 48 well plate at a density of 7,500 cells / well (0.5mL / well) in DMEM medium. Cells were then allowed to adhere for 24 h and then fixed.

3.2.13 Immunostaining and microscopy

Immunostaining. After 24 h incubation, cells were fixed with 4% paraformaldehyde (in PBS) for 10 min, permeabilized with 0.2% Triton X-100 (in PBS) for 5 min and blocked with a solution of 10% FBS and 0.25% gelatin for 1 h at room temperature. Phalloidin (for actin staining, 1:500) was added at this stage too. Samples were then incubated in DAPI (for nucleus staining, 1:1000) for 1 h at room temperature and washed again before being mounted on glass slides with Mowiol solutions.

3.2.14 Statistical analyses

All data were analyzed by Tukey's test and significance was determined by * $p <$ 0.05, ** $p < 0.01$: *** $p < 0.001$. A full summary of statistical analysis is provided in table b.1.

3.2.15 Synthesis of PMeOx thiol

1, 2-Diiodoethane (0.199 g, 0.71 mmol), MeOx (1.500 g, 17.63 mmol) and acetonitrile (2.0 mL) were added in the pre-dried microwave vials. In all cases, the monomer concentration was adjusted to 4 mol / L, and monomer to initiator ([M] / [I]) ratio 12.5, 25 and 50 were used. The vessels were capped with dedicated vessel caps and placed in the microwave synthesizer. Therefore, the reaction solution was heated to the desired temperature (160℃) after around 30 s preheating, and kept at this temperature whilst stirring for the desired reaction time (30 min). Subsequently, reaction mixtures were cooled to room temperature under a gas flow. Triethylamine (0.279 mL, 3.80 mmol) was added in a 5-fold excess. Subsequently, acrylic acid (0.321 mL, 4.24 mmol) was added in a 6-fold excess via syringe through the microwave vessel cap to the living oligo (MeOx). The amounts of methacrylic acid and triethyl amine were calculated from the used monomer to terminating agent's ratios. The reaction solution was heated to 80°C for 12 h. Acetonitrile was evaporated and the polymer was dissolved in chloroform. Therefore, the solution was re-dissolved in DCM and precipitated in cold diethyl ether for three times. Finally the solvent was evaporated under reduced pressure overnight before next functionalisation.

2I-PMeOx-acry (n=12.5) (1.500 g, 0.6 mmol) was dissolved with 10 mL H_2O in a round flask, and thioacetic acid (0.420 g, 5.5 mmol) was added in a 5-fold excess. NaOH (0.570 g, 5.5 mmol) was added in a 5-fold excess, and the reaction was stirred

overnight. Subsequently, hydroxylamine (0.34 mL, 5.5 mmol) was added in a 5-fold excess and stirred in ice bath for 2 h and 2 h at room temperature. Therefore, the polymers were recovered by freeze drying and precipitate in cold diethyl ether with DCM. Finally the solvent was evaporated under reduced pressure overnight and stored with nitrogen in the freezer. The amounts of thioacetic acid, sodium hydroxide and hydroxylamine were calculated from the caculated alkene per branch ratios.

Pentaerythrityl tetraiodide (n=25) (0.102 g, 0.18 mmol), MeOx (1.500 g, 17.63 mmol) and 1-Methyl-2-pyrrolidinone (2.0 mL) were added in the pre-dried microwave vials. In all cases, the monomer concentration was adjusted to 4 mol/L, and monomer to initiator ([M] / [I]) ratio 12.5, 25 and 50 were used. The vessels were capped with dedicated vessel caps and placed in the microwave synthesizer. Therefore, the reaction solution was heated to the desired temperature (200℃) after around 40 s preheating, and kept at this temperature whilst stirring for the desired reaction time (30 min). Subsequently, reaction mixtures were cooled to room temperature under a gas flow. Triethylamine (0.071 mL, 0.96 mmol) was added in a 5-fold excess. Subsequently, acrylic acid (0.077 mL, 1.02 mmol) was added in a 6-fold excess via syringe through the microwave vessel cap to the living oligo (MeOx). The amounts of acrylic acid and triethyl amine were calculated from the used monomer to terminating agent's ratios. The reaction solution was heated to 80°C for 12 h. Acetonitrile was evaporated and the polymer was dissolved in chloroform. Therefore, the solution was re-dissolved in DCM and precipitated in cold diethyl ether for three times. Finally the solvent was evaporated under reduced pressure overnight before next functionalization.

4I-PMeOx-acry (n=50) (0.820 g, 0.04 mmol) was dissolved with 10 mL H_2O in a round flask, and thioacetic acid (0.060 g, 0.79 mmol) was added in a 5-fold excess. NaOH

(0.032 g, 0.78 mmol) was added in a 5-fold excess, the reaction was stirred overnight. Subsequently, hydroxylamine (0.05 mL, 0.8 mmol) was added in a 5-fold excess and stirred under ice bath for 2 h and 2 h at room temperature. Therefore, the polymers were recovered by freeze drying and precipitate in cold diethyl ether with DCM. Finally the solvent was evaporated under reduced pressure overnight and stored with nitrogen in the freezer. The amounts of thioacetic acid, sodium hydroxide and hydroxylamine were calculated from the calculated alkene per branch ratios. The molar mass of 4I-PMeOx-acry was used from NMR result.

3.2.16 Synthesis of Bu-PMeOx-SH

Bu-PMeOx-OH (1.000 g, 75 mmol), 2-fold of thioacetic acid (0.327 g, 150 mmol) and 5 mol% of PI (0.044 g/mL Irgacure 2959) were dissolved in 1 mL MeOD, and then mixed solution was exposed to UV irradiation for 5 min with 50 mW/cm^2 intensity.

The Bu-PMeOx-thioacetate (1.000 g, 75 mmol) was placed in ethanol (10 mL) and stirred until fully dissolved. To this solution, 0.5 M NaOH/H_2O were added (4 mL, 1/1) and refluxed at 82°C for 2 h. Then, the solution n was neutralized by slowly adding 0.5 M HCl (4 mL), whilst stirring in ice bath. After this, evaporate the water and ethanol in the rotavap and redissolve in MeOH (2 mL) before precipitating in cold diethyl ether. Then redissolve in DCM and precipitate again in cold diethyl ether. The solvent was evaporated under high vacuum overnight and final product was stored in the freezer.

3.2.17 Photo rheology to fabricate hydrogels

To make a total amount of 200 µL gel curing solution, PBS was added for space, the solution was sandwiched with two methacrylate treated glass slide one stick on the quartz and the other one stick on a 20 nm plate. The fixed gap is 300 µm and Oscillations were set to controlled strain mode at 1 % strain. *In situ* monitoring the

gelation, time sweep was performed: 30 s of pre-perform without UV exposure, and then UV irradiation for 2 min, afterwards, without UV irradiation until the end of gelation. Frequency sweep, amplitude sweep and stress relaxation measurements were conducted after the UV cure to examine the *in situ* change in rheological behaviour.

Chapter 4

Synthesis of functional polyoxazolines with defined end-groups

4.1 Synthesis of polyoxazolines with well-defined end groups – state-of-the-art

Typically, the polymerization of oxazoline monomers is carried out with four different monomers: 2-methyl-2-oxazoline (PMeOx), 2-ethyl-2-oxazoline (PEtOx), 2-nonyl-2-oxazoline (PNonOx) and 2-phenyl-2-oxazoline (PPhOx) by Hoogenboom and colleagues. It was showed that microwave irradiation could decrease the reaction time as well as significantly improve the rate of polymerization[190, 191]. Synthesis of polyoxazoline takes advantage of cationic ring-opening polymerization as a result of suppressing side reactions (such as termination of chain growth/or chain-coupling) that can be performed in a manner. Thus, it enables to synthesis telechelic and semitelechelic polyoxazolines with quantitative termination of the polymerization[26].

Saegusa et al found that during the chain growth there may exist two active species in equilibrium: cationic chains, associated with a counterion defined by the initiator or any added salt and neutral chains in which the reactive centre remains tethered to the polymer chain via covalent bond. The position of the equilibrium depends on the basicity of the oxazoline monomer and the nucleophilicity of the counter ion[192], but the rate of the polymerization process highly depends on the formation of cationic species[193]. Temperature highly affects the position of the ionic-covalent equilibrium, and as a result the rate of the chain growth[194]. Although the polymerisation of oxazoline monomers can be carried out in living conditions if water and other termination agents are carefully excluded from the reaction mixture, it was reported that longer, well-defined polymer chains are difficult to achieve, as the average molecular

weight distributions broaden for polymerization when the degree of polymerization higher than 300[195]. Therefore short polyoxazolines appear better candidates for the design of macromolecules with controlled end functionalities and have been designed as block copolymers or oligomers with controlled reactive or functional end groups[196].

A variety of polyoxazolines have been studied, for instance, Schubert et al synthesized a range of amine end-functionalized PEtOx with different molecular weights (monomer to initiator ratio: 20, 40, 60, 80) and then immobilized on glass slides. They found that the coatings showed excellent anti-fouling behaviour when incubated in "real life" artificial river water streams which contains five different bacteria[197]. Moreover, multifunctional poly(2-oxazoline)s that carry alkene residues as well as hydroxyl groups or a dye have been designed to generate promising nanoparticles for cell studies such as cellular uptake of the nanoparticles[198].

Alkyl ester initiators such as tosylates[199], triflates, and halides have been widely used. For example, in the presence of methyl cations as initiators, the polymerization rates as follows: methyl triflate > methyl tosylate > methyl iodide[26]. Alkyl halide initiators range from chloride and bromide[40] to iodide, as well as acetyl halide[43]. While alkyl iodide initiators are mostly converted *in situ* from chloride[200] or bromide[201]. Initiators such as unsaturated aliphatic initiators with double[202, 203] or triple bonds[204] have attracted significant attention. This interest results from the unsaturated groups being suitable moieties for functionalization via two common types of "click" reactions: thiol-ene coupling (TEC) and copper-catalysed azide-alkyne cycloaddition (CuAAC)[205].

Schubert et al compared three different methods of end capping steps to obtain short POx polymers with methacrylate end functionalised poly (2-ethyl-2-oxazoline). The

most successful method was found to be the growth of a POx chain, followed by end capping with *in situ* formed triethylamonium methacrylate. This approach yields macro monomers (methacrylate POx) with high degree of conversion (≥ 80%) as well as low polydispersity (below 1.2)[45]. Choosing the right initiator is very important for controlled polymerizations and this principle can be applied to polyoxazolines. The chemical structure of the initiator determines the functionality of the resulting polymer as well as controlling the rate of initiation and the breadth of the initial molecular weight distribution[195].

To terminate the propagation of oxazolinium, a nucleophilic reagent is required to stop the propagation. The most popular terminating agent is by far water[206, 207], however, it was reported the weak nucleophilic resulted in kinetically controlled product which can be seen in scheme 3.1[206]. Therefore, hydroxyl ion in methanolic sodium hydroxide solutions[42] or sodium hydrogen carbonate[208] have also been widely used. Termination with amines is also particularly popular as it allows accessing other type of functionalities. For example, Saegusa and colleagues have successfully used primary amines such as 2-(N-2-2-aminoethyl-N-methyl) aminoethylstyrene (AAS) to terminate 2-methyl-2-oxazoline polymerisations[29]. Moreover, Schiavon et al using "grafting onto" method to form lipopolymers based on polyoxazolines that were end capped with α-ω- amino alkylalkoxysilanes[209].

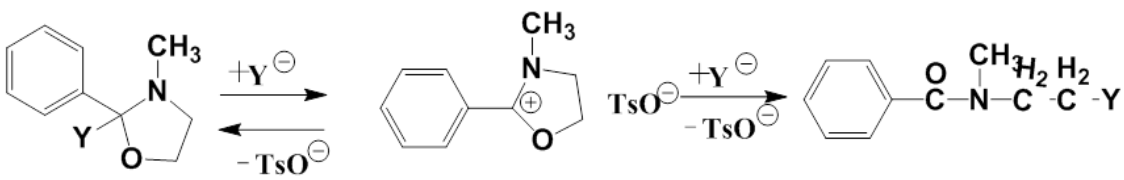

Scheme 4.1 Possible mechanism of oligomer (EtOx) terminated with water

Moreover, temperature is one of the important factor that highly impact on the polymerization of 2-phenyl-2-oxazoline, high polydispersity were obtained for the polymerization performed at 120°C or lower, which may due to slow initiating and thus not all polymer chains start to grow at the same time[208].

Interesting, the possibility to functionalise the lateral chain of reactive polyoxazolines makes POx an attractive alternative to PEG. For instance, Schlaad et al investigated the functionalization of POx via "thiol-click" reactions in mild conditions (generation of radicals with UV light at room temperature): radical addition of mercaptans (RSH) onto poly(2-(3-butenyl)-2-oxazoline) (ButNOx). Moreover, they found that a hydrophobic fluoropolymer can be prepared using the same way with 1H, 1H, 2H, 2H-perfluorooctanethiol as water soluble polymer or glycopolymer[210]. Furthermore, Hoogenboom and colleagues fabricated homogeneous hydrogels via thiol-ene conditions in the presence of dithiothreitol in water with copolymer poly(2-(3-butenyl)-2-oxazoline) (ButNOx)[136].

In addition, POx can be easily converted to polyamines (PEI) through partially or fully hydrolysing PEtOx side chains. PEI is a promising material for gene delivery and transfection, already commercially used for in vitro applications (e.g. in jetPEI). For example, polyethylenimines (PEI) was extensively studied as synthetic carriers for the delivery of plasmid DNA into cells in vitro and vivo[211, 212]. From previous studies, branched polyethyleneimine (BPEI) attracts lots of attention because of its highly efficiency gene delivery property both in vitro and in vivo[213]. However, it has been reported that linear PEI is less toxic than branched PEI[214] and low molecular weight of PEI shows less toxic than high molecular weight PEI[215].

Aims of this chapter. Hence it appears that POxs are attractive polymers for the introduction of defined end-functional groups to hydrophilic neutral polymer chains. These functionalities may in turn be applied to the design of biomaterials and surface coatings. Herein this chapter, we use microwave-mediated synthesis of POx for the design of well-defined short POx with different initiators and terminate reagent. Cationic ring opening polymerization of EtOx and MeOx were carried out here for four different initiators, acetonitrile as solvent and at 140°C microwave synthesizer assistance for 5 min, subsequently, the living chain ends were reacted with *in situ* formed triethyl ammonium (methacrylate, 2-Bromo-2-methylpropionic at low temperature) or terminate active oligo (EtOx and MeOx) chains with water and allylamine. In particular, we focused on the introduction of alkene functionalities that will be used in subsequent chapters for the design of polymer brushes and hydrogels.

4.2 Results and discussion

4.2.1 Synthesis of oligo (oxazoline)s from four different initiators and end capping with three different terminating agents.

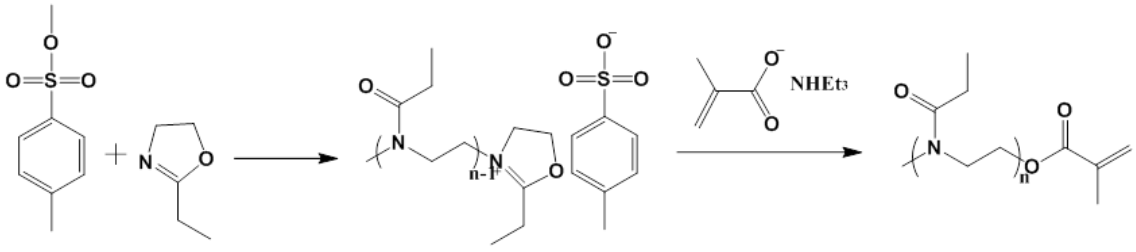

Scheme 4.2 Synthesis and mechanism of methacrylate end functionalized poly(2-ethyl-2-oxazoline)[45].

Scheme 4.2 presents the general mechanism for POx polymerisation followed by methacrylate end-functionalization, to form oligo (EtOx) (PEtOx). These PEtOx were initiated with methyl tosylate and then directly end capped with methacrylic acid.

Methyl tosylate was used as an initiator and acetonitrile as solvent for the polymerization of EtOx using microwave-assisted heating to 140°C. The living chains initiated can be terminated by reaction with *in situ* formed triethyl ammonium methacrylate, which was generated by the addition of methacrylic acid and triethylamine to the reaction solution. A series of well-defined oligo (PEtOx) can be synthesised via this ring opening polymerization method. The extent of control of the initiation and termination steps and the possible occurrence of side reactions (scheme 4.3) was characterized by ^{1}H-NMR and mass spectrometry.

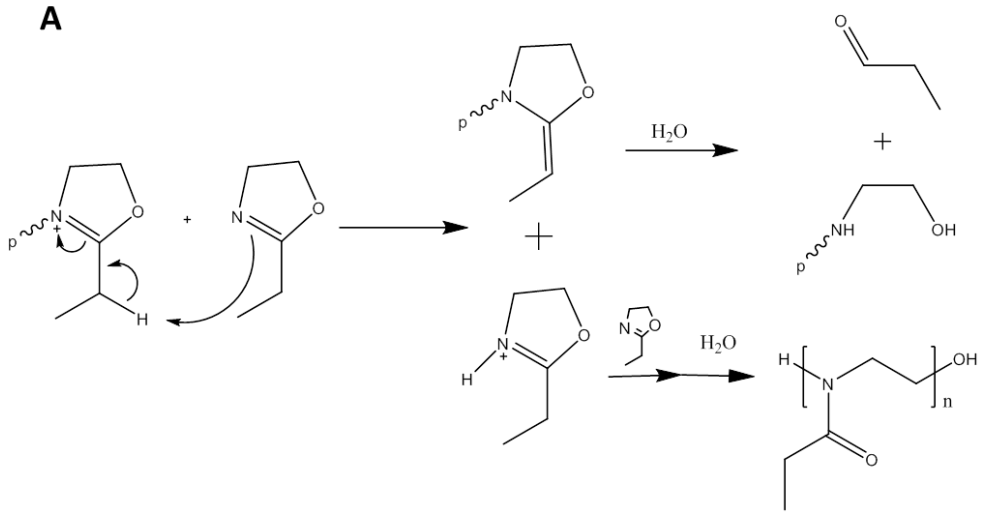

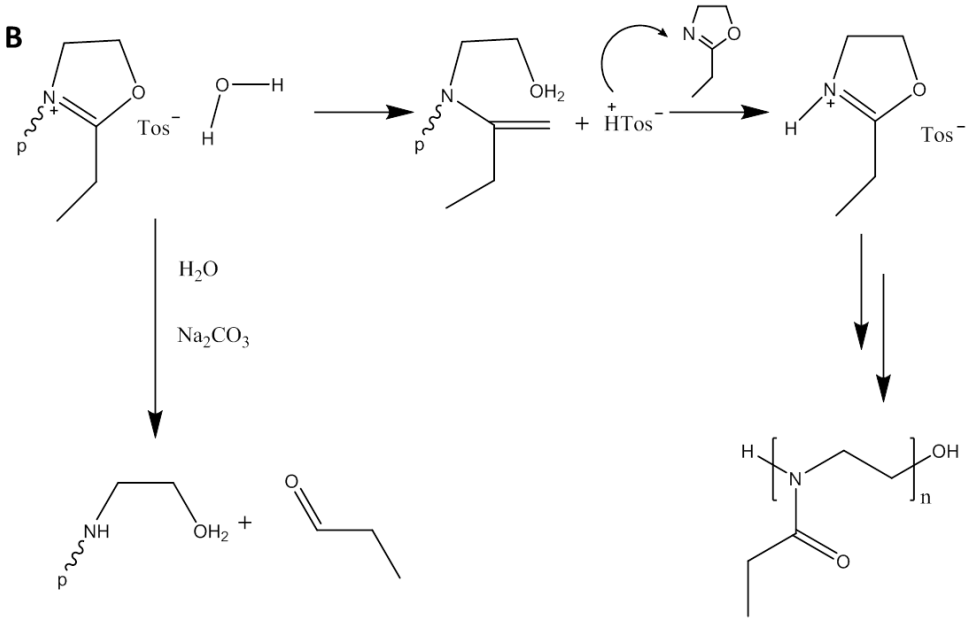

Scheme 4.3 Schematic representation of possible chain-transfer reactions during the polymerization of EtOx. (A) Possible chain transfer to monomer; (B) end-capping with H-nucleophilic and basic cleavage of oxazolinium species[216].

The polymers produced were purified by extraction and dissolved in $CDCl_3$ for characterization by ^{1}H-NMR spectroscopy. Samples were dissolved in DCM and added to a dithranol matrix for MALDI-ToF mass spectrometry. In the case of monomer to initiator ratios of 5:1, the reaction temperature was 140°C, and polymerisations were carried out for 5 min. Full assignment of protons corresponding to the poly (2-ethyl-2-oxazoline) can be seen in figure 4.1.

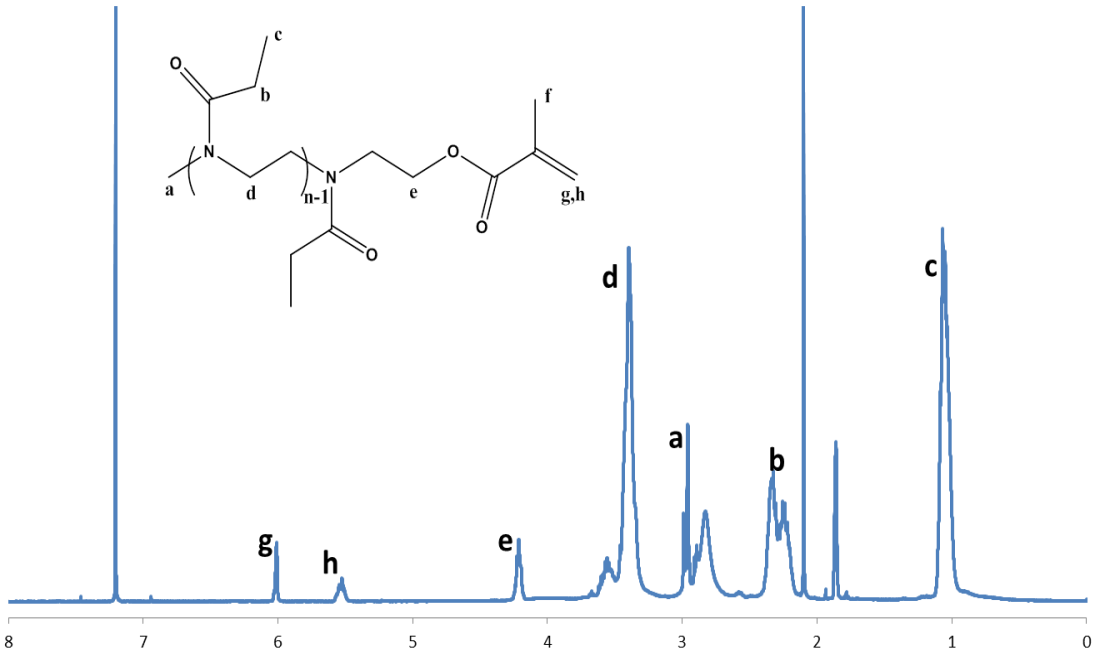

Figure 4.1 ^{1}H-NMR spectrum in $CDCl_3$ of oligo (EtOx) initiated by methyl tosylate and terminated with methacrylate acid.

As we can see from the ^{1}H-NMR spectra (figure 4.1), all peaks were assignable to corresponding protons of the chemical structure of poly (2-ethyl-2-oxazoline), including those associated with end groups. The ratios of the corresponding integrals allowed the confirmation of the molecular structure of the oligomers obtained and allowed to quantify their degree of polymerisation as well as the control of the end capping. According to the ratio H_d to H_g we can quantify the actual efficiency of the end-capping of the polymerised polyoxazoline chains, which was found to be close to the expected ratio for a 5:1 starting mixture of monomer: initiator (we found that H_d/H_g is 5.2 ± 0.3). Notably, all ratios are reported after correction for the number of protons involved in the respective peaks. Similarly H_d to H_f was found to be 5.2 ± 0.3, which is also very close to the expected ratio 5:1. Similarly, H_d to H_a was found to be 5.6 ± 0.8. H_a to H_g was

found to be 0.95 ± 0.10 shows that the amounts of initiating groups and methacrylate terminal groups are close to 1.0 as expected. The slightly lower ratio than predicted could highlight the occurrence of side reactions, which can be further characterised by MALDI-ToF (figure 4.2). Altogether, these results indicated a good control of the initiation and termination steps in short polyoxazoline oligomers.

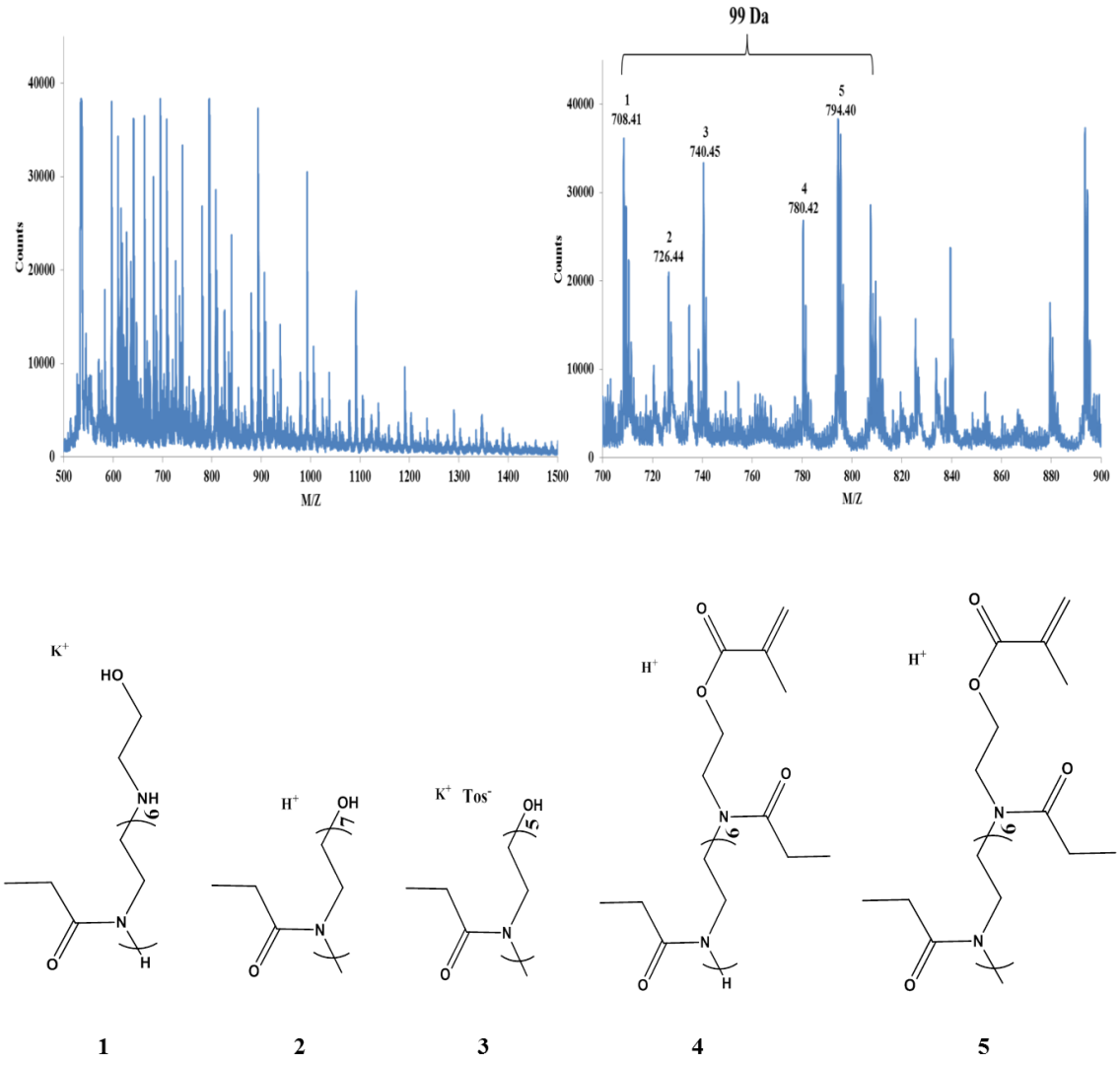

Figure 4.2 MALDI-ToF-MS of methyl oligo(EtOx) methacrylate obtained by end capping with methacrylate and initiated with methyl tosylate. (A) Full spectrum of

polymer, (B) zoom into the region m/z 700-900 and schematic representation of the proposed structures corresponding to the signals.

4.2.1.1 The impact of initiation on the control of telechelic oligo (oxazoline): Allyl p-toluenesulfonate, butenyl p-toluenesulfonate, undecenyl p-toluenesulfonate

Here we compared three different polymers. All of them have the same monomer to initiator ratio (5:1) and were terminated with methacrylate groups. These oligomers were however initiated with different tosylates: allyl tosylate, butenyl tosylate and undecenyl tosylate, respectively. The reaction temperature was 140°C, and polymerization time was 5 min, followed by end-capping reaction under 80°C overnight. After purification (extraction), all polymers were dissolved in $CDCl_3$ and then characterized by ^{1}H-NMR spectroscopy, and MALDI-ToF spectrometries were carried out with matrix dithranol.

Specific protons belonging to the different poly (2-ethyl-2-oxazoline)s obtained were highlighted in figure 4.3

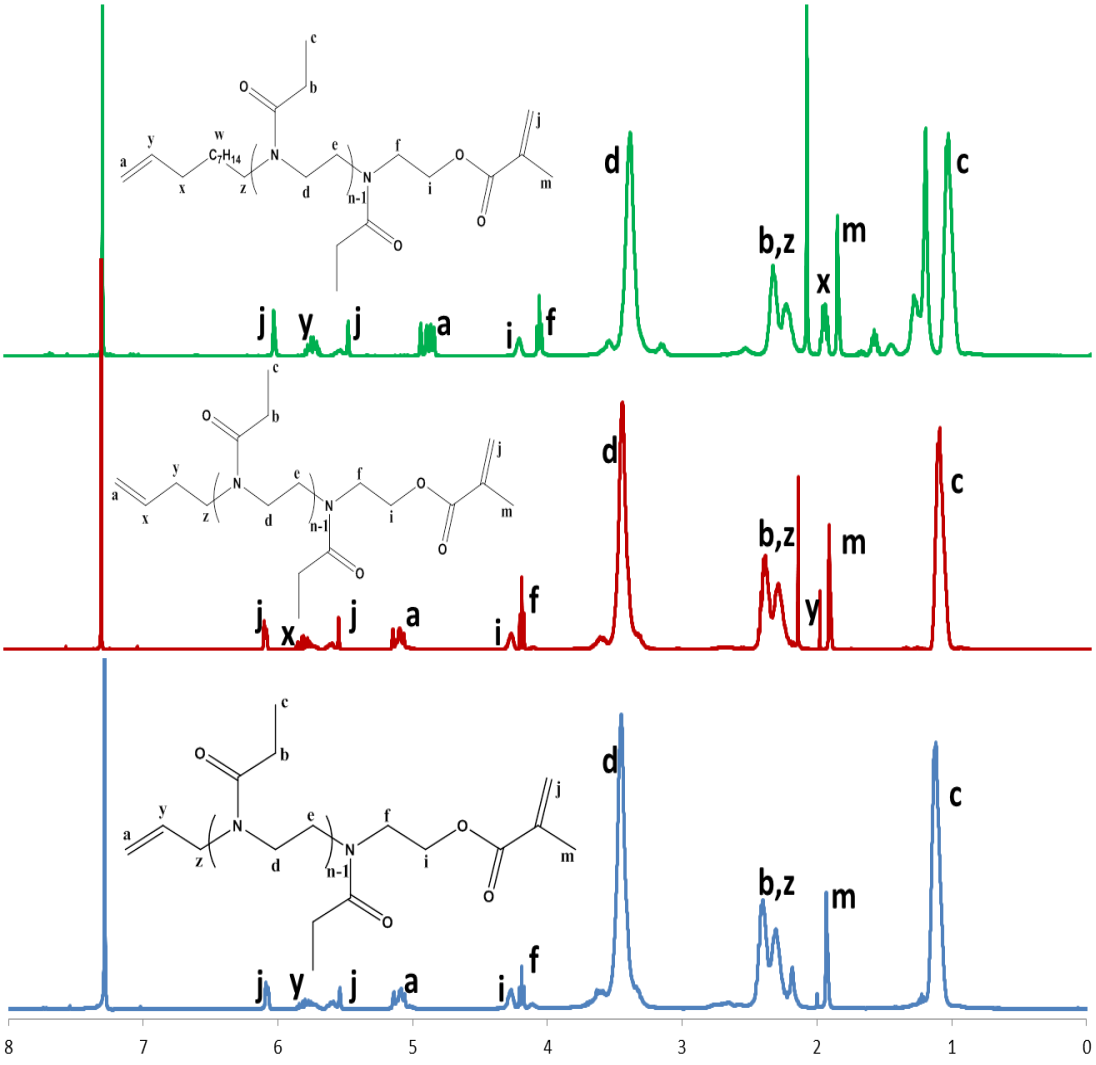

Figure 4.3 ^{1}H-NMR spectra in $CDCl_3$ of oligo (EtOx) initiated by three different and terminated with methacrylate acid. From bottom to top, blue: oligo (EtOx) initiated with allyl tosylate and end capping with methacrylate; red: oligo (EtOx) initiated with butenyl tosylate and end capping with methacrylate; green: oligo (EtOx) initiated with undecenyl tosylate and end capping with methacrylate. Monomer to initiator ratio is 5:1

Figure 4.3 presents the three ^{1}H-NMR traces corresponding to the different polymers (from bottom to top: oligo (EtOx) initiated with allyl tosylate, butenyl tosylate and undecenyl tosylate, respectively). These three polymers are all terminated with triethyl ammonium methacrylate. In general, all three polymers seem to be associated with a good control of initiation and termination, according to the ratios calculated from integrals of specific protons. For allyl tosylate initiation, the ratio of repeat units to initiator moieties H_d/H_a, was found to be slightly lower than expected, at 4.38 ± 0.08, but the ratio H_d/H_j, corresponding to termination moieties was found to be 5.08 ± 0.31, close to the monomer to initiator ratio of 5:1 used for these experiments. In agreement with the slightly lower H_d/H_a ratio than expected, the yield of polymer recovered was only 85%, although this is after purification. For butenyl tosylate initiation, comparison of H_d and H_a gave a ratio of 7.39 ± 0.37, whilst the H_d/H_j was 6.88 ± 0.10. Hence both ratios are higher than expected (monomer to initiator ratio of 5:1) and the overall yield of recovered polymer was higher (92%). Similarly, when PEtOx polymerisations were initiated with the undecenyl tosylate initiator H_d/H_a and H_d/H_j ratios were found to be 6.28 ± 0.31 and 5.13 ± 0.12, respectively with comparable yields to those observed for the butenyl initiation (Yield 93%). Overall, ^{1}H-NMR indicates a slightly uncontrolled of initiation and termination steps for the three alkene tosylate initiators, compared to methyl tosylate. However, NMR only provides an average picture of the polymer distributions and does not represent a true confirmation of the exact structure of individual polymer chains.

The synthesised oligo (oxazolines) initiated with allyl tosylate and terminated with methacrylate was characterized by MALDI-ToF first. Dithranol was used as matrix and DCM as solvent for the dissolution of the different reagents used to prepare samples for

analysis. Figure 3.4 displays a typical example of a full MALDI-ToF spectrum, showing main distributions separated by 99 Da, corresponding to the molar mass of one monomeric unit.

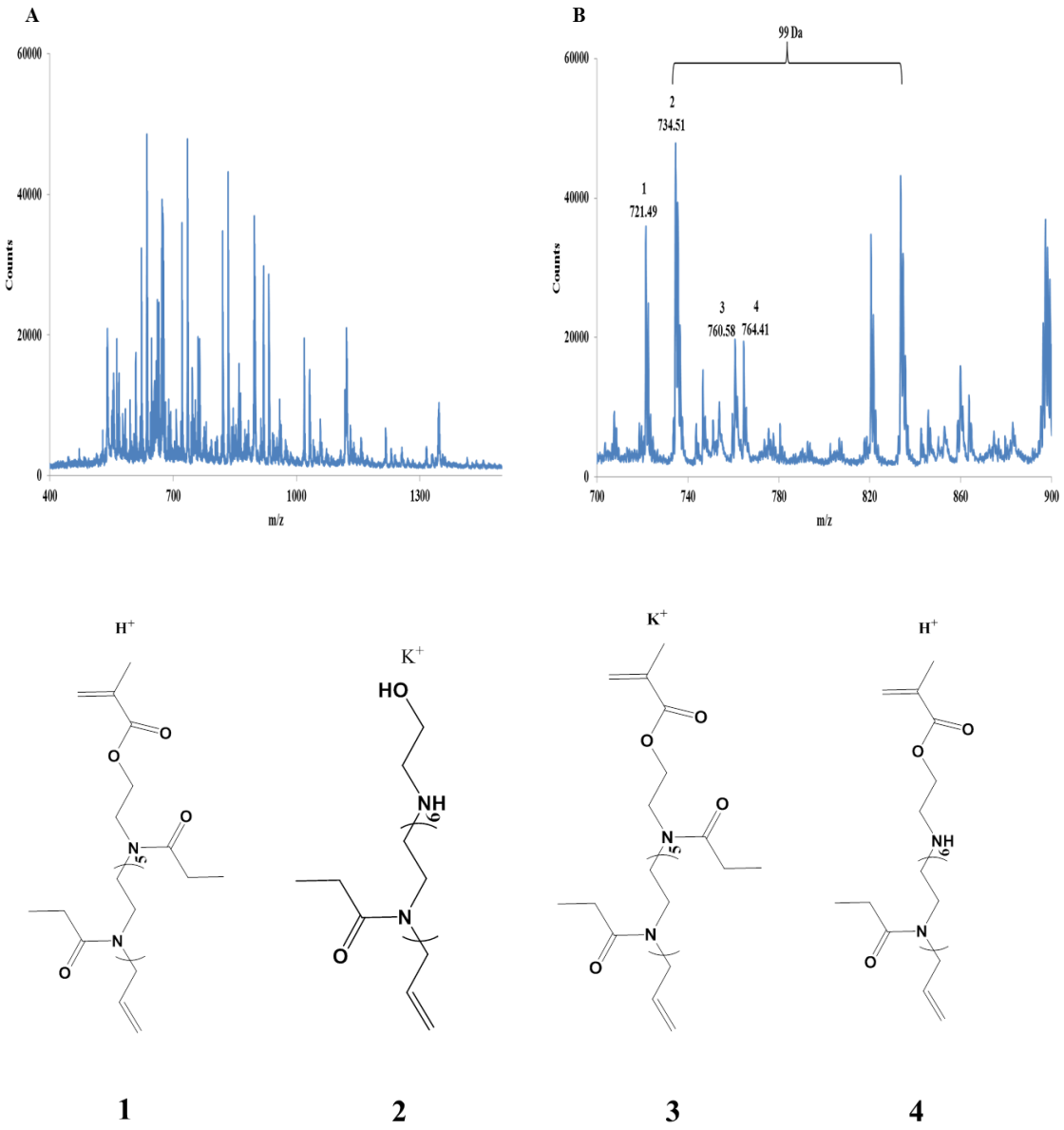

Figure 4.4 MALDI-ToF-MS of allyl oligo (EtOx) methacrylate obtained by end capping with methacrylate and initiated with allyl tosylate. (A) Full spectrum of polymer, (B) zoom into the region m/z 700-900 and schematic representation of the proposed structures corresponding to the signals.

From the full MALDI spectra we can see that a distribution of peaks with a main peak at 734.5 Da (expected 734.1) occurs for the allyl tosylate initiated oligomers but appears to be terminated with hydroxyl groups and missing one side chain, indicating some level of uncontrolled termination[216] or hydrolysis (or both). A second distribution with a main peak at 721.5 Da (expected 721.9) corresponds to the targeted structure with proton as counterions. This peak is in good agreement with NMR data as it confirms a degree of polymerisation of 6. This indicates that the degree of polymerization is indeed relatively well controlled. The molar masses of the other different peaks observed in the spectrograms, however, also indicate a mixture of methacrylate terminated chains (with various counterions) and side chain cleavage. Overall, these results contrast slightly with the NMR data obtained that had indicated a good match between the termination and initiation steps and indicate some level of hydrolysis of the oligomers, presumably during their purification (via extraction).

Similarly, oligo polyoxazoline initiated with butenyl tosylate and undecenyl tosylate and terminated with methacrylic acid were also further characterised by MALDI-ToF-MS.

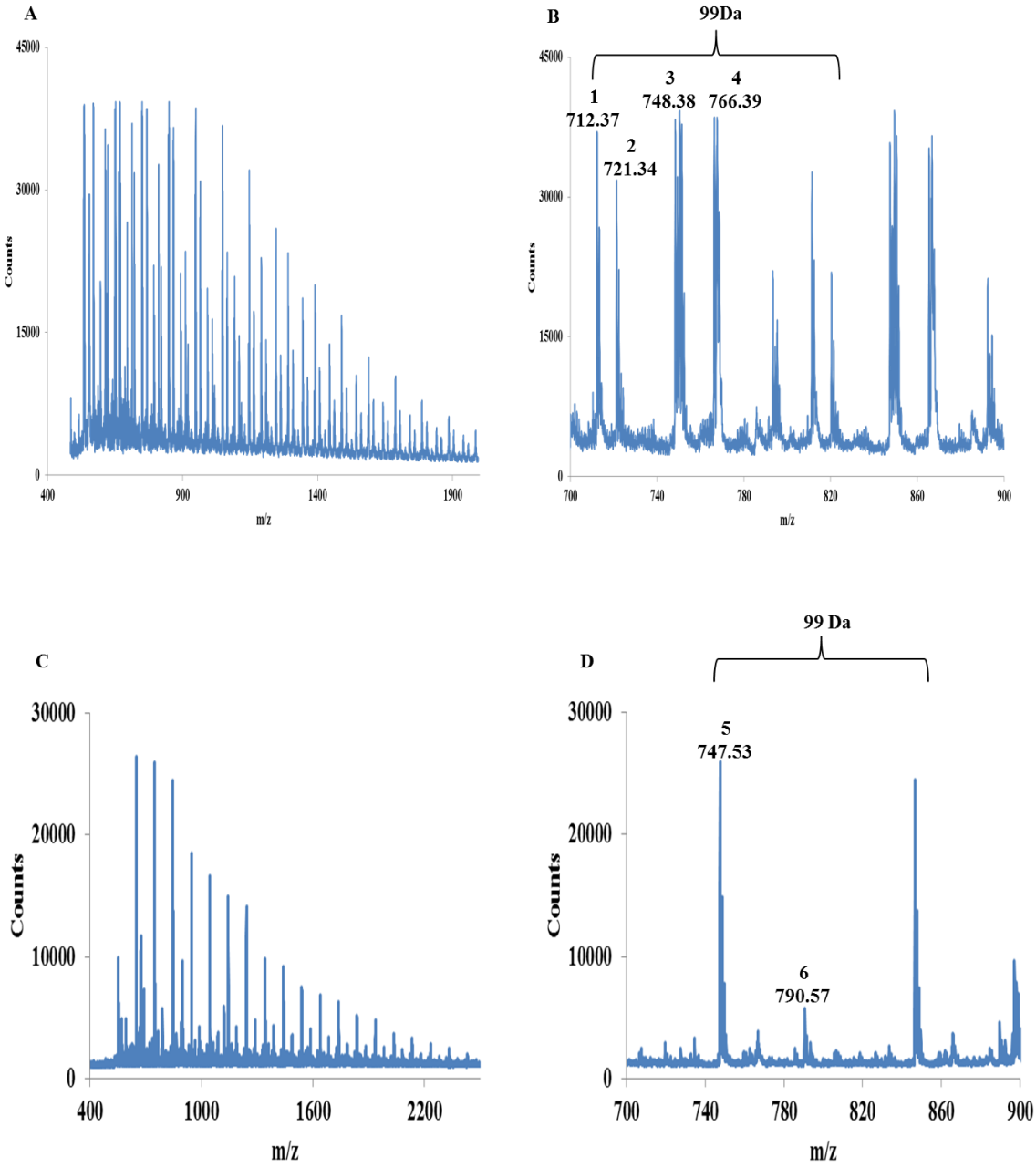
A
45000
30000
15000
0
Counts
400
900
1400
1900
m/z
B
99Da
45000
30000
15000
0
Counts
1
712.37
2
721.34
3
748.38
4
766.39
700
740
780
820
860
900
m/z
C
30000
20000
10000
0
Counts
400
1000
1600
2200
m/z
D
99 Da
30000
20000
10000
0
Counts
5
747.53
6
790.57
700
740
780
820
860
900
m/z

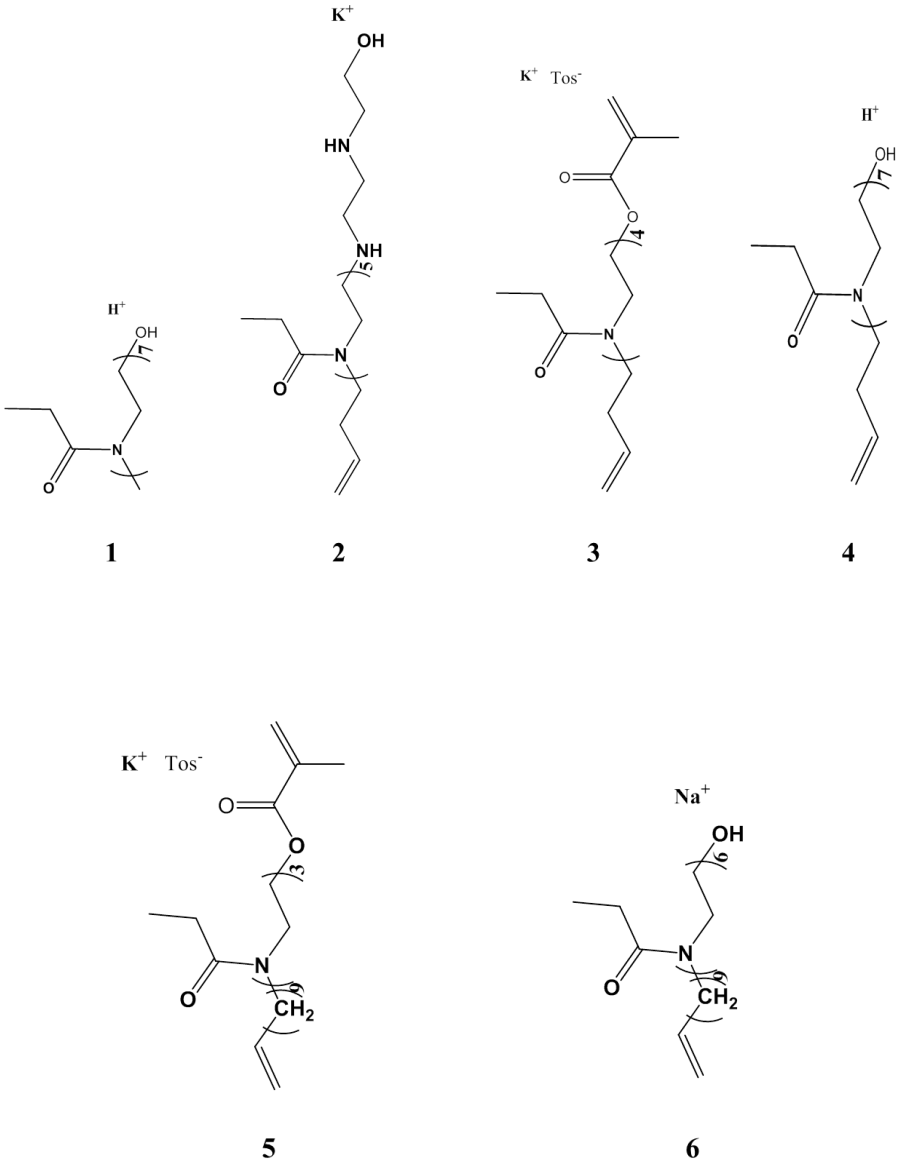

Figure 4.5 MALDI-ToF-MS of oligo(EtOx) methacrylate initiated with butenyl tosylate and undecenyl tosylate. (A) Full spectrum of Bu-PEtOxMA, (A) zoom into the region m/z 700-900 of Bu-PEtOxMA, (C) Full spectrum of Undecen-PEtOxMA, (D) zoom into the region m/z 700-900 of Undecen-PEtOxMA. Schematic representation of the proposed structures corresponding to the signals.

Apparently, peak 3 in figure 4.5 showed a distribution of peaks with a main peak at 748.4 Da (expected 747.0) occurs for the butenyl tosylate initiated oligomers and appears to be terminated with methacrylate, although with tosylate as counterions. A second distribution with a main peak at 766.4 Da (expected 767.0) corresponds to oligomers initiated with butenyl tosylate but end capping with hydroxyl. This peak is in good agreement with NMR data as it confirms a degree of polymerisation of 7. This indicates that the degree of polymerization is indeed relatively well controlled. The other two peaks 1 and 2 in figure 4.5 correspond to oligomers from side reactions[216] and some hydrolysis of lateral chain, respectively. Similarly, Oligo (EtOx) initiated with undecenyl tosylate and terminated with methacrylate acid, only one significant mass distribution was observed. Again, it seems to correspond to oligomers initiated with undecenyl tosylate and end capping with methacrylate, however, with tosylate as counterion. Hence our results contrast with those observed by NMR and indicate a poor level of control of termination events during the polymerisation of ethyl oxazoline.

4.2.1.2 The impact of termination on the control of telechelic oligo(oxazoline): H2O, 2-Bromo-2-methylpropionic acid and allylamine.

Here we compared three different polyoxazolines based on different terminate reagent. All monomer to initiator ratio keep constant at 5:1 and initiated with methyl tosylate. They are OEtOx terminated with H_2O in ice bath for 3 h and 80 °C oil bath for overnight, 2-Bromo-2-methylpropionic acid in ice bath for 3 h and allylamine at different conditions, respectively. The reaction temperature was 140°C, and polymerization time was 5 min. All of the final polymers were dissolved in $CDCl_3$ and then characterized by ^{1}H-NMR spectroscopy. For MALDI-ToF, the polymers were dissolved with dithranol in DCM.

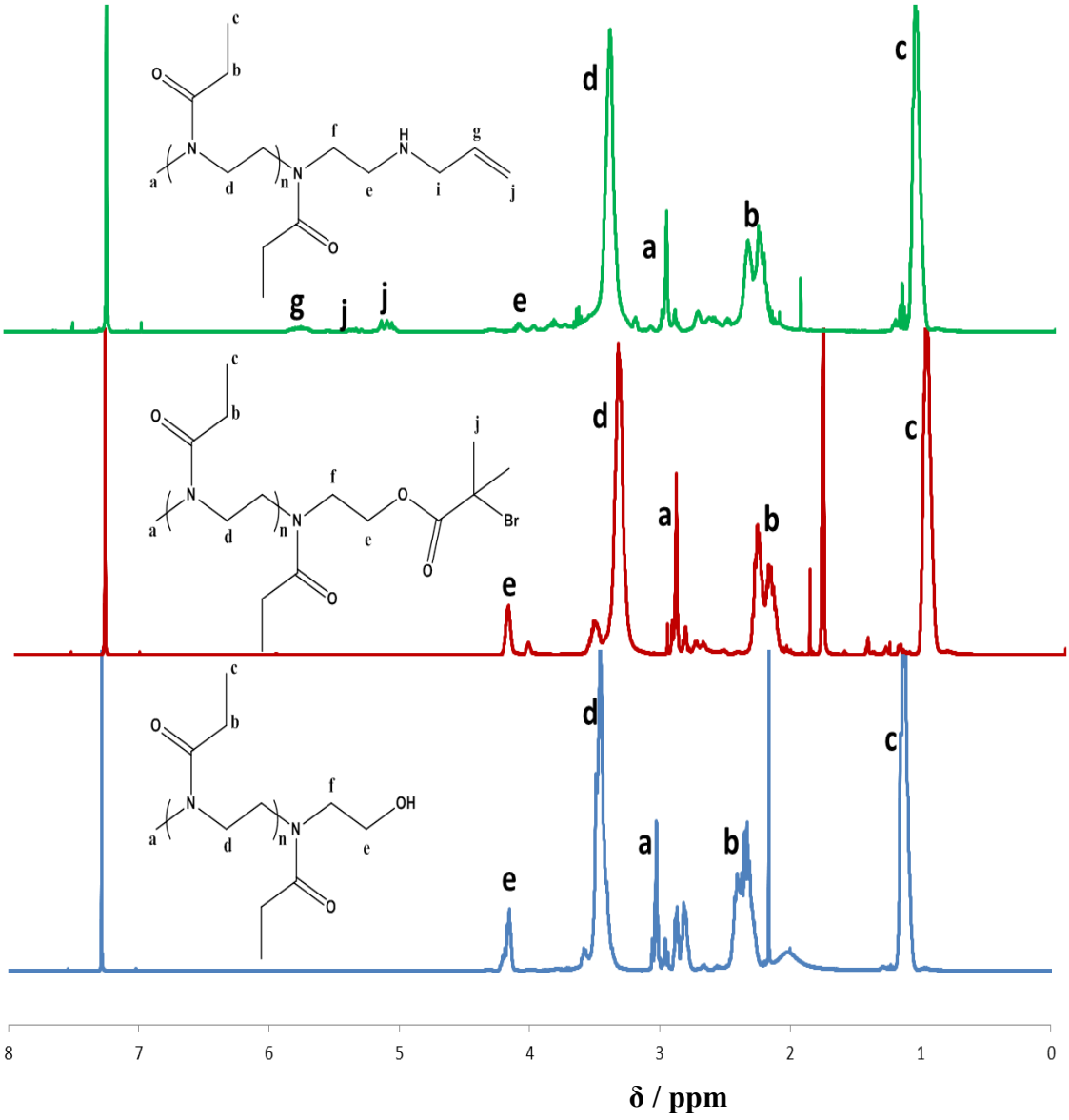

Figure 4.6 ^{1}H-NMR spectrum in $CDCl_3$ of oligo (EtOx) initiated with methyl tosylate and terminated with three different terminate reagent. From bottom to top, blue: oligo (EtOx) initiated with methyl tosylate and terminated with H_2O in ice bath; red: oligo (EtOx) initiated with methyl tosylate and terminated with 2-Bromo-2-methylpropionic acid obtained in ice bath for 3 h; green: oligo (EtOx) initiated with methyl tosylate and terminated with allylamine obtained in ice bath overnight. Monomer to initiator ratio is 5:1. All of the synthesizers were carried out by three times.

From figure 4.6 we can see specific protons belonging to the poly (2-ethyl-2-oxazoline) s are highlighted, and after assignment of every peaks to different protons belonging to poly(2-ethyl-2-oxazoline) that the expected structures were obtained. In order to investigate the nature of the end groups in the oligomers synthesised, the ratios of characteristic peaks were calculated from the corresponding integrals. Comparison between end groups and main chain protons was used to confirm the efficiency of end capping. Overall, all of these three polymers with different end capping can be relatively well controlled from ^{1}H-NMR results. For example, oligo (EtOx) initiated with methyl tosylate and terminated with allylamine in ice bath displays the characteristic ally multiplets at 5.2 ppm and 5.9 ppm. The corresponding ratios H_d/H_a is 7.72 ± 0.63 and H_d/H_j is 5.57 ± 0.23 indicate higher efficiencies of initiation than termination. In addition, both ratios are higher than the expected ratio 5:1 monomer to initiation/ termination, which may indicate incomplete initiation of the polymer chains.

In order to investigate further the end capping process, we compared end capping of POx chains with allylamine in different conditions. We observed that when end capping was carried out at 80°C overnight, NMRs indicated a poor control of termination steps and the isolated yields were generally around 47%. End capping at 80°C for 4 h in the presence of triethylamine indicated an even worse control of termination steps although yield was 45%. Moreover, without triethylamine and end capping at 80°C for 4 h, slightly better control of termination steps were observed as well as higher yield which was 52%. However, when end capping with allylamine under ice bath for 4 h, and significantly increase in allyl peaks and reasonable control of termination steps were observed although the lowest yield 36% was obtained. From calculated integrals with

lower temperature for end capping steps, we can confirm an excellent control of the end capping of oligo (EtOx) with allylamine. As can be seen in table 4.1.

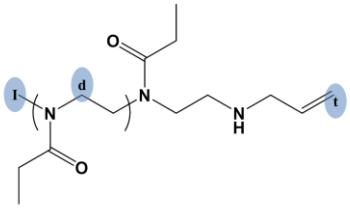

Table 4.1 Summary for oligo (EtOx) initiated with methyl tosylate and terminated with allylamine under different conditions.

	Ratio M/I	Temperature	Time/ min	H_d/H_i	H_m/H_t	H_i/H_t	Yield	Condition
Me-POx-Allylamine	**05:01**	**140**	**5**	**6.34**	**16.00**	**2.52**	**46.65%**	**80°C overnight**
Me-POx-allylamine	**05:01**	**140**	**5**	**5.57**	**7.72**	**1.39**	**36.29%**	**ice bath overnight**
Me-POx-allylamine	**05:01**	**140**	**5**	**7.93**	**46.44**	**5.86**	**44.63%**	**80°C 3-4 h TEA**
Me-POx-allylamine	**05:01**	**140**	**5**	**6.97**	**25.94**	**3.72**	**51.66%**	**80°C 3-4 h**

Oligo (EtOx) initiated with methyl tosylate and terminated with 2-Bromo-2-methylpropionic acid (in the presence of triethylamine) were analysed next. From NMR spectra we can see that H_d/H_j is 5.75 ± 0.27 and H_d/H_a is 5.57 ± 0.31, which showed both initiation and termination steps are relatively well controlled. It is also worth to note that the isolated yield is over 95%. Moreover, there is one more interesting phenomenon to report: at higher temperature (80°C) the end capping is not succeed as peaks were appeared from NMR at 5-6ppm, which correspond to alkenes. Therefore, at low temperatures for the end capping step, we observe that a successful termination of 2-Bromo-2-methylpropionic acid was obtained.

Finally, oligo(EtOx) initiated with methyl tosylate and terminated with water. The singlet H_e at 4.13 ppm was attributed to the $–CH_2$ next to the terminal hydroxyl. Here we can see that H_d/H_j is 4.63 ± 0.34 and H_d/H_a is 5.99 ± 0.53. A reverse result compared to previous studies, which shows more efficient end capping occurred than methyl tosylate initiation step. This could be due to side reactions where hydrogen initiated chains are formed[216].

The synthesized oligo (EtOx) initiated with methyl tosylate and terminated with water were characterized by MALDI-ToF, using similar conditions to those used for other POx samples. Distributions clearly displayed main peaks separated by 99 Da, again corresponding to ethyl-oxazoline repeat units (figure 4.7).

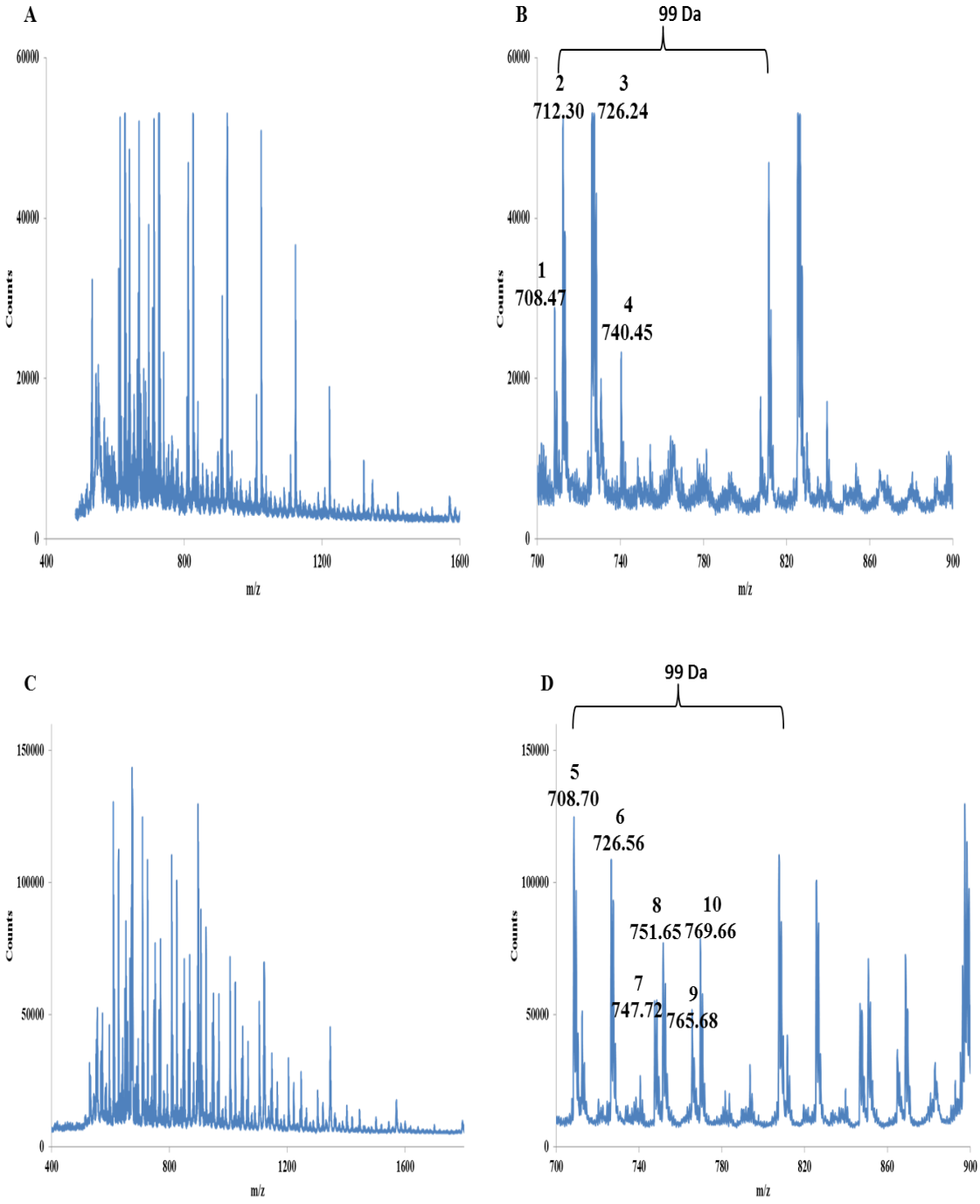
A
B
99 Da
2
712.30
3
726.24
1
708.47
4
740.45
C
D
99 Da
5
708.70
6
726.56
8
751.65
10
769.66
7
747.72
9
765.68
Counts
m/z

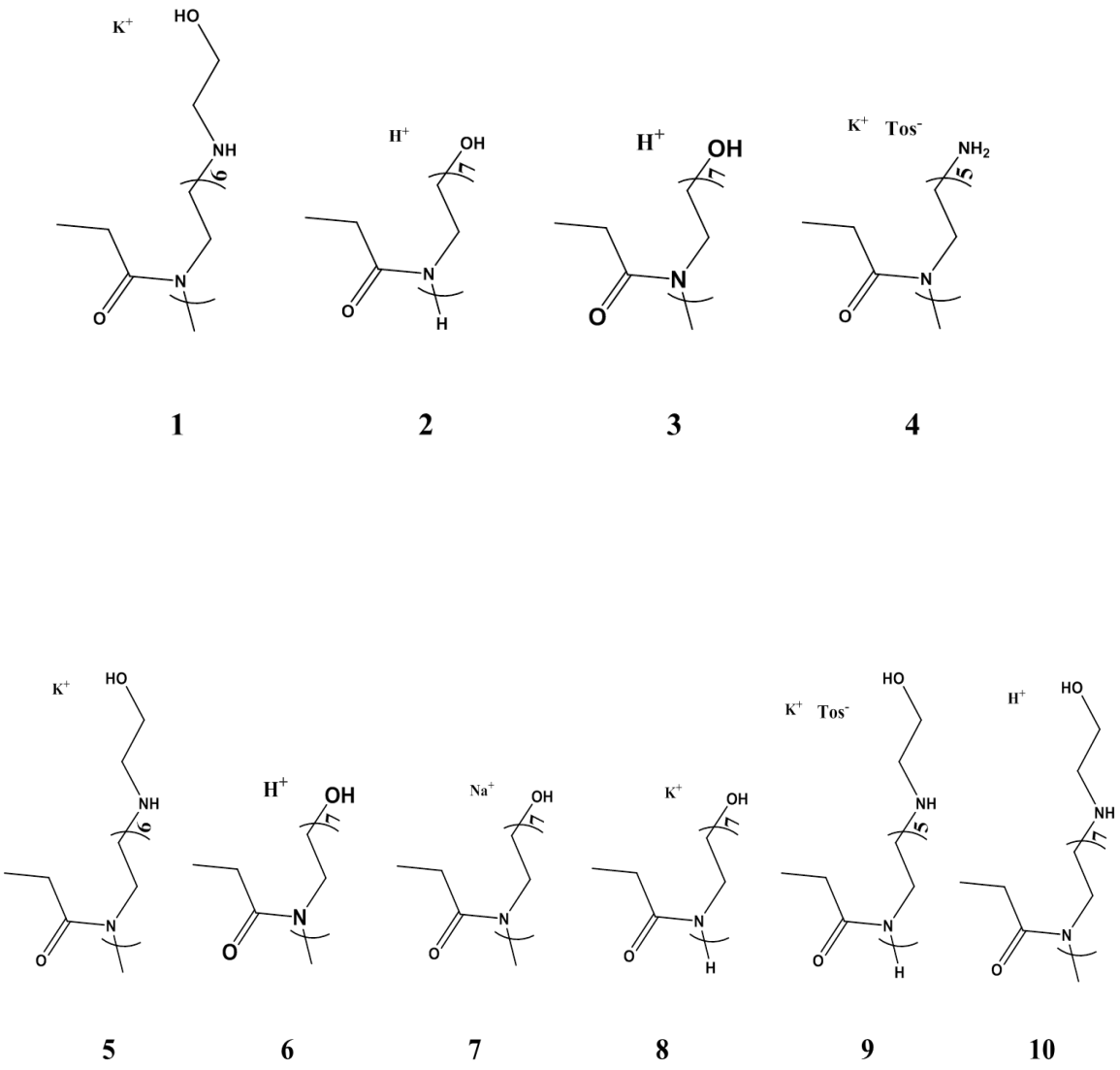

Figure 4.7 MALDI-ToF-MS of oligo (EtOx) initiated with methyl tosylate and terminated with H_2O at different conditions. (A) Full spectrum of MePEtOxOH synthesised under ice bath for 3 h, (B) zoom into the region m/z 700-900 of (A), (C) Full spectrum of MePEtOxOH synthesised under 80 °C overnight, (D) zoom into the region m/z 700-900 of (C). Schematic representation of the proposed structures corresponding to the signals.

From the spectra 4.7, there are four main peak distributions for oligomers initiated with methyl tosylate and terminated with water, and the most outstanding are two distributions: peak 2 and peak 3 from Figure 4.7. Peak 3 represent the target structure of oligo (EtOx) with methyl on the one end and hydroxyl on the other end, however, this peak is not in good agreement with NMR data as from NMR DP should be 6 while MALDI showed a degree of polymerisation of 7; a second main distribution peak 2 was contributed to oligo (EtOx) with proton on the one end and hydroxyl on the other end. The other two distributions correspond to the target POx but hydrolysis of lateral chain and with tosylate as counterions, respectively. When end capping steps at higher temperature 80°C overnight, more side reactions occurred which was confirmed by MALDI in figure 4.7D. We can see from the spectra that there are two outstanding distributions peak 5 and peak 6 in figure 4.7; peak 6 is target chemical structure while peak 5 arises from hydrolysed lateral chain of target structure. The molar masses of the other different peaks observed in the spectrograms, however, also indicate a mixture of proton terminated chains (with various counterions) and side chain cleavage. However, both of these two conditions result in high yields. Hence our results slightly contrast with those observed by NMR and indicate a better control of termination with water but at lower temperature during the polymerisation of ethyl oxazoline.

Synthesized oligo (EtOx) initiated with methyl tosylate and end-capped with allylamine and 2-Bromo-2-methylpropionic acid were also characterised by MALDI-ToF-MS to further verify the structures obtained.

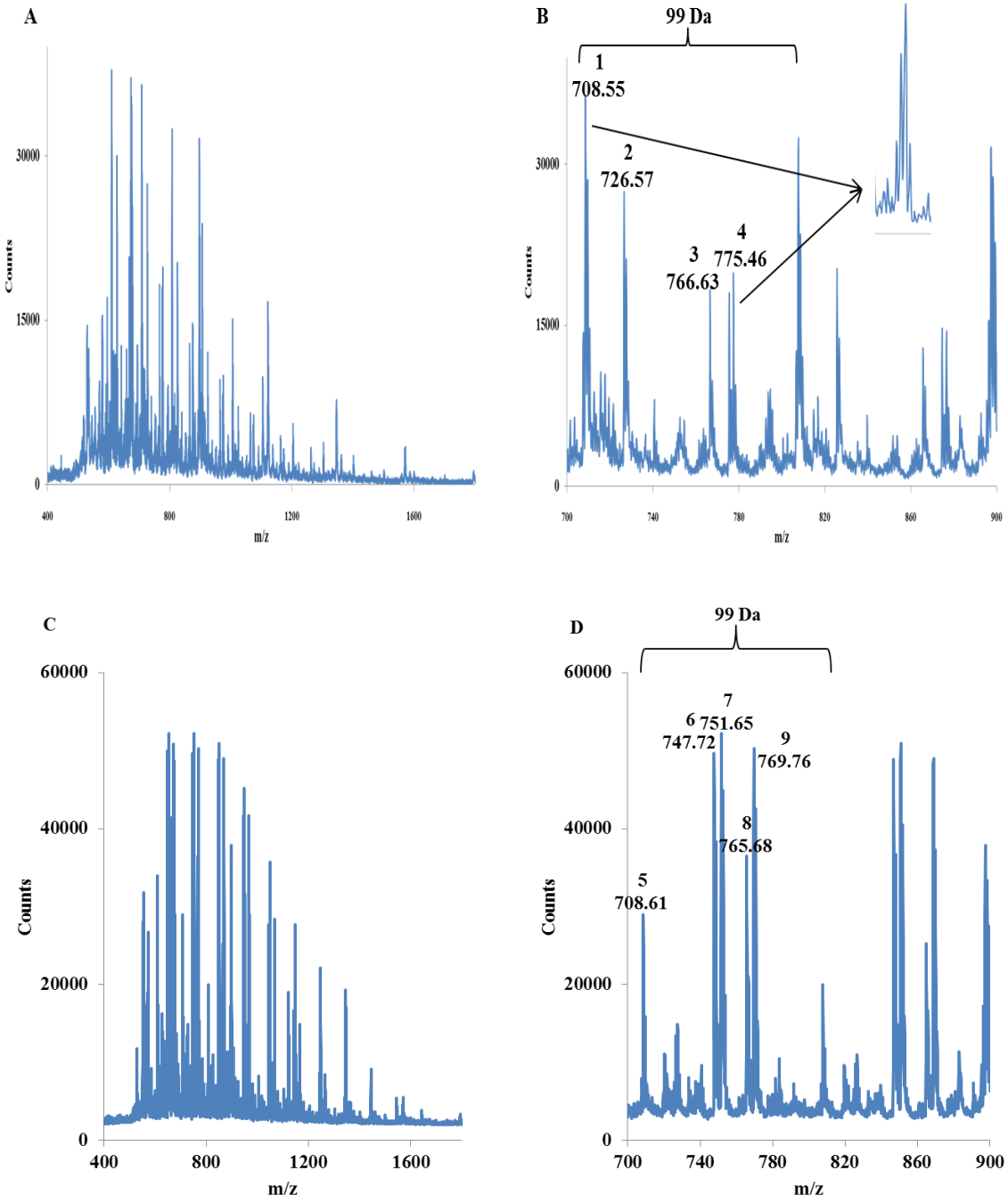
A
30000
15000
0
Counts
400
800
1200
1600
m/z
B
99 Da
1
708.55
2
726.57
3
766.63
4
775.46
30000
15000
0
Counts
700
740
780
820
860
900
m/z
C
60000
40000
20000
0
Counts
400
800
1200
1600
m/z
D
99 Da
60000
40000
20000
0
Counts
5
708.61
6
747.72
7
751.65
8
765.68
9
769.76
700
740
780
820
860
900
m/z

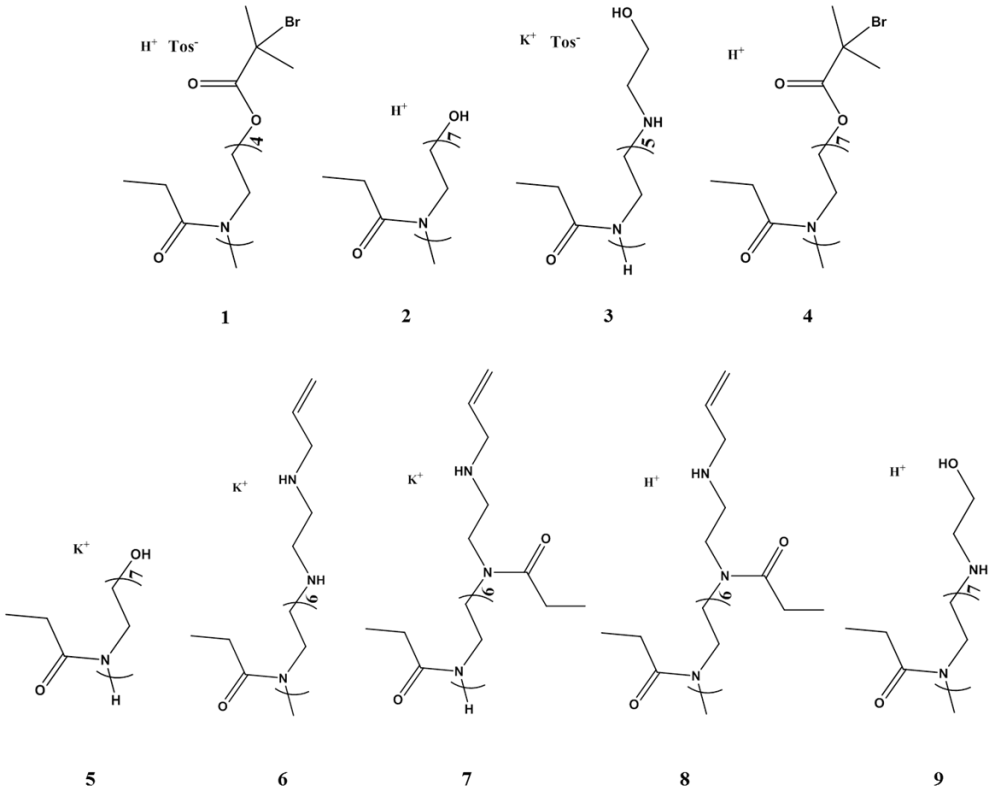

Figure 4.8 MALDI-TOF-MS of oligo(EtOx) initiated with methyl tosylate and terminated with 2-Bromo-2-methylpropionic acid and allylamine. (A) zoom into the region m/z 700-900 of Me-PEtOx-bromo (B) zoom into the region m/z 700-900 of me-PEtOx-allylamine. Schematic representation of the proposed structures corresponding to the signals.

According to the MALDI-ToF spectrograms presented in Figure 4.8A, several significant distributions are observed, displaying typical doublets associated with bromide-containing compounds (and separated by 3 Da although expected difference should be 2 Da). Peaks 1 and peak 4 is definitely end-capped with bromo acid as strong quarter peaks were appeared. However, peak 2 and peak 3 were contributed to side

reactions by-product. Eventually, oligo (PEtOx) end-capped with allylamine obtained more by-products from MALDI spectra. Peak 6, peak 7 and peak 8 were assigned to the right compound oligo (PEtOx) end-capped with allylamine. However, peak 6 was hydrolysed product. All other appeared structures were contributed to by-products from side reactions. Altogether, we propose MALDI-ToF-MS can show the possible structure of polymers but may not be accurate to determine the quantity of possible polymers.

4.2.2 Synthesis of copolymers of oxazoline derivatives

A number of studies have investigated the hydrolysis of poly(oxazoline)s. In 2005, Sung et al investigated two triblock copolymers and found PEI-PEG-PEI 4000-3400-4000 by hydrolysed PMeOx under 3 M HCl showed comparable transfection efficiency to branched PEI 25,000. Importantly, no inhibitive effect was found when serum was added to the transfection medium, which makes it more attractive than branched linear high molecular weight of PEI as less cytotoxicity for gene delivery systems[216]. Hoogenboom et al tried to hydrolysis poly (2-ethyl-2-oxazoline) and after 1 h at 270°C the polymer started degrading, highlighting the difficulty of hydrolysing PEtOx in neutral conditions. In addition, they varied the concentration of HCl and the reaction temperature and found that even at low concentrations of acid, higher temperature up to 180°C with microwave in sealed flasks can accelerate the hydrolysis rate[217]. Kronek and colleagues have studied partially hydrolysed PEtOx with different molar mass as well as degree of hydrolysis showed different cytotoxicity on three different cell lines. Importantly, fibroblasts showed the highest tolerance and higher molar mass copolymers showed sever toxicity on cell viability[218]. Similar result has been found by Hoogenboom et al as well[219].

2-(3-butenyl)-2-oxazoline was reported to be synthesised by three steps: starting from 4-pentenoic acid to N-(2-chlorethyl)-4-pentenamide, and then to 2-(3-butenyl)-2-oxazoline[210]. However, it took at least three days and the yield is around 50%. Moreover, the starting material 4-pentenoic acid is not a cheap material. Therefore, Schubert and colleagues investigated a method named "the modified α-deprotonation" to synthesise 2-(3-butenyl)-2-oxazoline in a simple way and only via one pot (two steps), while reasonable yields of this product was obtained[210].

Thus, we explored the use of macroinitiators PEG-di-tosylate for PEtOx to generate block copolymers in which PEtOx can be converted to PEI. Two target molecular weights of copolymers of POx-PEG-POx 3395-3400-3395 g/mol and 1377-3400-1377 g/mol were investigated. Moreover, 0.5 M HCl was applied to partially hydrolysed POx to PEI. In addition, we investigated the synthesis of monomer 2-(3-butenyl)-2-oxazoline by "the modified α-deprotonation" method, for subsequent copolymer synthesis. The scheme was shown in scheme 4.3.

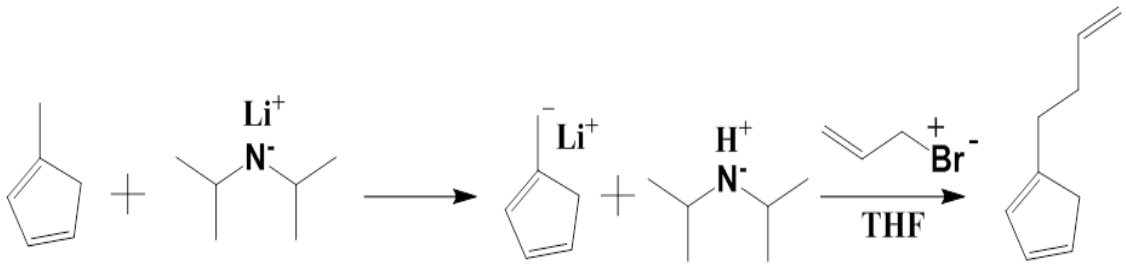

Scheme 4.3 Synthesis of ButNOx in a new α-deprotonation method

4.2.3 Synthesis of POx-PEG-POx and acid hydrolysis of POx-PEG-POx

Two different molecular weights of three block copolymer POx-PEG-POx were prepared via oligo (EtOx) initiated with PEG-di-tosylate at 160 °C for 10 min under

microwave assisted synthesizer. Furthermore, POx-PEG-POx was hydrolysed under 0.5 M HCl acid at room temperature for overnight.

All of the polymers were dissolved in D_2O and the chemical structure of the block copolymer synthesised before and after hydrolysis with different ratios of PEG and POx was characterised by ^{1}H-NMR spectroscopy to confirm the chemical structure of copolymer POx-PEG-POx and hydrolysed copolymer PEI-PEG-PEI.

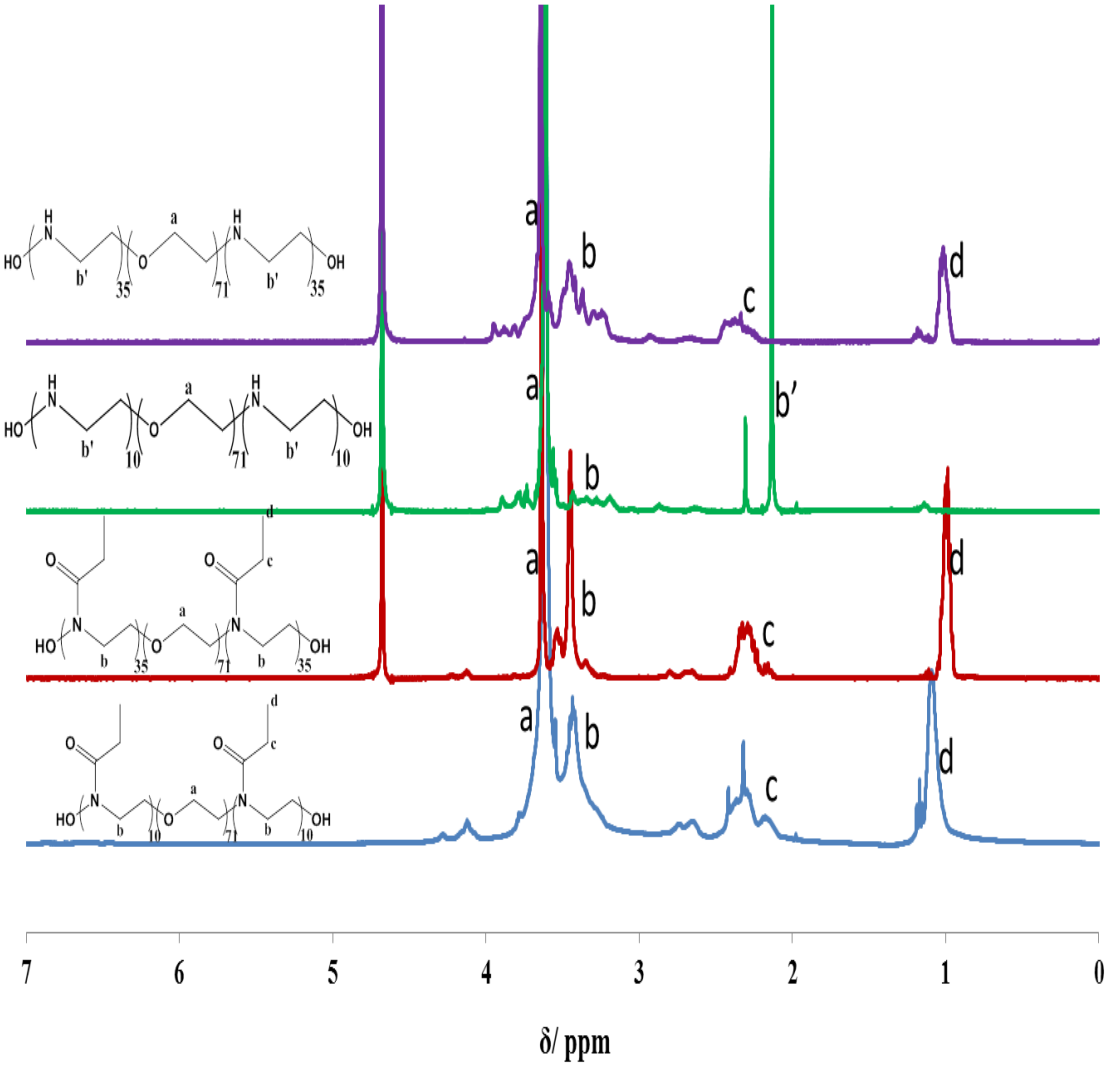

Figure 4.9 ^{1}H-NMR spectrum in D_2O of copolymer POx-PEG-POx and hydrolysed copolymer PEI-PEG-PEI. From top to bottom, purple: hydrolysed copolymer PEI-PEG-

PEI 35:1; green: hydrolysed copolymer PEI-PEG-PEI 10:1; red: copolymer POx-PEG-POx 35:1; blue: copolymer POX-PEG-POX 10:1.

From the ^{1}H-NMR spectra (figure 4.9), we can see the comparison between the four traces corresponding to the two different triblock copolymers POx-PEG-POx 10:1:10 and 35:1:35 before and after hydrolysis. Each peak was assigned to specific protons and the structure of each polymer was confirmed (see figure 4.9). The content of the different monomers, POx to PEG ratio, can be calculated from the integrals in the ^{1}H-NMR graphs. All of these four polymers showed a strong peak at 3.63 ppm, which represents the protons from the PEG backbone, and a peak at 3.47 ppm corresponding to methylene protons from POx main chain. On the basis of the ratio of the integrals of the signals 3.63 and 3.47, for target ratio 10:1:10, the number average molecular weights of the three triblock can be calculated to be 485-3400-485 g/mol, which is only half of the target 970-3400-970 g/mol. Similarly, the ratios of the integrals of those two signals indicated that for target ratio 35:1:35 (3395-3400-3395 g/mol) triblock copolymer has an average molecular weight of 1377-3400-1377 g/mol, which was half of the target molecular weight. A significantly decreased integral can be seen at peak 3.47 ppm for hydrolysed copolymers compared to the starting copolymer POx-PEG-POx. The peak at 2.7 ppm was assigned to the ethylenimine unit (-NH-) and a signal at 1.0 ppm was contributed to CH_3 group from lateral chain of POx. Especially, it should be noted that a small peak at 1.00, which could be attributed to residual acetyl groups, is also present. For POx-PEG-POx 10:1:10, it is estimated that the relative integrals at 1.00 and 3.63 that 89% of the acetyl groups have been removed. Similarly, PEI-PEG-PEI 35:1:35 showed decreased integrals for lateral chain comparing to starting POx-PEG-POx (75% of the acetyl groups have been removed).

Moreover, we characterized POx-PEG-POx (485-3400-485 g/mol) and POx-PEG-POx (1377-3400-1377 g/mol) with GPC, to verify the polydispersity as well as the molecular weight. However, POx-PEG-POx (485-3400-485 g/mol) was not soluble in DMF therefore no data was obtained.

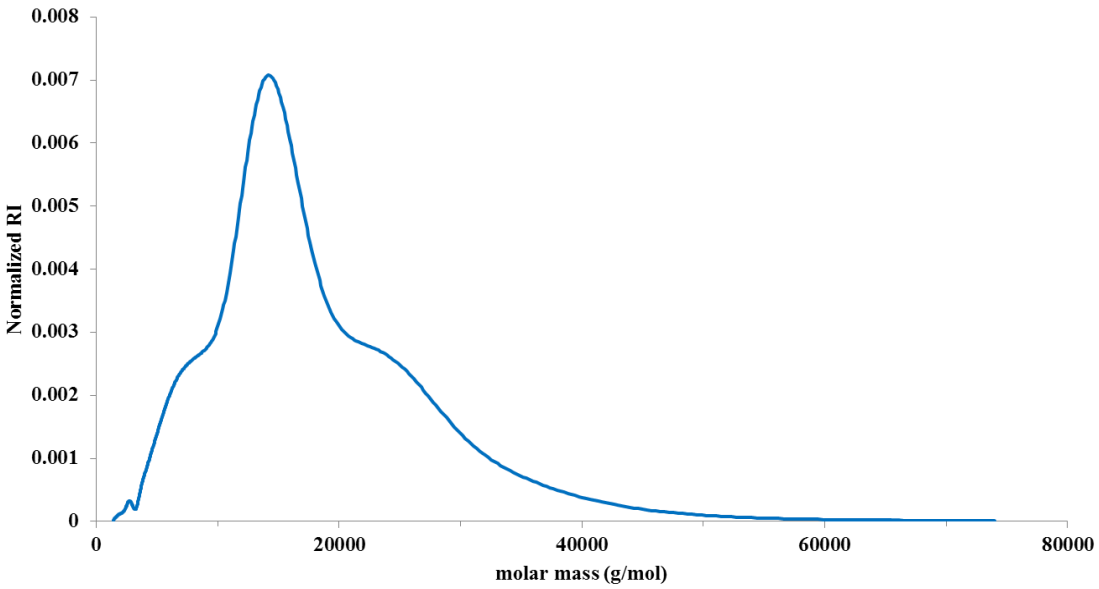

Figure 4.10 GPC chromatogram of the triblock copolymer of POx-PEG-POx (3395-3400-3395) in DMF.

Table 4.2 The triblock copolymer POx-PEG-POx (1377-3400-1377 g/mol) composition determined by GPC and NMR.

	GPC			NMR
Mw/ Mn	Mw	Mn	PD	Mn
1.4	13972	9973	1.40	6154

It is clear to see from GPC, polydispersity of 1.40 was obtained, however, we did not see any shoulder around 3400 g/mol that belongs to starting material PEG di-tosylate. It may indicate the successful initiation step was obtained and a full conversion initiated

by PEG di-tosylate. However, compared to Mn obtained from NMR, a much higher molecular weight was obtained and closer to target 10200 g/mol with 35 unit repeat on each arm.

After characterized with GPC and NMR, the chemical structure of the block copolymer synthesised before and after hydrolysis with different ratios of PEG and POx was characterised via Fourier Transformed Infrared spectroscopy (FTIR) and the results are shown in Figure 4.11 All of the polymers have been kept in high vacuum overnight to remove any residue of solvent introduced during the synthesis.

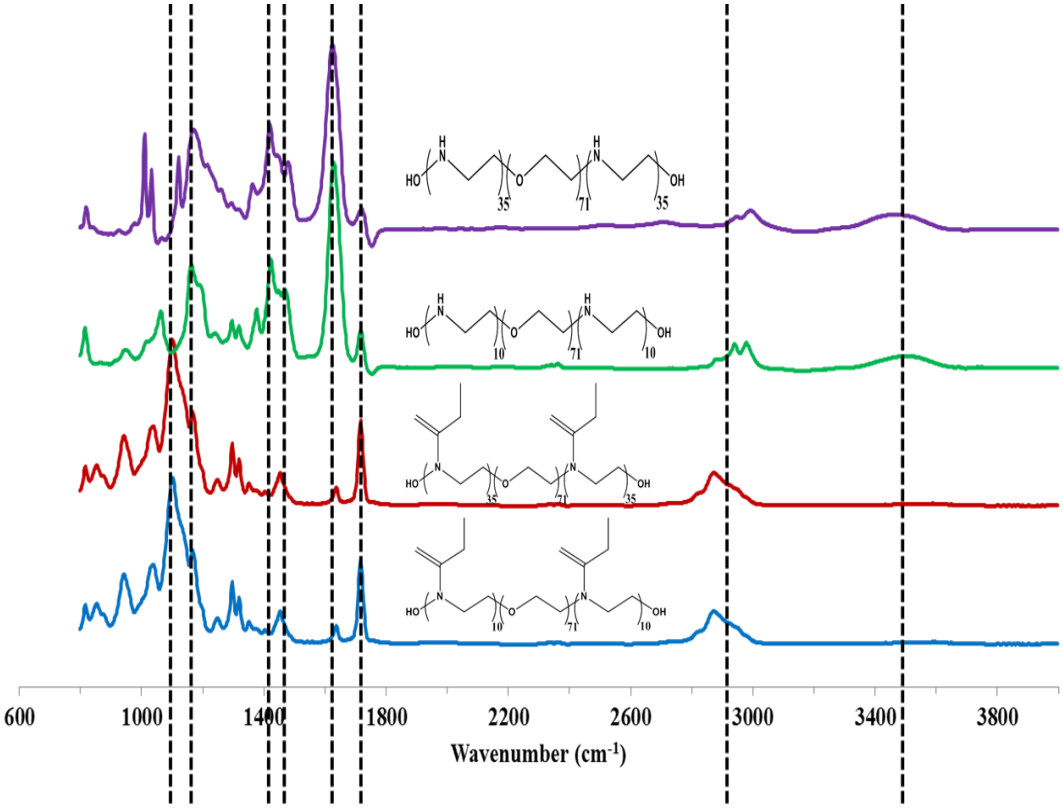

Figure 4.11 The FTIR spectra of copolymer POx-PEG-POx and hydrolysed copolymer PEI-PEG-PEI. blue: copolymer POx-PEG-POx 10:1; red: copolymer POx-PEG-POx 35:1; green: hydrolysed copolymer PEI-PEG-PEI 10:1; purple: hydrolysed copolymer PEI-PEG-PEI 35:1.

Characteristic peaks of pure block copolymers showed some strong absorption bands at 3020-2820 cm^{-1} (stretching vibrations of C-H), 1710-1720 cm^{-1} (stretching vibrations of C=O) and also displayed a distinct peak at 1100 cm^{-1}(stretching vibrations of C-H_2). However, hydrolysed block copolymers PEI-PEG-PEI showed a new strong band at 3650 - 3200 cm^{-1} (stretching vibration N–H), and bands at 3050–2830 cm^{-1} (stretching vibration C–H) was contributed to PEG main chain, however, it shifted a little bit when acid hydrolysis was applied as a result of acetyl groups cleaved, and bands near 1710-1720 cm^{-1} (stretching vibrations of C=O) decreased significantly as a result of cleavage of acetyl groups. Furthermore, a new strong peak at 1654 cm^{-1} (bending vibration N–H) was contributed by secondary amines and further confirmed a successful hydrolysis of the amide side chains, as well as peak at 1465 cm^{-1} (bending vibration C–H). From the FTIR spectra we can see that only the POx units have not fully hydrolysed, because we can still see peaks around 1720 cm^{-1}, although small. The degree of hydrolysis was caculated from ^{1}H-NMR, which will be presented later on.

4.2.4 Copolymer of butenyl and methyl/ethyl oxazoline

4.2.4.1 Synthesis of monomer butenyl oxazoline

Schlaad et al[210] developed an approach to synthesise ButNOx monomer starting from 4-pentenoic acid. N-(3-(dimethylamino)propyl)-N'-ethylcarbodiimide hydrochloride (EDC) and N-hydroxysuccinimide were used to couple it to 1-chloro-2-aminoethane and then intensive purification was applied. To overcome those limitations, the modified α-deprotonation method was described by Schubert[220]. Cheaper starting materials have been used and fewer steps were required for its synthesis. We used this approach to synthesise this monomer, which afforded the desired product in 43% yield. Characterisation is presented in Figures 3.12. Compared to the previous approach

developed in our group (yield 49%), this led to comparable in yield but significantly reduced the cost of reagents. The monomer ButNOx was dissolved in $CDCl_3$ and then characterized by ^{1}H-NMR spectroscopy to confirm the structure.

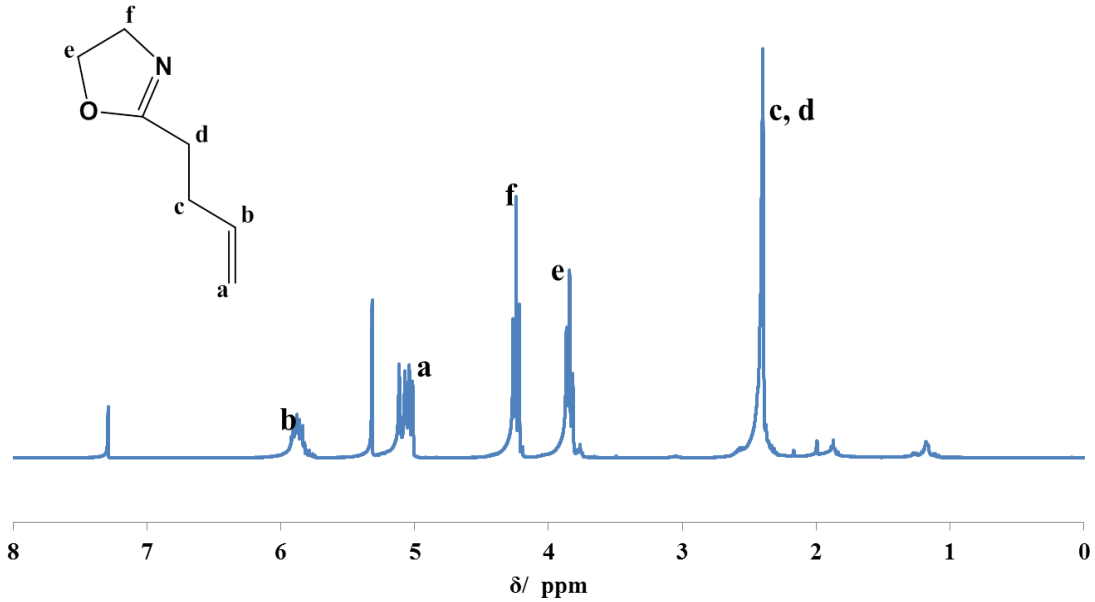

Figure 4.12 ^{1}H-NMR spectrum in $CDCl_3$ of monomer ButNOx

From the NMR graph, every peak was assigned to different protons which belongs to the 2-(3-butenyl)-2-oxazoline. The ratios were calculated from the integrals and allow the comparison of specific peaks on 2-(3-butenyl)-2-oxazoline and confirmation of the expected structure. This data is in good agreement with characterisation reported in the literature[136]. Peaks at 5.8 ppm and 5.2 ppm were assigned to alkenes on the lateral chain. Peaks at 3.9 ppm and 4.2 ppm were contributed to protons H_e and H_f. According to H_a/H_f, the actual ratio between alkene groups to protons on the oxazoline ring is precisely 1:1. A strong peak at 2.5 ppm was assigned to H_d showed that monomer 2-(3-butenyl)-2-oxazoline was obtained. (Yield is 43% after purification)

4.2.4.2 Synthesis of copolymer Bu-PEtOx and Bu-PMeOx polyoxazoline

Monomers ButNOx and MeOx (or EtOx) (40:100, n/n) were mixed together before initiated with methyl tosylate in acetonitrile at 160 °C, reactions were occurred in microwave synthesizer and target degree of polymerization were 200. Subsequently, water was quenched to the end to terminate polymerization. Copolymers BuPEtOxOH was dissolevd in $CDCl_3$ and BuPMeOxOH was dissolved in D_2O and characterised by ^{1}H-NMR to confirm the final structure.

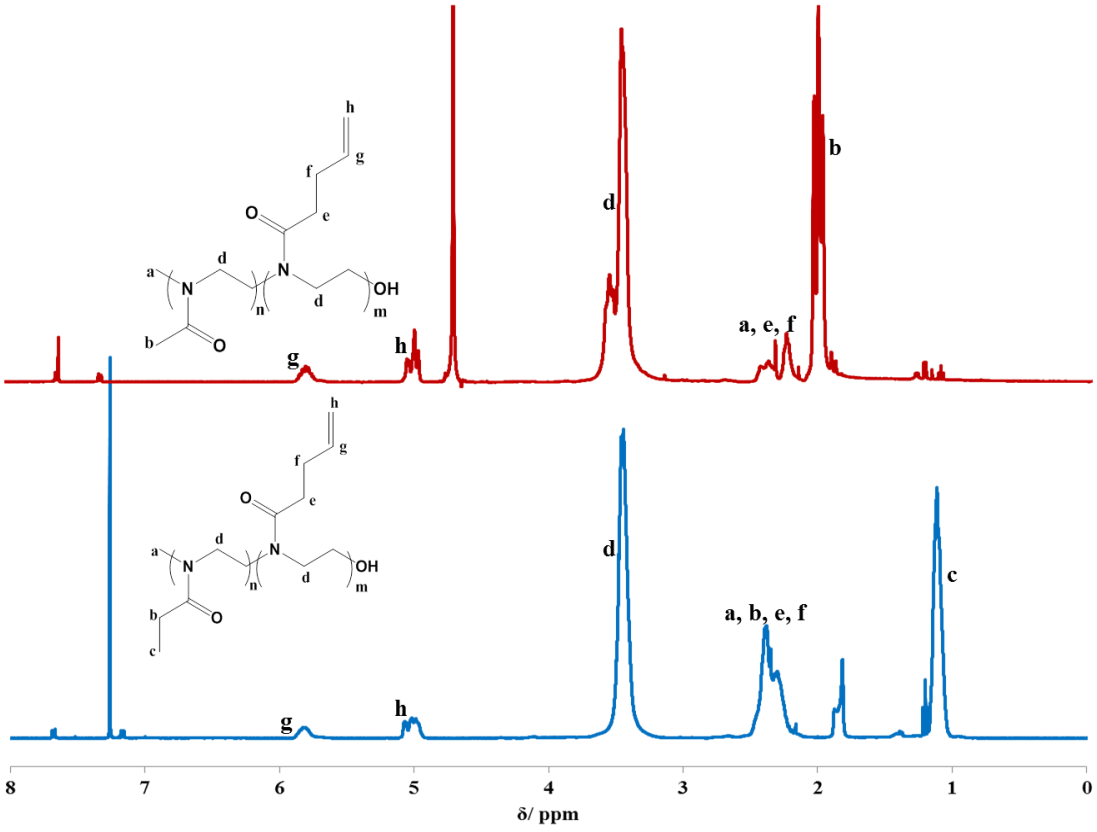

Figure 4.13 ^{1}H-NMR of copolymer BuPEtOxOH in $CDCl_3$ and BuPMeOxOH in D_2O

From the ^{1}H-NMR spectra, each peak corresponding to a specific proton in the copolymer structure has been assigned as detailed in figure 4.13. Peaks at 4.8 ppm and 5.8 ppm were assigned to alkenes from butenyl oxazoline for both of the copolymers.

By comparing the integrals of different specific protons we can confirm the percentage of alkene in the copolymers. For example, from copolymer BuPEtOxOH, the number of $H_h/(H_c+H_h)$ gives the percentage of alkene in the whole copolymer which is the same percentage of butenyl oxazoline in the copolymer. Here, for both copolymers the percentages of alkene are 15%. The total degree of polymerization was 148 for BuPMeOxOH.

4.3 Conclusions

So far, we have successfully controlled the initiation of short polyoxazolines. Investigating the control of the polymerisation with four different initiators and four different terminating agents, we observed that full control of the molecular structure of polyoxazolines was relatively difficult. Although initiation was found to be relatively efficient when initiated by methyl and ally tosylates, termination was found to be harder to control. For example, when oligo (EtOx) initiated with methyl tosylate and terminated with methacrylate, Schubert and colleagues found only one distribution for the target structure, however, in our study, we found relatively higher content of hydroxyl end group was obtained[45]. Similar result when allyl tosylate as initiator. But MALDI-ToF data showed significant capping of intermediates when using longer alkene initiators as well as terminate with bromoisobutyric acid, which may indicate weak nucleophiles were used resulted in by-product. No surprising that considering NMR results, which showed good agreement between initiator and terminating groups. Importantly, our efforts to end-cap POx at low temperature with different termination reagent identified that such milder conditions could improve significantly the control of termination steps. For example, allylamine and bromoisobutyric acid can only efficiently capping POx chains at low temperatures. Similarly, fewer side reactions

occurred when end-capping POx with water at low temperature. Moreover, except for end-capping POx with allylamine (36%), other functionalized POx all obtained high yield (>90%). However, overall our data suggests that oxazoline polymerisations only seem to confer a modest control of end groups, in a limited number of cases. This will limit the usefulness of polyoxazolines for the synthesis of defined telechelic POx substitutes.

However, compared to PEG polymerisation, copolymers of conventional oxazoline monomers (e.g. methyl and ethyl side chains) displayed interesting features. Triblock copolymers POx-PEG-POx were easily prepared from the corresponding PEG tosylate and acid hydrolysis of the resulting copolymers allowed hydrolysed PEI-PEG-PEI to be prepared. In addition, functionalities can be relatively easily introduced in the side chain of poly(oxazoline) copolymers, for example via alkene-functionalised POx copolymers. A time saving and cost effective method to obtain monomer 2-(3-butenyl)-2-oxazoline was used to synthesise an alkene functionalised oxazoline monomer which is in coincidence with the result from Dargaville's study[136]. Two promising copolymers that contain 15% alkene side chains were obtained for application in the design of hydrogels in chapter 6.

Chapter 5

Anti-fouling surface based on polyoxazoline methacrylate polymer brushes

5.1 The design of protein-resistant polymer brushes for biomedical applications

The quality and reproducibility of raw materials as well as the materials themselves play a pivotal role in cell culture systems. Currently functionalised polystyrene is used as plastic ware in tissue culture, however, the hydrophobic surface refuses cell adhesion; hence the need for a functionalized polystyrene surface that is hydrophilic and which allows protein adsorption so cell adhesion can be carried out via integrin binding. Proteins coming from biological sources always show variation from batch to batch, thus the production of synthetic surfaces with high reproducibility and biocompatibility for in vitro cell culture offers many advantages for obtaining adherent cells[221].

Modifying the surface with ultra-polymer brushes via controlled polymerization ATRP has been widely used and allows the surface to tailor functional groups. A variety of synthetic polymers as well as mechanical and chemical robustness make polymer brushes advantageous over other surface modification methods[111]. The synthesis of initiators for the surface initiation process is easier than free radical and NMP polymerizations, which require AIBN-silane derivatives or the nitroxide silane derivatives. In general, the process of ATRP is controlled with reversible activation-deactivation between the growing polymer chain and a copper-ligand species[111].

In terms of interaction of protein and polymer brushes, there are two adsorption mechanisms: one is primary adsorption at the surface as a result of the surface-protein attraction, and the second is ternary adsorption within the brush due to weak PEG-

protein attraction. Moreover, there is a combined mode of description for this system: the protein can attach on the surface while protruding out of the surface[222].

A hypothesized model of protein resistance on PEG surfaces was drawn up by Jeon and colleagues. From figure 5.1 we can see sandwiched PEG brushes in the middle of the protein water layer and hydrophobic substrate. The model proposes that the removal of water from hydrated polymer chains creates an osmotic penalty which further results in a repulsive force. The surface density as well as the chain length of PEG determines the magnitude of that force. It follows that, increasing the surface density as well as chain length may result in lower protein adsorption[223].

By modelling proteins as finite spherical particles Gennes et al. suggest that with the same surface density, increasing chain length can efficiently improve non-fouling properties[223].

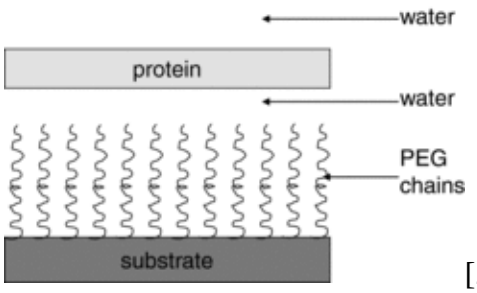

[223]

Figure 5.1 Model diagram showing a protein of infinite size in water with a solid substrate having terminally attached PEG chains.

Protein adsorption is related to the degree of polymerization for PEG brushes. With low *N*, for example, $N \leq 150$, the surfaces of PEG brushes are less adsorbing[224-226].

Dick and colleagues have found that PEO layers with an adverse grafting density (area per grafted PEO chain) which is less than the dimensions of the protein molecules

showed the best non-fouling properties although in some case protein can penetrate into the brush. By contrast, thinner brushes with adverse grafting density which is more than the dimensions of the protein molecules displayed increased protein adsorption. Moreover, with the same grafting density, increasing the thickness of the brush (ranging from 3 nm to 12 nm) results in more protein adsorption[225].

Neutral brushes such as PHEMA displayed good anti-fouling properties, and protein adsorption was initially decreased with increased brush thickness, reaching a plateau above 20 nm, before increasing again for thicker brushes (above 40-50 nm)[227]. Similar, results were obtained for PHEMA-*co*-POEGMA brushes[228].

Shorter PEG chain brushes result in higher surface density, which showed more efficient non-fouling ability when compared to brushes in the range of PEG (2 kDa) to PEG (5 kDa)[229]. Similarly, Nagasaki and colleagues have synthesised a heterotelechelic poly(ethylene glycol) (PEG) composing of a mercapto group on the one end and an acetal group at the other end (acetal-PEG-SH) and coated on a surface plasmon sensor (SPR) gold chip, and found shorter-PEG-SH (2 kDa) obtained higher PEG density than longer-PEG-SH (5 kDa). Moreover, by increasing the PEG density on SPR chip, lower nonspecific bovine serum albumin adsorption was obtained[230].

With increased PEG chain length decreased grafting density of PEG layer was obtained as a result of volume effect. More importantly, the extent of surface hydration plays a vital role in determining the materials biocompatibility rather than the molecular weight[231].

Stuart et al investigated the effect of grafting densities and chain length on PEG brushes with small molecules of BSA adsorbed. Figure 5.2, shows that with low grafting

densities the BSA can diffuse into the brush and adsorbed on the PEG chains, moreover, all three different chain lengths, and brushes showed the same BSA adsorption. However, only longer chain length of PEG brushes showed a maximum BSA adsorption at lower grafting densities, which is due to secondary adsorption occurring[232].

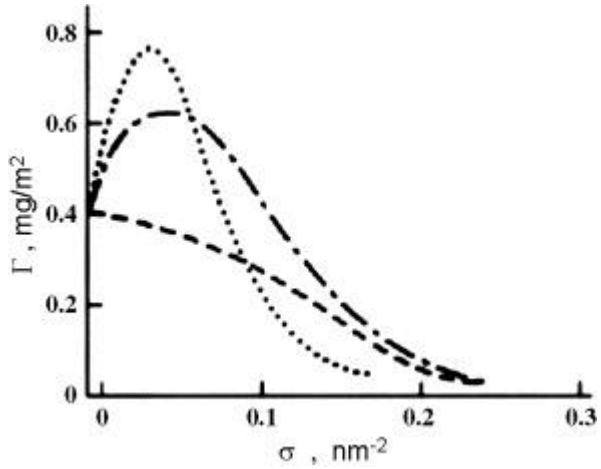

Figure 5.2 BSA adsorption on PEO brushes with different chain lengths: N = 700 (⋯), 445 (–·–), and 148 (- - -) (from Currie et al[233].

Meagher et al. found that 475 Da OEGMA (methyl ether terminated) showed less non-specific protein adsorption compared to 360 Da OEGMA (hydroxyl terminated)[234]. Moreover, several research groups reported that POEGMA brushes show better protein resistance than PEG brushes[235-237]. Even 20-fold reduced adsorption of kinesin to POEGMA surfaces compared to $(OEG)_3OH$-terminated SAM surfaces[238].

In addition, hydroxyl groups on side chains of POEGMA brushes can be further functionalised with carboxyl acid to generate carboxylic acid groups leading to immobilization of peptides[238]. Functionalised POEGMA brushes with nitrilotriacetic acid (NTA) moieties can be further immobilized with histidine-tagged (His-tagged) proteins with high stability and loading[239].

Benchmark anti-fouling poly (ethylene glycol) (PEG) surfaces were widely used in the past; however, PEGlated polymers are chemically unstable in the presence of oxygen[1]. Moreover, PEG brushes lose their protein resistance properties at 37 °C[240]. This shows that there is now an urgent need to find alternatives to PEGlated brushes.

Zwitterionic antifouling surfaces have attracted considerable attention recently due to their comparable anti-fouling properties with PEG surfaces. However, no observation has yet been found that shows zwitterionic antifouling surfaces to be advantageous over uncharged designs such as PEG surfaces.

Gong and colleagues have succeeded in fabricating PEG-COOH and phosphorylcholine zwitterionic polymer PMEN coatings on the sensor chip of the surface plasmon resonance (SPR) instrument. PMEN coating showed better resistance than that of PEG-COOH coating for BSA adsorption at low coating thickness (~ 1 nm). However, when the thickness is increased to 1.5 ~ 3.3 nm, the BSA resistant efficancy of PEG-COOH coating exceeded that of PMEN as a result of stronger steric repelling effect[241].

Muller and colleagues have been grafting pSBMA and linear PEG coatings on amine modified polycarbonate arrays to compare the difference in antifouling properties on wearable devices. Interestingly, more immunoglobulin G (IgG) or bovine serum albumin protein was immobilized on pSBMA surfaces than PEG surfaces, while non-specific adsorption was comparable to each other. Similarly, when two coatings were applied in wearable microprojection arrays, pSBMA polymers displayed significantly higher signal-to-noise ratio (>2-fold increase in signal) in comparison to PEG[241].

The extreme protein resistance of POEGMA brushes was investigated to achieve highly fidelity patterning of single cells[242], which pave the way for device production without comprising their nonfouling properties. Prime and colleagues have reported that oligo (ethylene glycol)-terminated SAMs on metals showed significant non-fouling properties. Consequently OEG and longer PEG brush surfaces have become the gold standard for “bioinert” model surfaces[243].

Hydrophilic POx exhibits very similar behavior with PEG owing to its peptdomimetic structure; however, POx shows higher chemical stability and can be further functionalized via substitute R in the side chains or at the end of the chain. In addition, PEtOx has been approved as an indirect food additive by FDA which may indicate the possibility of good immunogenicity of POx-based materials. Overall, POx is a good candidate for non-fouling biomedical applications[51].

Textor et al have studied the stability of two copolymer brushes under cell culture conditions; and found that PLL-g-PMeOx brushes showed better long-term stability than PLL-g-PEG brushes[7].

Jordan et al. investigated the impact of chemical composition and architecture of POx bottle-brush brushes (BBBs) on protein (fibronectin) adsorption and endothelial cell adhesion. They found that BBBs showed good non-fouling properties. Furthermore, when keeping the side chain length the same, the layer thickness has no effect on the hydrophilicity of the brushes. In addition, increasing the molar mass of monomer resulting a more hydrophilic surface[86].

A wide range of applications for protein resistant brushes have been explored: Label-free detection platforms included QCM[244], SPR[245-248], pulsed streaming

potentiometry[249], and voltammetry[250]; cell culture and implant design[251]; drug and gene delivery[66, 252-254]; antibacterial coatings[255, 256].

Aims of this chapter. PEG brushes have been widely studied, due to their immunogenicity, low toxicity, and anti-fouling properties. However, PEG polymers have been found to be unstable in the presence of oxygen and hard to be biofunctionalised. Thus, POx methacrylate brushes which preserve the very high level of crowding typical of PEG methacrylate brushes, such as non-fouling properties have also been studied. Moreover, POx allows simpler biofunctionalisation, for example alkene functionalised POx can be reacted with peptide via thiol-ene chemistry.

5.2 Results and discussion

5.2.1 Synthesis of polymer brushes

An important advantage of polymer brush growth via living radical polymerisations is that a linear relationship can often be achieved between the Mn of the polymer formed, the polymerisation time and the thickness of the coating generated. This has been achieved particularly successfully via ATRP, using a wide range of methacrylate monomers[111]. Fukuda et al. reported that the thickness of polymer brushes (Methyl Methacrylate as monomer) was dependent on the concentration of free initiator that was added. Higher concentrations of initiator resulted in higher rates of deactivation as fast reaction with Cu(I) species occurs, therefore limiting the lack of deactivation of systems initiated from the surface-tethered initiator only[257]. This allows a relatively linear increase in thickness, as a function of polymerisation time. Free initiators can also be substituted to Cu(II) species, acting as deactivators and allowing to regulate the living radical polymerisation process. Hence ATRP can be used to control the growth of polymer brushes with a linear relationship between polymerisation time, M_n of polymer

chains formed (on the surface or in solution) and the brush thickness. However, deviation from linearity is often reported at higher Mn and polymerisation times, due to the high surface density of brushes resulting in steric hindrance and burying of the reactive end chains within the coating, but also gradual deactivation of end chains via recombination due to their high surface density[258]. Interestingly, Armes and colleagues demonstrated that the copper (I)-mediated living radical polymerization of oligo(ethylene oxide) methacrylate (OEGMA), catalysed with a bipyridine-based catalyst and initiated with an alkyl halide initiator is relatively fast in aqueous solutions[259]. This enabled the formation of many hydrophilic coatings in mild conditions and relatively short polymerisation times. Huang et al compared the growth of PHEMA brushes on gold substrate via ATRP from Self-assembled monolayer (SAM) with and without the presence of water in the solvent. A 700 nm thick PHEMA film was obtained in the presence of water, whilst only 6 nm PHEMA films were grown from the surface in control experiments in the absence of water[260]. Interestingly, *in situ* reduction of the catalyst system can also be carried out, using ascorbic acid, in a process known as AGET ATRP, for a range acrylates, methacrylate and styrene monomers, such as methyl acrylate n-butyl acrylate, methyl methacrylate, and styrene[261].

Armes and colleagues have investigated the polymerization of methoxy-capped Oligo(ethylene glycol) methacrylate with various bromide-based initiators and in conjugation with a copper-based catalyst (CuCl), as well as bpy as ligand via ATRP. It confirmed a homopolymerization was carried out of ATRP due to relatively narrow polydispersity indexes (Mw/Mn < 1.30). Moreover, even decrease catalyst/initiator molar ratios to 0.10, a reasonable control was obtained which may indicate high activity for the Cu(I) catalyst. Furthermore, the rate of polymerization was significantly higher

in the presence of water. In addition, evolution of molecular weight and polydispersity with monomer conversion for the polymerization of OEGMA was shown in figure 5.3[129].

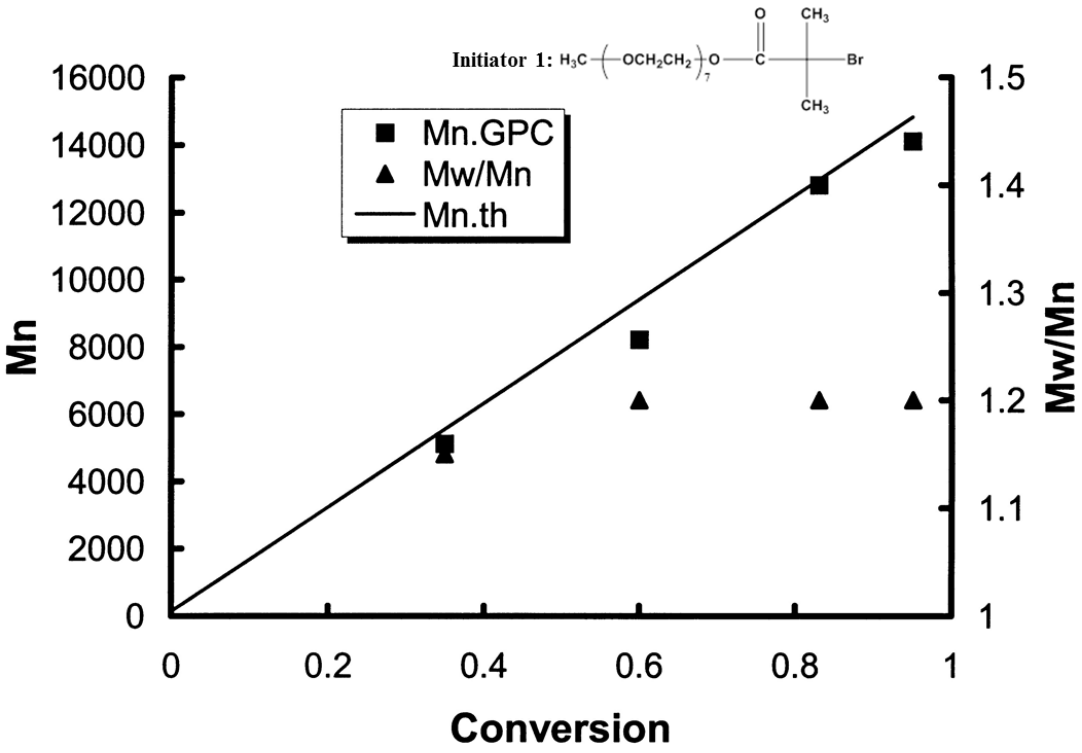

Figure 5.3 Evolution of molecular weight and polydispersity with monomer conversion for the polymerization of OEGMA using initiator 1 in aqueous media at 20 °C. Conditions: OEGMA = 10 g, D_2O = 5 g, [initiator] = 44 mM. The relative molar ratios of OEGMA: initiator: CuCl: bpy were 33:1:1:2.

Moreover, Huck and colleagues generally studied the controlling of polymerization of (mono-hydroxyl and mono-methoxyl terminated oligo(ethylene glycol) methacrylates (HOEGMA and MeOEGMA, respectively) from functionalised, planar surfaces via surface-initiated atom transfer radical polymerization (ATRP). They found a controlled polymerization was obtained when 0.2 mol% deactivating Cu(II)Br_2 was added to the polymerization solution (monomer 1 g/mL, bpy 5 mol%, CuCl 2 mol%, 11 mL water).

Although it was reported that amides are less efficient initiators for ATRP, MeOEGMA brushes grew from the ester silane, amide silane and thiol ester all showed roughly the same rate of polymerization, which may as a result of the large monomer MeOEGMA (MW 400) was insensitive to the exact nature of the initiator attached to the surface. Furthermore, they compared the growth of MeOEGMA (MW 400), and HOEGMA (MW 360 and 526). MeOEGMA (MW 400) and HOEGMA (MW 360) brushes displayed very similar rate of polymerization and obtained 50 nm after 120 min, however, HOEGMA (MW 526) showed higher rate of polymerization and obtained 55 nm after 90 min. Notably, both HOEGMA (MW 360 and MW 526) brushes gelled at 120 min and 90 min, respectively[118].

Ashutosh and colleagues have coated oligo(ethylene glycol) on SAM functionalized gold wafer via surface-initiated atom transfer radical polymerization. The polymerization was carried out in an oxygen free environment, using CuBr/bipyridine as catalyst in a 1:4 water/methanol (v/v) mixture with oligo(ethylene glycol) methyl methacrylate (OEGMA) as the monomer. Tuneable thicknesses in the 5-50 nm range were obtained by varying the concentration of SAM on gold wafers. Notably, 15 nm POEGMA brushes showed no protein adsorption either from 10 % fetal bovine serum (FBS), or 100% FBS[262].

Matyjaszewski et al. compared the growth of POEGMA brushes with two different complex systems and ascorbic acid as reducing agent via activators generated by electron transfer (AGET-ATRP), which are $CuBr_2$/TPMA and $CuCl_2$/TPMA complex, respectively. A better controlled polymerization with $CuCl_2$/TPMA complex was found than $CuBr_2$/TPMA. In addition, $CuBr_2$/bpy complex produced polymers with broader

molecular weight distribution than the $CuBr_2$/TPMA, which confer AGET ATRP retains all the benefits of normal ATRP[263].

A series of molecular brushes of poly(2-oxazoline)s methacrylate (POx) was obtained via aqueous ATRP with different ligands and catalyst system. Three different oligomers were poly(2-methyl-2-oxazoline methacrylate), poly(2-ethyl-2-oxazoline methacrylate) and poly(2-isopropyl-2-oxazoline methacrylate), respectively. All of the three molecular brushes displayed narrow molar mass distributions (Đ≤ 1.16) and maximum side chain grafting densities. Notably, oligo(2-methyl-2-oxazoline methacrylate) showed similar polymerization behaviour as oligo(ethylene glycol) methacrylate ($OEGMA_{475}$) from kinetics studies. In addition, bpy catalyst system showed the highest conversion (>99%) compared to PMDETA and Me6TREN. Moreover, bpy catalyst system with $CuBr_2$ displayed more controlled polymerization which obtained narrow polydispersity (Đ= 1.15)[126].

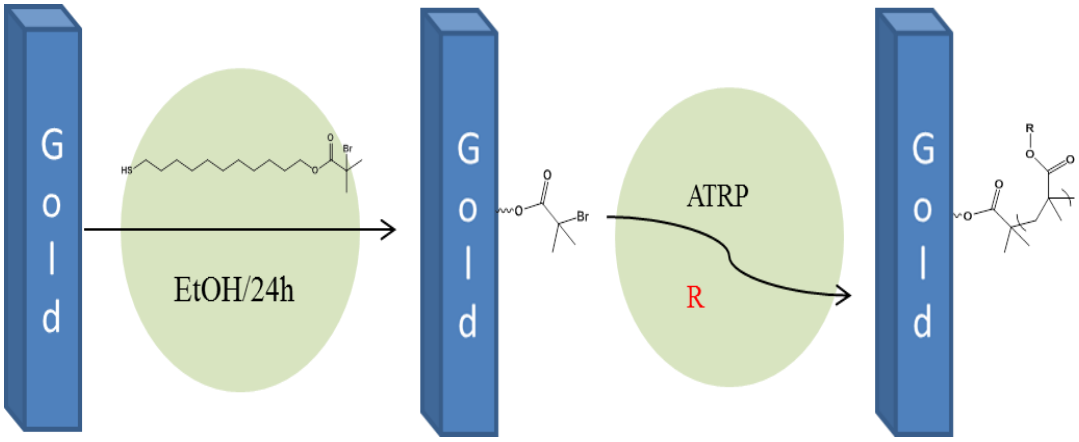

Figure 5.4 Deposition of ATRP initiator and subsequent atom transfer radical polymerization from gold substrates. R: polyoxazolines .

Considering the particularly successful growth of POEGMA brushes in mild aqueous conditions and their excellent protein resistant properties, our aim was to use low molar

mass oligooxazoline methacrylate monomers for the surface polymerization of POx brushes in two steps, including the initiator immobilisation to the surface of interest, gold in this study (figure 5.4).The impact of different catalyst systems on the growth of POx and POEGMA brushes was investigated. The resulting polymer brushes were characterised with contact angle goniometry, FTIR, XPS and AFM to study their surface properties. The protein resistance of these coatings was investigated by SPR. Patterned substrates were generated to control cell adhesion and studied using fluorescence microscopy.

5.2.1.1 Impact of ATRP catalytic system with POEGMA and PEtOxMA

PEtOxMA brushes were synthesised on gold treated silicon substrates via ATRP. We investigated the polymerization kinetic of two oligomers, OEGMA and OEtOxMA, and compared their growth and surface properties. The role of different ligands for the

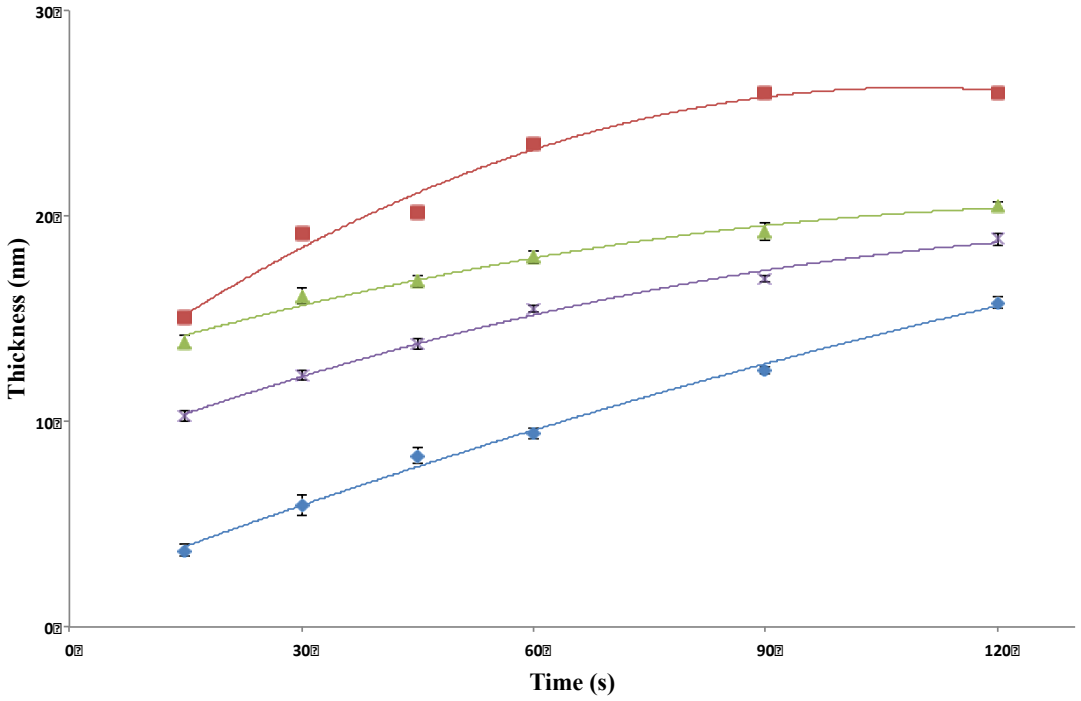

Figure 5.5 The kinetics of POEGMA brushes were measured by ellipsometry. blue: water/ ethanol (5/1), $CuBr_2$(18 mg), CuCl(82 mg), PMDETA(355 mg), red: water/ethanol(3/1), $CuBr_2$(9

mg), CuCl(41 mg), PMDETA(122 mg), green: water/ethanol(2/1), $CuBr_2$(4.6 mg), CuCl(41 mg), PMDETA(105 mg), purple: water/ethanol(3/1), $CuBr_2$(18 mg), CuCl(82 mg), PMDETA(152 mg).

catalytic system and solvents as well as deactivated catalyst has been investigated to explore conditions enabling improved control of the brush growth.

The polymerization of POEGMA with PMDETA based copper catalysts was investigated first. The thickness of POEGMA brushes was below 30 nm after 2 h of polymerisation. According to blue and purple traces in figure 4.6, with more non-polar solvent (ethanol) a thicker POEGMA brushes was obtained, in contrast to previous studies carried out with 1,1,4,7,10,10-hexamethyltriethylenetetramine (HMTETA) based catalysts[264]. Comparing conditions red and purple, the solvent was kept identical, but the amount of catalyst was increased, resulting in an increased thickness at lower catalyst concentrations, indicating that the deactivation process with PMDETA showed a significantly effect on the polymerization of OEGMA. Comparing conditions red and green in figure 5.5, in the case of less PMDETA system was added in condition green, as well as more polar solvent, previous results would have suggested that the rate of polymerization for condition green should be higher than that obtained in condition red[265]. On the contrary, our results showed that in 2 h a thinner POEGMA brush was obtained with condition green. This may be the result of disproportionation reactions occurring in the presence of water and leading to mixed polymerisation processes, between conventional ATRP and single electron transfer (SET) ATRP[266, 267]. However, it should be noted that in all cases, the slopes of the brush growth profiles are relatively comparable and the main difference between these conditions is the initial step observed in the brush growth. This suggests an initial fast uncontrolled growth

sensitive to the catalytic system, followed by partial deactivation and establishment of a slower growth process.

In addition, we investigated the growth POEGMA brushes via AGET, using ascorbic acid to reduce the catalyst *in situ*. In this system, we use ethanol/ water (9:1) as solvent and PMDETA cooper (II) as ligand catalyst.

The ARGET polymerizations kinetics of OEGMA with PMDETA and copper catalytic systems were investigated. We observed maximum thicknesses of 40 nm after 6 h for this system. According to blue and red conditions in figure 5.6, with less ascorbic acid thicker POEGMA brushes was obtained, which in good agreement with previous results and the notion that increased deactivation affords thicker brushes by preventing recombination[268].

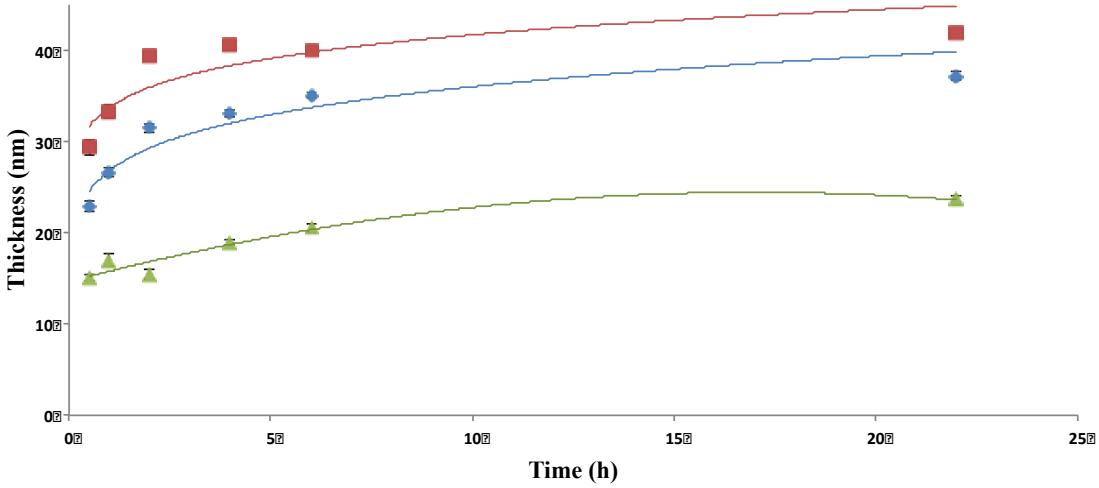

Figure 5.6 The polymerisation kinetics of POEGMA brushes with ascorbic acid system was measured by ellipsometry. blue: ethanol/ water (9/1), $CuCl_2$ (19.8 mg), PMDETA (31.5 µL), ascorbic acid (20.53 mg), red: ethanol/ water (9/1), $CuCl_2$ (19.8 mg), PMDETA (31.5 µL), ascorbic acid (10.27 mg), green: ethanol/ water (9/1), $CuCl_2$ (99.0 mg), PMDETA (157.5 µL), ascorbic acid (56 mg).

Similarly, comparing red with green conditions in figure 5.6, a 5 fold increase in concentration of the catalytic system resulted in thinner POEGMA brushes and the growth of polymerization was the weakest. This may indicate that increasing the concentration of all catalysts increased the radical density at the surface of the substrate and resulted in increased recombination.

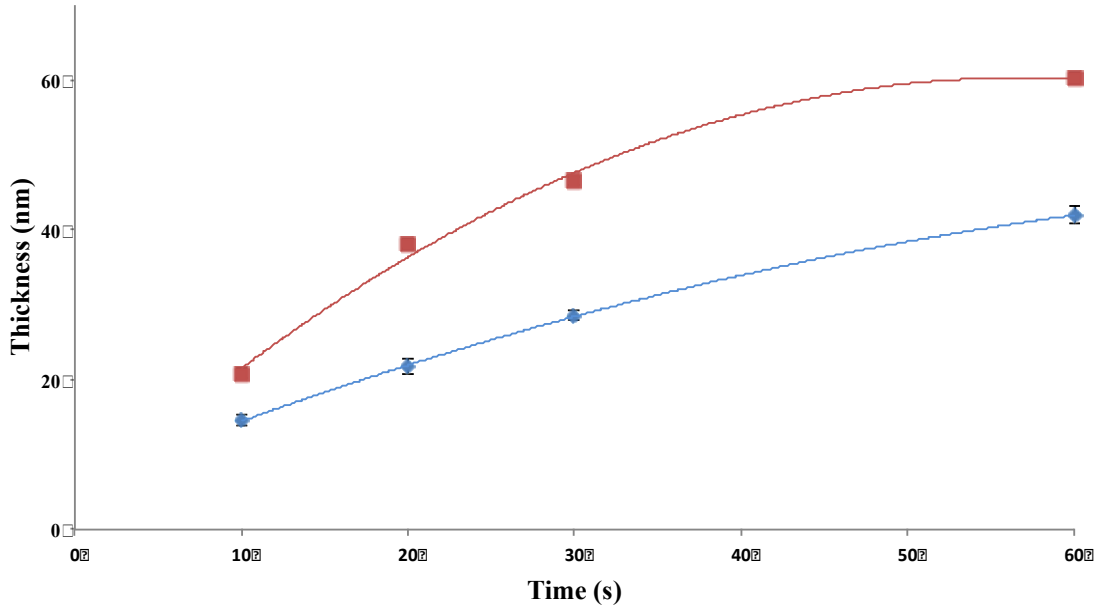

Figure 5.7 The polymerisation kinetics of POEGMA brushes with bpy-copper system was measured by ellipsometry. blue: water/ ethanol (4/1), $CuBr_2$ (18 mg), CuCl (82 mg), bipyridine (320 mg), red: water/ methanol (2/1), $CuBr_2$ (18 mg), CuBr (119.65 mg), bipyridine (320 mg).

The relatively low brush growth observed in figure 5.7 led us to propose that deactivation of the brush was insufficient and investigate the use of bipyridine ligands to decrease the K_{ATRP} and associated density of surface radicals[268]. In these conditions, overall, a 60 nm thickness of POEGMA brushes can be obtained in 1 h

(figure 5.7). In comparison to the results from PMDETA systems (figure 5.6), with similar catalytic conditions, but replacing the ligand type, resulted in 60 nm POEGMA brushes after only 1 h, without compromising the growth of brushes at later stages. This is in good agreement with the expected improvement in deactivation of the catalytic system and reduction in radical density at the growing surface, resulting in reduced levels of recombination. When CuBr was used instead of CuCl (condition red in figure 5.7), with expected increase in k_{act} thicker brushes of 60 nm in 1 h were obtained.

After having studied the kinetics of polymerizations of POEGMA, we investigated the kinetics of polymerizations of PEtOxMA with bpy-copper systems, as it was found to result in the highest thickness in the shortest times (figure 5.8).

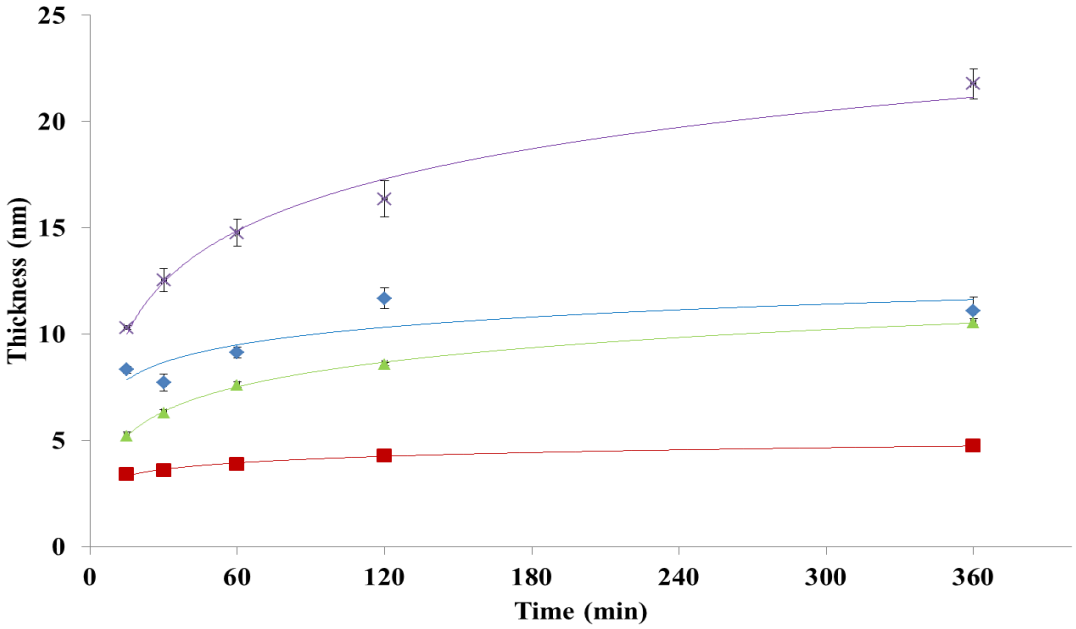

Figure 5.8 The polymerisation kinetics of PEtOxMA brushes carried out with ellipsometry.) water/ ethanol (2/1), $CuBr_2$ (18 mg), CuBr (119.65 mg), bipyridine (320 mg), red: water/ methanol (4/1), $CuBr_2$ (18 mg), CuCl (82 mg), bipyridine (320 mg), green: water/ methanol (2/1), $CuBr_2$ (18 mg), CuCl (82 mg), bipyridine (320 mg), purple: water/ methanol (2/1), $CuBr_2$ (18 mg), CuBr (119.65 mg), bipyridine (320 mg).

Polymerisations were carried out under inert conditions identical to those utilised for POEGMA brushes. Overall, we observed the formation of thinner brushes for OEtOxMA compared to OEGMA, with less evidence of controlled growth (linear increase over prolonged polymerisation time). As for PEtOxMA brushes, we measured the thickness of dry brushes on gold substrates by ellipsometry at different polymerisation times. In figure 5.8, comparing blue and purple, only changing the solvent from water/ethanol to water/methanol mixtures and keeping other condition identical, the growth kinetic of purple where methanol was used as solvent showed a steady increase in thickness and a more stable brush growth than in condition red where ethanol was used as co-solvent. This is in good agreement with results obtained for POEGMA by us and others[264], in which increasing the polarity of the solvent induced an increase in the polymerisation rate of methacrylate derivatives. In comparison, although steady growth of brushes was observed by ellipsometry for both conditions green and purple (comparing CuCl and CuBr mediated activation), thicker brushes were obtained for purple after the same polymerization time and double thickness of PEtOxMA was obtained for purple compared to green. Consistent with previous results, the increased k_{act} of CuBr compared to CuCl allowed faster growth of PEtOxMA brushes. However, according to red and green, further increasing the polarity of the solvent and the content of H_2O led to the formation of thinner brushes, presumably due to an increased rate of recombination. Hence we proposed that K_{ATRP} for red was increased to a level that did not allow the control of the polymerization. Hence it is apparent from our studies that a balance between activation and deactivation is essential to allow the growth of sufficiently large brushes without leading to recombination and uncontrolled polymer growth. Finally, the reduction rate observed for OEtOxMA compared to OEGMA (compare figure 5.8, condition purple to figure 5.7 condition red)

may be ascribed to the difference in molecular weight of these two monomer, as the larger OEtOxMA is expected to lead to slower polymerisation with higher levels of sterically-induced brush deactivation (growing radicals buried within the brush). This was also observed for OEGMA brushes with side chains of different lengths[269, 270]. Eventually, we decided to use water/ methanol 2:1 as solvent composition and CuBr as catalyst for further synthesis of polymer brushes.

5.2.1.2 Impact of the monomer on POxMA brush growth

The growth kinetics of polymer brushes with three different methacrylate oligomers was further investigated via spectroscopic ellipsometry, from initiator-coated gold substrates. Conditions used to synthesise polymer brushes were selected from 5.2.1.1 section,

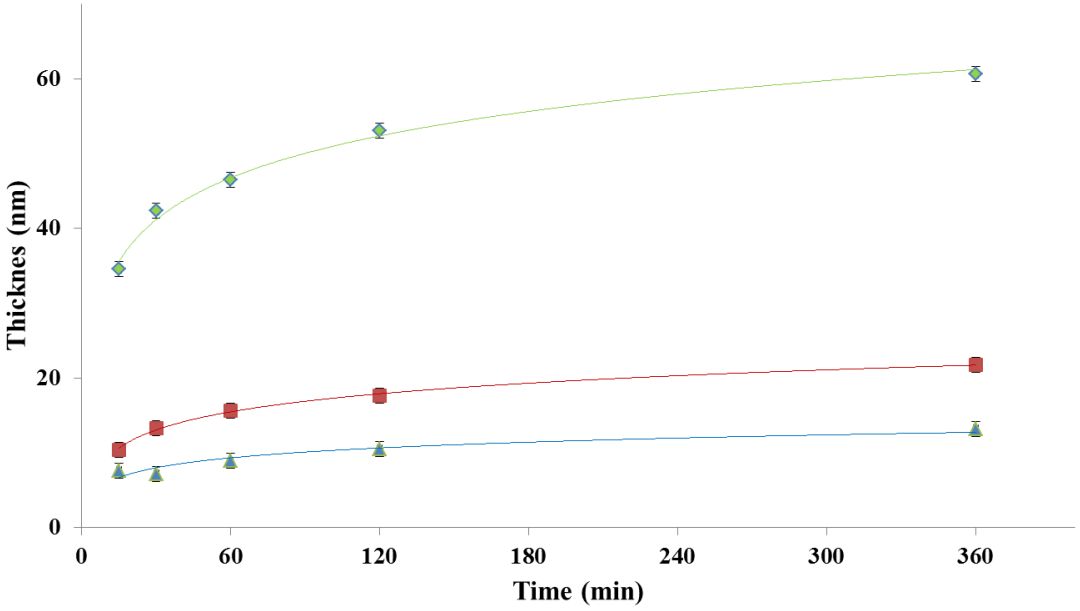

Figure 5.9 The polymerisation kinetics of polymer brushes synthesised with the same conditions (water/ methanol (2/1), $CuBr_2$ (18 mg), CuBr (119.65 mg), bipyridine (320 mg)) from three different oligomers: blue: OMeOxMA, red: OEtOxMA, green: OEGMA that measured by ellipsometry. All measurements were carried out with triplet.

where a more reactive copper (I) bromide with bpy ligands catalytic system was identified, resulting in high rates of polymerization. Three different oligomers were specifically studied for the growth of polymer brushes with reasonably high thicknesses: OEtOxMA, OMeOxMA and OEGMA.

The thickness of dry brushes was characterised by ellipsometry and, by varying polymerisation times, different thicknesses of polymer brushes were obtained. From figure 5.9 we can see that all three polymerization were in good control, with steady growth of polymer brushes over time. Clearly, POEGMA brushes grew faster and to higher thicknesses compared to the other two oligomers. With oligomer OEtOxMA and OMeOxMA, thinner brushes were formed, with maximum thicknesses of 13 nm and 22 nm, respectively. Such differences between oligo(ethylene glycol) and oligo(2-alkyl oxazolines) may be explained by differences in the size of these oligomers (OEGMA MW 300, OEtOxMA MW 600, OMeOxMA MW 525), but perhaps also by some level of hydrolytic degradation of oligo(oxazolines), resulting in secondary amines that can ligate ATRP catalysts and potentially deactivate them.

5.2.2 Surface characterisation

Having determined satisfactory protocols for the synthesis oligo(oxazoline) methacrylate brushes, we investigated next the surface properties of the resulting polymer brushes with XPS and FTIR to characterise the chemistry of these coatings as well as their hydrophilicity via water contact goniometry.

5.2.2.1 XPS

X-ray photoelectron spectroscopy analysis was carried out to confirm the successful polymerization of oligomer OEtOxMA and OMeOxMA and OAMeOxMA on silicon substrates.

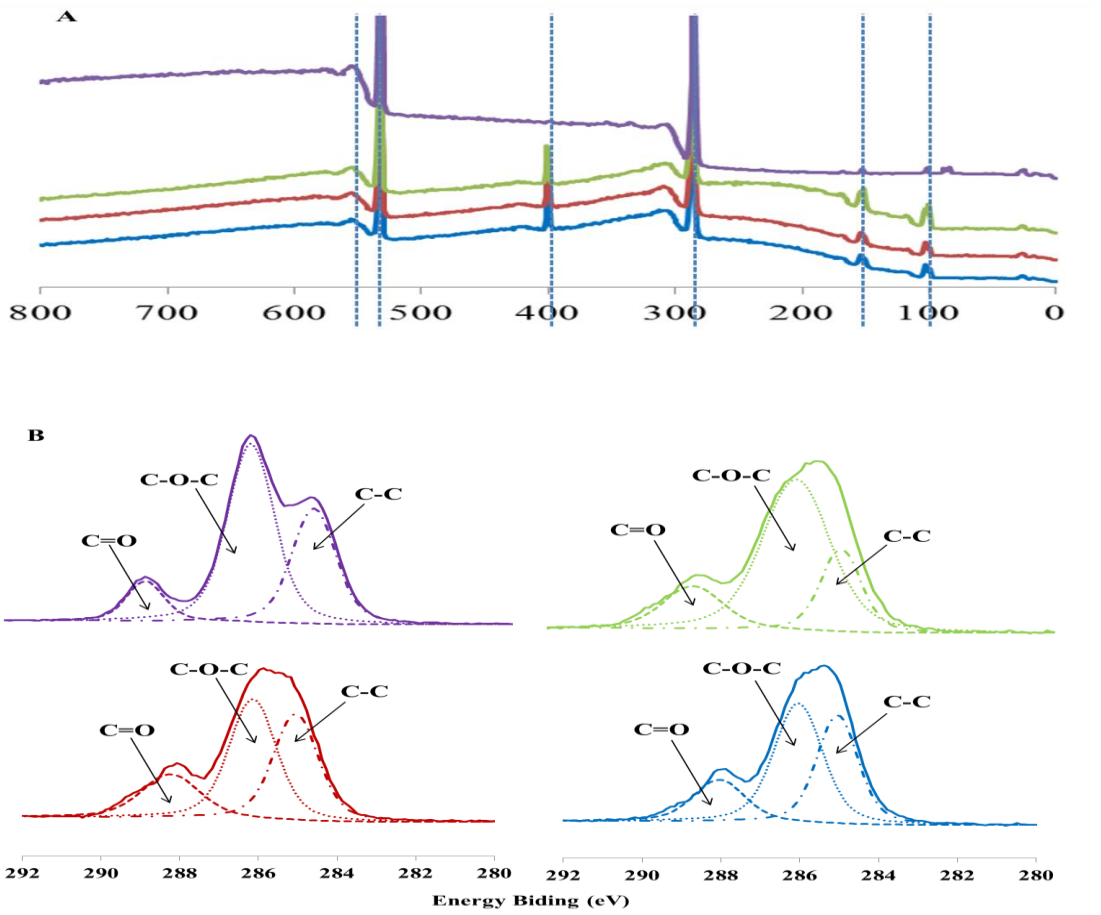

Figure 5.10 X-ray photoelectron spectra for three polymer brushes: A. Full spectra for three polymer brushes. B. C 1s spectra and N 1s spectra. blue: PEtOxMA brushes, red: PMeOxMA brushes, green: PAMeOxMA brushes

Table 5.1 Summary of atomic concentrations for three polymer brushes.

		Elements		
		C	O	N
PMeOxMA	expected at	67.57	18.92	13.51
	observed at	68.88	21.13	9.98
PEtOxMA	expected at	71.43	16.67	11.90
	observed at	71.54	18.32	10.14
PAMeOxMA	expected at	68.42	18.42	13.16
	observed at	68.27	22.76	8.97

The chemical compositions of three polymer brushes (PEtOxMA, PMeOxMA and PAMeOxMA) were confirmed by XPS analysis. Figure 5.10 shows the XPS C1s and N1s scans of three polymer brushes and table 5.1 summarizes the different binding energies and area ratios determined for each of the different carbon, oxygen and nitrogen atoms of the brushes. In agreement with the literature[271]. We can see that the XPS spectra of PEtOxMA, PMeOxMA and PAMeOxMA brushes all display four main signals: carbon, oxygen, silicon and nitrogen. Clear nitrogen signal at 400.2 eV confirm the successful polymerization of oxazoline oligomers from silicon wafers, as nitrogen is a specific element present in oxazolines. In addition, carbon levels are in good agreement with the expected structure of the polymer brushes, however, oxygen levels are higher while and nitrogen levels are lower than expected structure of the polymer brushes, which is surprising as cleavage of lateral chain should result in more levels of nitrogen.

5.2.2.2 FTIR

The chemical structure of three monomers OEGMA, OEtOxMA, OMeOxMA, three polymer brushes OPEGMA brushes, OEtOxMA brushes and OMeOxMA brushes have been analysed with FTIR and the results are shown in figure 5.11.

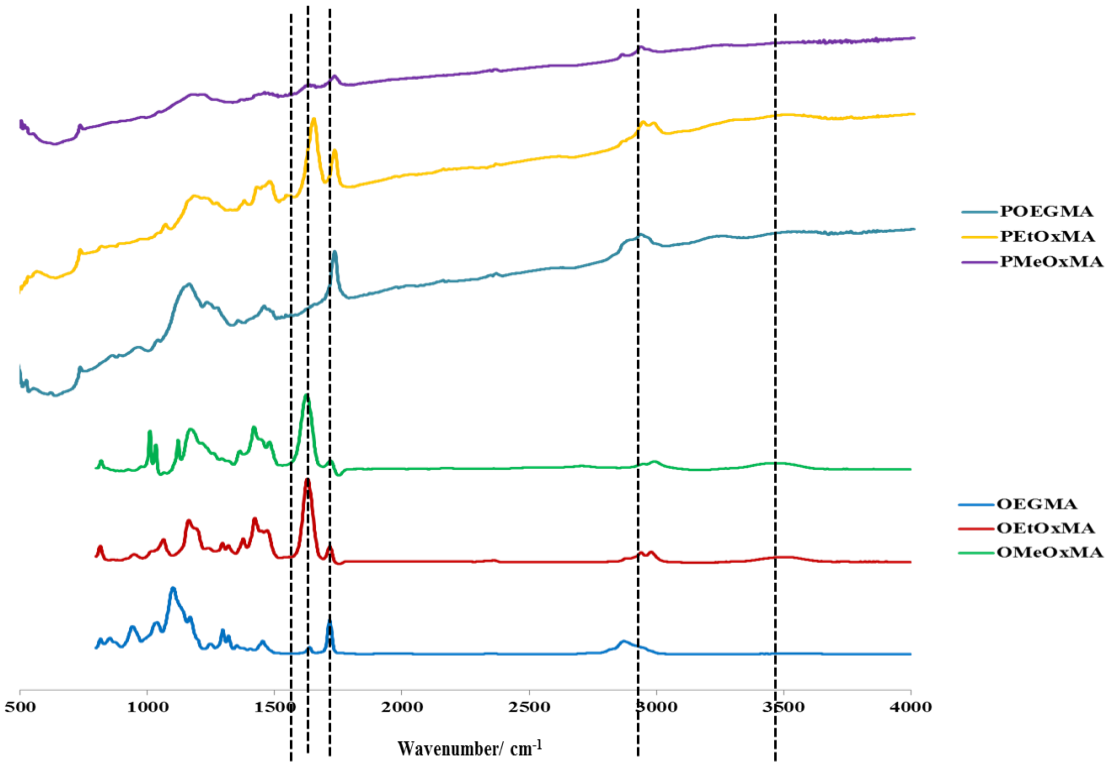

Figure 5.11 The FTIR spectra of three oligomers and three polymer brushes on gold substrates. Three oligomers are: OEGMA, OEtOxMA and OMeOxMA; three polymer brushes are: POEGMA, PEtOxMA and PMeOxMA.

The FTIR spectra display a characteristic band at 1630 cm^{-1}, typical amide stretching vibrations, which is in good agreement with literature[269]. Apparently, there is not much in OEGMA and none adsorption was found in POEGMA brushes as they do not display amide groups. However, very strong band were found in oxazoline oligomers, as well as in polyoxazoline brushes. Moreover, bands around 1700 cm^{-1} corresponding to –C=O vibrations from methacrylate group. All three monomers showed this typical band as well as all three polymer brushes, notably, significantly increased of band at 1700 cm^{-1} compared to band at 1600 cm^{-1} were found when comparing PEtOxMA and PMeOxMA brushes to their oligomers. It may indicate some lateral hydrolysis during

polymerization step. Furthermore, characteristic bands of the three polymer brushes all showed strong adsorption at 3020-2820 cm^{-1} (stretching vibrations of C-H)[272], which confirmed the successful polymer brushes adhered on gold substrates. However, significant lateral hydrolysis would be evidenced as a more pronounced tail around 2800 cm^{-1} for PEtOxMA and PMeOxMA brushes when comparing oxazoline monomers to OEGMA. We can see band at 1576 cm^{-1} (bending vibration N-H) which was contributed by hydrolysed lateral chain's product: secondary amines only from PEtOxMA brushes, which confer the hypothesis we made before that lateral hydrolysed during polymerization. In addition, band at 3350 cm^{-1} corresponding to –OH from methacrylate was found from oligomers OEtOxMA and OMeOxMA. However, rarely band can be found among polymer brushes.

5.2.2.1 Contact angle

The hydrophilicity of the polymer brushes indicates its ability to bond water molecules and is a first indicator of anti-fouling properties, although by no mean sufficient to guaranty protein resistance. For example, Yu Chang et al found that the electrostatic neutrality of surface coatings can reduce interaction between charged protein domains and corresponding surface[273]. Moreover, the hydrophilic nature can help reduce non polar interactions between proteins and hydrophobic surfaces[274], and prevent protein adsorption by steric hindrance[76].

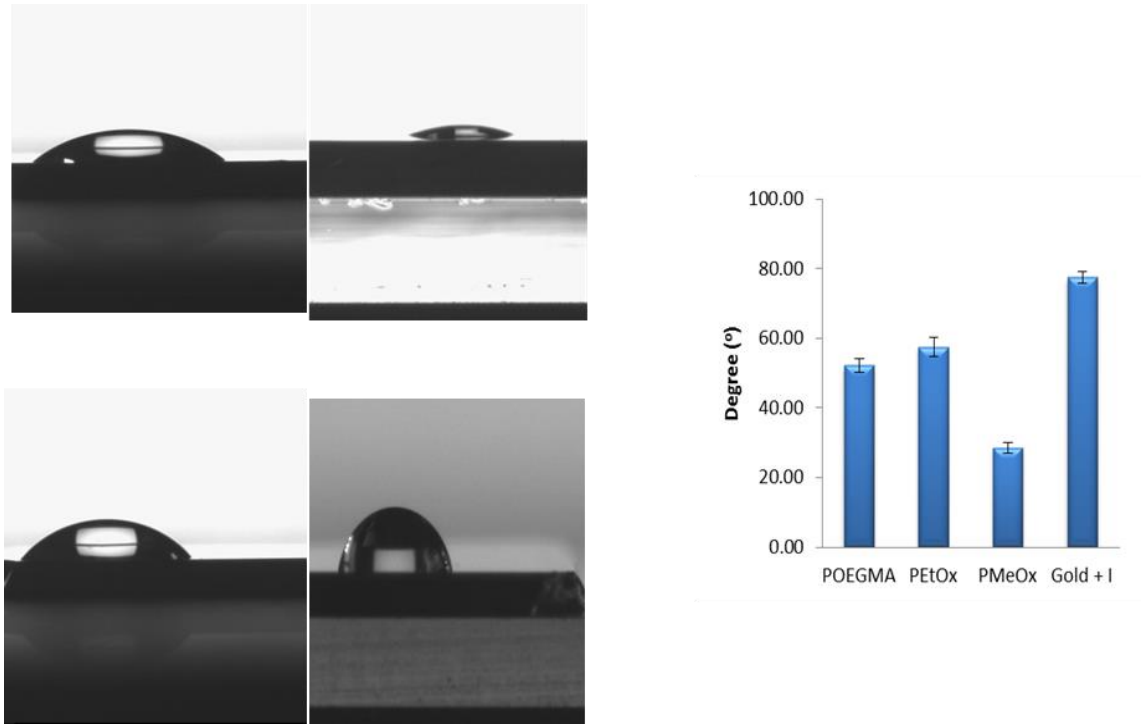

Figure 5.12 Characterize the hydrophilicity of polymer brushes with different monomers by contact angle. A) a drop of water on POEGMA polymer brushes; B) a drop of water on PMeOxMA polymer brushes; C) a drop of water on PEtOxMA polymer brushes; D) a drop of water on initiated gold wafer. All measurements were made triplet.

Here, the hydrophilicity of the polymer brushes surfaces was characterized by water contact angle. We used gold wafers coated with a monolayer of thiol initiators as comparison. PMeOxMA brushes showed particularly hydrophilic properties as the contact angle was decreased below 30°. In comparison, POEGMA brushes and PEtOxMA brushes showed similar hydrophilicity with contact angles of 52° and 57°, respectively. Initiator coated gold substrates presented the most hydrophobic character with the highest contact angle of 80°. Water contact angles measured for POEGMA are in line with those reported in the literature[275]. The higher hydrophobicity of

OEtOxMA compared to OMeOxMA is expected given the higher hydrophilicity and water solubility of methyl oxazoline derivatives compared to ethyl oxazolines[194].

5.2.3 Characterisation of protein adsorption

Halperin reported that there are two modes for protein adsorption: one is primary adsorption at the substrate, more typical of small proteins that can penetrate within the brush, and can be repressed by increasing the grafting density; the second mode is known as secondary adsorption which occurs at the surface of the polymer brushes (at the interface with the bulk of the liquid) and is strongly dependent on brush chemistry and attraction between brush and proteins[232]. Therefore, measuring protein resistance of ultra-low fouling coatings with single protein solution is insufficient, as it only probes one main type of interaction and does not account for secondary protein adsorption. Protein resistance is therefore better quantified using quartz crystal micro-balance or surface plasmon resonance in complex protein mixtures such as serum, blood or plasma. In particular, the use of serum is better suited and more relevant to applications such as cell patterning as serum is typically contained in cell culture media at concentrations ranging from 2 to 10%, but most commonly 10%[276].

Here we investigated the protein adsorption on four polymer brushes generated, with two different proteins: bovine serum albumin (BSA) and fibronectin (Fn), and one serum, fetal bovine serum (FBS). FBS was selected as an important marker of protein resistance at it is used in the medium of the cells selected for our study; however BSA and Fn were also tested due to their abundance in many physiological conditions and their importance to promote cell adhesion and patterning, respectively.

5.2.3.1 Non-specific protein adsorption (SPR)

The immobilization of non-specific proteins on four polymer brushes (21 nm PMeOxMA, 12 nm PEtOxMA brushes, 13 nm POEGMA brushes and 12 nm PMeOxMA brushes) was studied with two proteins and one serum, which are BSA, Fn and FBS, respectively, by SPR.

The quantification of protein adsorption can be monitored by SPR as it induces a change in the local refractive index close to the gold surface of the sensor, associated with changes in the gold plasmon band, which can be detected optically[277, 278]. PEG thiol monolayers deposited on gold were used as comparison as they are coating often used in biosensing and for biomedical applications, but do not display ultra-low fouling properties.

In general, for five functionalised wafers, among two proteins and one serum, BSA showed the lowest adsorption and serum FBS showed highest adsorption. Exposure of polymer brushes to a 1 mg/mL solution of BSA gave rise to a small shift in the surface bound mass of nearly 3 ± 0.62 ng/cm2 for 13 nm POEGMA brushes, 5 ± 0.73 ng/cm2 for 12 nm PMeOxMA brushes, 6 ± 1.90 ng/cm2 for 12 nm PEtOxMA brushes and 1 ± 0.87 ng/cm2 for 21 nm PEtOxMA brushes (for quantification, a change of 10 resonance units(RU) was assumed to correspond to a binding capacity of 1 ng/ cm2[279]). Similarly, exposure to 10 μg/mL Fibronectin (Fn) gave rise to a 1 ± 0.47 ng/ cm^2 increase on 13 nm POEGMA brushes, 2 ± 0.86 ng/ cm^2 increase on 21 nm PEtOxMA brushes, 2 ± 0.59 ng/ cm2 and 17 ± 7.90 ng/ cm2 increase on 12 nm PMeOxMA brushes and 12 nm PEtOxMA brushes, respectively. From the adsorption of these two protein solutions we can see that both of them showed similar non-fouling ability. However, when we

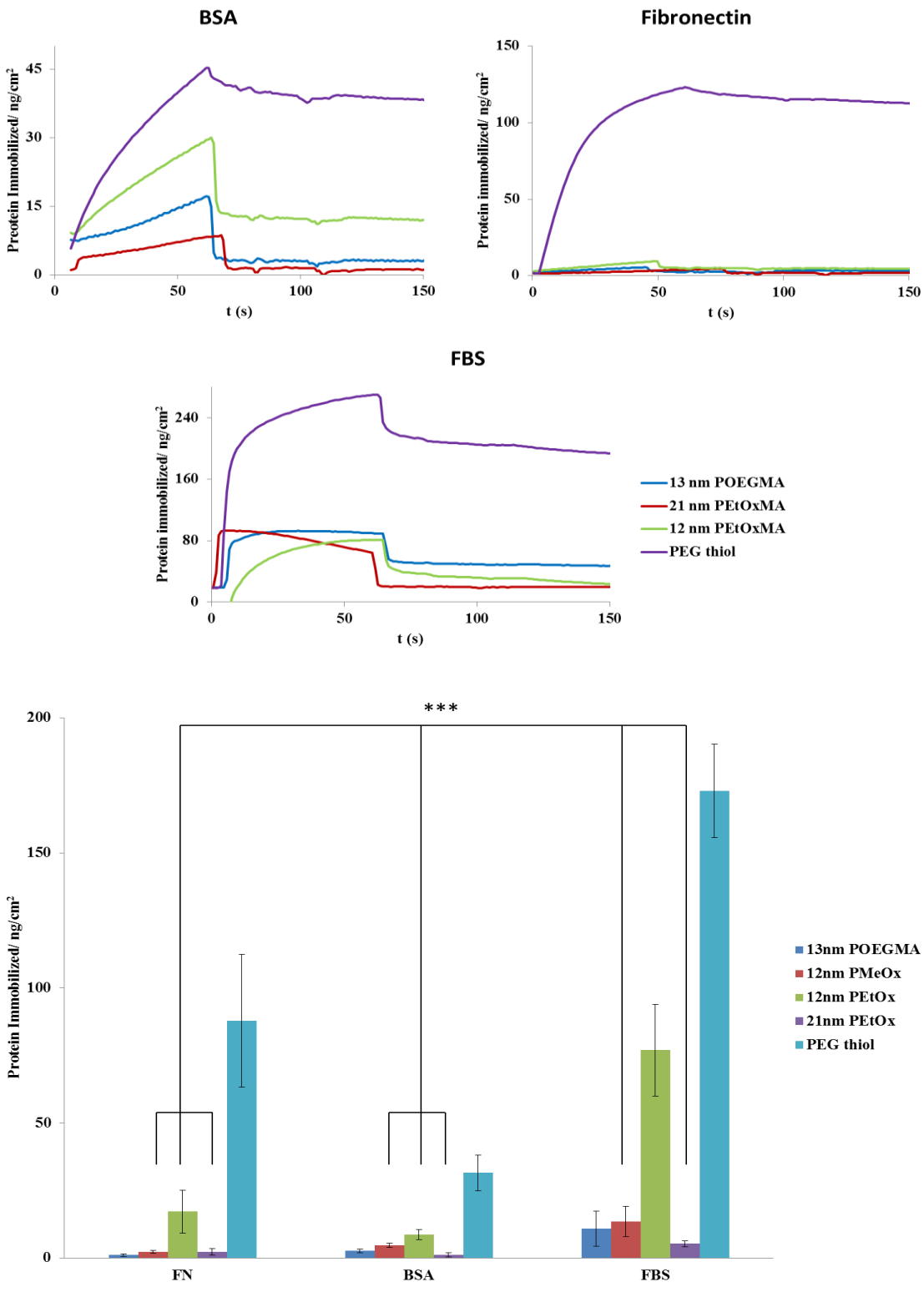

Figure 5.13 Protein resistance on polymer brushes and performed on Surface Plasmon resonance (SPR). (A) 1 mg/mL Bovine serum albumin (BSA), (B) 10 µg/mL Fibronectin (FN), (C) 10% Foetal bovine serum (FBS), (D) Summary graph of the

adsorption of two proteins (BSA and Fn) and one serum (FBS) on four polymer brushes: 13 nm POEGMA brushes, 12 nm PMeOxMA brushes, 12 nm PEtOxMA brushes and 21 nm PEtOxMA brushes, respectively. PEG thiol monolayer as control.

injected 10% FBS serum, different substrates showed significantly different adsorption profiles: 21 nm PEtOx brushes has the lowest adsorption with only 4 ± 1.07 ng/ cm2 and 13 nm POEGMA brushes came second with an increase of 11 ± 6.49 ng/ cm2; However, 14 ± 4.81 ng/ cm2 increase on 12 nm PMeOxMA brushes and significantly increase recorded from 12 nm PEtOx brushes, as 59.77 ± 16.94 ng/ cm2 was measured. However, our PEG thiol monolayer control showed the highest adsorption, which was 173 ± 17.35 ng/ cm^2 of adsorption measured from SPR. We suppose for thinner brushes, the adsorption of non-specific protein can be due to two reasons: 1. weak protein resistance of the polymer brush itself; 2. protein penetrates into thinner brushes. Both of these two reasons can result in a lower amount of protein adsorption. With the same thickness of polymer brushes, for example adsorption on 12 nm PEtOxMA brushes, 13 nm POEGMA and 12 nm PMeOxMA brushes, we can compare adsorption levels more directly. For two proteins: FN, BSA, 13 nm POEGMA and 12 nm PMeOxMA brushes showed comparably protein resistance. However, 12 nm PEtOxMA brushes showed significantly higher adsorption than 13 nm POEGMA and 12 nm PMeOxMA brushes. Similarly, when exposed to serum FBS, 13 nm POEGMA and 12 nm PMeOxMA brushes showed adsorption below 15 ng/ cm^2, while 12 nm PEtOxMA brushes showed the highest protein adsorption. Combine the result from contact angle; we suppose that 12 nm PEtOxMA brushes showed the poorest protein resistance among the other two brushes. When comparing 13 nm POEGMA brushes to 21 nm PEtOx brushes, although these two coatings displayed similar nonfouling ability when BSA and FN were applied,

considerably reduced protein adsorption was observed when FBS was injected to the 13 nm POEGMA brushes, perhaps as protein contained in serum can penetrate into thinner brushes that showed less protein adsorption at higher thicknesses. As was reported ~15 nm POEGMA brushes showed none protein adsorption[262]. Overall, 21 nm PEtOx brushes showed the best protein resistance property in serum FBS. However, 12 nm PMeOxMA brushes showed comparably protein resistance property with 13 nm POEGMA brushes. Considering the lower water contact angle of 12 nm PMeOxMA brushes, we assume that the high hydrophilicity of PMeOx, in combination with its high surface density, results in improved protein resistance, even at low brush thicknesses than 12 nm PEtOx brushes. A promising candidate as alternative to ~15 nm POEGMA brushes.

5.2.4 Cell patterning with PEtOx brushes and POEGMA brushes

The cell microenvironment (including soluble growth factors, cytokines and nutrients, neighbouring cells and extra-cellular matrix) is an important determinant of cell behaviour[280]. Therefore, studies focusing on mechanisms of how cells response to those environmental cues is very important to understand tissue homeostasis and the development of diseases such as cancer[242]. It is often not possible to observe cell responses *in vivo*, so recreating models *in vitro* is important to probe cell behaviour in detail and more realistic scenarios. Matrix engineering platforms have been developed to investigate cell-cell or cell-protein interactions with varied stiffness, topology and topography[281].

In particular, considering the importance of cell shape and size in determining phenotypes such as proliferation and differentiation, micro-patterning of cells is an attractive strategy to control cell spreading in well-defined areas and shapes[282]. For

example, by varying the shape and size of cell clusters the differentiations of embryonic stem cells was controlled[283]. In addition, a variety of shapes and sizes of single cell patterns has been studied. It was observed that cell symmetry mirrored closely the symmetry of the adhesive pattern, which was used to study the impact of matrix geometry and cell shape and symmetry on cell division axis[284], cell migration[285] and cell polarisation[286]. The protocol of preparing ECM protein deposited patterned polymer brushes was shown in figure 5.14.

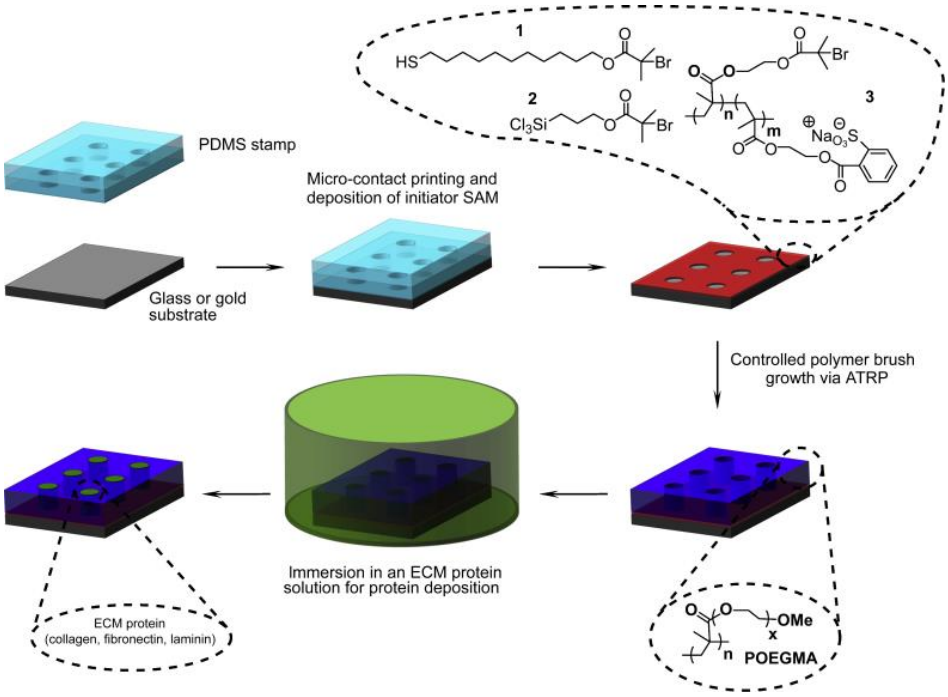

Figure 5.14 ECM protein patterning protocol. An initiator molecule or macromolecule is micro-contact printed on a substrate (gold-coated glass or glass), followed by POEGMA brush growth. At this stage, substrates can be stored in ambient conditions for several weeks without impairing their properties. For ECM protein deposition, a substrate is immersed in a solution of the desired protein, washed and used for cell seeding or immuno-staining.

Here, we investigated the ability to use POx brushes for the patterning of cells, using two different geometries of adhesive patterns: oval and circular. We carried out AFM to characterise the patterns; Fluorescent microscopy was used to investigate Fn deposition on unprotected surfaces and characterise the cell spreading on the resulting patterns.

5.2.4.2 AFM with patterned brushes

Atomic force microscopy was performed to confirm the thickness as well as the quality of POEGMA and PEtOx brush micropatterns with two different pattern shape: oval and circular.

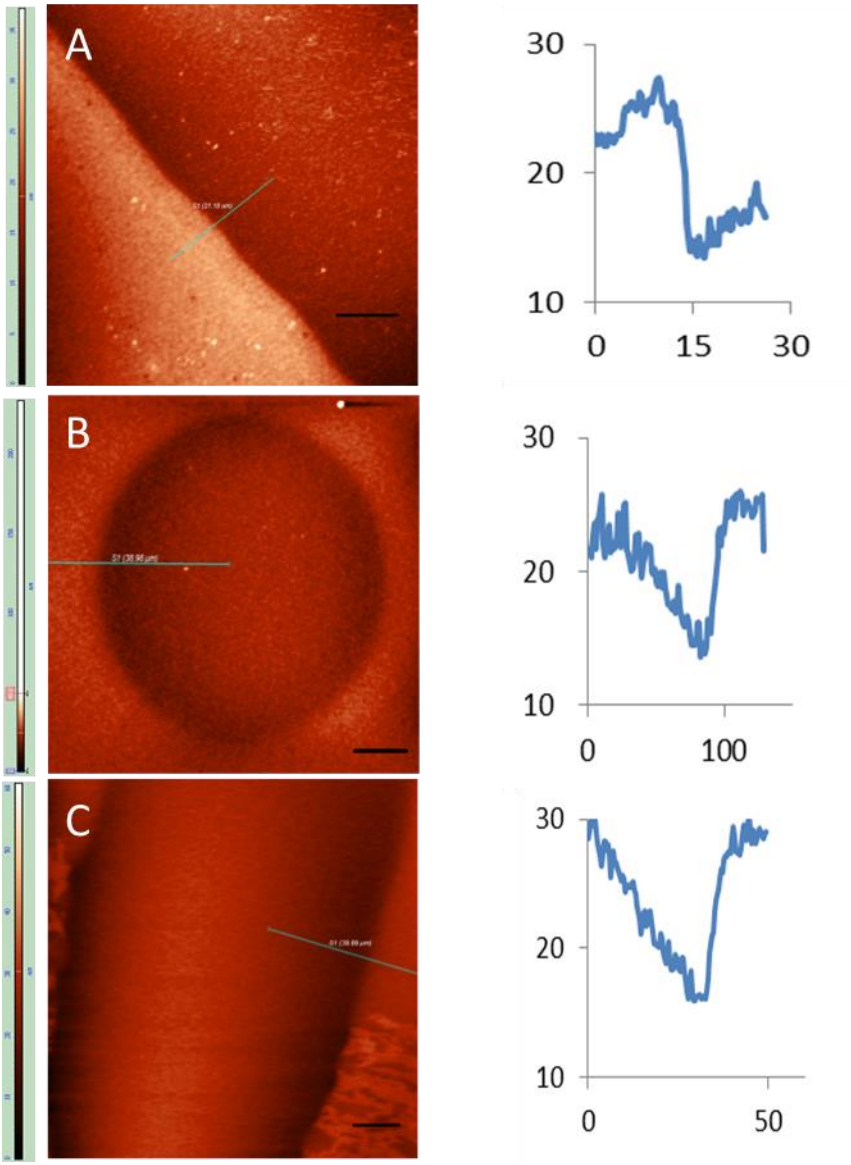

Figure 5.15 Shape of patterns generated with polymer brushes and thickness of the patterned polymer brushes monitored by Atomic-force microscopy (AFM). A. Oval pattern with POEGMA brushes, B. Circular pattern with PEtOxMA brushes, C. Oval pattern with PEtOxMA brushes.

AFM characterisation of POEGMA and PEtOxMA brush patterns allowed the determination of the height of polymer brushes patterned. For the height of POEGMA brushes was determined from these AFM scans to be close to 13 nm, in good agreement with ellipsometry. For PEtOxMA brushes, scans recorded for both circular and oval patterns showed a thickness around 15 nm. Overall, these AFM results confirmed the growth of PEtOxMA brushes with expected thicknesses, based on ellipsometry data.

5.2.4.1 Fibronectin deposition on pattening polymer brushes

It is reported that cell patterning was used to control single cell spreading, cell shape as well as the formation of cell clusters that attached to patterns of different shapes and sizes[242]. Here, we deposited fluorescent labeled fibronectin on POEGMA brushes and PEtOxMA brushes with two different patterns.

Fibronectin was deposited on 21 nm PEtOxMA and 13 nm POEGMA brushes based patterns with ellipsoidal shapes and subsequently immunostained for visualisation via epifluorescence microscopy. We can see that with PEtOxMA brushes, the background appears cleaner as no significant noise can be seen outside of patterned area. However, for POEGMA brush base patterns, relatively high background levels can be observed outside of the patterned area. In addition, the staining obtained on the fibronectin-deposited island itself was different depending on the nature of the brush defining the pattern. For POEGMA, the range of intensity profile was broader than when PEtOxMA was used for patterning (40-60 intensity units compared to 28-35 for POEGMA and

PEtOxMA, respectively). It may indicate that some POEGMA brushes were generated on the non-patterned areas, although inhomogeneously, perhaps as a result of lateral diffusion of the initiator ink during micro-contact printing, as previously reported[287-289]. It is possible that such inhomogeneity is not observed with patterns based on PEtOxMA brushes obtained via surface initiated ATRP strategy, although molecular diffusion of initiators would be expected to be comparable for both types of brushes studied. In

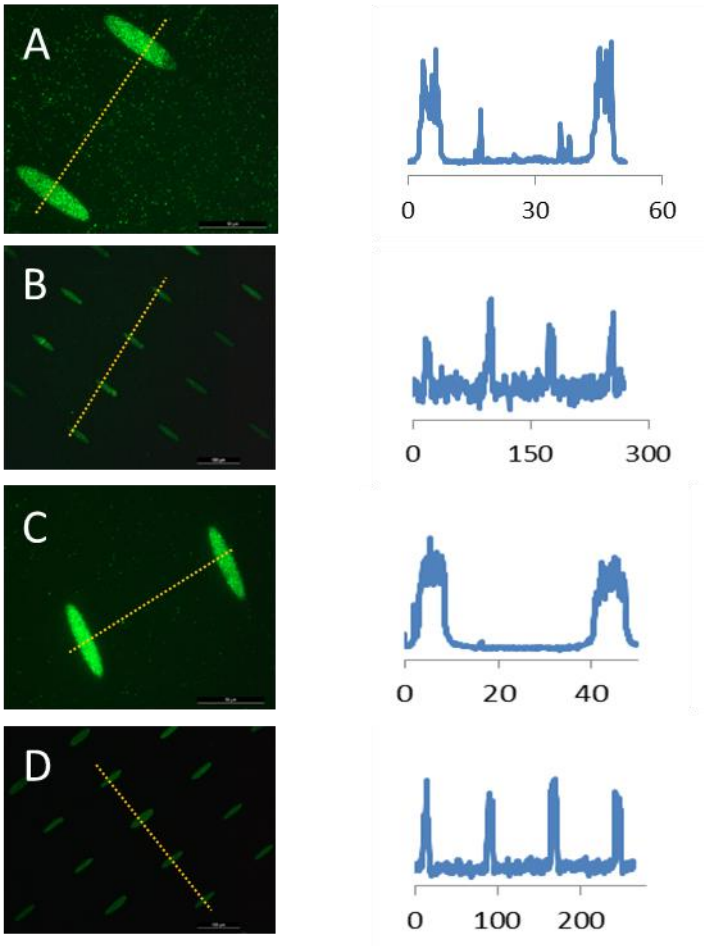

Figure 5.16 Deposition of FN on patterned POEGMA brushes and PEtOx brushes generated on gold substrates. A) FN on patterned POEGMA brushes, B) 63x on oil lens with A, PEtOx brushes were patterned on gold substrates with different patterns C) Fn on patterned PEtOx brushes, D) 63x oil lens with C. scale bar: 100 μm.

addition, based on figure 5.16, patterned PEtOxMA brushes display a clearer background compared to patterned POEGMA brushes. This is surprising considering the similarity in protein adsorption observed by SPR on these two materials, and even slightly higher protein resistance of PEtOxMA. Perhaps this could be explained by changes in brush heterogeneity observed by AFM in figure 5.15.

5.2.4.2 Cell patterning

Previous studies in our group had demonstrated the potential of micropatterning techniques for the study of basic cell biology as well as the design of cell-based assays[242, 290]. We next investigated the successful deposition of Fn protein using a non-fouling brush based micropatterns for control of cell patterning and shape. The patterning of GEβ3 cells was studied. Phalloidin (for actin staining, 1:500) and DAPI (for nucleus staining) staining, after cell seeding and cultured, were applied on the patterned POEGMA and PEtOx brush based patterns to study and control single cell shape and the formation of clusters of cells attached to patterns of different shapes and sizes.

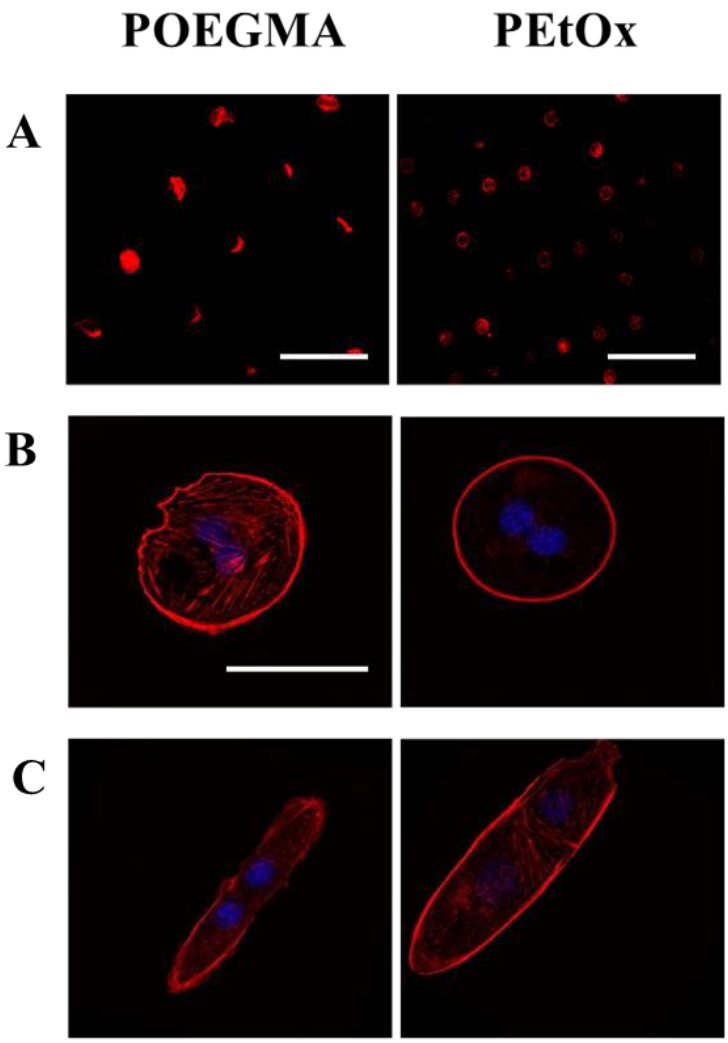

Figure 5.17 Patterning and spreading of GEβ3 cells on POEGMA brushes and PEtOx brushes were performed by fluorescent microscopy. A. Images of cell arrays (scale bar: 200 μm), B, C. single cells (scale bar: 30 μm) spreading on 50 μm islands, 3 h after seeding (staining: red, actin, blue, DAPI); the substrates used were silicon wafer.

GEβ3 cells were seeded on POEGMA and PEtOx coated islands (50 μm in diameter). On both brushes, GEβ3 cells were patterned on relatively larger areas, although not all adhesive islands were occupied by cells due to the low densities of seeding used in our assay. Perhaps a slightly higher level of coverage was achieved in PEtOx based patterns,

possibly due to the improved quality of deposition of fibronectin on islands based on these patterns. However, in both cases, patterned cells adopted the expected shapes and elongated on elliptical islands, confirming the ability to use both types of brushes for controlling cell spreading. In addition the structure of the actin network was found to be relatively similar for cells seeded on both types of patterns, with a dense network of actin fibres assembled at the cell periphery.

5.2.5 Thiol-ene chemistry

Julien and colleagues have modified poly (oligoethylene glycol methacrylate) (POEGMA) brushes with nitrilotriacetic acid (NTA) moieties, which can be immobilized with histidine-tagged (His-tagged) protein selectively and reversibly. A successful example of the application of POEGMA brushes in biomedical area such as microarrays, biosensing. The procedure was shown in figure 4.19. Apparently, POEGMA brushes need to be pre-functionalised and a few steps needed before perform to immobilise with protein[239]. Similarly, they functionalized POEGMA brushes with streptavidin and then react with protein, which also need two steps before immobilized with biotinylated antibodies[269]. Furthermore, have explored thiol-ene coupling to functionalized polyglycidyl methacrylate (PGMA) brushes with different thiols, and then PEGMA brushes was photo patterned to control the adsorption of bovine serum albumin as well as the generation of protein patterns[290].

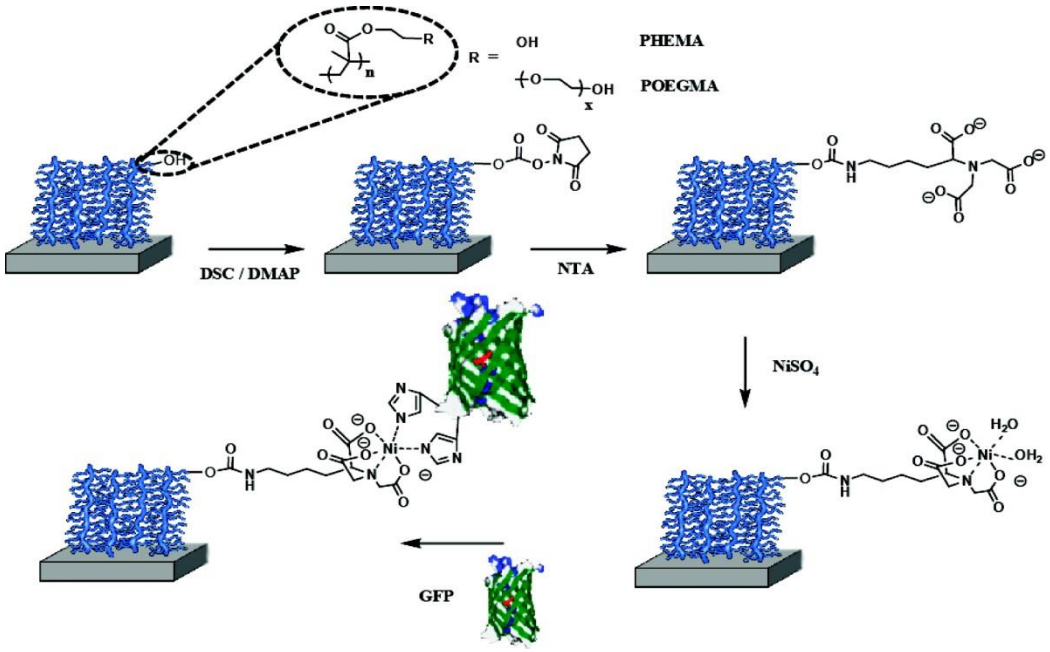

Figure 5.18 Structure and functionalization of polymer brushes with NTA ligands, followed by His-GFP immobilization[239].

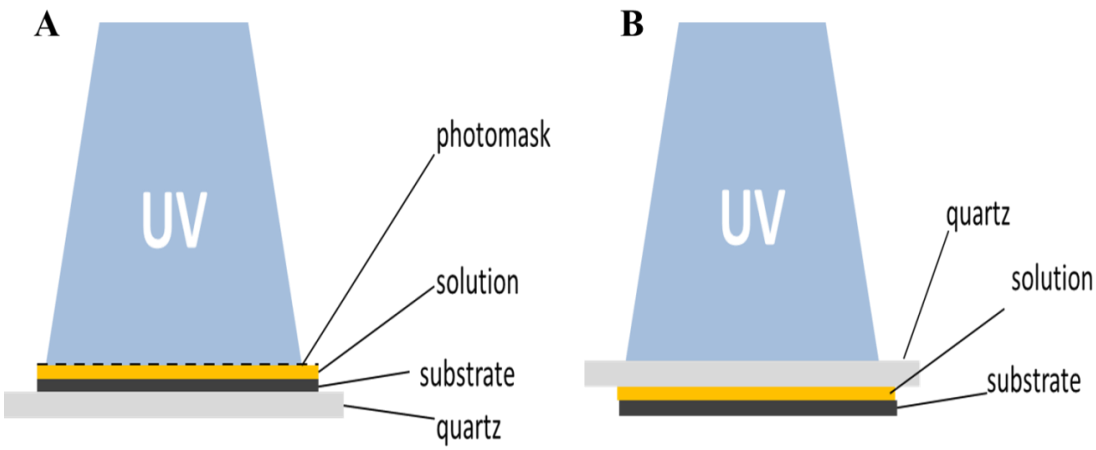

Figure 5.19 An illustration representing A. the thiol-ene pattering setup, B. the thiol-ene setup.

Hence, exploring the straight forward method to interact with protein was an alternative, such as thiol-ene coupling directly with polymer brushes. For this purpose, we used the method developed previously with the addition of a photomask to the system. Figure 5.19 shows an illustration of the setup. We first investigated the kinetics of surface initiated polymerization of OAMeOxMA by ellipsometry. After growth of reactive PAMeOxMA brushes, we carried out characterization of the resulting brushes and their functionalization via thiol-ene coupling with glutathione and FITC labeled peptides. The structures of glutathione and FITC labled peptides were shown in figure 5.20.

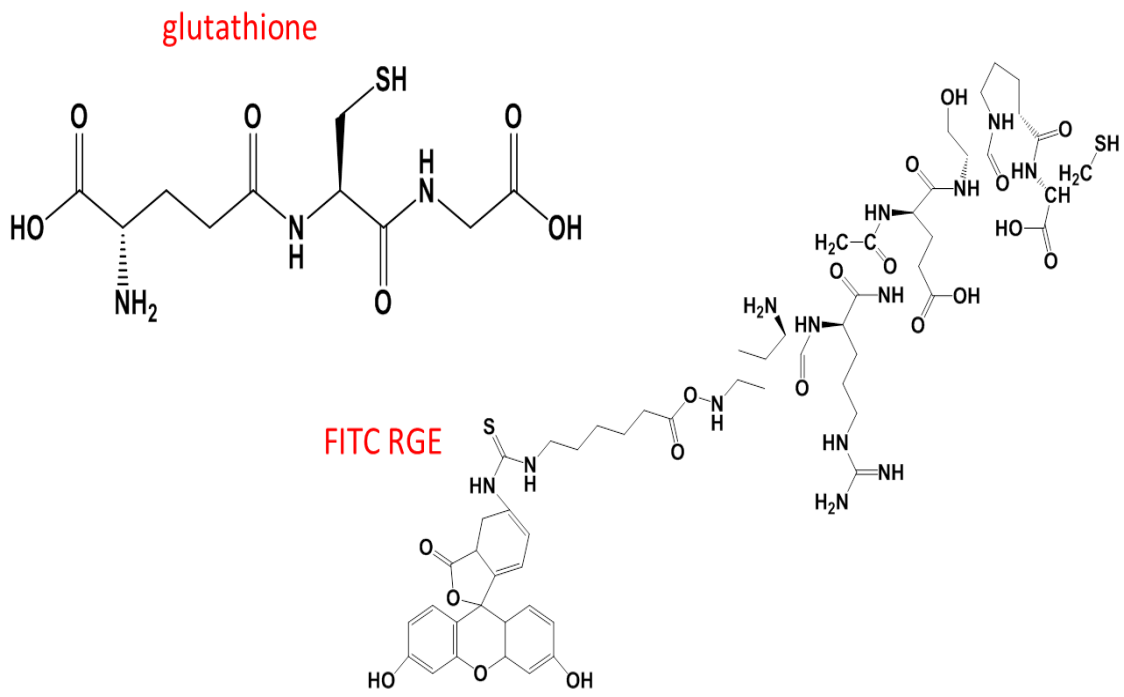

Figure 5.20 Structure of glutathione and FITC labbled RGE.

One of the advantages of poly(oxazolines) brushes, compared to commercially available monomers used to grow POEGMA brushes, is that it is possible to position functionalisable groups at the end of oligo(oxazoline methacrylate) monomers for subsequent functionalization after polymer brush growth. In particular, our group

recently showed the potential of thiol-ene based chemistry for biofunctionalisation of polymer brushes with peptides[290].

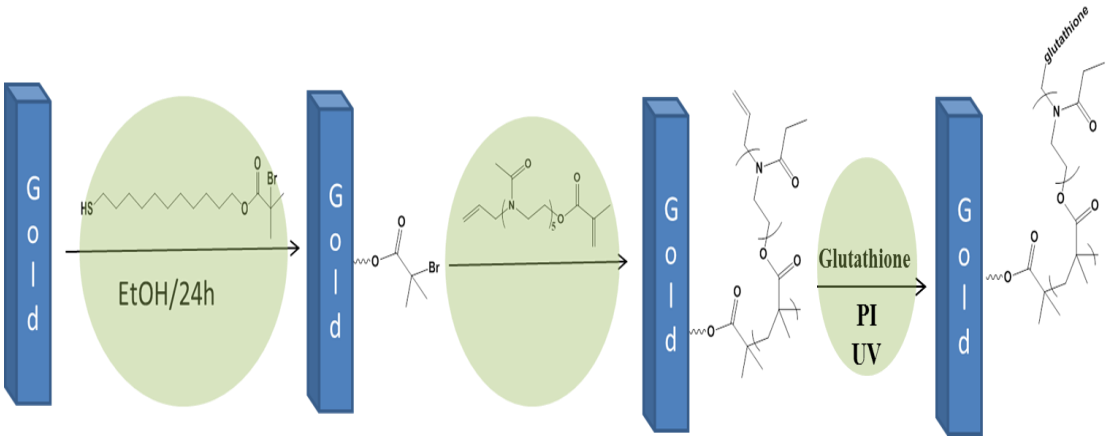

Figure 5.21 Scheme represents polymerization with AMeOxMA on gold substrates and then functionalised with glutathione via thiol-ene chemistry.

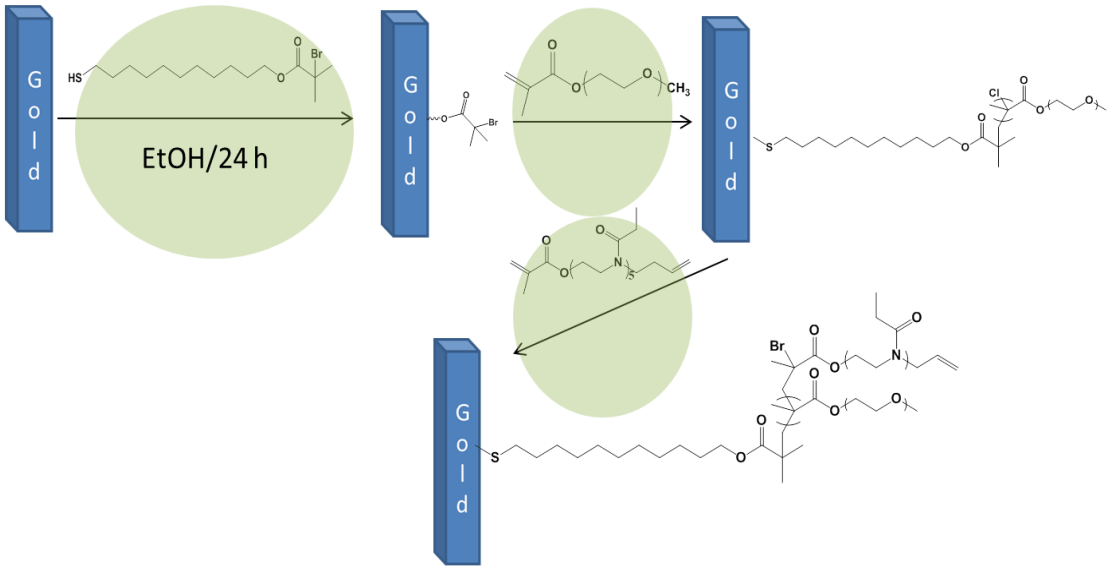

Figure 5.22 Scheme represents re-initiation of POEGMA brushes with AMeOxMA on gold substrates.

Therefore, we explore the potential of using telechelic oligo(oxazoline) monomers for the biofunctionalisation of polymer brushes. To this aim, we designed an allyl-initiated oligo(oxazoline methacrylate) monomer (figure 5.21). This monomer is designed to polymerise via ATRP via the reactive methacrylate side chain, but not significantly via the low reactivity allyl residue.

5.2.5.1 Characterisation of polymerisation via ellipsometry

OAMeOxMA is a very promising material for post polymerisation functionalization due to its alkene group that is relatively unreacted towards ATRP process but that can be activated via thiol-ene coupling. In order to confirm whether a well-controlled polymerization of oligomer OAMeOxMA can be achieved, the kinetics of PAMeOxMA brushes was investigated and performed by ellipsometry.

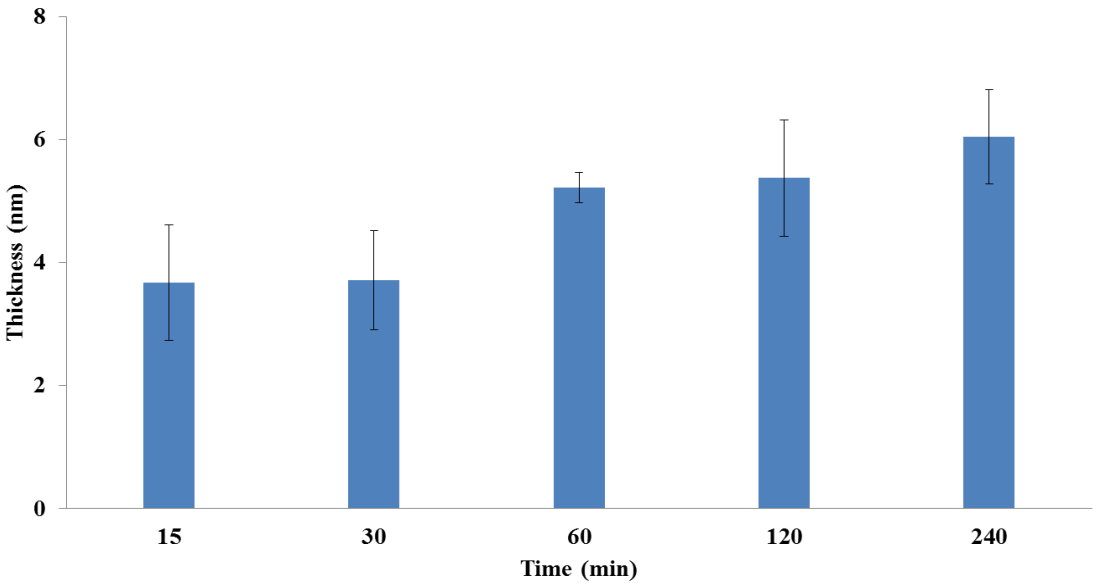

Figure 5.23 The polymerisation kinetics of polymer brushes synthesised with OAMeOxMA measured by ellipsometry. Conditions (water/ methanol (2/1), $CuBr_2$ (18 mg), CuBr (119.65 mg), bipyridine (320 mg) were carried out). All measurements were carried out with triplet.

A slight increase can be observed as a function of time during the polymerization of OAMeOxMA and after 4 h polymerization a final thickness of 7 nm can be obtained. Hence, polymerisation of allyl monomers, although possible, was slow and relatively uncontrolled compared to other oligo(oxazoline methacrylate) monomers and OEGMA. Biofunctionalisation strongly depends on the infiltration of molecules through polymer brushes[269, 290] and in many cases this process is restricted to the surface of polymer brushes. Therefore we proposed that thin coatings observed should be sufficient to confer surface functionalization of the coatings and those small molecules peptides such as glutathione and RGE peptides easily penetrate into brushes and therefore react with lateral chain of brushes. Here, we functionalised PAMeOxMA brushes with glutathione.

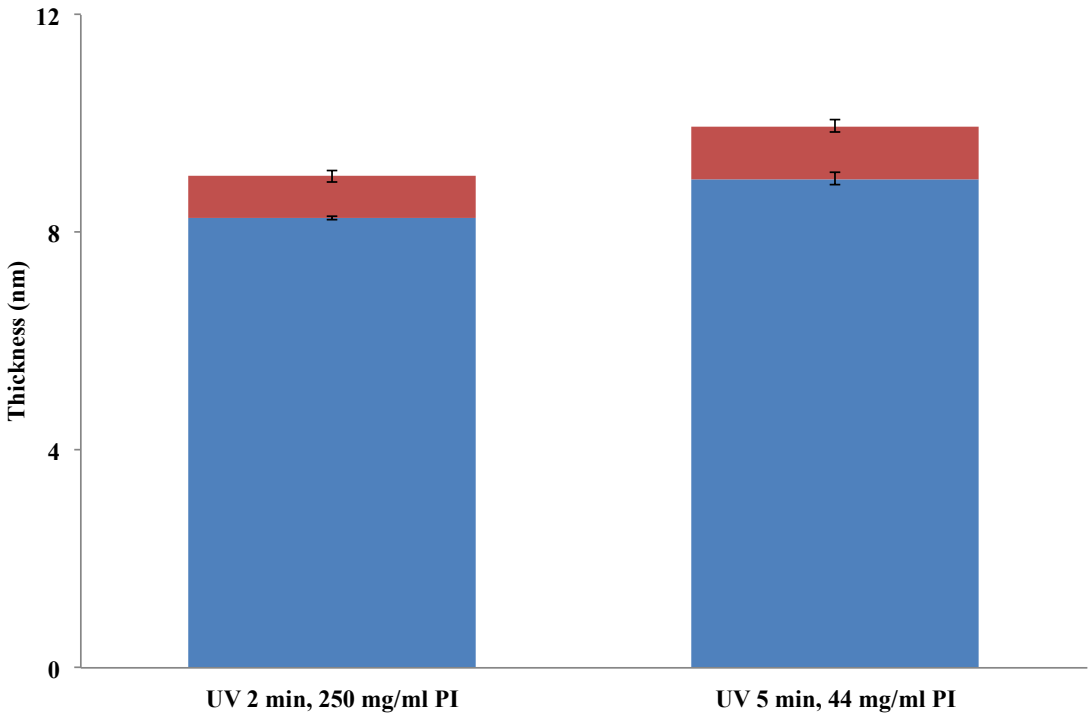

Figure 5.24 Thickness of PAMeOxMA brushes before and after react with glutathione under different UV exposure time and PI concentration monitored with ellipsometry. Glutathione react with gold wafer as control. (UV intensity: 17 mW/cm^2, time varied 2-5 min).

We further investigated the functionalised lateral chain of PAMeOxMA brushes by reacting with glutathione via photo thiol-ene chemistry. An increasing thickness of 0.8 nm was obtained for PAMeOxMA brushes under 2 min UV radiation and 250 mg/mL PI. However, increasing UV radiation time to 5 min and decreasing PI concentration to 44 mg/mL, the increased thickness was approximately up to 1 nm. It indicated that alkene groups was successfully anchored on gold substrates and can be further functionalised with small molecules such as glutathione. The functionalization of PAMeOxMA brushes via two different conditions with glutathione was 34% and 38%, respectively. (functionalization were calculated from literature[290])

Varying the thickness of PAMeOxMA brushes allows different surface properties. Copolymer brushes were synthesized to obtain thicker brushes that would better prevent protein adsorption via a first block of POEGMA brush, and re-initiated a second block of OAMeOxMA to generate block copolymer brushes that biofunctionalisation of the upper compartment of the brush (figure 5.25). The polymerization kinetics of re-initiation of copolymers was investigated with ellipsometry. Firstly POEGMA brushes of approximately 18 nm was synthesised and then re-initiate POEGMA brushes to grow PAMeOxMA brushes.

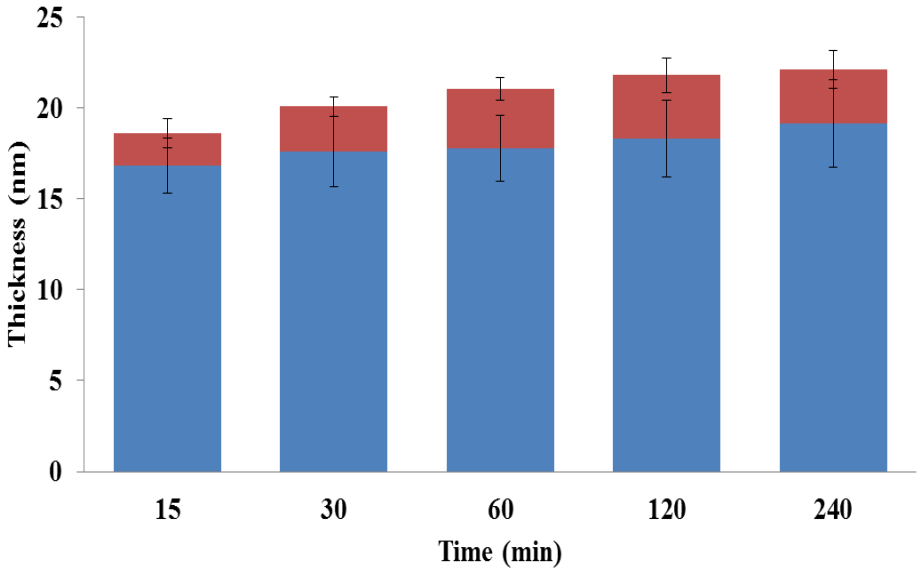

Figure 5.25 The polymerisation kinetics of copolymer brushes synthesised from POEGMA brushes and re-initiated to grow PAMeOxMA brushes were measured by ellipsometry. All measurements were carried out with triplicate. 17 nm POEGMA were obtained and remained in large expose of $CuBr_2$ solution for 5 min before re-initiate with PAMeOxMA brushes.

A moderate increase of polymer brush growth was observed after re-initiation with OAMeOxMA monomers from 18 nm POEGMA brushes. After 4 h growth, reinitiated brushes added 3 nm to the thickness of the first polymer block, in good agreement to what was observed when polymerising this monomer directly from initiator monolayers[193].

5.2.5.2 Patterning peptide on PAMeOxMA brushes

To demonstrate the biofunctionalisation of POx block copolymer brushes via thiol-ene coupling, we applied thiol-ene coupling to form patterned surfaces with FITC labeled peptide. 50 μm circles pattern were generated via the use of a photomask and FITC

labelled RGE peptides. After irradiation and washing of the surface, images were taken using an epifluorescent microscopy.

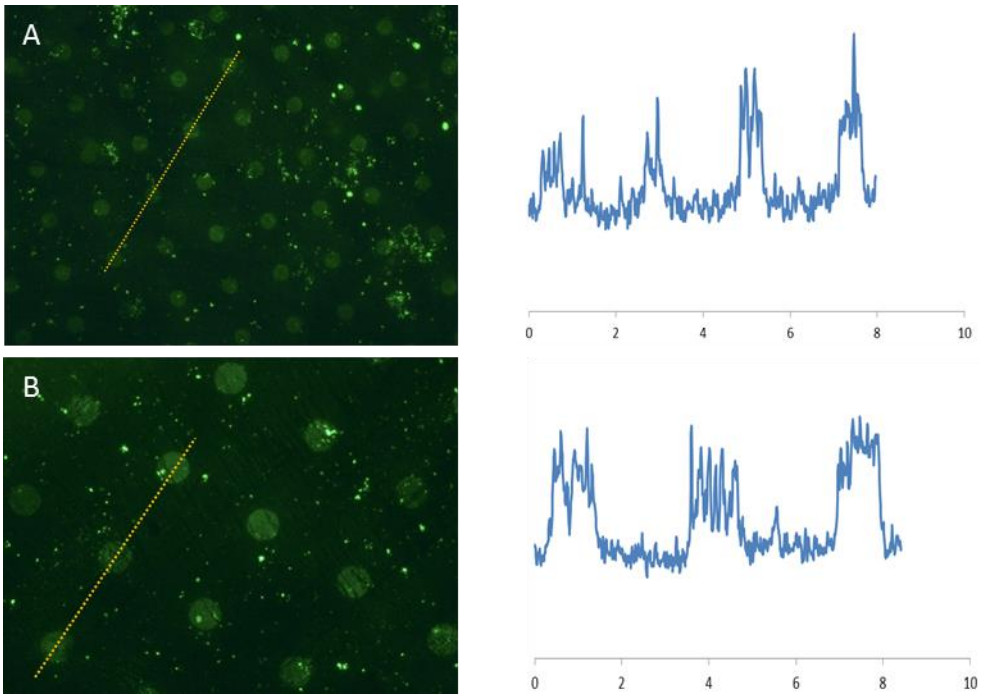

Figure 5.26 Epifluorescent images of FITC-RGE 50 μm circles patterned substrates, scale bar 100 μm. Reactions were carried out with 5 mol% PI and 300 s UV exposure. UV(intensity 17mW/cm^2).

A successfully circular pattern was achieved and evidenced by epifluroscent microscopy, which indicated that the lateral chain of PAMeOxMA brushes had successfully coupled with peptides via thiol-ene chemistry. Also from the profile we can see a relative good control of the contrast between exposed areas and the surrounding background. From figure 5.26 we can see the background of PAMeOxMA brushes is relatively clear which reflects their good protein resistance.

5.3 Conclusions

Polymer brushes are outstanding candidates to generate non-fouling surfaces and can be applied to study single cell behaviour in cell culture as well as the preparation of biosensors and biointerfaces promoting specific cell adhesion[242]. The present study focused on the synthesis of non-fouling POx brushes and characterisation. We monitored the surface properties of the resulting coatings via water contact angle, XPS, FTIR and Ellipsometry. We carried out protein resistance studies via SPR and identified similar non-fouling properties for PMeOx brushes compared to POEGMA brushes. However, PEtOx brushes showed the poorest non-fouling property between the other two brushes with the same thickness. Our results demonstrated that PEtOx brushes resulted in less protein adsorption compared with POEGMA brushes at the same height, which may due to changes in brush heterogeneity that was observed by AFM. Moreover, Jordan and colleagues found for hydrophilic POx bottle-brush brushes (BBBs) with PMeOx or PEtOx side chains fibronectin adsorption was (<6 ng/cm^{-2} exposed to 50 μg/mL), which is in good agreement with what we found that only 2 ng/cm^{-2} were obtained when exposed to 10 μg/mL[86]. In addition, micro patterning was used to study single cell spreading and patterning with PEtOxMA brushes and POEGMA brushes defining the non-fouling background. Our results demonstrated that PEtOxMA brushes integrate GEβ3 cells on circular pattern and allow the control of the cell spreading and formation of a structure yet templated cytoskeleton. Moreover, we explored PAMeOxMA brush functionalization with thiols such as glutathione as well as FITC peptide. Our results showed successful functionalization of polymer brushes that is suitable for the study of bioactive coatings for cell culture or potentially biosensing applications.

Chapter 6

Design of poly(oxazoline)-based peptide-functionalised hydrogels via thiol-ene chemistry

6.1 The use of thiol-ene chemistry to fabricate hydrogels

Synthetic hydrogels have been widely used as matrix to support cell growth in a controlled way due to its variety of chemistry and the control that can be achieved over physico-chemical and mechanical properties. In addition, synthetic hydrogels that show resistance to nonspecific protein adsorption provide a useful platform to selectively control cues support cell growth, including in 3D[291, 292].

Recently, PEG hydrogels formed by thiol-ene photo-click chemistry have been widely explored for cell encapsulation. Although both chain growth and step growth photopolymerizations offer spatial- temporal control over polymerization kinetics, step growth thiol-ene hydrogels offer more diverse and preferential properties. In Shih's study, they have investigated the advantage of step growth hydrogels such as cytocompatibility of the reactions, improved physical properties (higher gel fraction, higher mesh sizes, and higher mechanical properties) as well as the ability to encapsulate pancreatic β - cell in 3D culture[145].

In scheme 6.1, we can see a scheme that represents typical hydrogels fabricated via photo-click thiol-ene chemistry. PEG-tetra-norbornene (PEG4NB) reacts with a bi-functional crosslinker DTT (dithiothreitol), in a step-growth manner, to form thioester linkage and crosslinked hydrogels. Hydrolytic degradation of the network occurs due to easter bond hydrolysis.

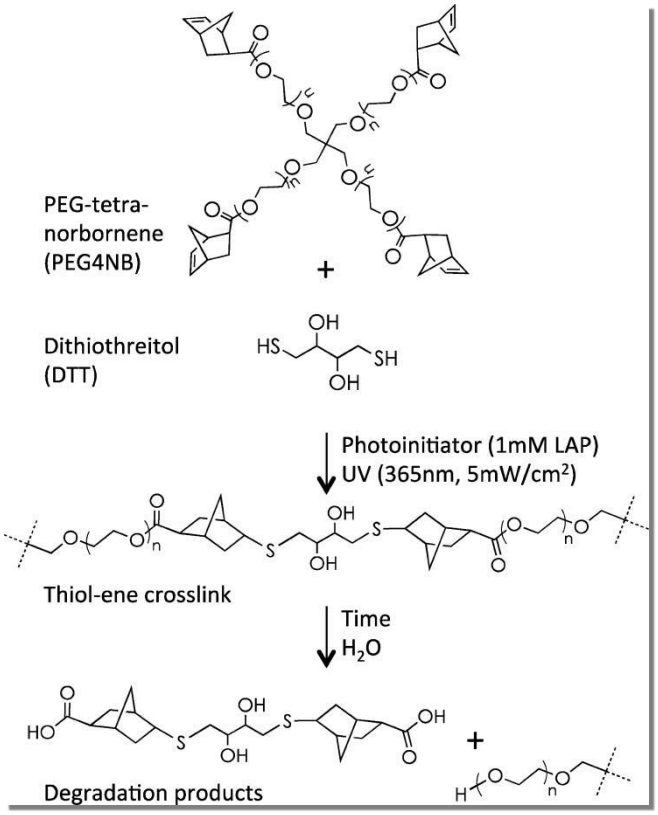

Scheme 6.1. Schematics of photopolymerization and hydrolytic degradation of step growth thiol-ene hydrogels.

A novel hydrogel system was formed via thiol-ene chemistry based on thiol functionalised PEG and allyloxycarbonyl functionalised peptides in the prescence of lithium acylphosphinate (LAP) or 2-hydroxy-1-[4-(2-hydroxyethoxy)phenyl]-2-methyl-1-propanone, (Irgacure 2959) photoinitiator and cytocompatible dose of UV light. LAP was selected due to more rapid polymerization against Irgacure 2959. Moreover, mechanics can be tuned by changing the concentration of thiol functionalised PEG[270].

PMeOx and PEtOx homopolymers are soluble in water at room temperature but lack the precursor for thiol-ene chemistry. To enable crosslinking via thiol-ene chemistry, alkenes were introduced via the alkyl substituent in the 2-position of the oxazoline

monomers. Hoogenboom et al have fabricated hydrogels based on (10% w/v) copolymer P(MeOx-co-DecEnOx) and dithiol or peptide via photopolymerization in the presence of (0 - 0.5% w/v) Irgacure 2959[293].

In addition, Kloxin and colleagues investigated the mechanical properties of hydrogels by varying the concentration of monomers (thiol functionalized PEG), to stabilise hydrogels in cell culture medium via *in situ* rheology. They found that this simple approach enabled the formation and characterization of PEG hydrogels with well-defined, spatial-defined properties. The scheme representing the photo polymerization principle used for the generation of these gels can be seen in figure 5.1, in addition to some of the advantages and applications associated with the resulting materials[294]. *In situ* gellation methods have attracted significant attention recently, as a result of their effectiveness at encapsulating cells and bioactive molecules[295].

Moreover, Burdick and colleagues investigated the mechanical properties of hydrogels based on norbornene functionalized hyaluronic acid and dithiothreitol via thiol-ene chemistry. Hydrogel mechanics from 1 kPa up to 70 kPa could be obtained by simply changing the amount of cross linker as well as the ratio of thiol to norbornene. For instance, with higher weight percentage of NorHA (0 – 12%), higher storage moduli were obtained (0 – 110 kPa). Similarly, with higher ratio of thiol to norbornene (until 1: 1), higher storage moduli was obtained, since then increased ratio obtained decreased storage moduli[296].

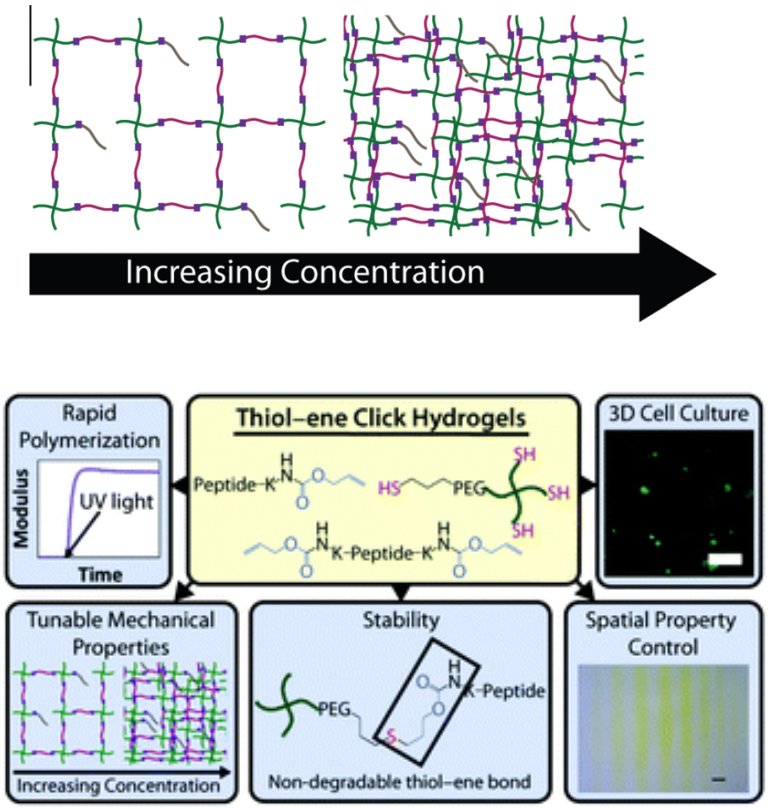

Figure 6.1 The mechanism of fabrication of hydrogels via thiol-ene chemistry and associated advantages and applications.

Furthermore, Chen and colleagues have developed PEG hydrogels with Methoxypolyethylene glycol maleimide (PEG-4Mal) and 4arm PEG thiol (PEG-4SH), with higher concentration of PEG-4SH bigger pore size of PEG hydrogel and shorter gelation time was obtained[297].

The mechanical properties of hydrogels affect cell behavior. For example, Hubbell and colleagues reported that cell invasion is highly dependent on network crosslink density, for example: decreasing PEG molecular mass from 20 to 15 kDa and the volumetric swelling ratio Q from ≈72 to 47, the rate of cell invasion decreased almost 4-fold. However this alteration was not linear with PEG structure (crosslink density) due to relatively dense networks (composed of 4armed-PEG-10kDa)[291]. Moreover, Burdick

and colleagues studied the influence of hyaluronic acid (HA) hydrogel crosslinking density and macromolecular diffusivity on human MSC chondrogenesis and hypertrophy. Variety of crosslinking densities were obtained by either changing the HA macromer concentration (1, 3, or 5% w/v at 15 min exposure) or the light exposure time (5% w/v at 5, 10, or 15 min). Increased crosslinking resulted in an overall decrease in cartilage matrix content and more restricted matrix distribution. Moreover, it promoted hypertrophic differentiation of the chondrogenically induced MSC and resulted in more matrix calcification in vitro[298]. It was reported by Mooney et al. that mesenchymal stem cell populations changes in response to the rigidity of 3D micro-environment, which indicate the matrix stiffness regulate the cells interpretation and in 3D hydrogels cell fate was related to morphology[299]. Anseth and colleagues found that hydrogels modified with RGD enhance the attachment, spreading, and cytoskeletal organization of rat calvarial osteoblasts on polymer surfaces[300]. RGD was reported a good candidate to promote cell adhesion since 1984[301].

POx offer great opportunities for the design of hydrogel structure because of the ease with which the side chain can be functionalized. By varying monomer with different side chains, a diverse range of POx structures with different hydrophilicity can be obtained. From inert to reactive leading to biomedical applications in protein conjugation, micelles, nanoparticles, and hydrogels[302].

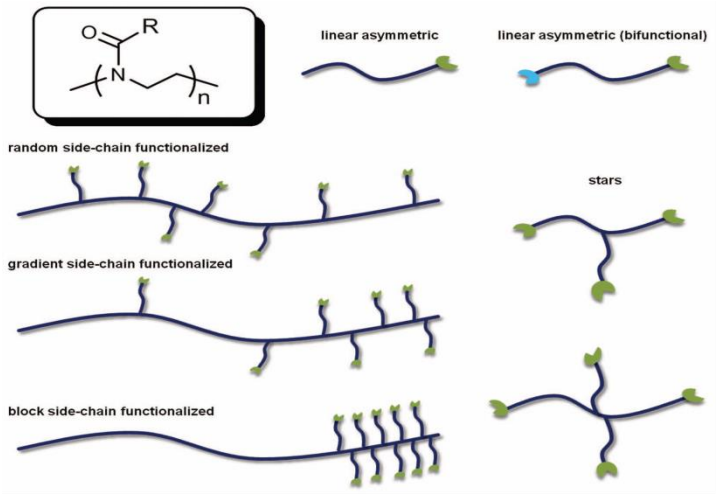

Figure 6.2 General structure of poly (2-oxazoline) and a selection of easily accessible functional POx structures ranging from linear with variable chain-ends or sidechain functionalities to stars, highlighting the structural versatility of this class of polymers.

Aims of this chapter: In this chapter, we proposed to design hydrogels based on poly(oxazolines), using thiol-ene coupling as the crosslinking reaction. Therefore, we investigated the synthesis and characterization of alkene- and thiol- functionalized POx and their crosslinking via radical-based thiol-ene chemistry via *in situ* rheology. In particular, we aimed to design multi-arm thiol crosslinkers able to achieve gelation of corresponding hydrogels at low concentrations or low levels of crosslinkers. However, these were not found to allow crosslinking.

Despite the inability to use thiol-functionalized POx for crosslinking hydrogel, we systematically studied how the concentration of multi-arm-PEG thiol crosslinkers affects the formulation of hydrogels. In addition, we studied how the functionality number of thiol crosslinkers (the number of thiol groups per molecule being varied via the introduction of different multi-arm PEG molecules) affects the mechanical

properties of hydrogels and their gelation. In situ rheology was carried out to investigate the gelation behaviour and mechanical properties of hydrogels.

6.2 Results and discussion

6.2.1 Synthesis of PMeOx thiol

Anseth et al. found that the initial macromer concentration used for the fabrication of PEG hydrogels affect the viability of osteoblasts photoencapsulated. For example, when PEG hydrogels formed with 10% of macromer a majority of osteoblasts survived the photoencapsulation process, however, after one day in vitro a decrease of osteoblasts viability to 25% and 38% from 30% and 40 wt. % of macromere concentration was obtained[300].

As the concentration of PEG macromere affects the viability of osteoblasts during the photoencapsulation process, with lower concentration of macromeres used for gelation, higher cell viability after photo-polymerization of the corresponding hydrogels would be expected in POx systems too. Hence, we proposed to synthesize thiol-end functionalized multi-arms POx crosslinkers that can be used to fabricate hydrogels with lower concentration of macromeres for POx hydrogels.

Here, we explored the synthesis of multi-arms PMeOx with thiol end capping and characterized the resulting materials (figure 6.11) via NMR, FTIR and mass spectrometry. Moreover, we synthesised a POx with thiolated pendant chains, Bu-PMeOx-OH, for which thiols were functionalized from the pendant alkenes from the copolymer Bu-PMeOx-OH. The resulting material was characterized by NMR and FTIR.

The different steps proposed for the synthesis of the thiolated telechelic PMeOx crosslinkers are presented in scheme 6.2.

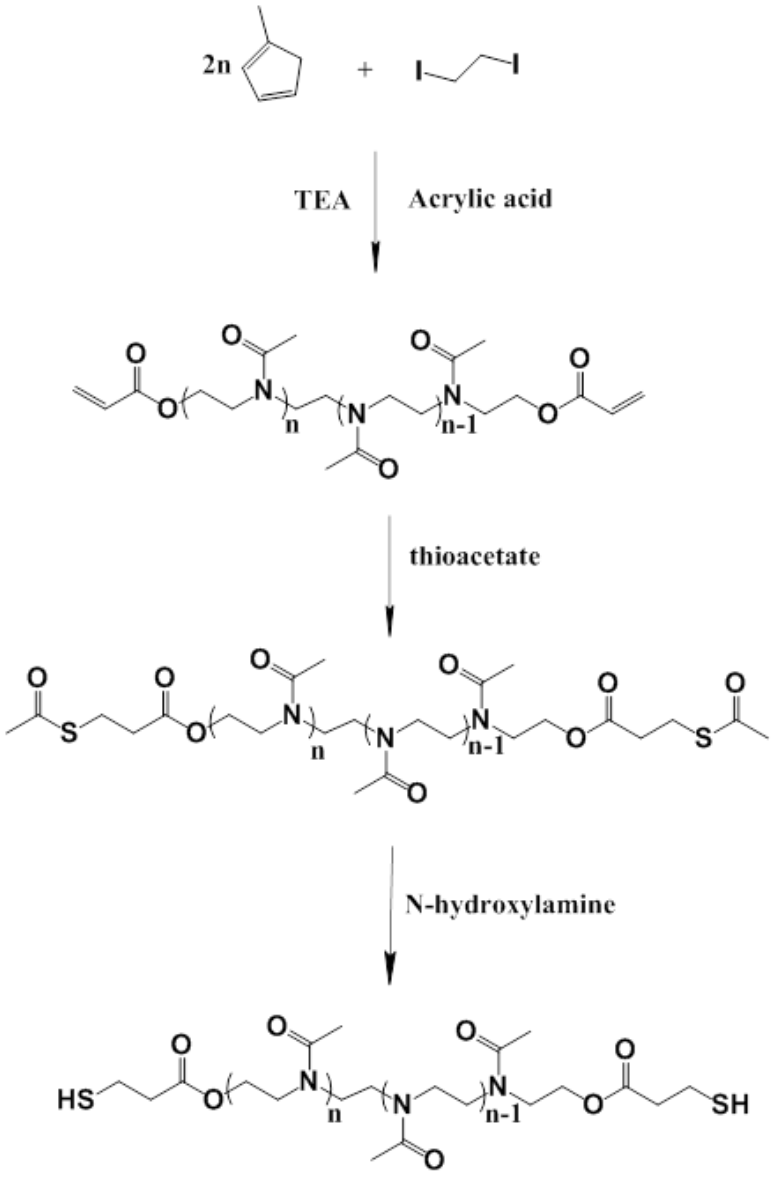

Scheme 6.2 Mechanism of synthesis thiol end functionalized two arm PMeOx.

6.2.1.1 Synthesis of two- and four-armed POx acrylates

MeOx was initiated with two different initiators: 1, 2-Diiodoethane and pentaerythrityl tetraiodide, and then end capped with acrylic acid under triethylamine base condition overnight. We tried to initiate with 1, 2-Dibromoethane and Pentaerythritol

tetrabromide, however, Pentaerythritol tetrabromide was not soluble in acetonitrile and NMP. Moreover, when initiated with 1, 2-Dibromoethane higher temperature was required compared to 1, 2-Diiodoethane for the initiation step. Therefore, 1, 2-Diiodoethane and pentaerythrityl tetraiodide were used. Notably, 1, 2-Diiodoethane is not soluble in acetonitrile at room temperature, so pre-stirring mixed solutes in 80°C oil bath before polymerized in 160°C microwave synthesizer for 30 min. However, pentaerythrityl tetraiodide was not soluble in acetonitrile at 80°C, and therefore, NMP (high boiling point and high solvency) was applied and pre-stir in 80°C oil bath before polymerized in 200°C microwave synthesiser for 30 min. Moreover, they all end capping with acrylic acid in the presence of triethylamine.

The polymers were purified by precipitation and dissolved in $CDCl_3$ for characterization by ^{1}H-NMR spectroscopy. We explored oligo (MeOx) initiated with 1, 2-Diiodoethane and acetonitrile as solvent for the polymerization via microwave assisted method under 160°C for 30 min. End capping was carried out with acrylic acid as in scheme 6.2. Full assignment of protons corresponding to the poly (2-Methyl-2-oxazoline) can be seen in figure 6.3.

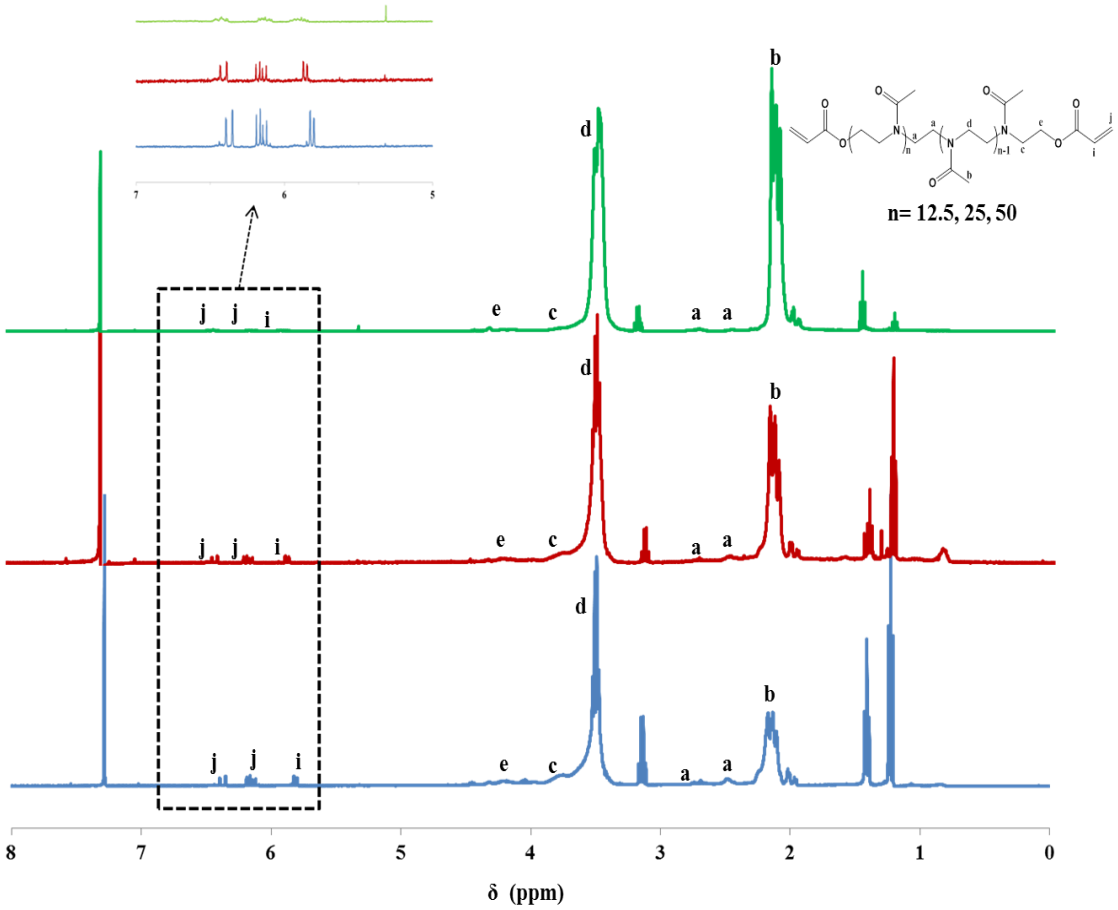

Figure 6.3 ^{1}H-NMR spectrum in $CDCl_3$ of three two arm polyoxazolines, which are oligo (MeOx) initiated with 1, 2-Diiodoethane and terminated with acrylic acid in the presence of triethyl amine. From bottom to top, represent polyoxazolines with different degree of polymerization (target number of repeat units). Blue: 12.5 repeat units per arm. Red: 25 repeat units per arm. Green: 50 repeat units per arm.

As we can see from the ^{1}H-NMR spectrometry, all peaks were assignable to corresponding protons of the chemical structure of 2I-PMeOx-acry, including those associated with end groups and initiation groups. The ratios of the corresponding integrals allowed the confirmation of the molecular structure of the oligomers obtained

and allowed to quantify their degree of polymerization as well as the control of end capping and initiation. According to the ratio H_d to H_a we can quantify the actual efficiency of initiation from 1, 2-Diiodoethane, and H_d to H_j we can quantify the actual efficiency of the end capping with acrylate. In addition, H_d to H_e represents the efficiency of the end capping with terminating agents. When the degree of polymerization of 2I-PMeOx-acry targeted was 12.5 repeat units on each arm, H_d to H_a was found to be higher than the expected ratio (i.e. 8.2), whilst the ratios H_d to H_e and H_d to H_j were found to be 9.8 and 19.5, respectively, which indicates the end capping of some oligomers with impurities, such as water, and associated side reactions that result in alternative end groups such as OH[197]. Similarly, for 2I-PMeOx-acry with 25 repeat units on each arm, H_d to H_a was found to be 13.51 which indicates a poorer control of initiation. Moreover, comparison of H_d and H_j gave a ratio of 36.47, whilst the ratio of H_d/H_e was 25.41. Although both ratios are higher than expected (monomer to initiator ratio 25:1), H_d/H_e was closer to the expected ratio and showed a good control of end capping with acrylate. Similarly, when the degree of polymerization goes higher to 50, H_d to H_a was found to be 41.20 which may indicate we can manage initiation step. However, H_d/H_e was 32 which almost double amount of the expected monomer to initiator ratio may due to side reactions such as OH end capping cause a reasonable ratio was found that H_d to H_j was 45.72. It showed that we cannot control the initiation and termination when the degrees of polymerization were 12.5 and 25. Overall, ^{1}H-NMR indicates a good control of initiation only for 50 repeat units, however, termination steps were not fully controlled for all three polymers.

Furthermore, we explored oligo (MeOx) initiated with pentaerythrityl tetraiodide at three different degree of polymerization: 12.5, 25, and 50 (targeted DP per arm). The

reaction temperature was kept at 200°C, and NMP as solvent for the 30 min polymerization in microwave. We tried acetonitrile as from literature it is a good solvent for polymerization of polyoxazoline[53], however, pentaerythrityl tetraiodide was not soluble in acetonitrile even at 160 degree and then an alternative solvent NMP was selected due to good solubility with pentaerythrityl tetraiodide. All of the final polymers were dissolved in $CDCl_3$ and then characterized by ^{1}H-NMR spectroscopy.

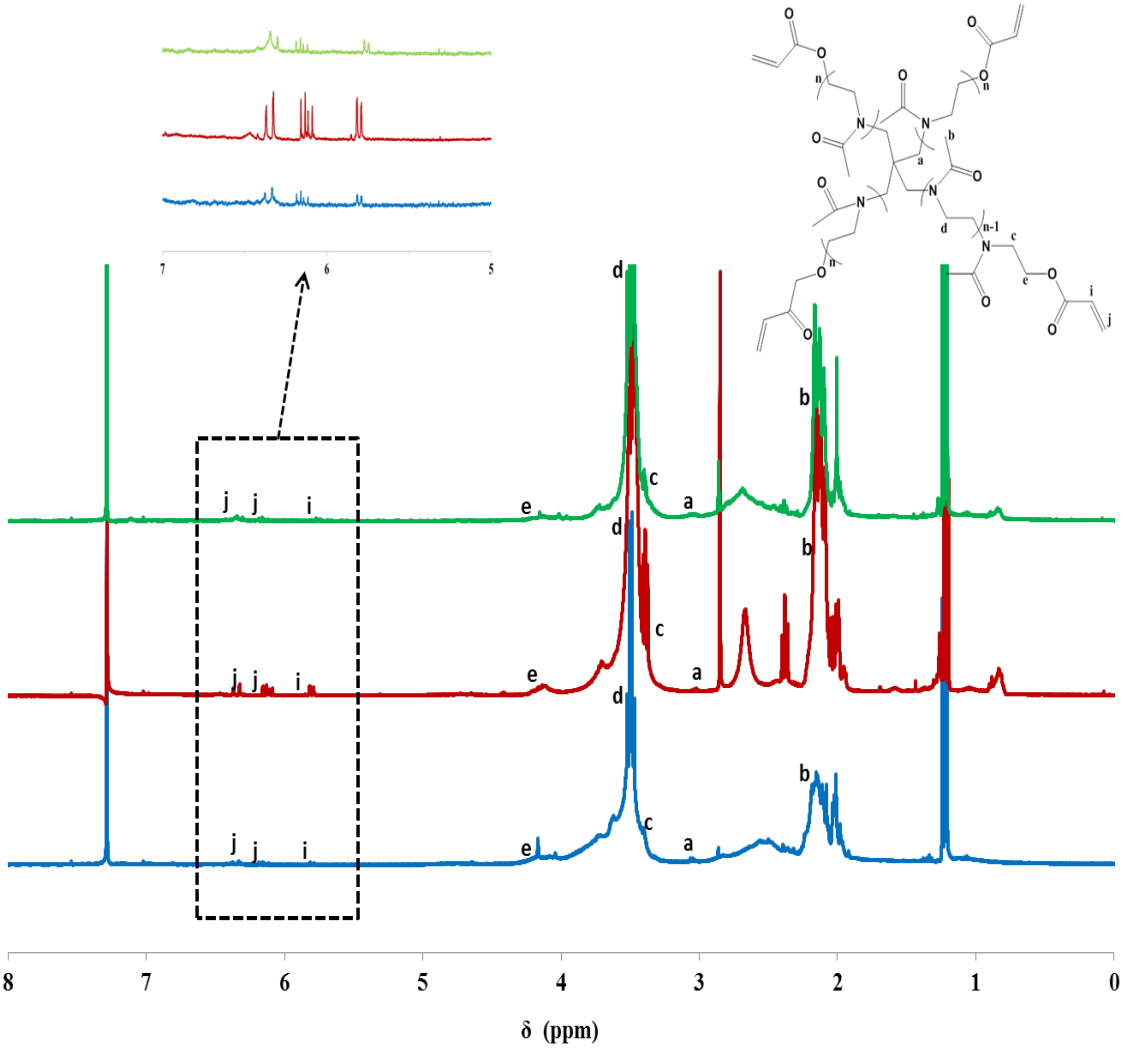

Figure 6.4 ^{1}H-NMR spectrum in $CDCl_3$ of three four arm polyoxazolines, which are oligo (MeOx) initiated with pentaerythrityl tetraiodide and terminated with acrylic acid.

From bottom to top, represent polyoxazolines with different degree of polymerization. Blue: 12.5 repeat units per arm. Red: 25 repeat units per arm. Green: 50 repeat units per arm (targeted degree of polymerization per arm).

For the NMR spectra we can see, after assignment of every peak to different protons belonging to poly (2-methyl-2-oxazoline), that the expected structures were obtained. In order to investigate the nature of the initiation groups and end groups in the oligomers synthesised, the ratios of characteristic peaks were calculated from the corresponding integrals. Again, comparison between end groups and main chain protons was used to confirm the efficiency of end capping. They all display the characteristic alkene multiplets at 6.31 ppm, 6.13 ppm and 5.79 ppm. When the degree of polymerization of 4I-PMeOx-acry targeted was 12.5 repeat units on each arm, corresponding ratios H_d/H_a was found to be 43.25, and H_d/H_j was found to be 131.77 which indicate very low efficiency of end capping with acrylate, both of the ratios are far higher than expected. In addition, H_d/H_e was found to be 6.99, which indicates no control of initiation as well as termination during the polymerization. When the degree of polymerization rise up to 25, again, the ratio of H_d/H_a was found to be 93.79, which indicates not control of initiation steps. Comparison of H_d and H_j gave a ratio of 70.81, which was higher than expected ratio 25 monomer to initiator/termination, but may indicate slightly better control of end capping with acrylate compared to 12.5 repeat units. More surprisingly, H_d/H_e was found to be 21.36 and may due to side reaction occured. For polymers with targeted 50 repeat units on each arm, surprisingly, H_d/H_a was found to be 48.32 which was very close to expected ratio 50 monomer to initiator/termination. It may indicate a control of initiation step. However, the corresponding ratios H_d/H_j and H_d/H_e were 56.76 and 19.98, respectively, which may indicate other side reactions occurred. Altogether

these ratios indicate uncontrolled end capping with acrylic acid. In all, all of the polymers showed no control over the initiation and termination step, except for targeted degree of polymerization was 50, initiation step was under control. It may due to steric hindrance so activated all two or four arms were very difficult.

6.2.1.2 Synthesis of two- and four-armed POx thiols

Although, from NMR, it seems we cannot control the polymerization of all two and four arms PMeOx, we observed reasonable control of alkene group end capping for some of the polymers and used these materials in following steps. Further functionalization with thioacetic acid and subsequent deacetylation steps was explored. Here, we functionalized 2I-PMeOx-acry and 4I-PMeOx-acry with thioacetic acid under base conditions, then cleaved the acetyl groups with hydroxylamine for 4 h.

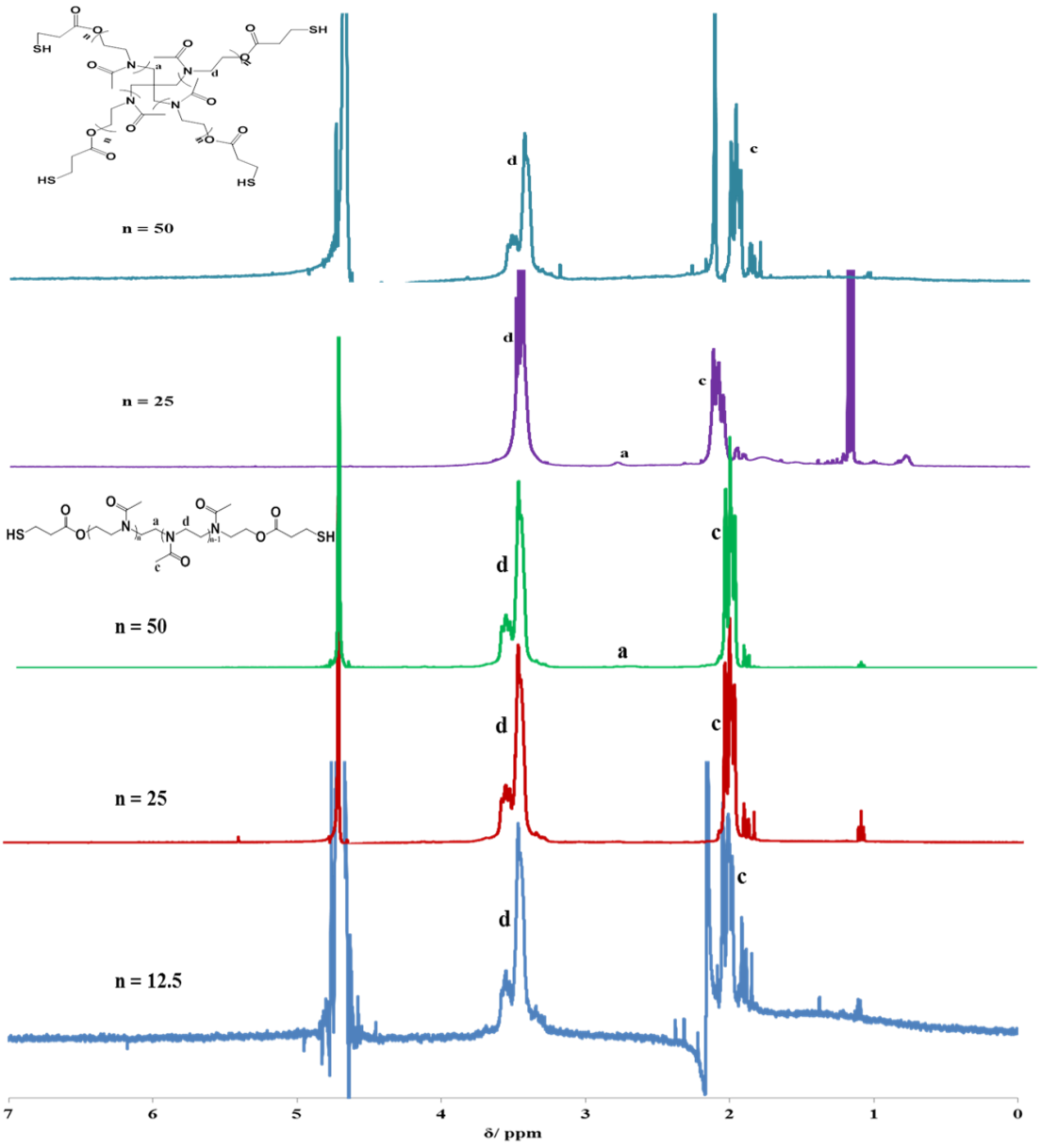

Figure 6.5 ^{1}H-NMR spectrum in $CDCl_3$ of five armed polyoxazolines, which are oligo (MeOx) initiated with two initiators: 1, 2-Diiodoethane and pentaerythrityl tetraiodide, and terminated with thiol. From bottom to top, represent armed polyoxazolines with different degree of polymerization. Blue: two arm polyoxazoline with 12.5 repeat units, red: two arm polyoxazoline with 25 repeat units, green: two arm polyoxazoline with 50 repeat units, purple: four arm polyoxazoline with 25 repeat units, indigo: four arm polyoxazoline with 50 repeat units. (DP are expected)

From figure 6.5 we can see the total disappearance of peaks at 6.31 ppm, 6.13 ppm and 5.79 ppm, which correspond to alkene groups from starting materials PMeOx-acry. This indicates that all polymers were successfully functionalized with thioacetic acid. Surprisingly, some of them did not show Ha which corresponds to initiation step. When the degree of polymerization of 2I-PMeOx-thiol targeted was 12.5 repeat units on each arm, we cannot determine the H_a, which may due to the cleavage. Apparently, we can see a peak at 2.25 ppm that corresponds to acetyl group, which indicate the hydrolysis step was not efficient. Similarly, when target degree of polymerization rise up to 25, no H_a was found from NMR spectra, however, no acetyl groups appeared. Furthermore, for polymers with targeted 50 repeat units on each arm, corresponding ratios H_d/H_a was found to be 41.95, while from 2I-PMeOx-acry DP was 32, which may be not very accurate integrals of H_a that was calculated as not clear peak shown in the spectra. For 4I-PMeOx-thiol, when the degree of polymerization was 25, we can see a significant peak belonging to H_a at 2.81 ppm, and H_d/H_a was found to be 29.03. In addition, when rise up the degree of polymerization to 50, we cannot see peak at 2.81 ppm, however, acetyl groups were found at 2.25 ppm indicate a failure of hydrolyse step. Overall, we suggest that a successful functionalization with thioacetic acid as alkene disappeared for all polymers, while deacetylation steps need to be improved.

Therefore, we did FTIR (not shown here) as well as MALDI for some sample to confirm the result from NMR.

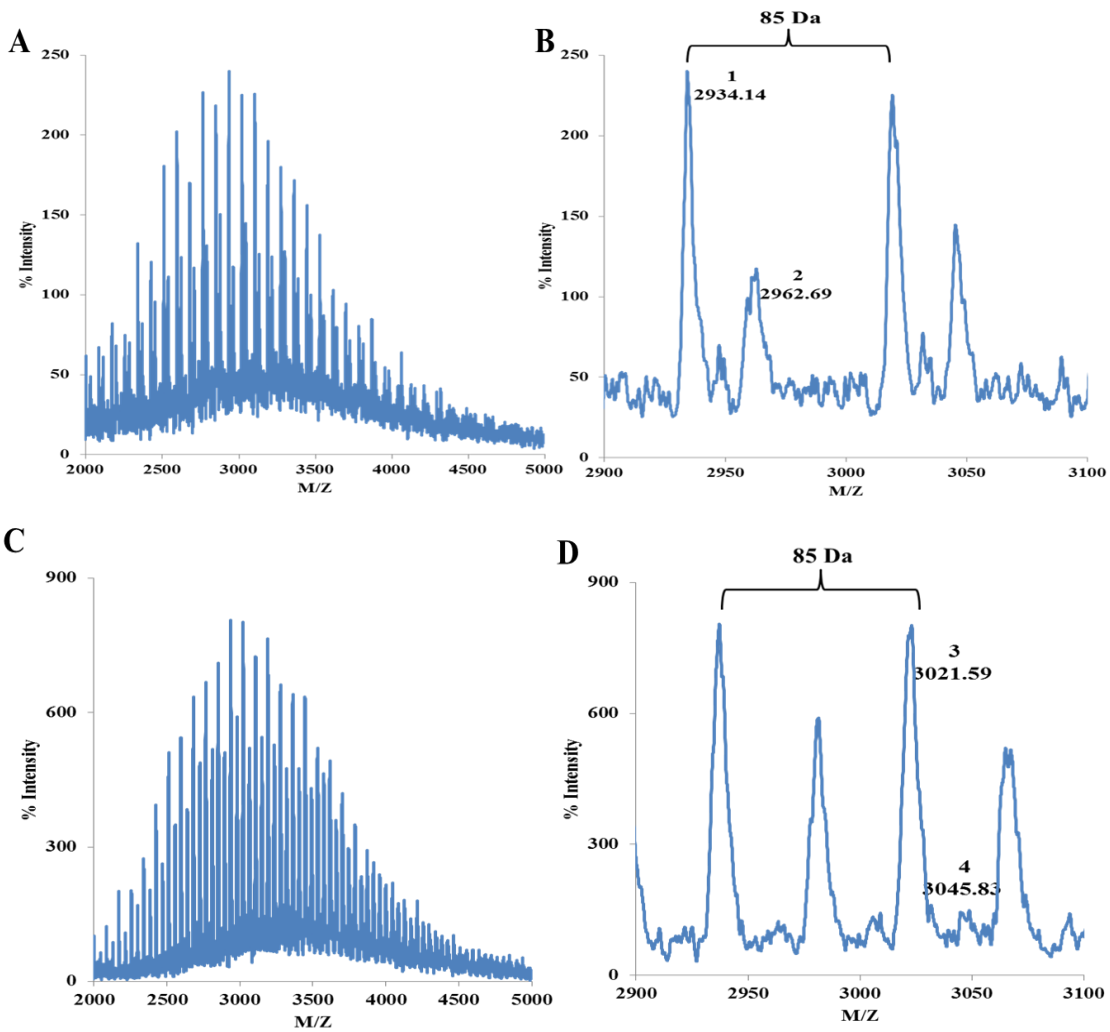
A
% Intensity
M/Z
B
85 Da
1
2934.14
2
2962.69
% Intensity
M/Z
C
% Intensity
M/Z
D
85 Da
3
3021.59
4
3045.83
% Intensity
M/Z

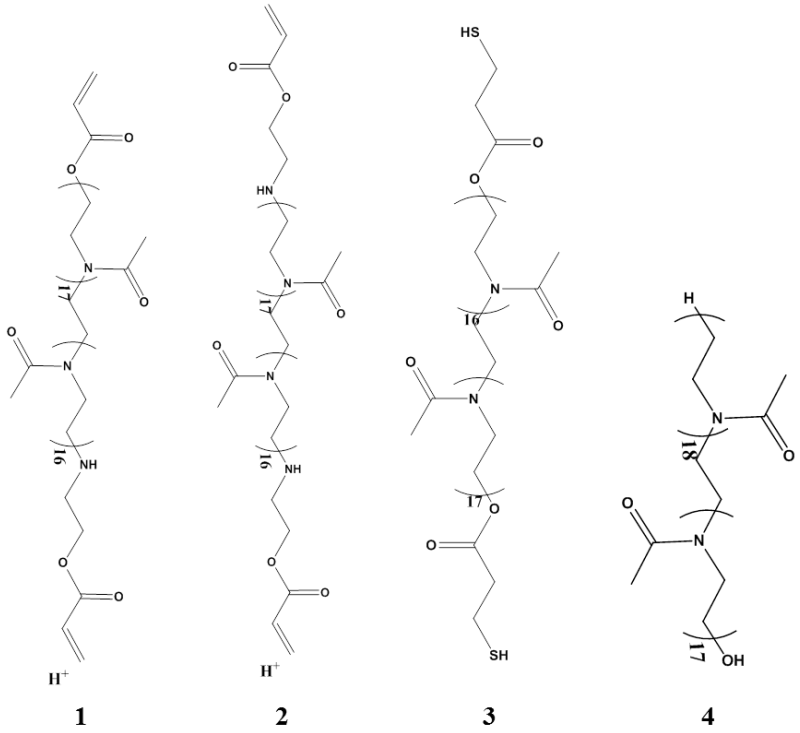

Figure 6.6 MALDI-ToF-MS of two arm PmeOx obtained by end capping with acrylate and and thiol. A. Full spectrum of 2I-PMeOx-acry, B. zoom into the region m/z 700-900 of A, C. Full spectrum of 2I-PmeOx-thiol, D. zoom into the region m/z 700-900 of C. Schematic representation of the proposed structures corresponding to the signals.

From the full MALDI spectra we can see that a distribution of peaks with a main peak at 2934.14 Da (expected 2934.34 Da) corresponds to the targeted structure but missing one side chain with proton as counterions. A degree of polymerization of 17 was obtained from MALDI which is higher than NMR result that 13.51 were obtained. A second distribution with a main peak at 2962.69 Da occurs for the 1, 2-Diiodoethane initiated oligomers (MeOx) but appears to be terminated with acrylic groups and missing two side chain, indicating some level of hydrolysis. For target 2I-PmeOx-thiol, only small distribution peak 4 in figure 6.7 was observed at 3021.59 Da (expected 3045.83 Da) for the target structure. A main peak at 3021.59 Da (expected 3021.21 Da)

represents 1, 2-Diiodoethane initiated oligomers (MeOx) and terminated with hydroxyl and proton, which indicates deacetylation steps with hydroxylamine was not selective. Overall, these results contrast slightly with the NMR data obtained that had indicated a good match between the termination and initiation steps and indicate some level of hydrolysis of the oligomers, presumably during their purification (via extraction). Distributions clearly displayed main peaks separated by 85 Da, which corresponding to methyl-oxazoline repeat units.

6.2.2 Synthesis of Bu-POx thiol

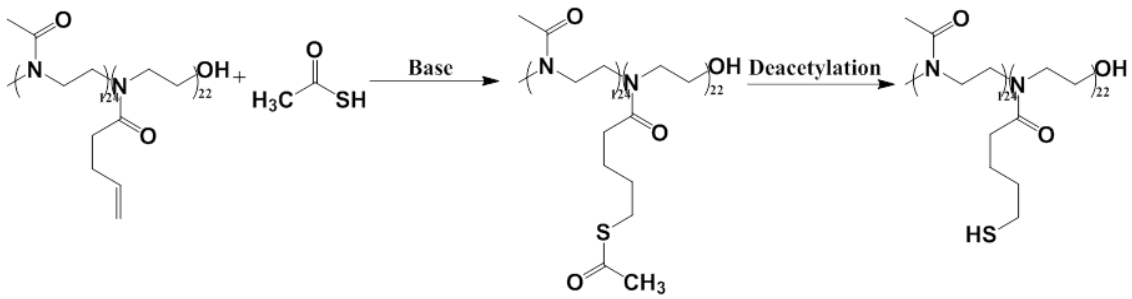

Scheme 6.3 Synthesis and mechanism of thiol functionalised poly(2-methyl-2-oxazoline) on lateral chain.

As from previous study, we cannot control the initiation with pentaerythrityl tetraiodide and terminated with acrylate, and to some extent we can control the initiation with 1, 2-diiodoethane but failed to control end capping with acrylate, we investigated another approach to synthesize thiolated poly(oxazolines). Here, we explored the functionalization of Bu-PMeOxOH with thiols lateral chains, using reaction of thioacetic acid, followed by deacetylation. Two different deacetylation methods were studied: in acid and base conditions. Base catalyzed deacetylation of corresponding

thioacetates allowed cleaving acetyl groups from thioacetate pendant chains. The mechanism of modified Bu-PMeOxOH side chain with thiol was shown in scheme 6.3.

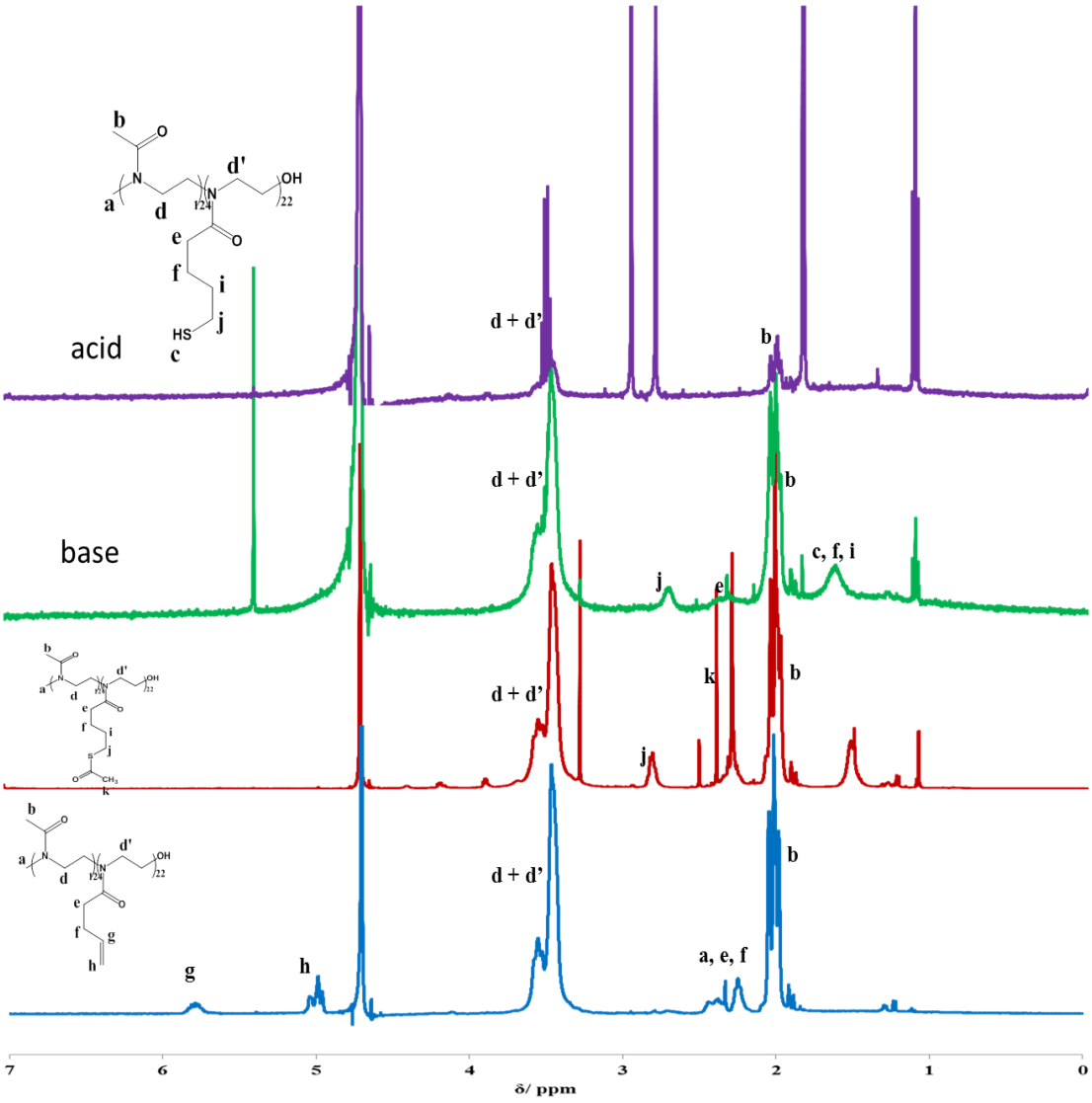

Figure 6.7 ^{1}H-NMR spectrum in D_2O of copolymer Bu-PMeOx, with different end groups and all initiated with methyl tosylate. From bottom to top, represent the typical product belonging to each functionalized step. blue: Bu-PMeOx, red: Bu-PMeOx

functionalized with thioacetic acid, green: Bu-PMeOx-SH hydrolyzed via base condition, purple: Bu-PMeOx-SH via hydroxylamine condition.

Figure 6.7 displays NMR spectra of Bu-PMeOx and corresponding intermediates before and after functionalization with thioacetic acid and after deacetylation of thioacetate groups. The copolymer Bu-PMeOxOH displays characteristic alkene multiplets at 5.81 ppm and 5.02 ppm, belonging to alkene group from lateral butene chains. It was shown in previous study that 15% of alkene from lateral chain in copolymers, in good agreement with previous reports and the expected comonomer ratio.[295] Furthermore, after Bu-PMeOx was functionalized with thioacetic acid under base conditions, alkene multiplets disappeared fully which indicate that alkene groups reacted fully with thioacetic acid. Peak at 2.40 ppm shown in figure 6.7 represent acetyl groups from thioacetic groups. Afterwards, we deacetylated acetyl group with base for 4 h (see Figure 6.7 green line). H_j and H_e appeared at 2.68 ppm and 2.77 ppm, moreover, peak at 1.63 ppm represent H_c, H_f and H_e. According to the calculated integrals, $H_{d'}/H_j$ was found to be 1.91 while the expected ratio should be 2. Moreover, $H_b/H_{(d+d')}$ was found to be 12%, which showed a decrease percentage of butene in copolymers, indicate some hydrolyze of lateral chain occurred during the deacetylation steps. Apparently H_b at 1.9 ppm dramatically decreased after hydrolyzed with hydroxylamine compared with hydrolyzed in base conditions, which indicate lateral chain (methyl) of copolymer was not stable in acid condition. Overall, we suppose the base condition to deacetylate is milder than hydroxylamine condition although still some of the alkene lateral chains have been cleaved.

6.2.3 Preparation of POx-based hydrogels via thiol-ene reaction

Flory-Stockmayer theory was conceptualized in 1941 and then further developed by Stockmayer in 1944, which was shown in figure 6.8. In this theory they made three assumptions that affect the gelation[303, 304].

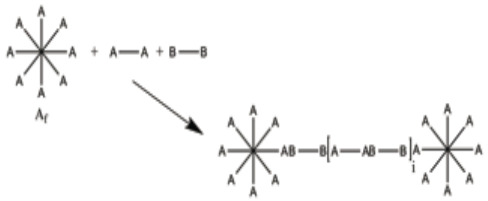

Figure 6.8 A general image of a multifunctional branch unit.

Three assumptions were

1. All functional groups on a branch unit are equally reactive.
2. All reactions occurs between A and B.
3. There are no intramolecular reactions.

It was reported that the functionality number is very important to achieve gelation at very low reactivities, and improve on the controlled degradation of the resulting gels. For example: having synthesised a range of alkene functionalised POx and thiol functionalised POx, we next examined their ability to generate hydrogels. the degree of functionality (i.e., the number of double bonds per polymer chain) influence the gel structure and gel properties. For example, the cross-linking density can be increased by simply increasing the number of functional groups on the polymer chains for a given molecular weight and macromer concentration[143]. Abdel and colleagues found that when trimethylolpropane trimethacrylate (TPT) as hexafunctional crosslinker was replaced by methylene bisacrylamide (MBA) as tetrafunctional crosslinker, the swelling

parameter EWC for crosslinked N-vinyl-2-pyrrolidone-*co*-butyl acrylate (VP-BA) copolymers decreased[305]. Moreover, Giridhar et al studied the effect of functionality of crosslinker on the swelling properties. Superabsorbents (SAPs) was prepared by monomer [2-(methacryloyloxy) ethyl] trimethylammonium chloride with different crosslinkers: hexafunctional trimethylpropane trimethacrylate (TMPTA), pentaerythritol triacrlylate (PETA), pentaerythritol tetraacrylate (PETTA), N, N-methylene bisacrylamide (MBA), ethylene glycol dimethacrylate(EGDMA). The order of swelling capacities in DI water is as follows: TMPTA > PETA > PETTA > MBA > EGDMA[305]. In addition, Marra et al. investigated the mechanical properties of multi-arm amino-terminated poly(ethylene glycol) (PEG) hydrogels that crosslinked with genipin via chain growth polymerization, they found that 8-arm PEG showed much slower gelation time compared to 4-arm PEG, moreover, 4-arm PEG displayed a porous structure, while 8-arm PEG displayed comparatively compact structure which indicate less cross link density was obtained[306].

Hence, we investigated the effect of different concentrations of multi-arm PEG-SH on the gelation behaviour and mechanical properties with *in situ* rheology when crosslinked with Bu-PMeOx-OH, the concentrations are C/2.5(540 mM), C/3 (450 mM), C/5 (270 mM), respectively. Moreover, we investigated the effect of the number of –SH on PEG-POx hydrogels, four different multi-arm PEG-SH crosslinked with Bu-PMeOx-OH via thiol-ene chemistry and they are PEG-2SH (1,000), PEG-4SH (5,000), PEG-4SH (20,000) and PEG-8SH (20,000), respectively. Furthermore, co-PEG thiol hydrogels that based on PEG-2SH (1,000) and PEG-8SH (20,000) cross linked with Bu-PMeOx-OH were characterized with *in situ* rheology. *In situ* rheology was carried out here to monitor the mechanical properties, mixed solution was exposed to 120 s UV

irradiation, and thiol to alkene is 90% and UV irradiation (17mw/cm^2). In addition, copolymer Bu-PMeOx-OH with thiol pendent was crosslinked with Bu-PMeOx-OH via Michael addition to fabricate pure POx hydrogels was also studied. Mixed solution was directly exposed to UV irradiation for 120 s and thiol to alkene is 90% and UV irradiation (50 mW/cm^2).

6.2.3.1 Attempts to prepare hydrogels purely based on POx precursors

Synthesized PMeOx-2SH (Mw=13,000 g/mol) was crosslinked with BuPMeOxOH at a concentration of C (13.5 x 10^{-4} mol/mL, 1350 mM) under exposure to UV irradiation for 120 s in the presence of photoinitiator (IRG 2959) with an intensity of 17 mW/cm^2. The formation of pure POx hydrogels was characterized by *in situ* rheology to investigate the mechanical properties of the resulting materials, during time sweeps, frequency sweeps, amplitude sweeps and stress relaxation.

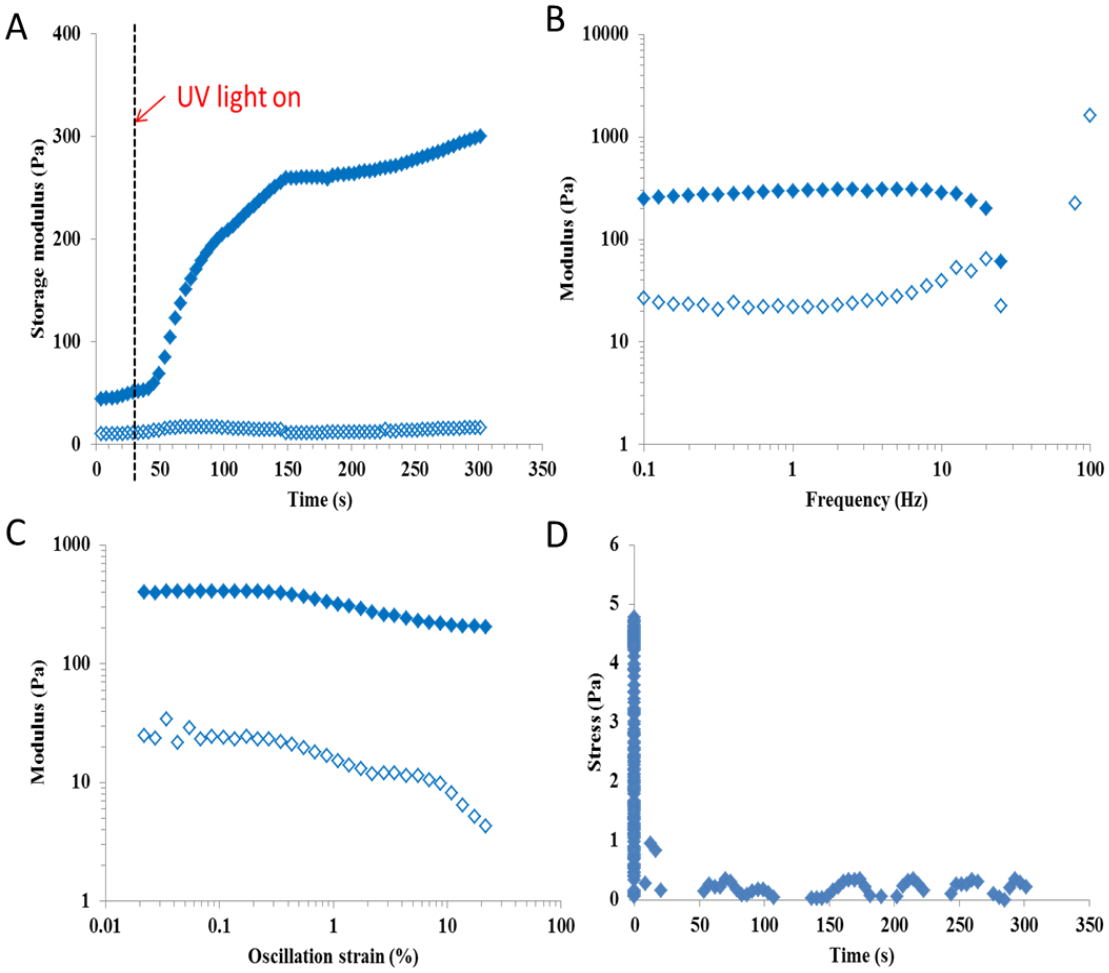

Figure 6.9 Example of gelation behaviour and mechanical properties of photo cross-linked hydrogels based on PMeOx-2SH (Mw=13,000 g/mol) and BuPMeOxOH via thiol-ene chemistry. A. Time sweep (frequency and strain of oscillation are 1 Hz and 2%, respectively) shows the evolution of storage modulus (G') and loss modulus (G'') during UV irradiation (UV irradiated at 17 mW/cm^2). The sample was conditioned for 30 s prior to UV exposure and irradiated for 120 s. B. Frequency sweeps (frequency varied from 0.1 Hz to 100 Hz) was used to confirm the structure of mixed POx-POx networks. C. Amplitude sweep (frequency is 1 Hz) was carried out to limit the value of the linear viscoelastic (LVE) range. D. Stress relaxation (strain of oscillation is 2%) was carried out to judge the elastic property of formed networks.

We first tested the preparation of POx hydrogels via thiol-ene chemistry and the mechanical properties were characterized by *in situ* rheology. From figure 6.9 we can see the storage moduli from time sweeps always higher than loss moduli, and start to increase once mixed with BuPMeOxOH. After 160 s it reached the highest storage moduli and then remained at 0.3 kPa until 300 s. This behaviour suggests some degree of reactivity, but the failure to generate a crosslinked macroscopic network. This was confirmed by the absence of gel after removal of the top geometry. Frequency and strain sweeps confirmed these behaviours. In fact, the strain sweeps gave some evidence of shear thinning behaviour that would be expected from polymer solutions[307]. In figure 6.9 D, it is also clear that no residual stress is retained even at early time points in stress relaxation experiments, consistent with the lack of elasticity of the materials obtained. Hence these results indicate that PMeOx-2SH (Mw=13,000 g/mol) partially crosslinked the alkene functionalized POx and resulted in solutions with increased viscosities, but no macroscopic hydrogel. None of the other POx thiols synthesized afforded any stronger evidence of crosslinking. Hence the subsequent sections focused on the formation of PEG-POx mixed hydrogels. We switched to this system as we rationalize that the lack of gelation resulted from the poor control we had on the structure of the multiarm POx thiols synthesised in the previous section.

Moreover, we tried to crosslink BuPMeOxOH with pendant thiols of PMeOx, but cannot see any hydrogel forming after the same condition, to verify whether pendent thiols of PMeOx can react with alkene, we characterised the product by NMR, which was shown in figure 5.10.

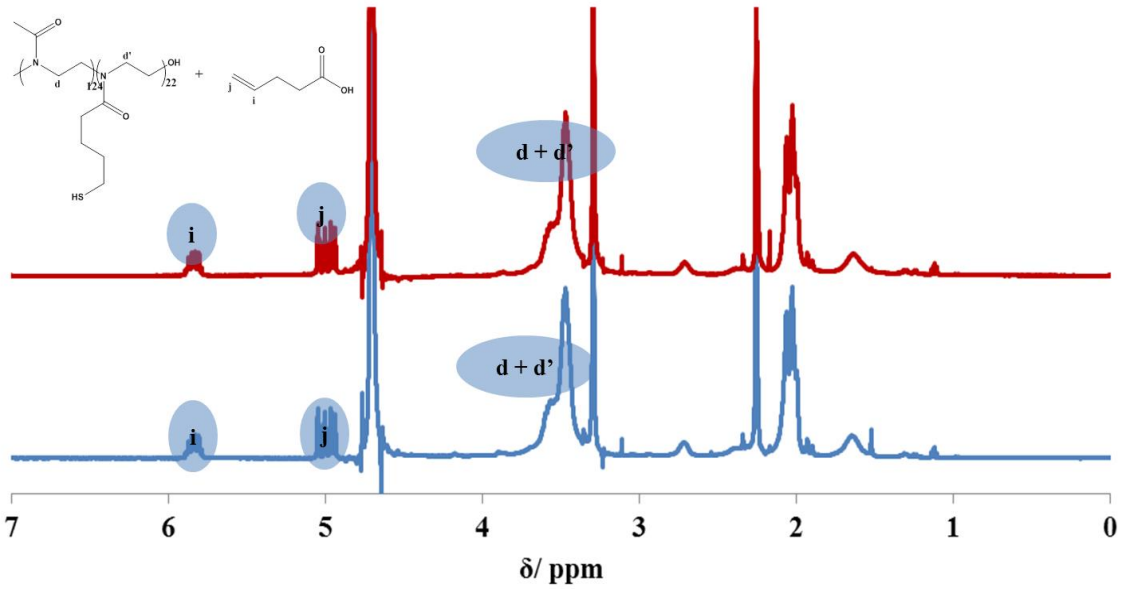

Figure 6.10 ^{1}H-NMR spectrum in D_2O of dialyzed pendent thiol of PMeOx with 4-Pentenoic acid in the presence of 50 mol% photoinitiator. blue: mixed solution before UV irradiation, red: mixed solution after UV irradiation. PH was adjusting to 7 before UV irradiation. UV intensity: 50 mW/cm^2, 300s.

Apparently, being exposed to UV light, peaks at 5.85 ppm and 5.04 ppm did not change at all. The ratios $H_j/H_{(d+d')}$ indicate alkene to main chain (3.47 ppm) were still the same. Therefore, it indicates something is killing the reactivity not only the problem of controlling the thiol.

6.2.3.2 Mixed PEG-POx hydrogels: Impact of total concentration

Two arm POx thiol n= 12.5, 25, 50

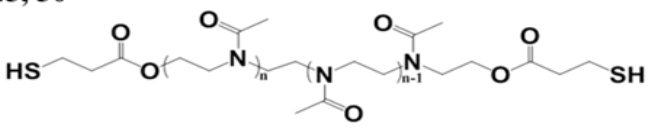

Four arm POx thiol n= 12.5, 25, 50

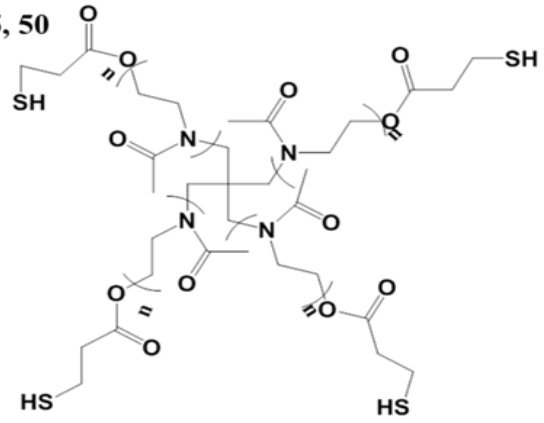

PEG di-thiol (Mn= 1000 g/mol)

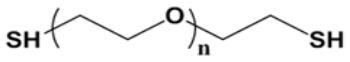

PEG tetra-thiol (Mn= 5000 g/mol, 20,000 g/mol)

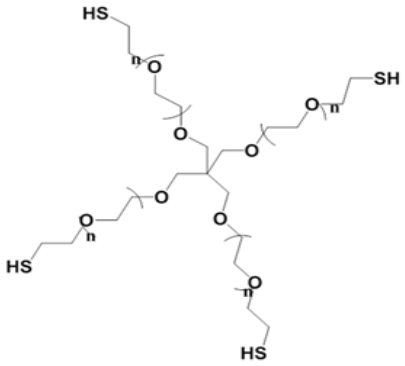

PEG hexa-thiol (Mn= 20,000 g/mol)

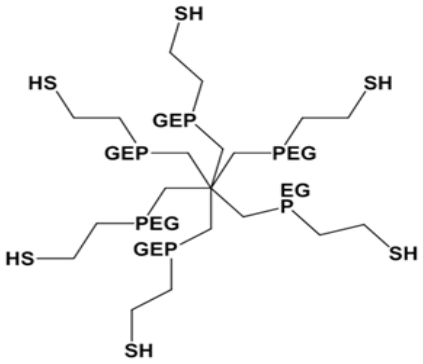

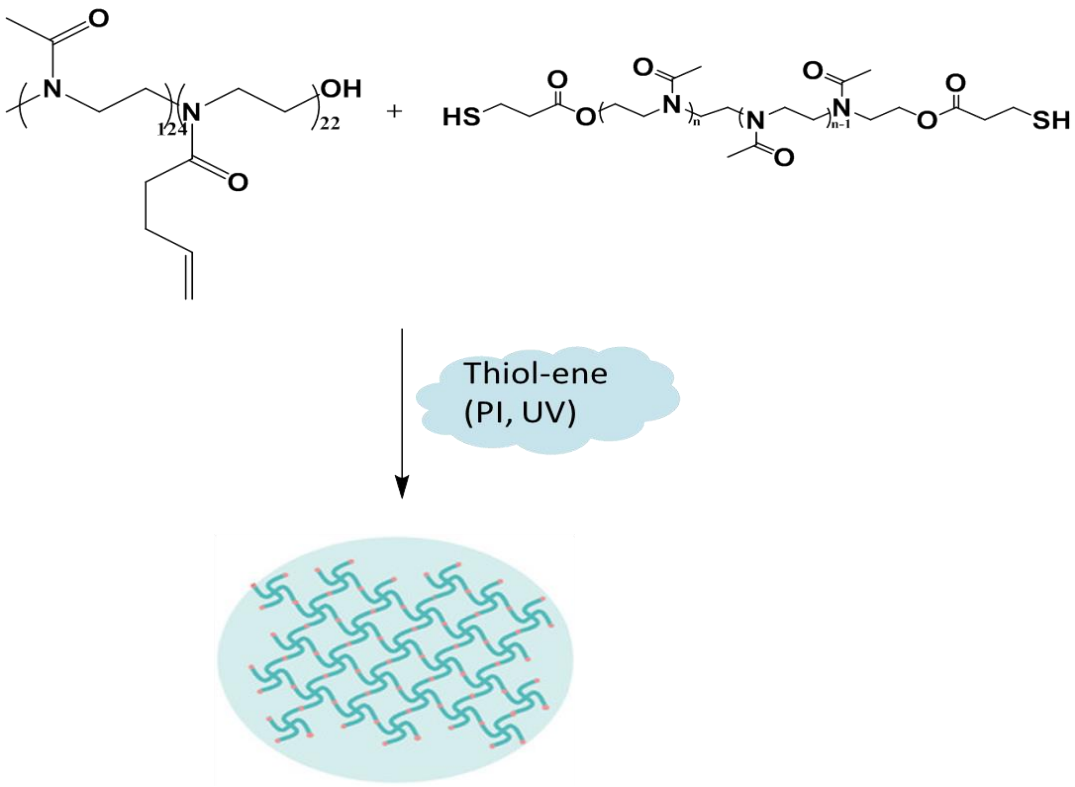

Figure 6.11 structure of thiols and alkene functionalized Pox, a general mechanism of thiol-ene chemistry to fabricate hydrogel.

We investigated next the preparation of mixed PEG-POx hydrogels. We first studied the impact of total thiol-ene concentration on fabricated PEG-POx hydrogels. To fabricate hydrogels for characterization, solutes were dissolved in PBS at three different concentrations, which are C2.5 (5.4 x 10^{-4} mol/mL, 540 mM), C3 (4.5 x 10^{-4} mol/mL, 450 mM) and C5 (2.7 x 10^{-4} mol/mL, 270 mM), respectively. Solutes are: polymer backbone (15% alkene of Bu-PMeOxOH), crosslinkers [four different multi-arms PEG-SH with different molecular weight are PEG-2SH (Mw=1,000 g/mol), PEG-4SH (Mw=5,000 g/mol), PEG-4SH (Mw=20,000 g/mol) and PEG-8SH (Mw=20,000 g/mol)] and IRG 2959 in ethanol (250mg/mL). Crosslinked hydrogels were generated using 5 mol% PI. The structure of thiols and alkene as well as a general mechanism of fabricating hydrogels was shown in figure 6.11.

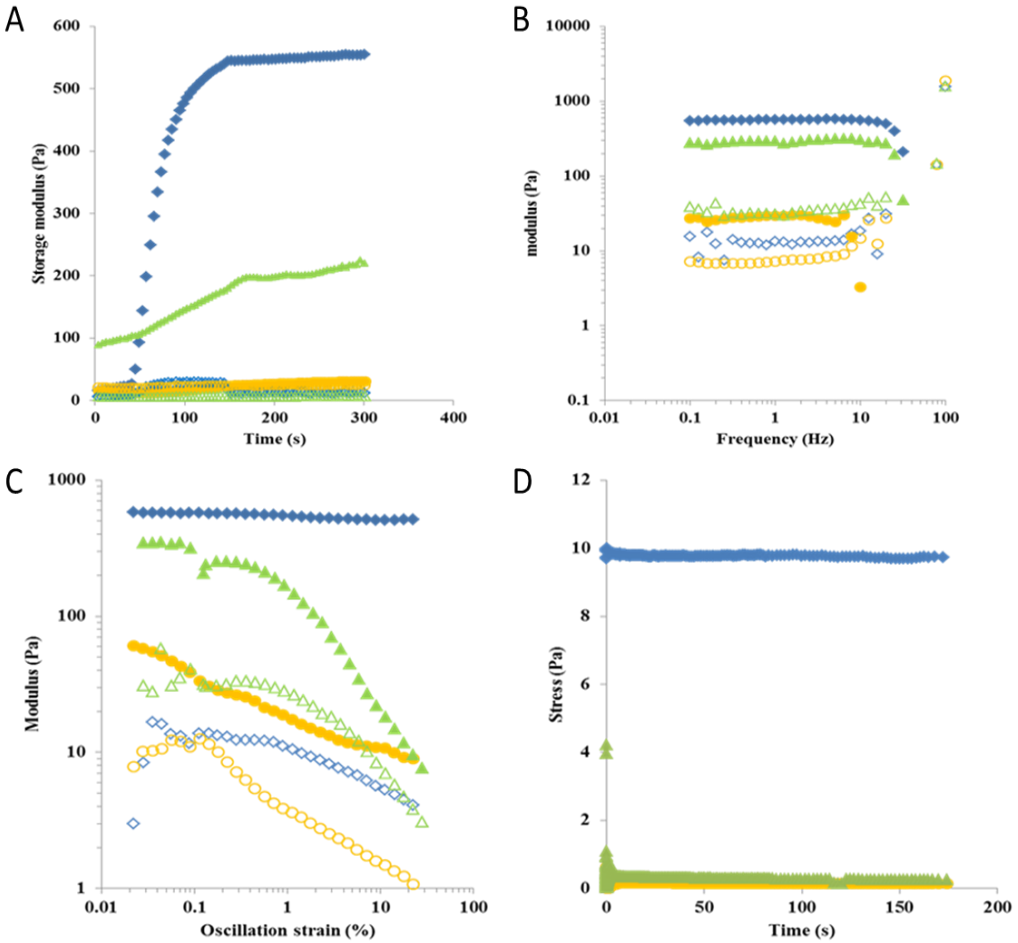

Figure 6.12 Impact of total concentration on the gelation behaviour and the mechanical properties of photo cross-linked hydrogels based on PEG-2SH (Mw=1,000 g/mol) and Bu-POx-OH via thiol-ene chemistry. A. Time sweep (frequency and strain of oscillation are 1 Hz and 2%, respectively) shows the evolution of storage modulus (G') and loss modulus (G'') during UV irradiation (UV irradiated at 17 mW/cm^2). The sample was conditioned for 30 s prior to UV exposure and irradiated for 120 s. B. Frequency sweeps (frequency varied from 0.1 Hz to 100 Hz) was used to confirm the structure of mixed PEG-POx networks. C. Amplitude sweep (frequency is 1 Hz) was carried out to limit the value of the linear viscoelastic (LVE) range. D. Stress relaxation (strain of oscillation is 2%) was carried out to judge the elastic property of formed networks.

As can be seen in figure 6.12, three different concentrations of thiol-ene solution were prepared when PEG-2SH (1000) crosslinked BuPMeOxOH. The respective ratios of alkene and thiols were kept constant. A full set of tests was carried out via *in situ* rheology: time sweeps, frequency sweeps, amplitude sweeps and stress relaxation. Rheology was carried out during and after 120 s UV irradiation. For the 540 mM gel, the shear moduli clearly increased shortly after the UV was switched on, indicating a rapid reactivity. By 148 s, a plateau was reached. Similar behaviours were observed at lower concentrations, although the increase in storage modulus was far less pronounced, especially for the 270 mM gels. Although the highest storage modulus was only around 0.6 kPa for concentration 540 mM, after remove the top geometry gel was observed, which indicate a cross-linked microscopic network was formed. However, when remove the top geometry no observation of gel was found from the other two lower concentration, this behavior suggests some degree of reactivity but the failure to generate a macroscopic network. Moreover, with 540 mM it displayed a rapidly increase of storage moduli after around 40 s and the UV irradiation was turn on at 30 s, which may indicate the radical polymerization undergo a pre-polymerization time for step growth polymerisation[308]. Furthermore, concentration 450 mM showed steady growth of storage modulus during 120 s of UV irradiation and obtained 0.2 kPa after 300 s. When remove the top geometry a sol-gel was found, which may indicate partially cross-linked macroscopic network was formed. In addition, concentration 270 mM obtained 0.05 kPa after 300 s, and this behavior may suggest high reactivity but failed to generate a macroscopic network, which was confirmed by removing the top geometry but no gel was found.

These results were confirmed by frequency sweeps and stress sweeps. Frequency sweeps for the 540 mM and 450 mM showed a relatively stable frequency independent profile, until 11 Hz, consistent with the formation of a macroscopic gel. However, 270 mM showed a marked decrease at much lower frequencies (5 Hz). Similarly the strain sweeps of 450 mM and 270 mM showed a considerable shear thinning profile, indicating weaker gels. These results were confirmed by stress relaxation experiments, which showed a clear elastic profile (very little relaxation) for the 540 mM gel, and high levels of stress relaxation for 450 mM gel.

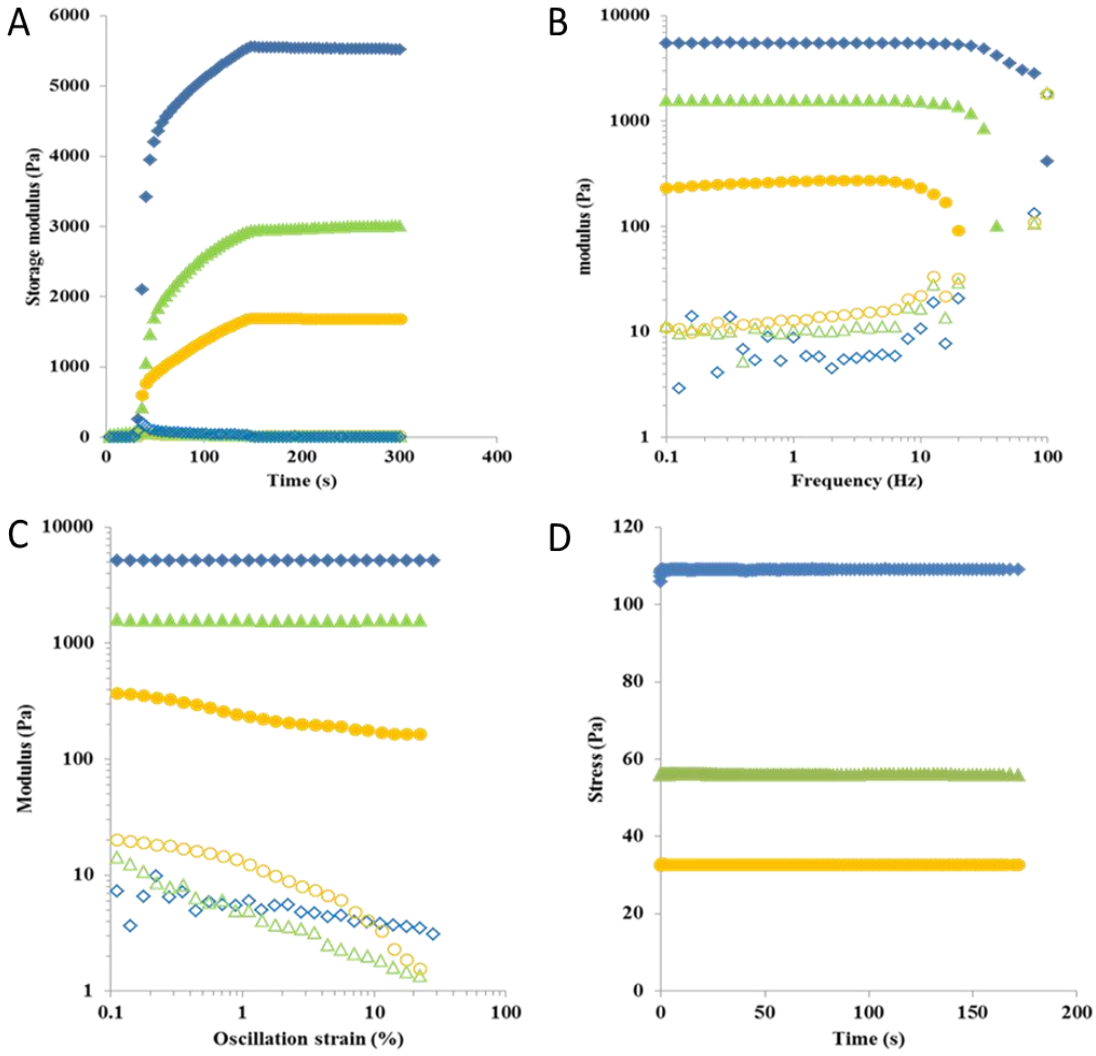

Figure 6.13 Impact of total concentration on the gelation behaviour and the mechanical properties of photo cross-linked hydrogels based on PEG-4SH (Mw=5,000 g/mol) and Bu-POx-OH via thiol-ene chemistry. A. Time sweep (frequency and strain of oscillation are 1 Hz and 2%, respectively) shows the evolution of storage modulus (G') and loss modulus (G'') during UV irradiation (UV irradiated at 17 mW/cm^2). The sample was conditioned for 30 s prior to UV exposure and irradiated for 120 s. B. Frequency sweeps (frequency varied from 0.1 Hz to 100 Hz) was used to confirm the structure of mixed PEG-POx networks. C. Amplitude sweep (frequency is 1 Hz) was carried out to limit the value of the linear viscoelastic (LVE) range. D. Stress relaxation (strain of oscillation is 2%) was carried out to judge the elastic property of formed networks.

In contrast, 270 mM displayed very little residual stress, consistent with the lack of macroscopic crosslinked network formed at this concentration.

From figure 6.13 we can see three different concentrations of thiol-ene solution were prepared when PEG-4SH (5000) cross-linked BuPMeOxOH. The respective ratios of alkene and thiols were kept constant. A full set of tests was carried out via *in situ* rheology: time sweeps, frequency sweeps, amplitude sweeps and stress relaxation. Rheology was carried out during and after 120 s UV irradiation. The storage moduli from time weep always higher than loss moduli, and start to increase rapidly after 7 s when exposed to UV-light. After 140 s it reached the highest storage moduli and then remained at a 1.7 kPa, 2.8 kPa, 5.8 kPa, respectively, after 300 s. This behavior suggests highly elastic materials were obtained. This was confirmed by the absence of gel after removal of the top geometry.

Moreover, frequency and strain sweeps confirmed these behaviors. Frequency sweeps for 540 mM and 450 mM showed a clear stable frequency independent profile, consistent with the formation of a microscopic gel. However, 270 mM showed a marked decrease at much lower frequencies (6 Hz). Similarly the strain sweep of 270 mM showed a considerable shear thinning profile, indicating weaker gels. These results were confirmed by stress relaxation experiments, which showed a clear elastic profile. These results were confirmed by stress relaxation experiments, which showed high stress retention, consistent with the macroscopic cross-linked network formed at these concentrations. Hence, these results indicate PEG-4SH (5000) highly cross-linked the alkene functionalized POx at three concentrations and resulted in macroscopic hydrogels.

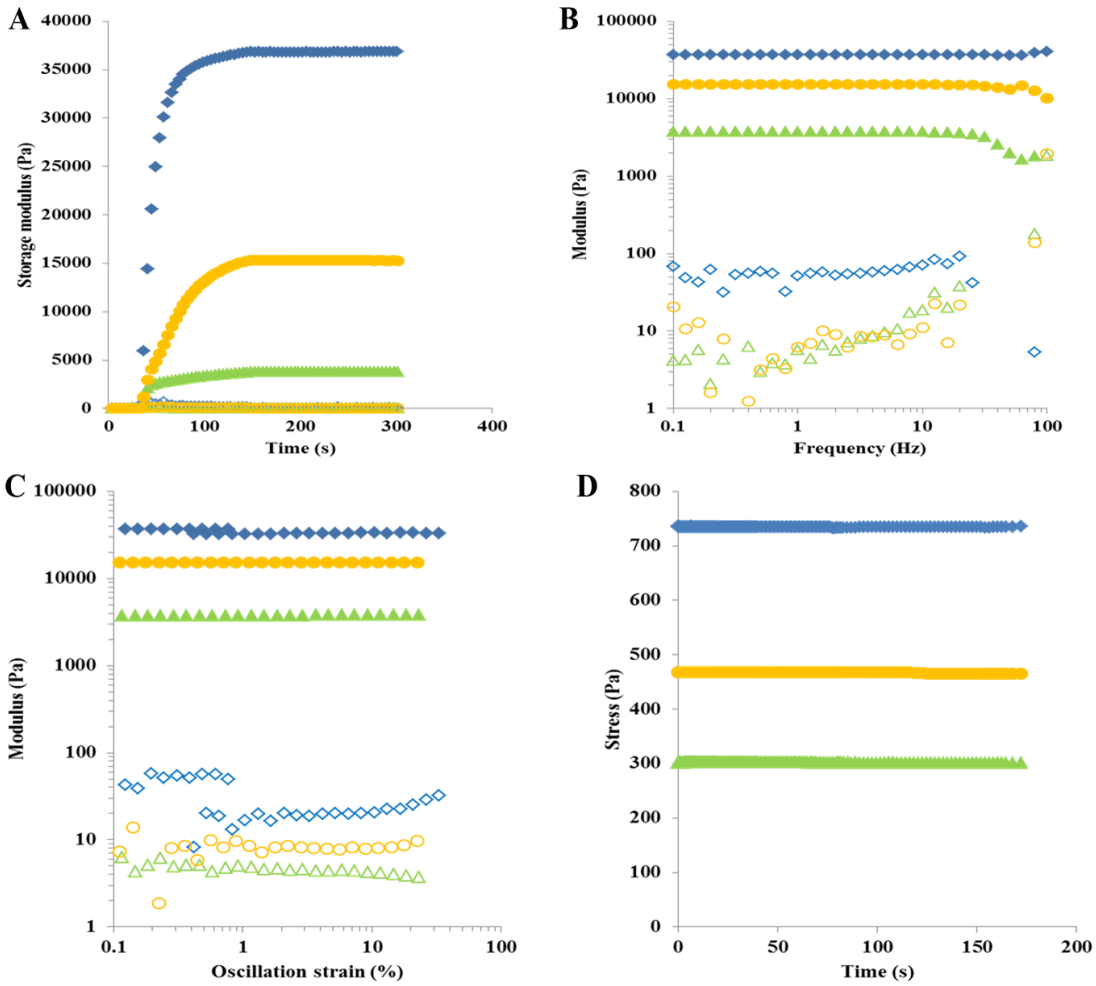

Figure 6.14 Impact of total concentration on the gelation behaviour and the mechanical properties of photo cross-linked hydrogels based on PEG-4SH (Mw=20,000 g/mol) and BuPOxOH via thiol-ene chemistry. A. Time sweep (frequency and strain of oscillation are 1 Hz and 2%, respectively) shows the evolution of storage modulus (G') and loss modulus (G'') during UV irradiation (UV irradiated at 17 mW/cm^2). The sample was conditioned for 30 s prior to UV exposure and irradiated for 120 s. B. Frequency sweeps (frequency varied from 0.1 Hz to 100 Hz) was used to confirm the structure of mixed PEG-POx networks. C. Amplitude sweep (frequency is 1 Hz) was carried out to limit the value of the linear viscoelastic (LVE) range. D. Stress relaxation (strain of oscillation is 2%) was carried out to judge the elastic property of formed networks.

As can be seen in figure 6.14, three different concentrations of thiol-ene solution were prepared when PEG-4SH (20,000) cross-linked BuPMeOxOH. The respective ratios of alkene and thiols were kept constant. A full set of tests was carried out via *in situ* rheology: time sweeps, frequency sweeps, amplitude sweeps and stress relaxation. Rheology was carried out during and after 120 s UV irradiation. For the three concentrations, the shear moduli clearly increased rapidly after 3 s when the UV was switched on, indicating a rapid reactivity. By 140 s, a plateau was reached. After remove the top geometry gels were found, which indicate highly cross-linked macroscopic networks were formed.

These results were confirmed by frequency sweeps and stress sweeps. Frequency sweeps for three concentrations showed a very stable frequency independent profile, until 12 Hz, consistent with the formation of a macroscopic gel. Similarly the strain sweeps of three concentrations showed a stable shear independent profile, indicating highly cross-linked gels. These results were confirmed by stress relaxation experiments, which showed high stress retention for three concentrations, consistent with the macroscopic cross-linked network formed.

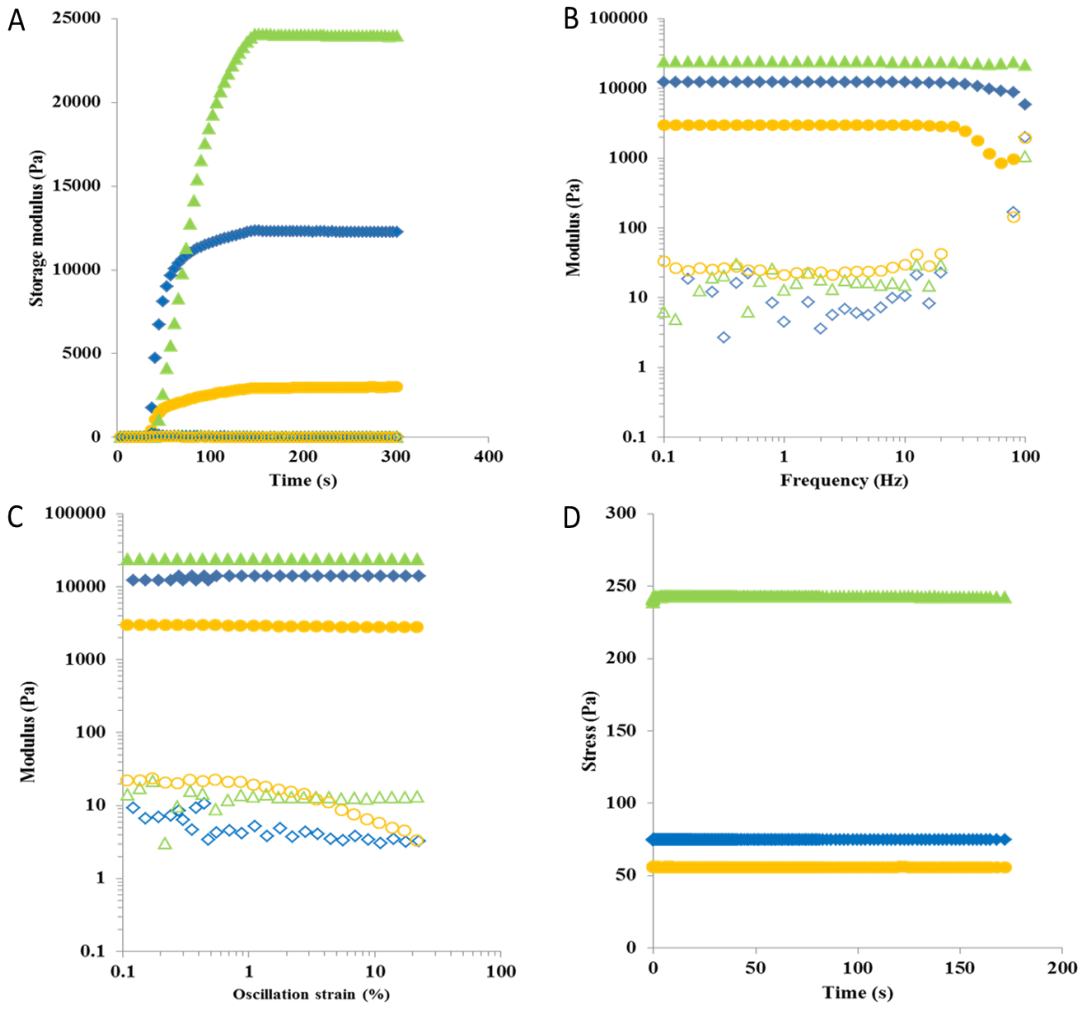

Figure 6.15 Impact of total concentration on the gelation behaviour and the mechanical properties of photo cross-linked hydrogels based on PEG-8SH (Mw=20,000 g/mol) and BuPOxOH via thiol-ene chemistry. A. Time sweep (frequency and strain of oscillation are 1 Hz and 2%, respectively) shows the evolution of storage modulus (G') and loss modulus (G'') during UV irradiation (UV irradiated at 17 mw/cm^2). The sample was conditioned for 30 s prior to UV exposure and irradiated for 120 s. B. Frequency sweeps (frequency varied from 0.1 Hz to 100 Hz) was used to confirm the structure of mixed PEG-POx networks. C. Amplitude sweep (frequency is 1 Hz) was carried out to limit the value of the linear viscoelastic (LVE) range. D. Stress relaxation (strain of oscillation is 2%) was carried out to judge the elastic property of formed networks.

As can be seen in figure 6.15, three different concentrations of thiol-ene solution were prepared when PEG-8SH (Mw=20,000 g/mol) cross-linked BuPMeOxOH. The respective ratios of alkene and thiols were kept constant. For the three concentrations, the shear moduli clearly increased rapidly after 7 s when the UV was switched on, indicating a rapid reactivity. By 144 s, a plateau was reached. After remove the top geometry gels were found, which indicate highly cross-linked macroscopic networks were formed.

These results were confirmed by frequency sweeps and stress sweeps. Frequency sweeps for three concentrations showed a very stable frequency independent profile, until 12 Hz, consistent with the formation of a macroscopic gel. Similarly the strain sweeps of three concentrations showed a stable shear independent profile, indicating highly cross-linked gels. These results were confirmed by stress relaxation experiments, which showed high stress retention for three concentrations, consistent with the macroscopic cross-linked network formed.

6.2.3.3 Mixed PEG-POx hydrogels: impact of the functionality number of PEG thiols

In order to investigate the impact of the functionality number of PEG-SH on PEG-POx hydrogels, four different types multi-arms PEG-SH were used here which are PEG-2SH (1,000), PEG-4SH (5,000), PEG-4SH (20,000) and PEG-8SH (20,000).

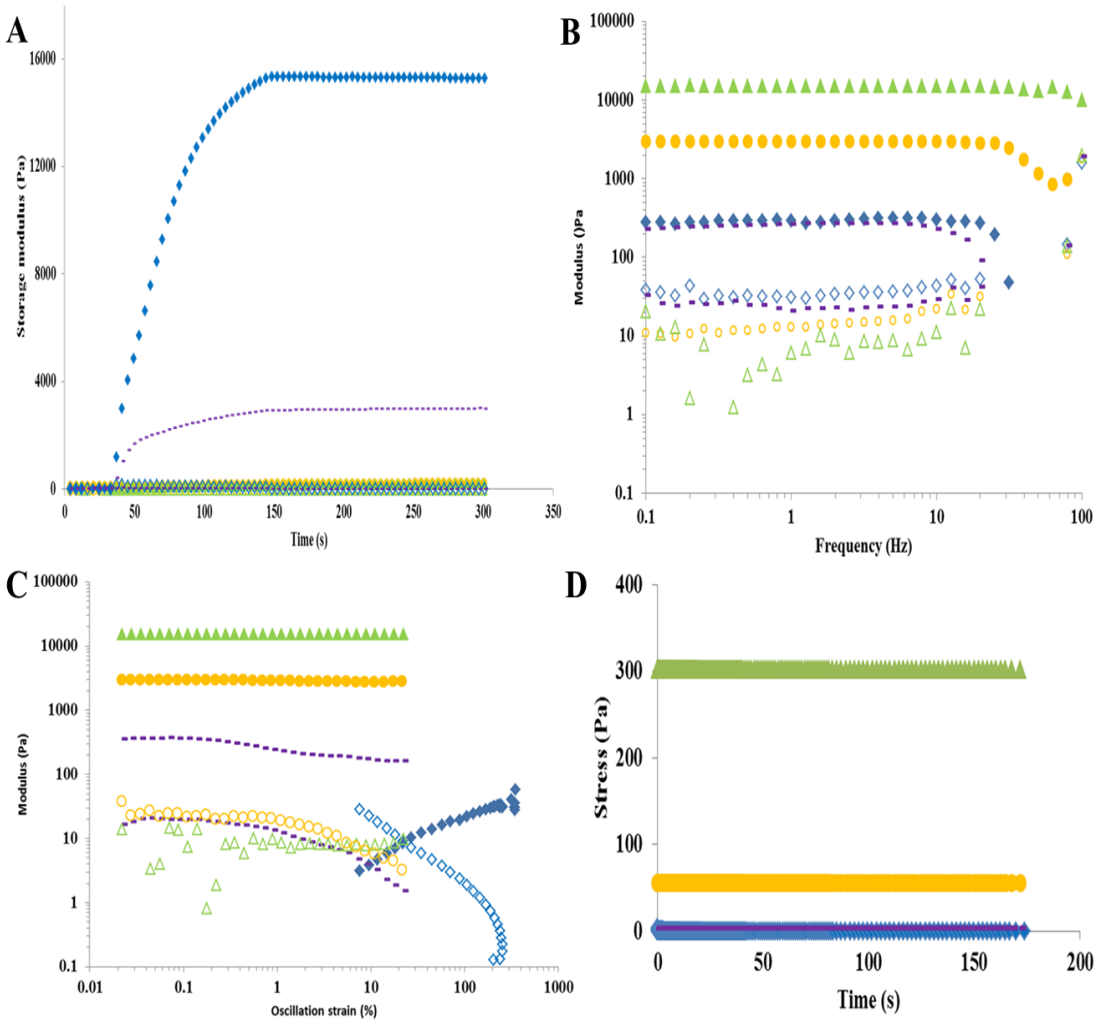

Figure 6.16 Impact of multi thiol type on the gelation behaviour and the mechanical properties of cross-linked POx network with 270 mM concentration of thiol-ene solution via thiol-ene chemistry and monitored by *in situ* rheology. A. Time sweep (frequency and strain of oscillation are 1 Hz and 2%, respectively) shows the evolution of storage modulus (G') and loss modulus (G'') during UV irradiation (UV irradiated at 17 mw/cm^2). The sample was conditioned for 30 s prior to UV exposure and irradiated for 120 s. B. Frequency sweeps (frequency varied from 0.1 Hz to 100 Hz) was used to confirm the structure of mixed PEG-POx networks. C. Amplitude sweep (frequency is 1 Hz) was carried out to limit the value of the linear viscoelastic (LVE) range. D. Stress relaxation (strain of oscillation is 2%) was carried out to judge the elastic property of

formed networks. blue: PEG-2SH (1,000), purple: PEG-4SH (5,000), green: PEG-4SH (20,000) and yellow: PEG-8SH (20,000).

At a concentration of 270 mM, thiol-ene solutions based on PEG-2SH (1,000) and PEG-4SH (5,000) displayed low storage moduli after 120 s of UV irradiation. In contrast, PEG-4SH (20,000) achieved the highest storage moduli as well as the shortest gelation time among other three type of multi-arm PEG (gelation started after 3 s of UV irradiation), followed by PEG-8SH (20,000). The results also indicate that with the same molecular weight of multi-arm PEG, the number of –thiols strongly affected the final shear modulus as the gel based on PEG-4SH (20,000) reached 15 kPa whereas that based on PEG-8SH (20,000) reached only 3 kPa after 120 s UV irradiation. However, with the same type of multi-arm-PEG (i.e. functionality number), increasing the molecular weight of PEG-SH increased the storage modulus of the gel obtained. For example, the gel based on PEG-4SH (5,000) achieved 0.2 kPa, while that based on PEG-4SH (20,000) achieved 15 kPa. Interestingly, visual observation of the materials resulting from crosslinking with PEG-8SH (20,000) and PEG-4SH (20,000) were clearly gelled. In contrast, the material obtained from PEG-2SH (1,000) a solution was clearly obtained, without apparent gel, while from PEG-4SH (5,000) was clearly gelled, despite its low modulus. Given that the concentrations of thiols and alkenes were kept constant across the family of materials studied, these results suggest that PEG-2SH (1,000) afforded microgels that do not form macroscopic hydrogels. Hence, the functionality number and distance between crosslinks appear as important parameters controlling the gelation process in this system. Too short and too few thiols per crosslinking molecules is likely to lead to significant defects within the hydrogel formed, resulting in weaker mechanical properties, delayed gelation and, in the extreme

case of the dithiol, microgels that do not sufficiently branch out to form a macroscopic network.

Similarly, at a concentration of 450 mM, thiol-ene solutions based on PEG-2SH (1,000) displayed low shear moduli around 0.03 kPa after 120 s of UV irradiation. In contrast, PEG-8SH (20,000) achieved the highest storage moduli among other three type of multi-arm PEG (gelation started after 3 s of UV irradiation), followed by PEG-4SH (20,000), PEG-4SH (5,000). Notably, the results showed reverse trend compared to concentration 270 Mm, which coincidence to Flory's theory that the number of –thiols strongly affected the final shear modulus. Similarly, keep the number of –SH constant, with increasing molecular weight, the storage moduli increased, which indicate the effect of steric hindrance. Notably, visual observation of the materials resulting from crosslinking with PEG-2SH (1,000) a semi-gel was clearly obtained, while the materials obtained from other three PEG-thiols were clearly gelled.

Although, the materials resulting from crosslinking with 540mM concentration was clearly gelled, they all follow the similar gelation process as concentration 270 mM.

6.2.3.3 Mixed PEG-POx hydrogels: based on co-PEG thiols

From previous study we found that although PEG-4SH displayed the highest storage moduli in time sweeps, but when removal of the top geometry, gel was formed at lower concentration of thiol. However, with PEG-8SH (20,000) cross linker (storage moduli below 0.5 kPa) gels were formed. Hence, it is worth to test the mechanical properties of hydrogels formed with PEG-8SH (20,000)-co-PEG-2SH (1,000).

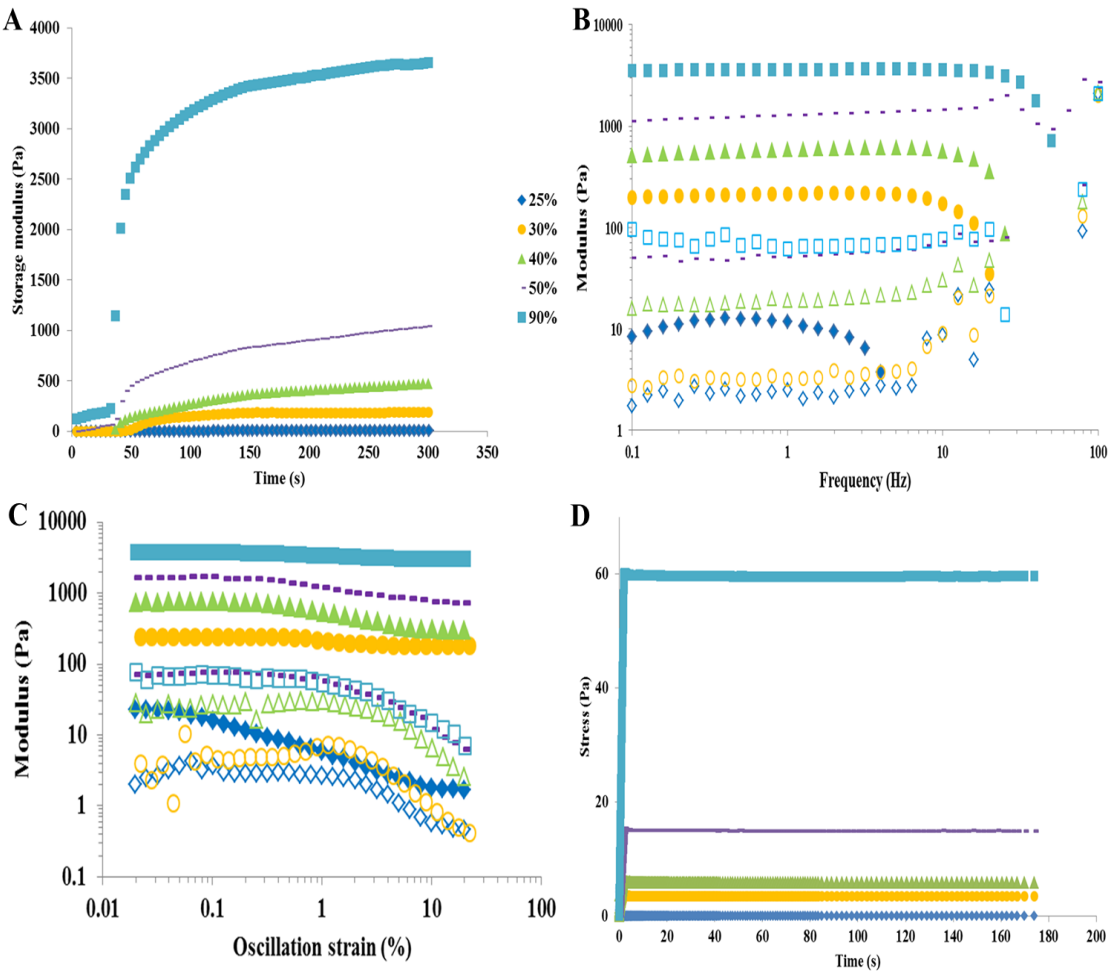

Figure 6.17 Impact of the different ratios of alkene and thiols on the gelation behavior and the mechanical properties of photo cross-linked hydrogels based on PEG-8SH (Mw=20,000 g/mol) cross linked with BuPOxOH via thiol-ene chemistry. Five ratios were applied: 25%, 30%, 40%, 50% and 90%, respectively. Concentrations were kept at 270 mM. A. Time sweep (frequency and strain of oscillation are 1 Hz and 2%, respectively) shows the evolution of storage modulus (G') and loss modulus (G'') during UV irradiation (UV irradiated at 17 mW/cm^2). The sample was conditioned for 30 s prior to UV exposure and irradiated for 120 s. B. Frequency sweeps (frequency varied from 0.1 Hz to 100 Hz) was used to confirm the structure of mixed PEG-POx networks. C. Amplitude sweep (frequency is 1 Hz) was carried out to limit the value of

the linear viscoelastic (LVE) range. D. Stress relaxation (strain of oscillation is 2%) was carried out to judge the elastic property of formed networks.

As can be seen in figure 6.17, five ratios of thiol to alkene of thiol-ene solution were prepared when PEG-8SH (20,000) cross-linked BuPMeOxOH. The respective ratios of thiol to alkene were 25%, 30%, 40%, 50% and 90%, respectively. A full set of tests was carried out via *in situ* rheology: time sweeps, frequency sweeps, amplitude sweeps and stress relaxation. Rheology was carried out during and after 120 s UV irradiation. For the 90% PEG-8SH (20,000), the shear moduli dramatically increased after the UV was switched on, indicating a rapid reactivity. In addition, it achieved the highest storage moduli as well as the shortest gelation time among other four ratios. Similar behaviors were observed at 50% PEG-8SH (20,000), although the increase in storage modulus was far less pronounced. In contrast, for the 40%, 30% and 25% PEG-8SH (20,000), slowly increases of shear moduli were obtained after the UV was switched on. Interestingly, the materials resulting from crosslinking with 25% PEG-8SH (20,000) a semi-gel was obtained although the storage modulus was 0.01 kPa. However, the materials cross-linked from the rest ratios all showed clearly gelled after removal of the top geometry. These behaviors indicate cross-linked macroscopic networks were formed even with only 30% PEG-8SH (20,000).

These results were confirmed by frequency sweeps and stress sweeps. Frequency sweeps for 90%, 50%, 40% and 30% PEG-8SH (20,000) all showed relatively stable frequency independent profiles, consistent with the formation of a macroscopic gel. However, 25% PEG-8SH (20,000) showed a marked decrease at much lower frequencies (1Hz). Similarly the strain sweeps of 90%, 50% and 30% PEG-8SH (20,000) showed stable independent strain profiles, indicating strong gels. In contrast,

25% PEG-8SH (20,000) showed considerable shear thinning profile while 40% PEG-8SH (20,000) showed shear thinning profile since 0.14% strain were applied, indicating weaker gels were formed. These results were confirmed by stress relaxation experiments, which showed high levels of stress retention for 90%, 50%, 40% and 30% PEG-8SH (20,000) gels. However, clear elastic profile (very little relaxation) for 25% PEG-8SH (20,000) gel, consistent with the lack of macroscopic cross-linked network formed at this concentration.

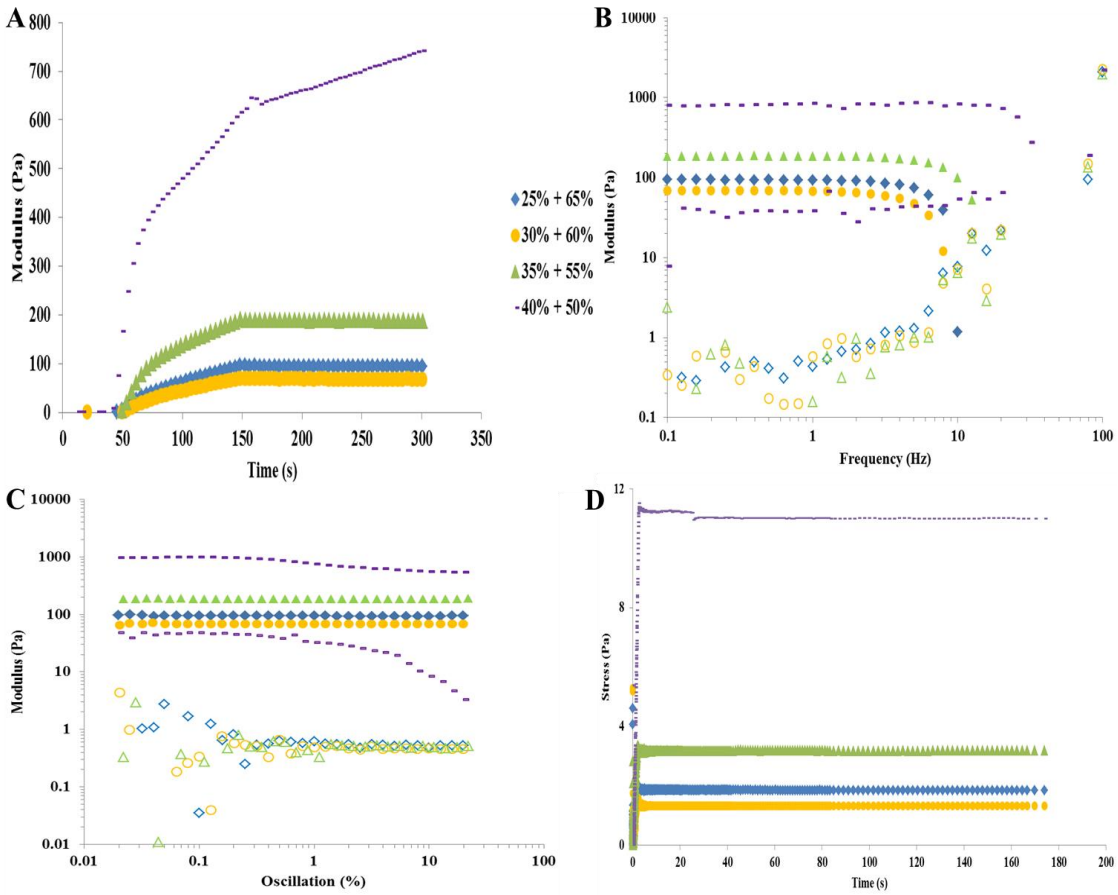

Figure 6.18 Impact of the different ratios of alkene and co-thiols on the gelation behavior and the mechanical properties of photo cross-linked hydrogels based on PEG-8SH (20,000) cross linked with BuPOxOH via thiol-ene chemistry. Four ratios of alkene and co-thiols were applied (PEG-8SH and PEG-2SH): 25% +65%, 30% + 60%, 35% + 55%, 40% + 50%, respectively. Concentrations were kept at 270 mM. A. Time sweep

(frequency and strain of oscillation are 1 Hz and 2%, respectively) shows the evolution of storage modulus (G') and loss modulus (G'') during UV irradiation (UV irradiated at 17 mW/cm^2). The sample was conditioned for 30 s prior to UV exposure and irradiated for 120 s. B. Frequency sweeps (frequency varied from 0.1 Hz to 100 Hz) was used to confirm the structure of mixed PEG-POx networks. C. Amplitude sweep (frequency is 1 Hz) was carried out to limit the value of the linear viscoelastic (LVE) range. D. Stress relaxation (strain of oscillation is 2%) was carried out to judge the elastic property of formed networks.

As can be seen in figure 6.18, five ratios of alkene and co-thiols of thiol-ene solution were prepared when PEG-8SH (20,000) cross-linked with BuPMeOxOH. The respective ratios of alkene and co-thiols were 25% +65%, 30% + 60%, 35% + 55%, 40% + 50%, respectively. For the 40% + 50% PEG-8SH (20,000) and PEG-2SH (1,000) gel, the shear moduli dramatically increased after 11 s when UV was switched on, indicating a rapid reactivity. Also, slowly increases of shear moduli was obtained until 300 s. Compared to 40% pure PEG-8SH (20,000) as cross linker, the shear moduli increased from 0.5 kPa to 0.7 kPa, which may be due to additional PEG-2SH (1,000) added. In contrast, when the ratio of co-thiol was 30% + 60%, a slightly decrease of storage moduli was obtained, shear moduli was decreased from 0.2 kPa to 0.1 kPa. Interestedly, 25% +65% co-thiols obtained 0.1 kPa shear moduli while it did not show any shear moduli before. Notably, 25% +65% co-thiols with alkene functionalized POx generate a macroscopic network, which was confirmed by removing the top geometry and sol-gel was found.

From frequency sweeps and stress sweeps, however, only 40% + 50% co-thiols showed relatively stable frequency independent profiles, consistent with the formation of a

macroscopic gel. However, since 2.5% strain was applied it showed shear thinning profile which may indicate a weak gel was formed. Since 0.6% strain was applied, 35% + 55%, 30% + 60% and 25% +65% all showed shear thicken profile, which is slightly contrary to frequency sweep as they did not show any independent profile. Interestingly, results from stress relaxation experiments, which showed high levels of stress relaxation for 40% + 50% co-thiols but low stress relaxation for 35% + 55%, 30% + 60% and 25% +65% gel, which in consistent with the sol-gel cross-linked network formed at these concentration.

Overall, the mechanical properties of hydrogels did not change a lot when compared pure PEG-8SH (20,000) system with co-thiol system, which may indicate when replacing PEG-2SH(1,000) with growth factor or peptide, the mechanical properties of gels won't change a lot as well. Therefore, co-thiol system is a simple system to study the mechanical properties of gels before replacing with expensive peptide or growth factor, moreover, it pave the way for application as cell matrix.

6.3 Conclusions

Multi-arm thiols are promising crosslinkers to generate hydrogels via thiol-ene chemistry. The present study focused on the synthesis of multi-arm POx thiols and characterization; moreover, multi-PEG-thiols were used as crosslinkers to fabricate hydrogels. We characterized the synthesized POx-thiols with NMR, FTIR and MALDI. Moreover, we monitored the mechanical properties of hydrogels via *in situ* rheology.

Investigating the control of the polymerisation with two initiators and thiol as terminate reagent, we observed that full control of the molecular structure of polyoxazolines was very difficult. When initiated with 1, 2-Diiodoethane, the initiation step was relatively controlled compared to use pentaerythrityl tetraiodide as initiator. Moreover, all

termination showed a large amount of side reactions occured when terminated with acrylic acid, which affect further deacetylation reaction that only a small distribution was obtained from MALDI. In addition, we investigated thiol-ene chemistry of pendant thiol functionalized Bu-PMeOxOH with Bu-PMeOxOH, however, no gel was obtained. Furthermore, pendant thiol functionalized Bu-PMeOxOH was reacted with 4-Pentenoic acid via michael addition, again no reaction occured, which may explain that no gels formed via pure POx system was not due to steric hindrance, may result from some radical reaction that kill the gelation process.

In addition, we investigated the impact of concentration of total thiol-ene solution as well as the type of different PEG-SH on fabrication of hydrogels. We observed that keep the type of thiol constant, increased shear moduli were obtained with increasing concentration of total thiol-ene solution. Similar to molecular weight, when keep the type of thiol the same, with higher molecular weight of thiols obtained higher shear moduli, which may be due to less steric hindrance of thiols in one molecular. Generally, the number of thiol highly affects the gelation process. For example, stiffer hydrogels were obtained when the number of thiol increased from two arms PEG-thiol to four arms PEG-thiol. However, when the number increased from four to eight, gelation process was more complicated and not in line with the number of thiol. Moreover, we investigated the mechanical properties of co-thiols: PEG-8SH (20,000) and PEG-2SH (1,000). We found that the shear moduli were not changing a lot when additional PEG-2SH (1,000) was added to make up to 90% thiol in total.

Chapter 7

Conclusions and future directions

In this thesis, synthesis of polyoxazolines was intensively studied. The cationic ring-opening polymerization of 2-oxazoline monomer take advantage of its high regioselectivity and only occurs at the nitrogen atom of a 2-oxazoline monomer. Moreover, POx shows highly chemical stability and can be easily further functionalised via substitute R in the side chains or terminate with dedicated functional groups. Based upon these advantages, a variety of telechelic polyoxazolines were synthesised with different initiators and termination agents. Results showed that for initiation steps, in the presence of acetonitrile, all showed relatively high efficiency; however, in comparison initiators methyl tosylate to allyl tosylate, methyl tosylate initiated POx showed more controlled initiation step. In addition, termination step was more complicated. Conditions such as temperature as well as reaction time were important factors to determine the effectively end capping step. For instance, bromoisobutyric acid can only cap with POx under mild conditions (low temperature). Moreover, hydroxyl end group was obtained in all synthesised polyoxazolines, which confer a critical synthesis condition is needed and limits the usefulness of polyoxazolines for the synthesis of defined telechelic POx substitutes. However, synthesis of telechelic POx was reported with promising control of initiation and termination steps from Schubert's study. As a suggestion for future work, terminate reagent should be purified before end-capped with POx to improve the efficiency. Moreover, synthesized polyoxazoline with bromo end group can be applied as initiator of silicon wafer, offering pure POx brushes system.

Phenotypes of cell such as cell shape and sizes determine the proliferation and differentiation, therefore, cell microenvironment such as matrix that manipulate cell

shape and sizes allows systematically study cell biology in well-defined conditions. Non-fouling polymer brushes was exploited to achieve high fidelity patterning of single cells, therefore, these coatings can be patterned with different shapes and sized to manipulate the cell's shapes and sizes. In our result, a comparable non-fouling property of PMeOxMA brushes was obtained compared to benchmark POEGMA brushes with the similar thickness. Moreover, our result demonstrates a straight forward way of functionalise POx brushes with peptide was successfully obtained, which confirm the diversity use of POx. However, only a thinner PAMeOxMA brushes was obtained which may due to impurities of the oligomer OAMeOxMA. From chapter 3 we know that initiation step need to be improved especially when allyl tosylate was used as initiator. Moreover, thinner thickness may also due to two reactive alkene end groups react before polymerization. As a suggestion for future work, explore other ATRP system to obtain thicker POx brushes especially for oligomer OMeOxMA is needed, owing to the thickness and grafting density of polymer brushes that affect the anti-fouling properties. Our results demonstrated that even thinner PAMeOxMA brushes can be further functionalised with peptide in a simpler way compared to POEGMA brushes, which confirm functionalised oligomer MeOx is a better candidate compared to PEG for non-fouling biomedical applications.

Synthetic hydrogels attract lots of attention recently as a result of its tuneable mechanical and biochemical properties. Cell matrix determine cell phenotype and POx was approved a good non-fouling property from our study (chapter 5), and therefore synthetic hydrogels based on POx is a very promising candidate for cell matrix. Results showed that initiation of oligo (MeOx) with di-iodide; relatively controlled initiation step was obtained compared to tetra-iodide as initiator, which confirm the role of

initiator was very important. Moreover, the selection of solvent was comparably important; the failure of the initiation step may due to the wrong solvent that was chosen. Furthermore, uncontrolled termination step occurred again compared to the results from chapter 4 when lower degree of polymerization was applied. In addition, from our previous study (chapter 4) that some of the lateral chain can be cleaved during the polymerization. Hence, choosing the right initiators as well as solvent is highly demand. Our results also showed that the number of –SH did highly affect the gelation, and therefore help scientists to select the suitable crosslinker when fabricating hydrogels. Furthermore, with additional PEG-2SH to PEG-8SH hydrogel system, the shear moduli slightly improved, which reminds scientists that replacing PEG-2SH with peptide may not change the mechanical properties of hydrogels a lot. As a suggestion for future work, synthesis of crosslinker POx with other controlled initiators, such as arm p-toluenesulfonate, or use mixture of solvent such as acetonitrile mixed with NMP for initiation step. When end capping with acrylic acid, it is worth to try mild conditions as in chapter 4 we did, and then deacetylate in base condition as we can see clearly for pendant thiol functionalized POx lateral chain were highly cleaved. Also PEG-8SH can be applied to fabricate hydrogel as it showed very promising shear moduli as well as from observation.

References

1. McDonnell, T., Y. Ioannou, and A. Rahman, *PEGylated drugs in rheumatology—why develop them and do they work?* Rheumatology, 2013. **53**(3): p. 391-396.
2. McGary, C., *Degradation of poly (ethylene oxide).* Journal of Polymer Science Part A: Polymer Chemistry, 1960. **46**(147): p. 51-57.
3. Branch, D.W., et al., *Long-term stability of grafted polyethylene glycol surfaces for use with microstamped substrates in neuronal cell culture.* Biomaterials, 2001. **22**(10): p. 1035-1047.
4. Zhang, F., et al., *Modification of Si (100) surface by the grafting of poly (ethylene glycol) for reduction in protein adsorption and platelet adhesion.* Journal of Biomedical Materials Research Part A, 2001. **56**(3): p. 324-332.
5. Sharma, S., R.W. Johnson, and T.A. Desai, *Evaluation of the stability of nonfouling ultrathin poly (ethylene glycol) films for silicon-based microdevices.* Langmuir, 2004. **20**(2): p. 348-356.
6. Schellekens, H., W.E. Hennink, and V. Brinks, *The immunogenicity of polyethylene glycol: facts and fiction.* Pharmaceutical research, 2013. **30**(7): p. 1729-1734.
7. Pidhatika, B., et al., *Comparative stability studies of poly (2-methyl-2-oxazoline) and poly (ethylene glycol) brush coatings.* Biointerphases, 2012. **7**(1-4): p. 1.
8. Xue, X., et al., *Heat treatment increases the bioactivity of C-terminally PEGylated staphylokinase.* Process Biochemistry, 2014. **49**(7): p. 1092-1096.
9. Xu, P., et al., *Hydrogen-bonded and reduction-responsive micelles loading atorvastatin for therapy of breast cancer metastasis.* Biomaterials, 2014. **35**(26): p. 7574-7587.
10. Kang, T., et al., *iNGR-modified PEG-PLGA nanoparticles that recognize tumor vasculature and penetrate gliomas.* Biomaterials, 2014. **35**(14): p. 4319-4332.
11. Bai, J., Y. Liu, and X. Jiang, *Multifunctional PEG-GO/CuS nanocomposites for near-infrared chemo-photothermal therapy.* Biomaterials, 2014. **35**(22): p. 5805-5813.
12. Mei, L., et al., *Increased tumor targeted delivery using a multistage liposome system functionalized with RGD, TAT and cleavable PEG.* International journal of pharmaceutics, 2014. **468**(1-2): p. 26-38.
13. Kim, K.S., et al., *A cancer-recognizable MRI contrast agents using pH-responsive polymeric micelle.* Biomaterials, 2014. **35**(1): p. 337-343.
14. Song, W., et al., *Anti-tumor efficacy of c (RGDfK)-decorated polypeptide-based micelles co-loaded with docetaxel and cisplatin.* Biomaterials, 2014. **35**(9): p. 3005-3014.
15. Jeon, O., J.E. Samorezov, and E. Alsberg, *Single and dual crosslinked oxidized methacrylated alginate/PEG hydrogels for bioadhesive applications.* Acta biomaterialia, 2014. **10**(1): p. 47-55.
16. Cencer, M., et al., *Effect of pH on the rate of curing and bioadhesive properties of dopamine functionalized poly (ethylene glycol) hydrogels.* Biomacromolecules, 2014. **15**(8): p. 2861-2869.
17. Dang, L.T., et al., *Inhibition of apoptosis in human induced pluripotent stem cells during expansion in a defined culture using angiopoietin-1 derived peptide QHREDGS.* Biomaterials, 2014. **35**(27): p. 7786-7799.
18. Dehority, W., et al., *Polyethylene Glycol-Surfactant for Lavage Lung Injury in Rats.* Pediatric Research, 2005. **58**(5): p. 913-918.
19. *Indirect Additives used in Food Contact Substances*.
20. Fiume, M.M., et al., *Safety Assessment of Alkyl PEG/PPG Ethers as Used in Cosmetics.* International Journal of Toxicology, 2012. **31**.
21. Jang, H., C.Y. Shin, and K. Kim, *Safety Evaluation of Polyethylene Glycol (PEG) Compounds for Cosmetic Use.* Toxicology Research, 2015. **31**(2): p. 105-136.

22. Webster, R., et al., *PEGylated proteins : Evaluation of their safety in the absence of definitive metabolism studies.* Drug Metabolism and Disposition, 2006. **35**(1): p. 9-16.
23. Mcgraw, T., *Safety of polyethylene glycol 3350 solution in chronic constipation: randomized, placebo-controlled trial.* Clinical and Experimental Gastroenterology, 2016. **9**: p. 173-180.
24. Turecek, P., et al., *PEGylation of Biopharmaceuticals: A Review of Chemistry and Nonclinical Safety Information of Approved Drugs.* Journal of Pharmaceutical Sciences, 2016. **105**(2): p. 460-475.
25. Bodner, T., et al., *Delocalized π‐electrons in 2‐oxazoline rings resulting in negatively charged nitrogen atoms: revealing the selectivity during the initiation of cationic ring‐opening polymerizations.* Polymer International, 2011. **60**(8): p. 1173-1179.
26. Rossegger, E., V. Schenk, and F. Wiesbrock, *Design strategies for functionalized poly (2-oxazoline) s and derived materials.* Polymers, 2013. **5**(3): p. 956-1011.
27. Hoogenboom, R. and U.S. Schubert, *Microwave‐Assisted Polymer Synthesis: Recent Developments in a Rapidly Expanding Field of Research.* Macromolecular Rapid Communications, 2007. **28**(4): p. 368-386.
28. Diehl, C. and H. Schlaad, *Polyoxazoline‐based Crystalline Microspheres for Carbohydrate‐Protein Recognition.* Chemistry-A European Journal, 2009. **15**(43): p. 11469-11472.
29. Konradi, R., et al., *Poly-2-methyl-2-oxazoline: a peptide-like polymer for protein-repellent surfaces.* Langmuir, 2008. **24**(3): p. 613-616.
30. Knop, K., et al., *Poly (ethylene glycol) in drug delivery: pros and cons as well as potential alternatives.* Angewandte chemie international edition, 2010. **49**(36): p. 6288-6308.
31. Metselaar, J.M., in *Dept. Pharmaceutics, UtrechtInstitute for Pharmaceutical Sciences*. 2006, Dept. Pharmaceutics, UtrechtInstitute for Pharmaceutical Sciences.
32. Hadjichristidis, N., et al., *Polymers with complex architecture by living anionic polymerization.* Chemical reviews, 2001. **101**(12): p. 3747-3792.
33. Hawker, C.J., A.W. Bosman, and E. Harth, *New polymer synthesis by nitroxide mediated living radical polymerizations.* Chemical reviews, 2001. **101**(12): p. 3661-3688.
34. Tomalia, D. and D. Sheetz, *Homopolymerization of 2‐alkyl‐and 2‐aryl‐2‐oxazolines.* Journal of Polymer Science Part A: Polymer Chemistry, 1966. **4**(9): p. 2253-2265.
35. Seeliger, W., et al., *Recent syntheses and reactions of cyclic imidic esters.* Angewandte Chemie International Edition, 1966. **5**(10): p. 875-888.
36. Kagiya, T., et al., *Ring‐opening polymerization of 2‐substituted 2‐oxazolines.* Journal of Polymer Science Part C: Polymer Letters, 1966. **4**(7): p. 441-445.
37. Bassiri, T., A. Levy, and M. Litt, *Polymerization of cyclic imino ethers. I. Oxazolines.* Journal of Polymer Science Part C: Polymer Letters, 1967. **5**(9): p. 871-879.
38. Saegusa, T., H. Ikeda, and H. Fujii, *Isomerization polymerization of 2-oxazoline. IV. Kinetic study of 2-methyl-2-oxazoline polymerization.* Macromolecules, 1972. **5**(4): p. 359-362.
39. Buzin, P., G. Schwarz, and H.R. Kricheldorf, *Cationic polymerizations of 2‐alkyloxazolines catalyzed by bismuth salts.* Journal of Polymer Science Part A: Polymer Chemistry, 2008. **46**(14): p. 4777-4784.
40. Cirpan, A., et al., *Synthesis and electroactivity of pyrrole end-functionalized poly (2-methyl-2-oxazoline).* European polymer journal, 2001. **37**(11): p. 2225-2229.
41. Volet, G., et al., *Synthesis of monoalkyl end-capped poly (2-methyl-2-oxazoline) and its micelle formation in aqueous solution.* Macromolecules, 2005. **38**(12): p. 5190-5197.

42. Aoi, K. and M. Okada, *Polymerization of oxazolines.* Progress in polymer science, 1996. **21**(1): p. 151-208.
43. Paulus, R.M., et al., *Acetyl Halide Initiator Screening for the Cationic Ring‐Opening Polymerization of 2‐Ethyl‐2‐Oxazoline.* Macromolecular Chemistry and Physics, 2008. **209**(8): p. 794-800.
44. Hoogenboom, R., M.W. Fijten, and U.S. Schubert, *Parallel kinetic investigation of 2‐oxazoline polymerizations with different initiators as basis for designed copolymer synthesis.* Journal of Polymer Science Part A: Polymer Chemistry, 2004. **42**(8): p. 1830-1840.
45. Weber, C., et al., *Preparation of methacrylate end-functionalized poly (2-ethyl-2-oxazoline) macromonomers.* Designed monomers and polymers, 2009. **12**(2): p. 149-165.
46. Obeid, R., et al., *Temperature response of self-assembled micelles of telechelic hydrophobically modified poly (2-alkyl-2-oxazoline) s in water.* Macromolecules, 2009. **42**(6): p. 2204-2214.
47. Huber, S., N. Hutter, and R. Jordan, *Effect of end group polarity upon the lower critical solution temperature of poly (2-isopropyl-2-oxazoline).* Colloid and Polymer Science, 2008. **286**(14-15): p. 1653-1661.
48. Wiesbrock, F., et al., *Investigation of the living cationic ring-opening polymerization of 2-methyl-, 2-ethyl-, 2-nonyl-, and 2-phenyl-2-oxazoline in a single-mode microwave reactor.* Macromolecules, 2005. **38**(12): p. 5025-5034.
49. Luxenhofer, R., et al., *Poly (2‐oxazoline) s as Polymer Therapeutics.* Macromolecular rapid communications, 2012. **33**(19): p. 1613-1631.
50. Konradi, R., C. Acikgoz, and M. Textor, *Polyoxazolines for nonfouling surface coatings—a direct comparison to the gold standard PEG.* Macromolecular rapid communications, 2012. **33**(19): p. 1663-1676.
51. Victor, R., *Poly (2-oxazoline) s as materials for biomedical applications.* Journal of Materials Science: Materials in Medicine, 2014. **25**(5): p. 1211-1225.
52. Waschinski, C.J., et al., *Influence of satellite groups on telechelic antimicrobial functions of polyoxazolines.* Macromolecular bioscience, 2005. **5**(2): p. 149-156.
53. Viegas, T.X., et al., *Polyoxazoline: chemistry, properties, and applications in drug delivery.* Bioconjugate chemistry, 2011. **22**(5): p. 976-986.
54. Vicent, M.J., H. Ringsdorf, and R. Duncan, *Polymer therapeutics: clinical applications and challenges for development*. 2009, Elsevier.
55. Leader, B., Q.J. Baca, and D.E. Golan, *Protein therapeutics: a summary and pharmacological classification.* Nature reviews Drug discovery, 2008. **7**(1): p. 21.
56. Jevševar, S., M. Kunstelj, and V.G. Porekar, *PEGylation of therapeutic proteins.* Biotechnology journal, 2010. **5**(1): p. 113-128.
57. Mero, A., et al., *Synthesis and characterization of poly (2-ethyl 2-oxazoline)-conjugates with proteins and drugs: suitable alternatives to PEG-conjugates?* Journal of Controlled Release, 2008. **125**(2): p. 87-95.
58. Velander, W.H., et al., *Polyoxazoline‐Peptide adducts that retain antibody avidity.* Biotechnology and bioengineering, 1992. **39**(10): p. 1024-1030.
59. Seidel, A., *Characterization and analysis of polymers*. 2008: John Wiley & Sons.
60. Canal, F., J. Sanchis, and M.J. Vicent, *Polymer–drug conjugates as nano-sized medicines.* Current opinion in biotechnology, 2011. **22**(6): p. 894-900.
61. Velander, W.H., et al., *The use of Fab‐masking antigens to enhance the activity of immobilized antibodies.* Biotechnology and bioengineering, 1992. **39**(10): p. 1013-1023.

62. Moreadith, R., et al. *Ser-214, a novel polymer-conjugated rotigotine formulation affords greatly extended duration of anti-parkinsonian effect and enhanced plasma exposure following a single administration in rodents and primates*. in *Proceedings of the 16th international conference of Parkinson's disease and movement disorders, movement disorder society*. 2012.
63. Morille, M., et al., *Progress in developing cationic vectors for non-viral systemic gene therapy against cancer.* Biomaterials, 2008. **29**(24-25): p. 3477-3496.
64. Thomas, M., et al., *Full deacylation of polyethylenimine dramatically boosts its gene delivery efficiency and specificity to mouse lung.* Proceedings of the National Academy of Sciences of the United States of America, 2005. **102**(16): p. 5679-5684.
65. Jeong, J.H., et al., *DNA transfection using linear poly (ethylenimine) prepared by controlled acid hydrolysis of poly (2-ethyl-2-oxazoline).* Journal of controlled Release, 2001. **73**(2-3): p. 391-399.
66. Hsiue, G.-H., et al., *Nonviral gene carriers based on diblock copolymers of poly (2-ethyl-2-oxazoline) and linear polyethylenimine.* Bioconjugate chemistry, 2006. **17**(3): p. 781-786.
67. von Erlach, T., et al., *Formation and characterization of DNA-polymer-condensates based on poly (2-methyl-2-oxazoline) grafted poly (l-lysine) for non-viral delivery of therapeutic DNA.* Biomaterials, 2011. **32**(22): p. 5291-5303.
68. Chacko, R.T., et al., *Polymer nanogels: a versatile nanoscopic drug delivery platform.* Advanced drug delivery reviews, 2012. **64**(9): p. 836-851.
69. Matsumura, Y. and K. Kataoka, *Preclinical and clinical studies of anticancer agent‐incorporating polymer micelles.* Cancer science, 2009. **100**(4): p. 572-579.
70. Onaca, O., et al., *Stimuli‐Responsive Polymersomes as Nanocarriers for Drug and Gene Delivery.* Macromolecular bioscience, 2009. **9**(2): p. 129-139.
71. Hoogenboom, R., et al., *Synthesis and aqueous micellization of amphiphilic tetrablock ter-and quarterpoly (2-oxazoline) s.* Macromolecules, 2007. **40**(8): p. 2837-2843.
72. Krumm, C., et al., *Well‐Defined Amphiphilic Poly (2‐oxazoline) ABA‐Triblock Copolymers and Their Aggregation Behavior in Aqueous Solution.* Macromolecular rapid communications, 2012. **33**(19): p. 1677-1682.
73. Ben-Haim, N., et al., *Cell-specific integration of artificial organelles based on functionalized polymer vesicles.* Nano Letters, 2008. **8**(5): p. 1368-1373.
74. Broz, P., et al., *Inhibition of macrophage phagocytotic activity by a receptor-targeted polymer vesicle-based drug delivery formulation of pravastatin.* Journal of cardiovascular pharmacology, 2008. **51**(3): p. 246-252.
75. Greco, F. and M.J. Vicent, *Combination therapy: opportunities and challenges for polymer–drug conjugates as anticancer nanomedicines.* Advanced drug delivery reviews, 2009. **61**(13): p. 1203-1213.
76. Banerjee, I., R.C. Pangule, and R.S. Kane, *Antifouling coatings: recent developments in the design of surfaces that prevent fouling by proteins, bacteria, and marine organisms.* Advanced Materials, 2011. **23**(6): p. 690-718.
77. Ostuni, E., et al., *Self-assembled monolayers that resist the adsorption of proteins and the adhesion of bacterial and mammalian cells.* Langmuir, 2001. **17**(20): p. 6336-6343.
78. Waschinski, C.J. and J.C. Tiller, *Poly (oxazoline) s with telechelic antimicrobial functions.* Biomacromolecules, 2005. **6**(1): p. 235-243.
79. Nikitin, A.G., A.V. Kabashin, and H. Dallaporta, *Plasmonic resonances in diffractive arrays of gold nanoantennas: near and far field effects.* Optics express, 2012. **20**(25): p. 27941-27952.
80. Braun, S., W.R. Salaneck, and M. Fahlman, *Energy‐level alignment at organic/metal and organic/organic interfaces.* Advanced materials, 2009. **21**(14‐15): p. 1450-1472.

81. Comminges, C. and U. Wollenberger, *Surface modification of gold electrodes for a switchable biosensor.*
82. Siegwart, D.J., J.K. Oh, and K. Matyjaszewski, *ATRP in the design of functional materials for biomedical applications.* Progress in polymer science, 2012. **37**(1): p. 18-37.
83. Grubbs, R.B., *Nitroxide-mediated radical polymerization: limitations and versatility.* Polymer Reviews, 2011. **51**(2): p. 104-137.
84. Otsu, T., *Iniferter concept and living radical polymerization.* Journal of Polymer Science Part A: Polymer Chemistry, 2000. **38**(12): p. 2121-2136.
85. Ma, H., et al., *Protein-resistant polymer coatings on silicon oxide by surface-initiated atom transfer radical polymerization.* Langmuir, 2006. **22**(8): p. 3751-3756.
86. Zhang, N., et al., *Tailored Poly (2‐oxazoline) Polymer Brushes to Control Protein Adsorption and Cell Adhesion.* Macromolecular bioscience, 2012. **12**(7): p. 926-936.
87. Nath, N. and A. Chilkoti, *Creating "smart" surfaces using stimuli responsive polymers.* Advanced materials, 2002. **14**(17): p. 1243-1247.
88. Wischerhoff, E., et al., *Smart bioactive surfaces.* Soft Matter, 2010. **6**(4): p. 705-713.
89. Dimitrov, I., et al., *Thermosensitive water-soluble copolymers with doubly responsive reversibly interacting entities.* Progress in Polymer Science, 2007. **32**(11): p. 1275-1343.
90. Weber, C., R. Hoogenboom, and U.S. Schubert, *Temperature responsive bio-compatible polymers based on poly (ethylene oxide) and poly (2-oxazoline) s.* Progress in Polymer Science, 2012. **37**(5): p. 686-714.
91. Woodle, M.C., C.M. Engbers, and S. Zalipsky, *New amphipatic polymer-lipid conjugates forming long-circulating reticuloendothelial system-evading liposomes.* Bioconjugate chemistry, 1994. **5**(6): p. 493-496.
92. David, G., et al., *Poly (N-isopropylacrylamide)/poly [(N-acetylimino) ethylene] thermosensitive block and graft copolymers.* European polymer journal, 2003. **39**(6): p. 1209-1213.
93. Rueda, J., et al., *Synthesis and characterization of thermoresponsive graft copolymers of NIPAAm and 2-alkyl-2-oxazolines by the "grafting from" method.* Macromolecules, 2005. **38**(17): p. 7330-7336.
94. Vasilev, K., J. Cook, and H.J. Griesser, *Antibacterial surfaces for biomedical devices.* Expert review of medical devices, 2009. **6**(5): p. 553-567.
95. Willcox, M., et al., *A novel cationic‐peptide coating for the prevention of microbial colonization on contact lenses.* Journal of applied microbiology, 2008. **105**(6): p. 1817-1825.
96. Cole, N., et al., *In vivo performance of melimine as an antimicrobial coating for contact lenses in models of CLARE and CLPU.* Investigative ophthalmology & visual science, 2010. **51**(1): p. 390-395.
97. Wisniewski, N. and M. Reichert, *Methods for reducing biosensor membrane biofouling.* Colloids and Surfaces B: Biointerfaces, 2000. **18**(3-4): p. 197-219.
98. Meyer, B., *Approaches to prevention, removal and killing of biofilms.* International Biodeterioration & Biodegradation, 2003. **51**(4): p. 249-253.
99. Yebra, D.M., S. Kiil, and K. Dam-Johansen, *Antifouling technology—past, present and future steps towards efficient and environmentally friendly antifouling coatings.* Progress in organic coatings, 2004. **50**(2): p. 75-104.
100. Hucknall, A., S. Rangarajan, and A. Chilkoti, *In pursuit of zero: polymer brushes that resist the adsorption of proteins.* Advanced Materials, 2009. **21**(23): p. 2441-2446.
101. Kane, R.S., P. Deschatelets, and G.M. Whitesides, *Kosmotropes form the basis of protein-resistant surfaces.* Langmuir, 2003. **19**(6): p. 2388-2391.

102. Llanos, G.R. and M.V. Sefton, *Review Does polyethylene oxide possess a low thrombogenicity?* Journal of Biomaterials Science, Polymer Edition, 1993. **4**(4): p. 381-400.
103. Skoda, M., et al., *Protein density profile at the interface of water with oligo (ethylene glycol) self-assembled monolayers.* Langmuir, 2009. **25**(7): p. 4056-4064.
104. Jung, I.K., et al., *Surface Graft Polymerization of Poly (ethylene glycol) Methacrylate onto Polyurethane via Thiol–Ene Reaction: Preparation and Characterizations.* Journal of Biomaterials Science, Polymer Edition, 2009. **20**(10): p. 1473-1482.
105. Hamming, L.M. and P.B. Messersmith, *Fouling resistant biomimetic poly (ethylene glycol) based grafted polymer coatings.* Mater. Matters, 2008. **3**(52).
106. Wang, H., et al., *Evaluation of photochemically immobilized poly (2-ethyl-2-oxazoline) thin films as protein-resistant surfaces.* ACS applied materials & interfaces, 2011. **3**(9): p. 3463-3471.
107. Fairbanks, B.D., et al., *A versatile synthetic extracellular matrix mimic via thiol‐norbornene photopolymerization.* Advanced Materials, 2009. **21**(48): p. 5005-5010.
108. Zhang, X., et al., *Ugi reaction of natural amino acids: a general route toward facile synthesis of polypeptoids for bioapplications.* ACS Macro Letters, 2016. **5**(9): p. 1049-1054.
109. Agrawal, M., et al., *Facile approach to grafting of poly (2-oxazoline) brushes on macroscopic surfaces and applications thereof.* ACS applied materials & interfaces, 2012. **4**(3): p. 1357-1364.
110. Azzaroni, O., *Polymer brushes here, there, and everywhere: Recent advances in their practical applications and emerging opportunities in multiple research fields.* Journal of Polymer Science Part A: Polymer Chemistry, 2012. **50**(16): p. 3225-3258.
111. Edmondson, S., V.L. Osborne, and W.T. Huck, *Polymer brushes via surface-initiated polymerizations.* Chemical society reviews, 2004. **33**(1): p. 14-22.
112. Jeon, N.L., et al., *Patterned polymer growth on silicon surfaces using microcontact printing and surface-initiated polymerization.* Applied Physics Letters, 1999. **75**(26): p. 4201-4203.
113. Matyjaszewski, K., et al., *Controlled/"living" atom transfer radical polymerization of methyl methacrylate using various initiation systems.* Macromolecules, 1998. **31**(5): p. 1527-1534.
114. Ding, S., J.A. Floyd, and K.B. Walters, *Comparison of surface confined ATRP and SET‐LRP syntheses for a series of amino (meth) acrylate polymer brushes on silicon substrates.* Journal of Polymer Science Part A: Polymer Chemistry, 2009. **47**(23): p. 6552-6560.
115. Baum, M. and W.J. Brittain, *Synthesis of polymer brushes on silicate substrates via reversible addition fragmentation chain transfer technique.* Macromolecules, 2002. **35**(3): p. 610-615.
116. Lindqvist, J., et al., *Intelligent dual-responsive cellulose surfaces via surface-initiated ATRP.* Biomacromolecules, 2008. **9**(8): p. 2139-2145.
117. Henze, M., et al., *"Grafting through": mechanistic aspects of radical polymerization reactions with surface-attached monomers.* Macromolecules, 2014. **47**(9): p. 2929-2937.
118. Brown, A.A., et al., *Synthesis of oligo (ethylene glycol) methacrylate polymer brushes.* European polymer journal, 2005. **41**(8): p. 1757-1765.
119. Braunecker, W.A., et al., *Origin of activity in Cu-, Ru-, and Os-mediated radical polymerization.* Macromolecules, 2007. **40**(24): p. 8576-8585.
120. Matyjaszewski, K. and J. Xia, *Atom transfer radical polymerization.* Chemical reviews, 2001. **101**(9): p. 2921-2990.

121. Fischer, H., *The persistent radical effect: a principle for selective radical reactions and living radical polymerizations.* Chemical reviews, 2001. **101**(12): p. 3581-3610.
122. Patten, T.E. and K. Matyjaszewski, *Atom transfer radical polymerization and the synthesis of polymeric materials.* Advanced Materials, 1998. **10**(12): p. 901-915.
123. Matyjaszewski, K., *Transition metal catalysis in controlled radical polymerization: atom transfer radical polymerization.* Chemistry-A European Journal, 1999. **5**(11): p. 3095-3102.
124. Queffelec, J., S.G. Gaynor, and K. Matyjaszewski, *Optimization of atom transfer radical polymerization using Cu (I)/tris (2-(dimethylamino) ethyl) amine as a catalyst.* Macromolecules, 2000. **33**(23): p. 8629-8639.
125. Tang, W. and K. Matyjaszewski, *Effects of initiator structure on activation rate constants in ATRP.* Macromolecules, 2007. **40**(6): p. 1858-1863.
126. Gieseler, D. and R. Jordan, *Poly (2-oxazoline) molecular brushes by grafting through of poly (2-oxazoline) methacrylates with aqueous ATRP.* Polymer Chemistry, 2015. **6**(25): p. 4678-4689.
127. Matyjaszewski, K., Y. Nakagawa, and C.B. Jasieczek, *Polymerization of n-butyl acrylate by atom transfer radical polymerization. Remarkable effect of ethylene carbonate and other solvents.* Macromolecules, 1998. **31**(5): p. 1535-1541.
128. Wang, X.-s., N. Luo, and S.-k. Ying, *Controlled radical polymerization of methacrylates at ambient temperature and the synthesis of block copolymers containing methacrylates.* Polymer, 1999. **40**(14): p. 4157-4161.
129. Wang, X.-S. and S. Armes, *Facile atom transfer radical polymerization of methoxy-capped oligo (ethylene glycol) methacrylate in aqueous media at ambient temperature.* Macromolecules, 2000. **33**(18): p. 6640-6647.
130. Perrier, S., et al., *Copper (I) - mediated radical polymerization of methacrylates in aqueous solution.* Journal of Polymer Science Part A: Polymer Chemistry, 2001. **39**(10): p. 1696-1707.
131. Xia, J. and K. Matyjaszewski, *Controlled/"living" radical polymerization. Atom transfer radical polymerization using multidentate amine ligands.* Macromolecules, 1997. **30**(25): p. 7697-7700.
132. Nicodemus, G.D. and S.J. Bryant, *Cell encapsulation in biodegradable hydrogels for tissue engineering applications.* Tissue Engineering Part B: Reviews, 2008. **14**(2): p. 149-165.
133. Kim, H.-D., et al., *Epidermal growth factor–induced enhancement of glioblastoma cell migration in 3D arises from an intrinsic increase in speed but an extrinsic matrix-and proteolysis-dependent increase in persistence.* Molecular biology of the cell, 2008. **19**(10): p. 4249-4259.
134. Cushing, M.C. and K.S. Anseth, *Hydrogel cell cultures.* Science, 2007. **316**(5828): p. 1133-1134.
135. Schweikl, H., G. Spagnuolo, and G. Schmalz, *Genetic and cellular toxicology of dental resin monomers.* Journal of dental research, 2006. **85**(10): p. 870-877.
136. Dargaville, T.R., et al., *Unexpected switching of the photogelation chemistry when cross-linking poly (2-oxazoline) copolymers.* Macromolecules, 2016. **49**(13): p. 4774-4783.
137. Liu, S.Q., et al., *Synthetic hydrogels for controlled stem cell differentiation.* Soft Matter, 2010. **6**(1): p. 67-81.
138. Wichterle, O. and D. Lim, *Hydrophilic gels for biological use.* Nature, 1960. **185**(4706): p. 117.

139. Kaihara, S., S. Matsumura, and J.P. Fisher, *Synthesis and properties of poly [poly (ethylene glycol)-co-cyclic acetal] based hydrogels.* Macromolecules, 2007. **40**(21): p. 7625-7632.
140. Kloxin, A.M., et al., *Photodegradable hydrogels for dynamic tuning of physical and chemical properties.* Science, 2009. **324**(5923): p. 59-63.
141. Shin, H., et al., *In vivo bone and soft tissue response to injectable, biodegradable oligo (poly (ethylene glycol) fumarate) hydrogels.* Biomaterials, 2003. **24**(19): p. 3201-3211.
142. Ifkovits, J.L. and J.A. Burdick, *Photopolymerizable and degradable biomaterials for tissue engineering applications.* Tissue engineering, 2007. **13**(10): p. 2369-2385.
143. Ma, P.X. and J. Elisseeff, *Scaffolding in tissue engineering*. 2005: CRC press.
144. Tibbitt, M.W., et al., *Mechanical properties and degradation of chain and step-polymerized photodegradable hydrogels.* Macromolecules, 2013. **46**(7): p. 2785-2792.
145. Lin, C.-C., A. Raza, and H. Shih, *PEG hydrogels formed by thiol-ene photo-click chemistry and their effect on the formation and recovery of insulin-secreting cell spheroids.* Biomaterials, 2011. **32**(36): p. 9685-9695.
146. Decker, C., *UV-curing chemistry: past, present, and future.* JCT, Journal of coatings technology, 1987. **59**(751): p. 97-106.
147. Nguyen, K.T. and J.L. West, *Photopolymerizable hydrogels for tissue engineering applications.* Biomaterials, 2002. **23**(22): p. 4307-4314.
148. Benoit, D.S., et al., *Small functional groups for controlled differentiation of hydrogel-encapsulated human mesenchymal stem cells.* Nature materials, 2008. **7**(10): p. 816.
149. Yang, F., et al., *The effect of incorporating RGD adhesive peptide in polyethylene glycol diacrylate hydrogel on osteogenesis of bone marrow stromal cells.* Biomaterials, 2005. **26**(30): p. 5991-5998.
150. Nuttelman, C.R., et al., *The effect of ethylene glycol methacrylate phosphate in PEG hydrogels on mineralization and viability of encapsulated hMSCs.* Biomaterials, 2006. **27**(8): p. 1377-1386.
151. Hwang, N.S., et al., *Effects of Three‐Dimensional Culture and Growth Factors on the Chondrogenic Differentiation of Murine Embryonic Stem Cells.* Stem cells, 2006. **24**(2): p. 284-291.
152. Hwang, N.S., et al., *In vivo commitment and functional tissue regeneration using human embryonic stem cell-derived mesenchymal cells.* Proceedings of the National Academy of Sciences, 2008. **105**(52): p. 20641-20646.
153. Williams, C.G., et al., *Variable cytocompatibility of six cell lines with photoinitiators used for polymerizing hydrogels and cell encapsulation.* Biomaterials, 2005. **26**(11): p. 1211-1218.
154. Bryant, S.J., C.R. Nuttelman, and K.S. Anseth, *Cytocompatibility of UV and visible light photoinitiating systems on cultured NIH/3T3 fibroblasts in vitro.* Journal of Biomaterials Science, Polymer Edition, 2000. **11**(5): p. 439-457.
155. Shu, X.Z., et al., *Disulfide cross-linked hyaluronan hydrogels.* Biomacromolecules, 2002. **3**(6): p. 1304-1311.
156. Park, Y., et al., *Bovine primary chondrocyte culture in synthetic matrix metalloproteinase-sensitive poly (ethylene glycol)-based hydrogels as a scaffold for cartilage repair.* Tissue engineering, 2004. **10**(3-4): p. 515-522.
157. Metters, A. and J. Hubbell, *Network formation and degradation behavior of hydrogels formed by Michael-type addition reactions.* Biomacromolecules, 2005. **6**(1): p. 290-301.
158. Lutolf, M., et al., *Systematic modulation of Michael-type reactivity of thiols through the use of charged amino acids.* Bioconjugate chemistry, 2001. **12**(6): p. 1051-1056.
159. Shu, X.Z., et al., *In situ crosslinkable hyaluronan hydrogels for tissue engineering.* Biomaterials, 2004. **25**(7-8): p. 1339-1348.

160. Rydholm, A.E., C.N. Bowman, and K.S. Anseth, *Degradable thiol-acrylate photopolymers: polymerization and degradation behavior of an in situ forming biomaterial.* Biomaterials, 2005. **26**(22): p. 4495-4506.
161. Salinas, C.N., et al., *Chondrogenic differentiation potential of human mesenchymal stem cells photoencapsulated within poly (ethylene glycol)–arginine-glycine-aspartic acid-serine thiol-methacrylate mixed-mode networks.* Tissue engineering, 2007. **13**(5): p. 1025-1034.
162. Rydholm, A.E., et al., *Gel Permeation Chromatography Characterization of the Chain Length Distributions in Thiol− Acrylate Photopolymer Networks.* Macromolecules, 2006. **39**(23): p. 7882-7888.
163. Rydholm, A.E., et al., *Controlling network structure in degradable thiol− acrylate biomaterials to tune mass loss behavior.* Biomacromolecules, 2006. **7**(10): p. 2827-2836.
164. Lodge, T.P., *A virtual issue of Macromolecules:"Click chemistry in macromolecular science"*. 2009, ACS Publications.
165. Kolb, H.C., M. Finn, and K.B. Sharpless, *Click chemistry: diverse chemical function from a few good reactions.* Angewandte Chemie International Edition, 2001. **40**(11): p. 2004-2021.
166. Malkoch, M., et al., *Synthesis of well-defined hydrogel networks using click chemistry.* Chemical Communications, 2006(26): p. 2774-2776.
167. Ossipov, D.A. and J. Hilborn, *Poly (vinyl alcohol)-based hydrogels formed by "click chemistry".* Macromolecules, 2006. **39**(5): p. 1709-1718.
168. Liu, S.Q., et al., *Biodegradable poly (ethylene glycol)–peptide hydrogels with well-defined structure and properties for cell delivery.* Biomaterials, 2009. **30**(8): p. 1453-1461.
169. Caliari, S.R. and J.A. Burdick, *A practical guide to hydrogels for cell culture.* Nature methods, 2016. **13**(5): p. 405.
170. Adzima, B.J., et al., *Spatial and temporal control of the alkyne–azide cycloaddition by photoinitiated Cu (II) reduction.* Nature Chemistry, 2011. **3**(3): p. 256-259.
171. Shih, H. and C.-C. Lin, *Cross-linking and degradation of step-growth hydrogels formed by thiol–ene photoclick chemistry.* Biomacromolecules, 2012. **13**(7): p. 2003-2012.
172. Gerlach, G. and K.-F. Arndt, *Hydrogel sensors and actuators: engineering and technology*. Vol. 6. 2009: Springer Science & Business Media.
173. Ingber, D.E., *Cellular mechanotransduction: putting all the pieces together again.* The FASEB journal, 2006. **20**(7): p. 811-827.
174. Schwarz, U.S. and R. Alon, *L-selectin-mediated leukocyte tethering in shear flow is controlled by multiple contacts and cytoskeletal anchorage facilitating fast rebinding events.* Proceedings of the National Academy of Sciences of the United States of America, 2004. **101**(18): p. 6940-6945.
175. D.J. Almdal K, H.S., Kramer O, *What is a gel?*, M.C.M. Symp, Editor.
176. Zuidema, J.M., et al., *A protocol for rheological characterization of hydrogels for tissue engineering strategies.* Journal of Biomedical Materials Research Part B: Applied Biomaterials, 2014. **102**(5): p. 1063-1073.
177. Engler, A.J., et al., *Matrix elasticity directs stem cell lineage specification.* Cell, 2006. **126**(4): p. 677-689.
178. Guvendiren, M. and J.A. Burdick, *Stiffening hydrogels to probe short-and long-term cellular responses to dynamic mechanics.* Nature communications, 2012. **3**: p. 792.
179. Elkin, B.S., et al., *Mechanical heterogeneity of the rat hippocampus measured by atomic force microscope indentation.* Journal of neurotrauma, 2007. **24**(5): p. 812-822.

180. Lu, Y.-B., et al., *Viscoelastic properties of individual glial cells and neurons in the CNS.* Proceedings of the National Academy of Sciences, 2006. **103**(47): p. 17759-17764.
181. Saha, K., et al., *Substrate modulus directs neural stem cell behavior.* Biophysical journal, 2008. **95**(9): p. 4426-4438.
182. Engler, A.J., et al., *Myotubes differentiate optimally on substrates with tissue-like stiffness: pathological implications for soft or stiff microenvironments.* J Cell Biol, 2004. **166**(6): p. 877-887.
183. Discher, D.E., P. Janmey, and Y.-l. Wang, *Tissue cells feel and respond to the stiffness of their substrate.* Science, 2005. **310**(5751): p. 1139-1143.
184. Flory, P.J., *Principles of polymer chemistry*. 1953: Cornell University Press.
185. Kizilay, M.Y. and O. Okay, *Effect of hydrolysis on spatial inhomogeneity in poly (acrylamide) gels of various crosslink densities.* Polymer, 2003. **44**(18): p. 5239-5250.
186. Branco, M.C., et al., *Macromolecular diffusion and release from self-assembled β-hairpin peptide hydrogels.* Biomaterials, 2009. **30**(7): p. 1339-1347.
187. Stellwagen, N.C., *Apparent pore size of polyacrylamide gels: Comparison of gels cast and run in Tris‐acetate‐EDTA and Tris‐borate‐EDTA buffers.* Electrophoresis, 1998. **19**(10): p. 1542-1547.
188. Olofsson, K., M. Malkoch, and A. Hult, *Soft hydrogels from tetra-functional PEGs using UV-induced thiol–ene coupling chemistry: a structure-to-property study.* RSC Advances, 2014. **4**(57): p. 30118-30128.
189. Khetan, S., et al., *Degradation-mediated cellular traction directs stem cell fate in covalently crosslinked three-dimensional hydrogels.* Nature materials, 2013. **12**(5): p. 458.
190. Wiesbrock, F., R. Hoogenboom, and U.S. Schubert, *Microwave‐assisted polymer synthesis: state‐of‐the‐art and future perspectives.* Macromolecular Rapid Communications, 2004. **25**(20): p. 1739-1764.
191. Hoogenboom, R., et al., *Microwave-assisted cationic ring-opening polymerization of 2-oxazolines: a powerful method for the synthesis of amphiphilic triblock copolymers.* Macromolecules, 2006. **39**(14): p. 4719-4725.
192. Saegusa, T., H. Ikeda, and H. Fujii, *Alternating Copolymerization of 2-Oxazoline with β-Propiolactone.* Macromolecules, 1972. **5**(4): p. 354-358.
193. Dworak, A., *The role of cationic and covalent active centers in the polymerization of 2‐methyl‐2‐oxazoline initiated with benzyl bromide.* Macromolecular Chemistry and Physics, 1998. **199**(9): p. 1843-1849.
194. Dworak, A., et al., *Polyoxazolines-mechanism of synthesis and solution properties.* Polimery, 2014. **59**(1): p. 88-94.
195. Guillerm, B., et al., *How to modulate the chemical structure of polyoxazolines by appropriate functionalization.* Macromolecular rapid communications, 2012. **33**(19): p. 1600-1612.
196. Wang, C.-H. and G.-H. Hsiue, *New amphiphilic poly (2-ethyl-2-oxazoline)/poly (L-lactide) triblock copolymers.* Biomacromolecules, 2003. **4**(6): p. 1487-1490.
197. Tauhardt, L., et al., *Amine end-functionalized poly (2-ethyl-2-oxazoline) as promising coating material for antifouling applications.* Journal of Materials Chemistry B, 2014. **2**(30): p. 4883-4893.
198. Kempe, K., et al., *Multifunctional Poly (2‐oxazoline) Nanoparticles for Biological Applications.* Macromolecular rapid communications, 2010. **31**(21): p. 1869-1873.
199. Fijten, M.W., et al., *Clickable Poly (2‐Oxazoline) s as Versatile Building Blocks.* Macromolecular Chemistry and Physics, 2008. **209**(18): p. 1887-1895.

200. Rueda, J.C., et al., *Synthesis of New Hydrogels by Copolymerization of Poly (2‐methyl‐2‐oxazoline) Bis (macromonomers) and N‐Vinylpyrrolidone.* Macromolecular Chemistry and Physics, 2003. **204**(7): p. 947-953.
201. Zalipsky, S., et al., *Evaluation of blood clearance rates and biodistribution of poly (2‐oxazoline)‐grafted liposomes.* Journal of pharmaceutical sciences, 1996. **85**(2): p. 133-137.
202. Chujo, Y., et al., *A novel silane coupling agent. 1. Synthesis of trimethoxysilyl-terminated poly (N-acetylethylenimine).* Macromolecules, 1989. **22**(5): p. 2040-2043.
203. Einzmann, M. and W.H. Binder, *Novel functional initiators for oxazoline polymerization.* Journal of Polymer Science Part A: Polymer Chemistry, 2001. **39**(16): p. 2821-2831.
204. Guillerm, B., et al., *Synthesis and evaluation of triazole-linked poly (ε-caprolactone)-graft-poly (2-methyl-2-oxazoline) copolymers as potential drug carriers.* Chemical Communications, 2012. **48**(23): p. 2879-2881.
205. Mansfeld, U., et al., *Clickable initiators, monomers and polymers in controlled radical polymerizations–a prospective combination in polymer science.* Polymer Chemistry, 2010. **1**(10): p. 1560-1598.
206. Nuyken, O., et al., *Systematic investigations on the reactivity of oxazolinium salts.* Macromolecular Chemistry and Physics, 1996. **197**(1): p. 83-95.
207. Kobayashi, S., et al., *Synthesis of acryl-and methacryl-type macromonomers and telechelics by utilizing living polymerization of 2-oxazolines.* Macromolecules, 1989. **22**(7): p. 2878-2884.
208. Hoogenboom, R., M.W. Fijten, and U.S. Schubert, *The Effect of Temperature on the Living Cationic Polymerization of 2‐Phenyl‐2‐oxazoline Explored Utilizing an Automated Synthesizer.* Macromolecular rapid communications, 2004. **25**(1): p. 339-343.
209. Förtig, A., et al. *Solid‐supported biomimetic membranes with tailored lipopolymer tethers*. in *Macromolecular Symposia*. 2004. Wiley Online Library.
210. Gress, A., A. Völkel, and H. Schlaad, *Thio-click modification of poly [2-(3-butenyl)-2-oxazoline].* Macromolecules, 2007. **40**(22): p. 7928-7933.
211. Huang, S. and R. Zhuo, *Recent progress in polymer-based gene delivery vectors.* Chinese Science Bulletin, 2003. **48**(13): p. 1304-1309.
212. Demeneix, B., Z. Hassani, and J.-P. Behr, *Towards multifunctional synthetic vectors.* Current gene therapy, 2004. **4**(4): p. 445-455.
213. Pollard, H., et al., *Polyethylenimine but not cationic lipids promotes transgene delivery to the nucleus in mammalian cells.* Journal of Biological Chemistry, 1998. **273**(13): p. 7507-7511.
214. Wightman, L., et al., *Different behavior of branched and linear polyethylenimine for gene delivery in vitro and in vivo.* The journal of gene medicine, 2001. **3**(4): p. 362-372.
215. Fischer, D., et al., *A novel non-viral vector for DNA delivery based on low molecular weight, branched polyethylenimine: effect of molecular weight on transfection efficiency and cytotoxicity.* Pharmaceutical research, 1999. **16**(8): p. 1273-1279.
216. Wiesbrock, F., et al., *Microwave-assisted synthesis of a 42-membered library of diblock copoly (2-oxazoline) s and chain-extended homo poly (2-oxazoline) s and their thermal characterization.* Macromolecules, 2005. **38**(19): p. 7957-7966.
217. Victor, R., et al., *Fast and accurate partial hydrolysis of poly (2-ethyl-2-oxazoline) into tailored linear polyethylenimine copolymers.* Polymer Chemistry, 2014. **5**(17): p. 4957-4964.
218. Shah, R., et al., *In vitro study of partially hydrolyzed poly (2-ethyl-2-oxazolines) as materials for biomedical applications.* Journal of Materials Science: Materials in Medicine, 2015. **26**(4): p. 157.

219. Lin, C.-P., Y.-C. Sung, and G.-H. Hsiue, *Non-viral pH-sensitive Gene Carriers based on Poly ((2-ethyl-2-oxazoline)-co-ethylenimine)-block-Poly (2-ethyl-2-oxazoline): A Study of Gene Release Behavior.* J Med Biol Eng, 2012. **32**: p. 365-72.
220. Kempe, K., et al., *Rational design of an amorphous poly (2-oxazoline) with a low glass-transition temperature: monomer synthesis, copolymerization, and properties.* Macromolecules, 2010. **43**(9): p. 4098-4104.
221. Tait, A., et al., *Biocompatibility of poly (2-alkyl-2-oxazoline) brush surfaces for adherent lung cell lines.* Biomaterials, 2015. **61**: p. 26-32.
222. Halperin, A., et al., *Primary versus ternary adsorption of proteins onto PEG brushes.* Langmuir, 2007. **23**(21): p. 10603-10617.
223. Jeon, S., et al., *Protein—surface interactions in the presence of polyethylene oxide: I. Simplified theory.* Journal of colloid and interface science, 1991. **142**(1): p. 149-158.
224. Efremova, N.V., et al., *Measurements of interbilayer forces and protein adsorption on uncharged lipid bilayers displaying poly (ethylene glycol) chains.* Biochemistry, 2000. **39**(12): p. 3441-3451.
225. Norde, W. and D. Gage, *Interaction of bovine serum albumin and human blood plasma with PEO-tethered surfaces: influence of PEO chain length, grafting density, and temperature.* Langmuir, 2004. **20**(10): p. 4162-4167.
226. Bosker, W., et al., *BSA adsorption on bimodal PEO brushes.* Journal of colloid and interface science, 2005. **286**(2): p. 496-503.
227. Zhao, C., et al., *Effect of film thickness on the antifouling performance of poly (hydroxy-functional methacrylates) grafted surfaces.* Langmuir, 2011. **27**(8): p. 4906-4913.
228. Yandi, W., et al., *Hydration and chain entanglement determines the optimum thickness of poly (HEMA-co-PEG10MA) brushes for effective resistance to settlement and adhesion of marine fouling organisms.* ACS applied materials & interfaces, 2014. **6**(14): p. 11448-11458.
229. Uchida, K., et al., *A reactive poly (ethylene glycol) layer to achieve specific surface plasmon resonance sensing with a high S/N ratio: the substantial role of a short underbrushed PEG layer in minimizing nonspecific adsorption.* Analytical chemistry, 2005. **77**(4): p. 1075-1080.
230. Uchida, K., et al., *Creation of a mixed poly (ethylene glycol) tethered-chain surface for preventing the nonspecific adsorption of proteins and peptides.* Biointerphases, 2007. **2**(4): p. 126-130.
231. Otsuka, H., Y. Nagasaki, and K. Kataoka, *Surface characterization of functionalized polylactide through the coating with heterobifunctional poly (ethylene glycol)/polylactide block copolymers.* Biomacromolecules, 2000. **1**(1): p. 39-48.
232. Halperin, A., *Polymer brushes that resist adsorption of model proteins: design parameters.* Langmuir, 1999. **15**(7): p. 2525-2533.
233. Currie, E., et al., *Stuffed brushes: theory and experiment.* Pure and applied chemistry, 1999. **71**(7): p. 1227-1241.
234. Rodda, A.E., et al., *Optimization of Aqueous SI‐ATRP Grafting of Poly (Oligo (Ethylene Glycol) Methacrylate) Brushes from Benzyl Chloride Macroinitiator Surfaces.* Macromolecular bioscience, 2015. **15**(6): p. 799-811.
235. Ling, Y., et al., *POEGMA-based disulfide-containing fluorescent probes for imitating and tracing noninternalization-based intracellular drug delivery.* Chemical Communications, 2016. **52**(24): p. 4533-4536.
236. Shi, X., et al., *Cell adhesion on a POEGMA-modified topographical surface.* Langmuir, 2012. **28**(49): p. 17011-17018.
237. Cheng, G., et al., *Inhibition of bacterial adhesion and biofilm formation on zwitterionic surfaces.* Biomaterials, 2007. **28**(29): p. 4192-4199.

238. Katira, P., et al., *Quantifying the Performance of Protein‐Resisting Surfaces at Ultra‐Low Protein Coverages using Kinesin Motor Proteins as Probes.* Advanced Materials, 2007. **19**(20): p. 3171-3176.
239. Gautrot, J.E., et al., *Protein-resistant NTA-functionalized polymer brushes for selective and stable immobilization of histidine-tagged proteins.* ACS applied materials & interfaces, 2009. **2**(1): p. 193-202.
240. Efremova, N., S. Sheth, and D. Leckband, *Protein-induced changes in poly (ethylene glycol) brushes: molecular weight and temperature dependence.* Langmuir, 2001. **17**(24): p. 7628-7636.
241. Xing, C.-M., et al., *Quantitative fabrication, performance optimization and comparison of PEG and zwitterionic polymer antifouling coatings.* Acta biomaterialia, 2017. **59**: p. 129-138.
242. Gautrot, J.E., et al., *Exploiting the superior protein resistance of polymer brushes to control single cell adhesion and polarisation at the micron scale.* Biomaterials, 2010. **31**(18): p. 5030-5041.
243. Prime, K.L. and G.M. Whitesides, *Self-assembled organic monolayers: model systems for studying adsorption of proteins at surfaces.* Science, 1991: p. 1164-1167.
244. Kurosawa, S., et al., *Synthesis of tethered-polymer brush by atom transfer radical polymerization from a plasma-polymerized-film-coated quartz crystal microbalance and its application for immunosensors.* Biosensors and Bioelectronics, 2004. **20**(6): p. 1165-1176.
245. Yang, W., et al., *Pursuing "zero" protein adsorption of poly (carboxybetaine) from undiluted blood serum and plasma.* Langmuir, 2009. **25**(19): p. 11911-11916.
246. Hu, W., et al., *Poly [oligo (ethylene glycol) methacrylate‐co‐glycidyl methacrylate] Brush Substrate for Sensitive Surface Plasmon Resonance Imaging Protein Arrays.* Advanced Functional Materials, 2010. **20**(20): p. 3497-3503.
247. Vaisocherova, H., et al., *Ultralow fouling and functionalizable surface chemistry based on a zwitterionic polymer enabling sensitive and specific protein detection in undiluted blood plasma.* Analytical chemistry, 2008. **80**(20): p. 7894-7901.
248. Huang, C.-J., Y. Li, and S. Jiang, *Zwitterionic polymer-based platform with two-layer architecture for ultra low fouling and high protein loading.* Analytical chemistry, 2012. **84**(7): p. 3440-3445.
249. Luna-Vera, F., J.D. Ferguson, and J.C. Alvarez, *Real time detection of lysozyme by pulsed streaming potentials using polyclonal antibodies immobilized on a renewable nonfouling surface inside plastic microfluidic channels.* Analytical chemistry, 2011. **83**(6): p. 2012-2019.
250. Welch, M.E., et al., *Generalized platform for antibody detection using the antibody catalyzed water oxidation pathway.* Journal of the American Chemical Society, 2014. **136**(5): p. 1879-1883.
251. Tugulu, S., et al., *RGD—Functionalized polymer brushes as substrates for the integrin specific adhesion of human umbilical vein endothelial cells.* Biomaterials, 2007. **28**(16): p. 2536-2546.
252. Bharali, D.J., et al., *Organically modified silica nanoparticles: a nonviral vector for in vivo gene delivery and expression in the brain.* Proceedings of the National Academy of Sciences of the United States of America, 2005. **102**(32): p. 11539-11544.
253. Pack, D.W., et al., *Design and development of polymers for gene delivery.* Nature reviews Drug discovery, 2005. **4**(7): p. 581.
254. Sun, J.-T., C.-Y. Hong, and C.-Y. Pan, *Fabrication of PDEAEMA-coated mesoporous silica nanoparticles and pH-responsive controlled release.* The Journal of Physical Chemistry C, 2010. **114**(29): p. 12481-12486.

255. Cloete, T., *Biofouling control in industrial water systems: What we know and what we need to know.* Materials and Corrosion, 2003. **54**(7): p. 520-526.
256. Da Silva, E.P. and E.C.P. De Martinis, *Current knowledge and perspectives on biofilm formation: the case of Listeria monocytogenes.* Applied microbiology and biotechnology, 2013. **97**(3): p. 957-968.
257. Ejaz, M., et al., *Controlled graft polymerization of methyl methacrylate on silicon substrate by the combined use of the langmuir− blodgett and atom transfer radical polymerization techniques.* Macromolecules, 1998. **31**(17): p. 5934-5936.
258. Matyjaszewski, K., et al., *Polymers at interfaces: using atom transfer radical polymerization in the controlled growth of homopolymers and block copolymers from silicon surfaces in the absence of untethered sacrificial initiator.* Macromolecules, 1999. **32**(26): p. 8716-8724.
259. Wang, X.-S., et al., *Facile synthesis of well-defined water-soluble polymers via atom transfer radical polymerization in aqueous media at ambient temperature.* Chemical Communications, 1999(18): p. 1817-1818.
260. Kim, J.-B., et al., *Synthesis of triblock copolymer brushes by surface-initiated atom transfer radical polymerization.* Macromolecules, 2002. **35**(14): p. 5410-5416.
261. Min, K., H. Gao, and K. Matyjaszewski, *Use of ascorbic acid as reducing agent for synthesis of well-defined polymers by ARGET ATRP.* Macromolecules, 2007. **40**(6): p. 1789-1791.
262. Ma, H., et al., *"Non‐Fouling" Oligo (ethylene glycol)‐Functionalized Polymer Brushes Synthesized by Surface‐Initiated Atom Transfer Radical Polymerization.* Advanced Materials, 2004. **16**(4): p. 338-341.
263. Oh, J.K., K. Min, and K. Matyjaszewski, *Preparation of poly (oligo (ethylene glycol) monomethyl ether methacrylate) by homogeneous aqueous AGET ATRP.* Macromolecules, 2006. **39**(9): p. 3161-3167.
264. Horn, M. and K. Matyjaszewski, *Solvent effects on the activation rate constant in atom transfer radical polymerization.* Macromolecules, 2013. **46**(9): p. 3350-3357.
265. Braunecker, W.A., et al., *Thermodynamic components of the atom transfer radical polymerization equilibrium: quantifying solvent effects.* Macromolecules, 2009. **42**(17): p. 6348-6360.
266. Rosen, B.M. and V. Percec, *Single-electron transfer and single-electron transfer degenerative chain transfer living radical polymerization.* Chemical reviews, 2009. **109**(11): p. 5069-5119.
267. Nguyen, N.H., et al., *SET-LRP of N-(2-hydroxypropyl) methacrylamide in H 2 O.* Polymer Chemistry, 2013. **4**(8): p. 2424-2427.
268. Tang, W., et al., *Understanding atom transfer radical polymerization: effect of ligand and initiator structures on the equilibrium constants.* Journal of the American Chemical Society, 2008. **130**(32): p. 10702-10713.
269. Trmcic-Cvitas, J., et al., *Biofunctionalized protein resistant oligo (ethylene glycol)-derived polymer brushes as selective immobilization and sensing platforms.* Biomacromolecules, 2009. **10**(10): p. 2885-2894.
270. Qi, Y., et al., *A brush-polymer/exendin-4 conjugate reduces blood glucose levels for up to five days and eliminates poly (ethylene glycol) antigenicity.* Nature biomedical engineering, 2017. **1**(1): p. 0002.
271. Joh, D.Y., et al., *Poly (oligo (ethylene glycol) methyl ether methacrylate) Brushes on High-κ Metal Oxide Dielectric Surfaces for Bioelectrical Environments.* ACS applied materials & interfaces, 2017. **9**(6): p. 5522-5529.
272. Du, Z., et al., *Optimizing conditions of preparation of thermoresponsive SiO2-POEGMA particles via AGET-ATRP.* Applied Surface Science, 2015. **329**: p. 234-239.

273. Shih, Y.-J., et al., *Hemocompatibility of polyampholyte copolymers with well-defined charge bias in human blood.* Langmuir, 2014. **30**(22): p. 6489-6496.
274. Chen, S., et al., *Surface hydration: principles and applications toward low-fouling/nonfouling biomaterials.* Polymer, 2010. **51**(23): p. 5283-5293.
275. Fan, X., L. Lin, and P.B. Messersmith, *Cell fouling resistance of polymer brushes grafted from Ti substrates by surface-initiated polymerization: effect of ethylene glycol side chain length.* Biomacromolecules, 2006. **7**(8): p. 2443-2448.
276. Ladd, J., et al., *Zwitterionic polymers exhibiting high resistance to nonspecific protein adsorption from human serum and plasma.* Biomacromolecules, 2008. **9**(5): p. 1357-1361.
277. Homola, J., S.S. Yee, and G. Gauglitz, *Surface plasmon resonance sensors.* Sensors and Actuators B: Chemical, 1999. **54**(1-2): p. 3-15.
278. Nguyen, H.H., et al., *Surface plasmon resonance: a versatile technique for biosensor applications.* Sensors, 2015. **15**(5): p. 10481-10510.
279. Liedberg, B., I. Lundström, and E. Stenberg, *Principles of biosensing with an extended coupling matrix and surface plasmon resonance.* Sensors and Actuators B: Chemical, 1993. **11**(1-3): p. 63-72.
280. Wilgus, T.A., *Growth factor–extracellular matrix interactions regulate wound repair.* Advances in wound care, 2012. **1**(6): p. 249-254.
281. Lutolf, M.P., P.M. Gilbert, and H.M. Blau, *Designing materials to direct stem-cell fate.* Nature, 2009. **462**(7272): p. 433.
282. Ochsner, M., et al., *Micro-well arrays for 3D shape control and high resolution analysis of single cells.* Lab on a Chip, 2007. **7**(8): p. 1074-1077.
283. Peerani, R., et al., *Niche‐mediated control of human embryonic stem cell self‐renewal and differentiation.* The EMBO journal, 2007. **26**(22): p. 4744-4755.
284. Théry, M., et al., *The extracellular matrix guides the orientation of the cell division axis.* Nature cell biology, 2005. **7**(10): p. 947.
285. Jiang, X., et al., *Directing cell migration with asymmetric micropatterns.* Proceedings of the National Academy of Sciences of the United States of America, 2005. **102**(4): p. 975-978.
286. Théry, M., et al., *Anisotropy of cell adhesive microenvironment governs cell internal organization and orientation of polarity.* Proceedings of the National Academy of Sciences, 2006. **103**(52): p. 19771-19776.
287. Yanker, D.M. and J.A. Maurer, *Direct printing of trichlorosilanes on glass for selective protein adsorption and cell growth.* Molecular Biosystems, 2008. **4**(6): p. 502-504.
288. Jeon, N.L., et al., *Structure and stability of patterned self-assembled films of octadecyltrichlorosilane formed by contact printing.* Langmuir, 1997. **13**(13): p. 3382-3391.
289. Delamarche, E., et al., *Transport mechanisms of alkanethiols during microcontact printing on gold*. 1998, ACS Publications.
290. Tan, K.Y., et al., *Study of thiol–ene chemistry on polymer brushes and application to surface patterning and protein adsorption.* Polymer Chemistry, 2016. **7**(4): p. 979-990.
291. Lutolf, M., et al., *Synthetic matrix metalloproteinase-sensitive hydrogels for the conduction of tissue regeneration: engineering cell-invasion characteristics.* Proceedings of the National Academy of Sciences, 2003. **100**(9): p. 5413-5418.
292. Grafahrend, D., et al., *Degradable polyester scaffolds with controlled surface chemistry combining minimal protein adsorption with specific bioactivation.* Nature materials, 2011. **10**(1): p. 67.
293. Farrugia, B.L., et al., *Poly (2-oxazoline) hydrogels for controlled fibroblast attachment.* Biomacromolecules, 2013. **14**(8): p. 2724-2732.

294. Sawicki, L.A. and A.M. Kloxin, *Design of thiol–ene photoclick hydrogels using facile techniques for cell culture applications.* Biomaterials science, 2014. **2**(11): p. 1612-1626.
295. Choi, B., et al., *Introduction to in situ forming hydrogels for biomedical applications*, in *In-Situ Gelling Polymers*. 2015, Springer. p. 5-35.
296. Gramlich, W.M., I.L. Kim, and J.A. Burdick, *Synthesis and orthogonal photopatterning of hyaluronic acid hydrogels with thiol-norbornene chemistry.* Biomaterials, 2013. **34**(38): p. 9803-9811.
297. Yu, J., et al., *In situ covalently cross-linked PEG hydrogel for ocular drug delivery applications.* International journal of pharmaceutics, 2014. **470**(1-2): p. 151-157.
298. Bian, L., et al., *The influence of hyaluronic acid hydrogel crosslinking density and macromolecular diffusivity on human MSC chondrogenesis and hypertrophy.* Biomaterials, 2013. **34**(2): p. 413-421.
299. Huebsch, N., et al., *Harnessing traction-mediated manipulation of the cell/matrix interface to control stem-cell fate.* Nature materials, 2010. **9**(6): p. 518.
300. Burdick, J.A. and K.S. Anseth, *Photoencapsulation of osteoblasts in injectable RGD-modified PEG hydrogels for bone tissue engineering.* Biomaterials, 2002. **23**(22): p. 4315-4323.
301. Hersel, U., C. Dahmen, and H. Kessler, *RGD modified polymers: biomaterials for stimulated cell adhesion and beyond.* Biomaterials, 2003. **24**(24): p. 4385-4415.
302. Hoogenboom, R., *Poly (2‐oxazoline) s: a polymer class with numerous potential applications.* Angewandte Chemie International Edition, 2009. **48**(43): p. 7978-7994.
303. Flory, P.J., *Molecular size distribution in three dimensional polymers. i. gelation1.* Journal of the American Chemical Society, 1941. **63**(11): p. 3083-3090.
304. Stauffer, D., A. Coniglio, and M. Adam, *Gelation and critical phenomena*, in *Polymer networks*. 1982, Springer. p. 103-158.
305. Atta, A.M. and A.A.A. Abdel‐Azim, *Effect of crosslinker functionality on swelling and network parameters of copolymeric hydrogels.* Polymers for Advanced Technologies, 1998. **9**(6): p. 340-348.
306. Tan, H., et al., *Novel multiarm PEG‐based hydrogels for tissue engineering.* Journal of Biomedical Materials Research Part A, 2010. **92**(3): p. 979-987.
307. Muller, F.L. and J.F. Davidson, *Rheology of shear thinning polymer solutions.* Industrial & engineering chemistry research, 1994. **33**(10): p. 2364-2367.
308. Nguyen, K.D., et al., *Ultrafast diffusion-controlled thiol–ene based crosslinking of silicone elastomers with tailored mechanical properties for biomedical applications.* Polymer Chemistry, 2016. **7**(33): p. 5281-5293.

Appendix A

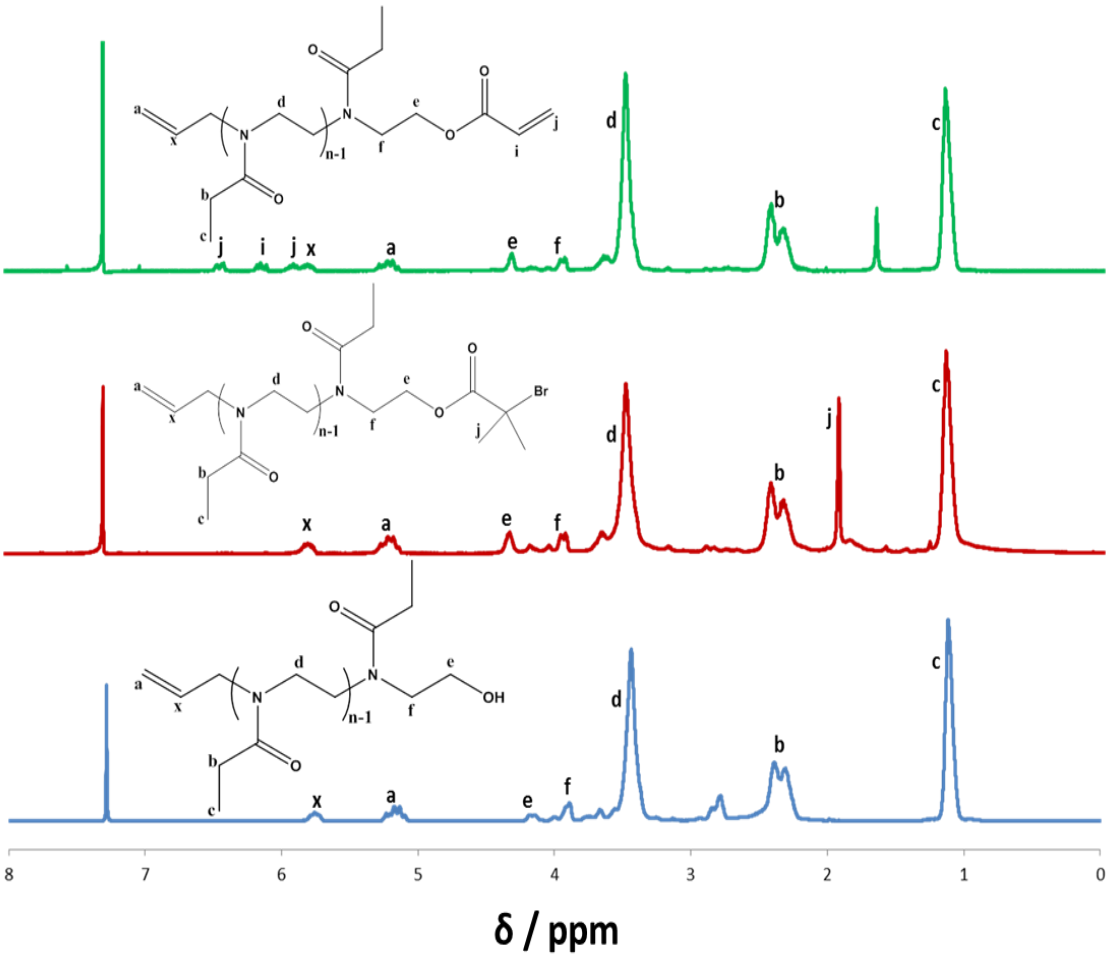

Figure a.1 ^{1}H-NMR spectrum in $CDCl_3$ of three polyoxazolines. From bottom to top, blue: oligo (EtOx) initiated with allyl tosylate and terminated with H_2O, red: oligo (EtOx) initiated with allyl tosylate and terminated with 2-Bromo-2-methylpropionic acid, green: oligo (MeOx) initiated with allyl tosylate and terminated with acrylic acid. Monomer to initiator ratio is 5:1

Table a.1 Summary of yield and conditions for oligo (EtOx) initiated with allyl tosylate and three terminate agent: 2-Bromo-2-methylpropionic acid, acrylic acid, and H_2O.

	Yield	Condition
Allyl-PEtOX-Bromo	93.27%	ice bath 3-4h
Allyl-PEtOX-Acry	99.89%	ice bath 3-4h
Allyl-PEtOX-OH	85.67%	80°C overnight

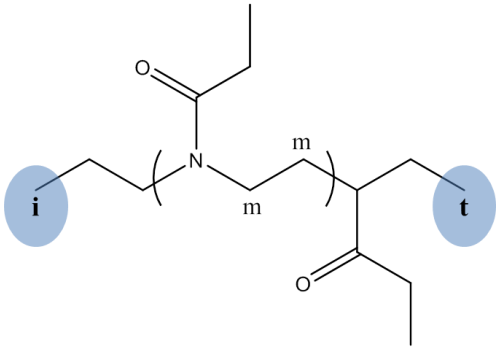

Table a.2 Summary of yield and conditions for oligo (EtOx) initiated with three initiators (methyl tosylate, butenyl tosylate, undecenyl tosylate) and three terminate agent (2-Bromo-2-methylpropionic acid, acrylic acid, and H_2O).

	Ratio M/I	Temperature	Time/mins	Hm/Hi	Hm/Ht	Hi/Ht	Yield	Conditions
Me-POX-OH	**05:01**	**140**	**5**	**5.99**	**4.63**	**0.76**	**91.24%**	**80°C overnight**
Me-POX-allylamine	**05:01**	**140**	**5**	**5.57**	**7.72**	**1.39**	**36.29%**	**ice bath overnight**
Me-POX-bromo	**05:01**	**140**	**5**	**5.57**	**5.75**	**1.03**	**91.32%**	**ice bath 3-4hrs**
Allyl-POX-MAA	**05:01**	**140**	**5**	**4.38**	**5.08**	**1.16**	**86.33%**	**80°C overnight**
Buten-POX-MAA	**05:01**	**140**	**5**	**6.88**	**7.39**	**1.07**	**92.42%**	**80°C overnight**
Undecen-POX-MAA	**05:01**	**140**	**5**	**5.13**	**6.28**	**1.22**	**94.50%**	**80°C overnight**

Table b.1 Summary of statistical data analysis obtained for the adsorption of protein on different polymer brushes via SPR. n.s., non significant; *, $p < 0.05$; **, $p < 0.01$: ***, $p < 0.001$.

	MeanDiff	Prob	
Fn 12nm PMeOx Fn 13nm POEGMA	1.16779	1	n.s.
Fn 12nm PEtOx Fn 13nm POEGMA	16.0984	0.90977	n.s.
Fn 12nm PEtOx Fn 12nm PMeOx	14.93062	0.89189	n.s.
Fn 21nm PEtOx Fn 13nm POEGMA	1.17183	1	n.s.
Fn 21nm PEtOx Fn 12nm PMeOx	0.00404	1	n.s.
Fn 21nm PEtOx Fn 12nm PEtOx	-14.9266	0.91958	n.s.
Fn PEG thiol Fn 13nm POEGMA	86.70981	6.80E-08	***
Fn PEG thiol Fn 12nm PMeOx	85.54202	5.61E-08	***
Fn PEG thiol Fn 12nm PEtOx	70.61141	7.16E-07	***
Fn PEG thiol Fn 21nm PEtOx	85.53798	6.10E-08	***
BSA 13nm POEGMA Fn 13nm POEGMA	1.53124	1	n.s.
BSA 13nm POEGMA Fn 12nm PMeOx	0.36346	1	n.s.
BSA 13nm POEGMA Fn 12nm PEtOx	-14.5672	0.95647	n.s.
BSA 13nm POEGMA Fn 21nm PEtOx	0.35942	1	n.s.
BSA 13nm POEGMA Fn PEG thiol	-85.1786	7.55E-08	***
BSA 12nm PMeOx Fn 13nm POEGMA	3.61109	1	n.s.
BSA 12nm PMeOx Fn 12nm PMeOx	2.4433	1	n.s.
BSA 12nm PMeOx Fn 12nm PEtOx	-12.4873	0.9712	n.s.
BSA 12nm PMeOx Fn 21nm PEtOx	2.43926	1	n.s.
BSA 12nm PMeOx Fn PEG thiol	-83.0987	6.03E-08	***
BSA 12nm PMeOx BSA 13nm POEGMA	2.07984	1	n.s.
BSA 12nm PEtOx Fn 13nm POEGMA	7.54012	0.99999	n.s.
BSA 12nm PEtOx Fn 12nm PMeOx	6.37233	1	n.s.
BSA 12nm PEtOx Fn 12nm PEtOx	-8.55828	0.99991	n.s.
BSA 12nm PEtOx Fn 21nm PEtOx	6.36829	1	n.s.
BSA 12nm PEtOx Fn PEG thiol	-79.1697	6.73E-07	***
BSA 12nm PEtOx BSA 13nm POEGMA	6.00888	1	n.s.
BSA 12nm PEtOx BSA 12nm PMeOx	3.92903	1	n.s.
BSA 21nm PEtOx Fn 13nm POEGMA	0.06475	1	n.s.
BSA 21nm PEtOx Fn 12nm PMeOx	-1.10304	1	n.s.
BSA 21nm PEtOx Fn 12nm PEtOx	-16.0337	0.87086	n.s.
BSA 21nm PEtOx Fn 21nm PEtOx	-1.10708	1	n.s.
BSA 21nm PEtOx Fn PEG thiol	-86.6451	5.04E-08	***
BSA 21nm PEtOx BSA 13nm POEGMA	-1.4665	1	n.s.
BSA 21nm PEtOx BSA 12nm PMeOx	-3.54634	1	n.s.
BSA 21nm PEtOx BSA 12nm PEtOx	-7.47538	0.99998	n.s.
BSA PEG thiol Fn 13nm POEGMA	30.42181	0.23822	n.s.
BSA PEG thiol Fn 12nm PMeOx	29.25402	0.19056	n.s.
BSA PEG thiol Fn 12nm PEtOx	14.3234	0.98114	n.s.
BSA PEG thiol Fn 21nm PEtOx	29.24998	0.23092	n.s.
BSA PEG thiol Fn PEG thiol	-56.288	6.84E-04	***
BSA PEG thiol BSA 13nm POEGMA	28.89056	0.31167	n.s.
BSA PEG thiol BSA 12nm PMeOx	26.81072	0.30813	n.s.
BSA PEG thiol BSA 12nm PEtOx	22.88169	0.77038	n.s.
BSA PEG thiol BSA 21nm PEtOx	30.35706	0.18501	n.s.

FBS 13nm POEGMA Fn 13nm POEGMA	9.7974	0.9994	n.s.
FBS 13nm POEGMA Fn 12nm PMeOx	8.62962	0.99959	n.s.
FBS 13nm POEGMA Fn 12nm PEtOx	-6.301	0.99999	n.s.
FBS 13nm POEGMA Fn 21nm PEtOx	8.62558	0.99974	n.s.
FBS 13nm POEGMA Fn PEG thiol	-76.9124	3.02E-07	***
FBS 13nm POEGMA BSA 13nm POEGMA	8.26616	0.99991	n.s.
FBS 13nm POEGMA BSA 12nm PMeOx	6.18632	0.99999	n.s.
FBS 13nm POEGMA BSA 12nm PEtOx	2.25728	1	n.s.
FBS 13nm POEGMA BSA 21nm PEtOx	9.73266	0.99901	n.s.
FBS 13nm POEGMA BSA PEG thiol	-20.6244	0.81215	n.s.
FBS 12nm PMeOx Fn 13nm POEGMA	12.39292	0.99322	n.s.
FBS 12nm PMeOx Fn 12nm PMeOx	11.22513	0.99371	n.s.
FBS 12nm PMeOx Fn 12nm PEtOx	-3.70548	1	n.s.
FBS 12nm PMeOx Fn 21nm PEtOx	11.22109	0.99569	n.s.
FBS 12nm PMeOx Fn PEG thiol	-74.3169	6.23E-07	***
FBS 12nm PMeOx BSA 13nm POEGMA	10.86167	0.99818	n.s.
FBS 12nm PMeOx BSA 12nm PMeOx	8.78183	0.99951	n.s.
FBS 12nm PMeOx BSA 12nm PEtOx	4.8528	1	n.s.
FBS 12nm PMeOx BSA 21nm PEtOx	12.32817	0.98944	n.s.
FBS 12nm PMeOx BSA PEG thiol	-18.0289	0.91947	n.s.
FBS 12nm PMeOx FBS 13nm POEGMA	2.59551	1	n.s.
FBS 12nm PEtOx Fn 13nm POEGMA	75.8152	4.04E-07	***
FBS 12nm PEtOx Fn 12nm PMeOx	74.64741	1.34E-07	***
FBS 12nm PEtOx Fn 12nm PEtOx	59.71679	2.88E-05	***
FBS 12nm PEtOx Fn 21nm PEtOx	74.64337	2.27E-07	***
FBS 12nm PEtOx Fn PEG thiol	-10.8946	0.9996	n.s.
FBS 12nm PEtOx BSA 13nm POEGMA	74.28395	6.29E-07	***
FBS 12nm PEtOx BSA 12nm PMeOx	72.20411	2.31E-07	***
FBS 12nm PEtOx BSA 12nm PEtOx	68.27508	1.80E-05	***
FBS 12nm PEtOx BSA 21nm PEtOx	75.75045	1.75E-07	***
FBS 12nm PEtOx BSA PEG thiol	45.39339	0.01406	**
FBS 12nm PEtOx FBS 13nm POEGMA	66.01779	8.82E-06	***
FBS 12nm PEtOx FBS 12nm PMeOx	63.42228	2.09E-05	***
FBS 21nm PEtOx Fn 13nm POEGMA	4.16714	1	n.s.
FBS 21nm PEtOx Fn 12nm PMeOx	2.99935	1	n.s.
FBS 21nm PEtOx Fn 12nm PEtOx	-11.9313	0.98037	n.s.
FBS 21nm PEtOx Fn 21nm PEtOx	2.99531	1	n.s.
FBS 21nm PEtOx Fn PEG thiol	-82.5427	5.84E-08	n.s.
FBS 21nm PEtOx BSA 13nm POEGMA	2.63589	1	n.s.
FBS 21nm PEtOx BSA 12nm PMeOx	0.55605	1	n.s.
FBS 21nm PEtOx BSA 12nm PEtOx	-3.37298	1	n.s.
FBS 21nm PEtOx BSA 21nm PEtOx	4.10239	1	n.s.
FBS 21nm PEtOx BSA PEG thiol	-26.2547	0.3401	n.s.
FBS 21nm PEtOx FBS 13nm POEGMA	-5.63027	1	n.s.
FBS 21nm PEtOx FBS 12nm PMeOx	-8.22578	0.99976	n.s.
FBS 21nm PEtOx FBS 12nm PEtOx	-71.6481	2.67E-07	***

FBS PEG thiol Fn 13nm POEGMA	171.7591	0	***
FBS PEG thiol Fn 12nm PMeOx	170.5913	0	***
FBS PEG thiol Fn 12nm PEtOx	155.6607	0	***
FBS PEG thiol Fn 21nm PEtOx	170.5873	0	***
FBS PEG thiol Fn PEG thiol	85.04932	1.64E-07	***
FBS PEG thiol BSA 13nm POEGMA	170.2279	0	***
FBS PEG thiol BSA 12nm PMeOx	168.148	0	***
FBS PEG thiol BSA 12nm PEtOx	164.219	0	***
FBS PEG thiol BSA 21nm PEtOx	171.6944	0	***
FBS PEG thiol BSA PEG thiol	141.3373	5.82E-07	***
FBS PEG thiol FBS 13nm POEGMA	161.9617	0	***
FBS PEG thiol FBS 12nm PMeOx	159.3662	0	***
FBS PEG thiol FBS 12nm PEtOx	95.94393	6.03E-08	***
FBS PEG thiol FBS 21nm PEtOx	167.592	0	***

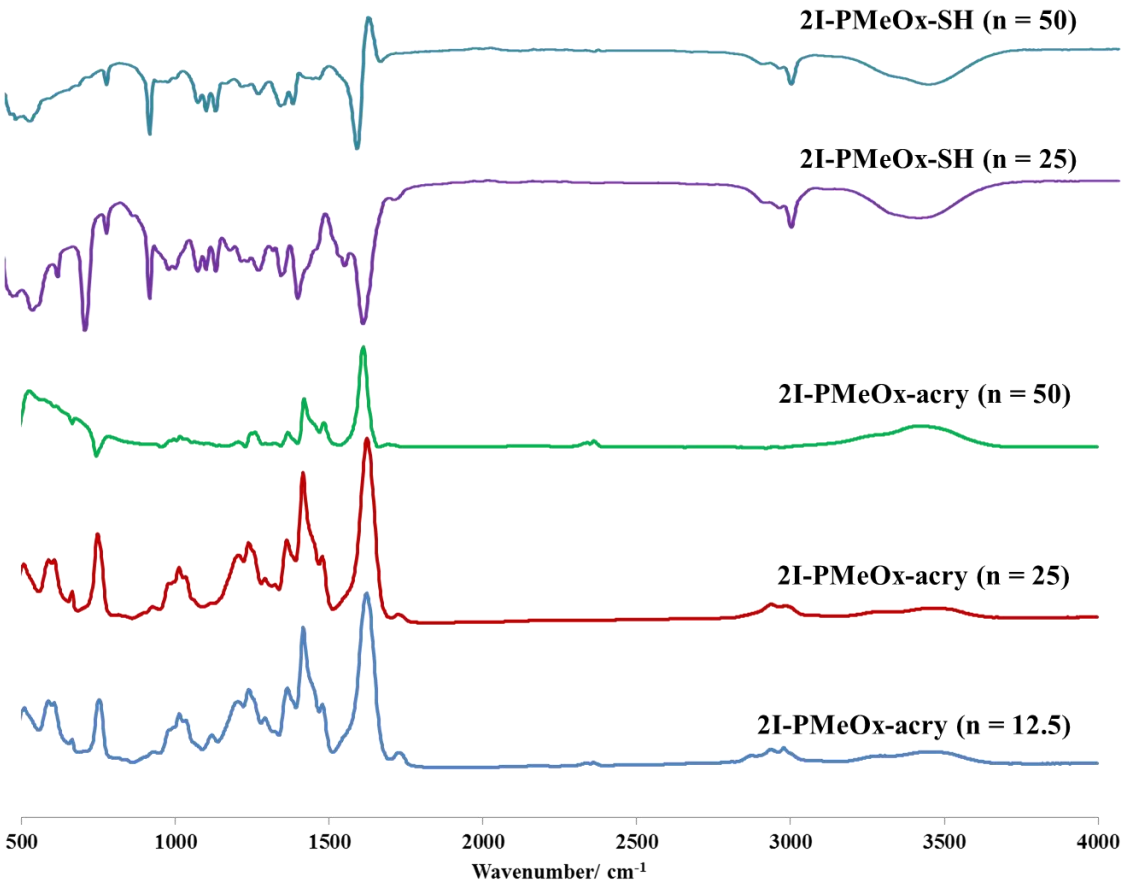

Figure c.1 FTIR for two arm PMeOx with arylic end and thiol end.

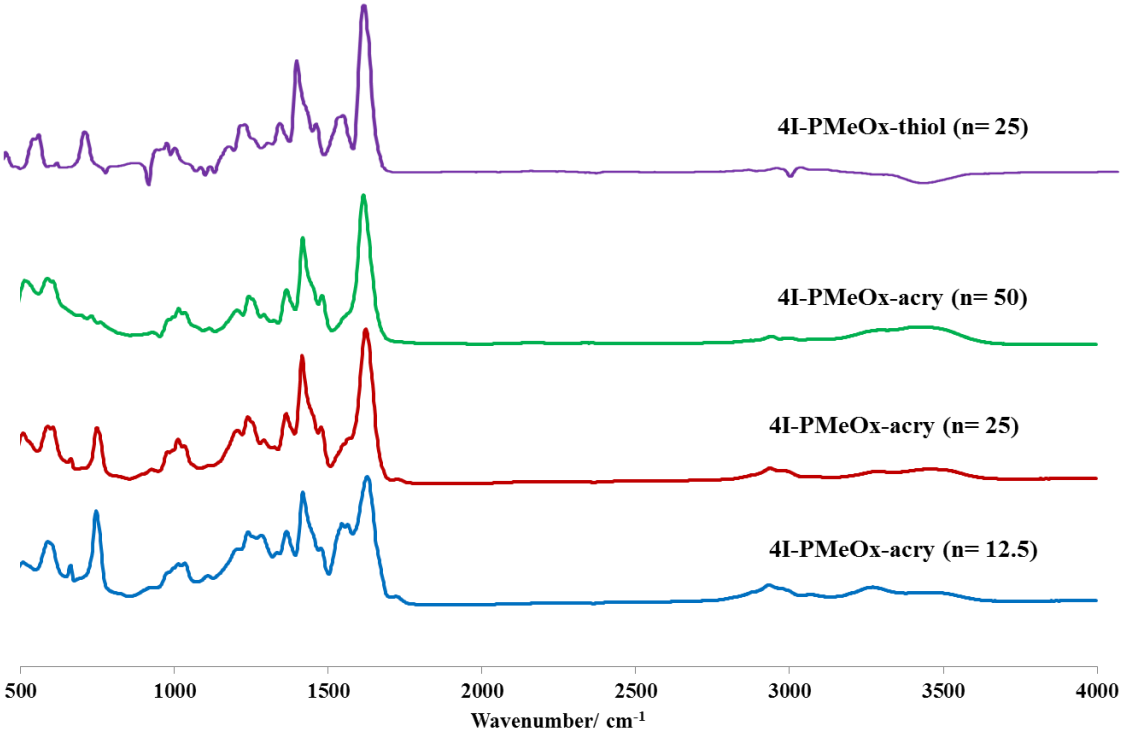

Figure c.2 FTIR for four arm PMeOx with arylic end and thiol end.

Appendix B

Instruments

NMR

Nuclear magnetic resonance is a physical phenomenon in which nuclei in a magnetic field absorb and re-emit electromagnetic radiation in an applied magnetic field. The frequency of the magnetic field as well as the magnetic properties of the isotope of the atoms determines the energy of the resonance frequency. Specific isotopes that contain an odd number of protons and/or neutrons have an intrinsic magnetic moment and angular momentum, in other words a nonzero spin; only these specific isotopes can spin and applied for NMR use.

^{1}H-NMR characterisation was carried out using Bruker AV 400 and AVIII 400. Abbreviations for NMR peaks: s- singlet, d-doublet, t-triplet, q-quartet, dt-doublet of triplets, dq-doublet of quartets, tt-triplet of triplets and m-multiplet. Detection limit was 1 mg/mL and the minimum limit depends on the frequency of the magnetic field, analysis time and concentration of sample solution. Experimental error was ± 0.1 ppm.

MALDI-ToF

Matrix-assisted laser desorption/ionization is a technique that trigger laser (nitrogen laser light) absorbing matrix to emit ion from large molecular, and those ionized molecules will be protonated or deprotonated in the hot plum of ablated gases and then accelerated before being detected.

Mass spectrometry was carried out using a matrix-assisted laser desorption/ionization (MALDI) system Ultraflex 3 ToF/ToF (Bruker Daltonics). 1 mg/mL of sample solutions were prepared in DCM and 20 mg/mL matrix solutions were prepared with dithranol in DCM. Finally, 1 μL sample solution was mixed with 49 μL matrix solutions for MALDI-ToF characterisation. The detection limit of mass range was 600 Da – 3500 Da. Mass accuracy of better than 20 ppm (0.02 Da for an m/z of 1000) can be obtained.

ATR-FTIR

Attenuated total reflectance Fourier transform infrared spectroscopy measure the changes in an optical dense crystal that occur in a totally internally reflected infrared beam. An infrared beam as an incident light irradiate an optically dense crystal with a high refractive index at a certain angle. This internal reflectance creates an evanescent wave that extends beyond the surface of the crystal into the sample held in contact with the crystal.

Grazing angle FTIR was produced by a Bruker Bruker Tensor 27 spectrometer equipped with a MCT detector, results were acquired at a resolution of 16 cm^{-1} and a total of 128 scans per run in the region of 400-4000 cm^{-1}; abbreviations for the peaks: s-strong, m-medium and w-weak. In principle, detection limit for polymer brushes was below 5 – 10 nm and for monolayers was around 1 nm.

Ellipsometry

Ellipsometry is a non-destructive, light optical technique to investigate dielectric properties of thin films. Basically, incident light goes through a polarization and then reflected off the surface of a material, the change of polarization is detected by an analyser, parameters such as amplitude ratio, Ψ, and the phase difference, Δ are used to calculate the dielectric properties of thin films.

Dry brush thicknesses were measured by ellipsometry at a 70° incidence angle using a α-SE instrument from J.A. Woolam co. Inc. A simple gold substrate/Cauchy film model was used and fitted between 400 and 900 nm. On the condition of visible-to-near infrared measurements, the maximum thickness is less than 5 microns that can be measured. Moreover, ellipsometry is very sensitive to the presence of surface layers and the sensitivity depends on changes in phase. However, the interaction of light and ultra-thin films does not provide adequate sensitivity to simultaneously measure both thickness and refractive index, so we assume minimum thickness is ultra-thin layers. Experimental error was ± 1 nm.

in-situ rheology

Rheometer is used to measure the response of the flow of matter under applied forces. Here we use rotational cylinder to apply forces on samples. Samples were placed sandwiched between cylinders from rheometer. One of the cylinders is rotated at a set speed, which determines the shear rate. Owing to the rotated cylinder, materials tend to drag the other cylinder round, and the force exerts on that cylinder was measured and converted as shear stress.

Rheology were carried out with DHR-3 from TA instrument fitted with a UV accessory and a 20 nm upper parallel plate. The UV curable gel was sandwiched between two functionalized coverslips glues to the cylinders of the rheometer at a fixed gap of 250 μm. Oscillations were set to controlled strain mode at 2%. For in situ monitoring the progressing of gelation, a time sweep was performed: 30 s of equilibrium without UV exposure, UV irradiation for 2 min and the UV light was turned off for the remaining part of the experiment. Frequency sweep and amplitude sweep measurements were conducted after the UV cure to examine the change in rheological behaviour.

SPR

A parallel beam is passing through the edge of Au or Ag coated glass (prism), when the momentum of incidence matches to the surface Plasmon, resonance from the metal surface named plasmon wave was created, and then refractive index of metal surface changed and resulting the change of angle of reflection.

Surface Plasmon Resonance (SPR) was performed on a Biacore 3000. SPR chips (Ssens) were coated with the desired polymer brush (20 nm). Treated chips were docked, primed with buffer (PBS) twice, and equilibrated at 20 μL/min for 30 min or until a stable baseline was obtained. For measurements of nonspecific binding, an example of the programmed sequence was the following: wash with PBS and equilibrate for 5 min, expose to a protein solution for 5 min (BSA of 1 mg/mL, 10 μg/mL FN or 10% FBS). The flow rate was 20 μL/min. Measurements were carried out in triplicate. The minimum detection limit for SPR is around 0.6 RU, however, the sensitivity of SPR is related to the index of refraction of the fluid medium.

Contact angle Goniometer

A liquid drop rests on a flat, horizontal solid surface. The contact angle is defined as the angle formed by the intersection of the liquid-solid interface and the liquid-vapour interface and determined from Young-Laplace equation.

The experimental error was ± 2 degrees.

XPS

X-ray photoelectron spectroscopy is a surface quantitative spectroscopy that measure the elemental composition, chemical state and electronic state of elements that within the materials on the surface. Basically, a beam of X-ray is irradiated on the surface coated with samples, and meanwhile detector is simultaneously measuring the kinetic energy and number of electrons that emitted from the top 0-10 nm of the sample that being analysed. The detection limits was determined by the X-ray sources used.

Appendix C

Chemical structures

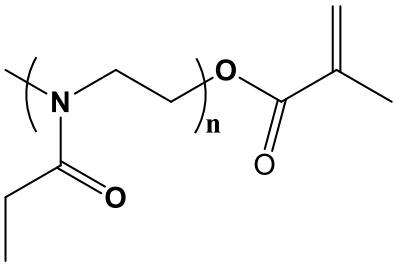

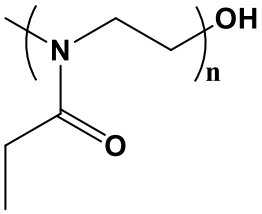

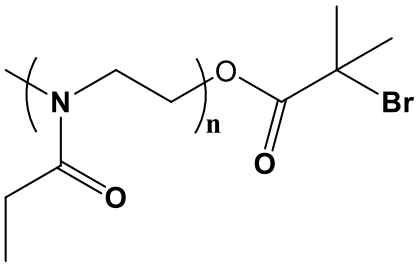

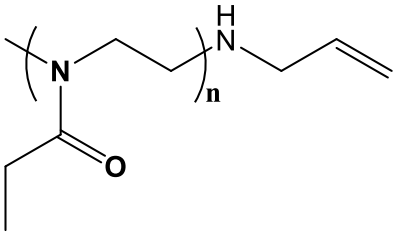

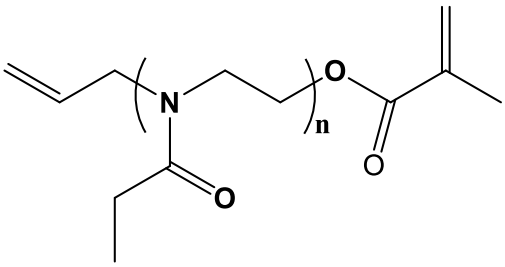

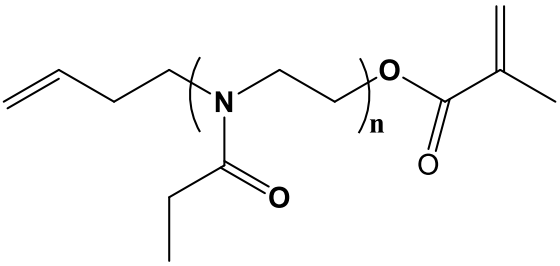

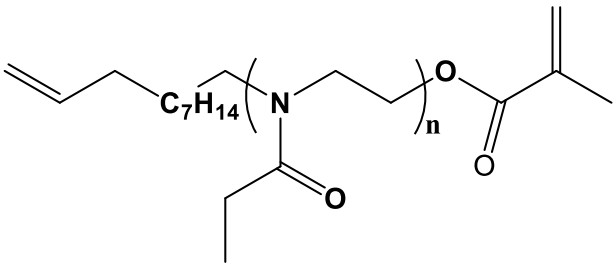

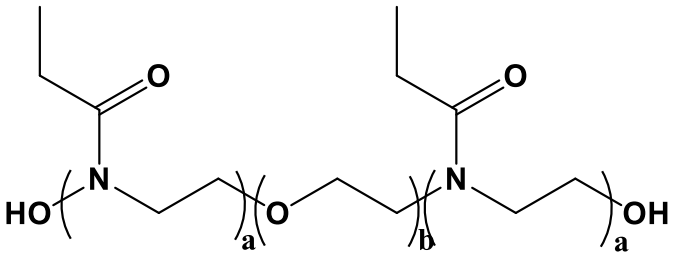

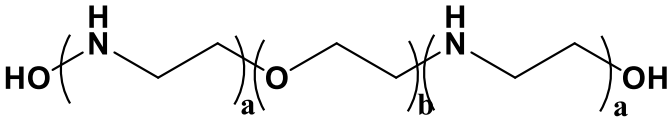

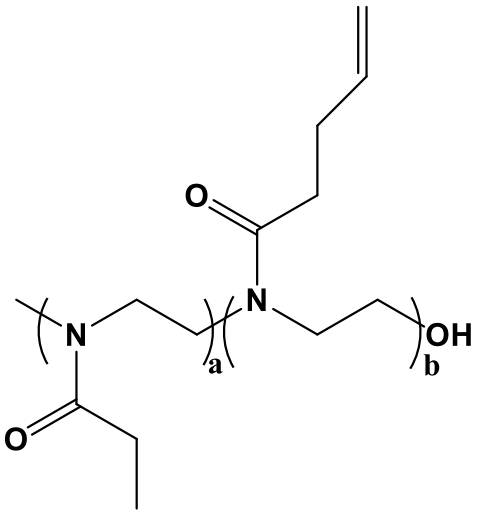

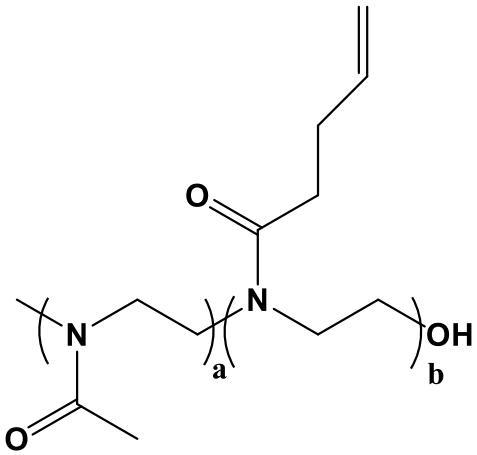

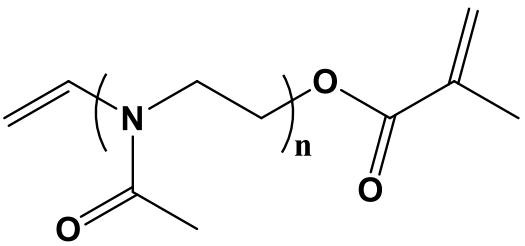

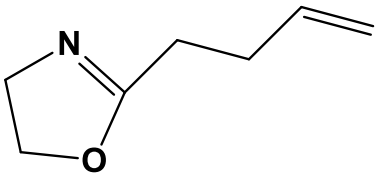

Two arm POx thiol n= 12.5, 25, 50

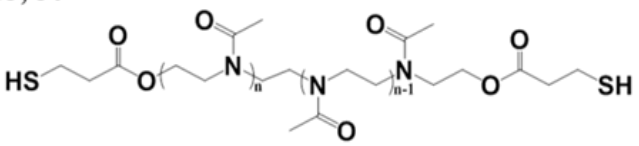

Four arm POx thiol n= 12.5, 25, 50

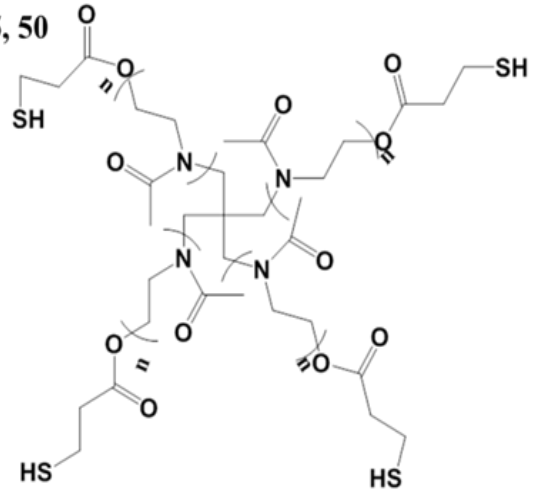

PEG di-thiol (Mn= 1000 g/mol)

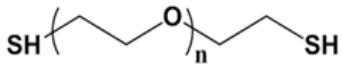

PEG tetra-thiol (Mn= 5000 g/mol, 20,000 g/mol)

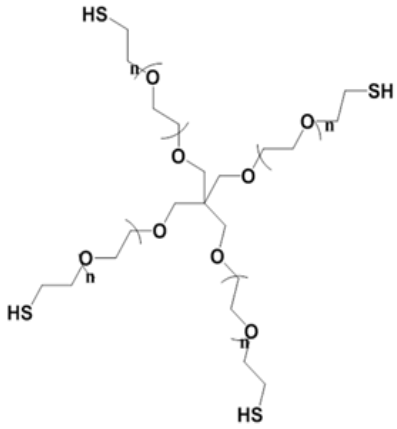

PEG hexa-thiol (Mn= 20,000 g/mol)